Terms and Conditions of Use of Digitised Theses from Trinity College Library Dublin

Copyright statement

All material supplied by Trinity College Library is protected by copyright (under the Copyright and Related Rights Act, 2000 as amended) and other relevant Intellectual Property Rights. By accessing and using a Digitised Thesis from Trinity College Library you acknowledge that all Intellectual Property Rights in any Works supplied are the sole and exclusive property of the copyright and/or other IPR holder. Specific copyright holders may not be explicitly identified. Use of materials from other sources within a thesis should not be construed as a claim over them.

A non-exclusive, non-transferable licence is hereby granted to those using or reproducing, in whole or in part, the material for valid purposes, providing the copyright owners are acknowledged using the normal conventions. Where specific permission to use material is required, this is identified and such permission must be sought from the copyright holder or agency cited.

Liability statement

By using a Digitised Thesis, I accept that Trinity College Dublin bears no legal responsibility for the accuracy, legality or comprehensiveness of materials contained within the thesis, and that Trinity College Dublin accepts no liability for indirect, consequential, or incidental, damages or losses arising from use of the thesis for whatever reason. Information located in a thesis may be subject to specific use constraints, details of which may not be explicitly described. It is the responsibility of potential and actual users to be aware of such constraints and to abide by them. By making use of material from a digitised thesis, you accept these copyright and disclaimer provisions. Where it is brought to the attention of Trinity College Library that there may be a breach of copyright or other restraint, it is the policy to withdraw or take down access to a thesis while the issue is being resolved.

Access Agreement

By using a Digitised Thesis from Trinity College Library you are bound by the following Terms & Conditions. Please read them carefully.

I have read and I understand the following statement: All material supplied via a Digitised Thesis from Trinity College Library is protected by copyright and other intellectual property rights, and duplication or sale of all or part of any of a thesis is not permitted, except that material may be duplicated by you for your research use or for educational purposes in electronic or print form providing the copyright owners are acknowledged using the normal conventions. You must obtain permission for any other use. Electronic or print copies may not be offered, whether for sale or otherwise to anyone. This copy has been supplied on the understanding that it is copyright material and that no quotation from the thesis may be published without proper acknowledgement.

Manipulation of Decellularized Porcine Scaffolds for Tissue Engineering Vascular Grafts

A thesis submitted to the University of Dublin in partial fulfilment of the requirements for the degree of

Doctor in Philosophy

Trinity College Dublin

2014

William Sheridan, BEng

Supervisors

Dr Bruce Murphy

Dr Garry Duffy

Declaration

I declare that I am the sole author of this thesis and that all work presented in it, unless otherwise referenced, is my own. I also declare that the work has not been submitted, in whole or in part, to any other university for a degree or other qualification.

I authorise the library of Trinity College Dublin to lend or copy this thesis upon request.

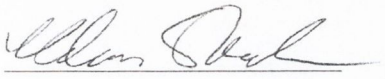

William Sheridan

May 2014

Declaration

I declare that I am the sole author of this thesis and that all work presented in it, unless otherwise referenced, is my own. I also declare that the work has not been submitted, in whole or in part, to any other university for a degree or other qualification.

I authorise the library of Trinity College Dublin to lend or copy this thesis upon request.

_____

William Sheridan

May 2014

Summary

The prevalence of vascular disease continues to increase worldwide, the treatment for which relies heavily on diseased vessel replacement. Tissue engineering vascular grafts potentially offers a new solution for addressing the shortage of autologous vessel grafts. Challenges such as suitable mechanical properties, viable cell sources, inefficient seeding techniques, lengthy manufacturing times, sustainable shelf life and high costs have hindered this translation. Decellularized scaffolds could potentially offer a solution to this clinical problem; however, their translation has been limited by their highly dense matrix architecture which can prevent cell repopulation. This thesis aims to advance new methods to manipulate decellularized tissue for use as vascular grafts.

Direct injection of cells via medial injection channels allowed for rapid bulk seeding of decellularized scaffolds. Further manipulation by small collagen fiber digestion increased the porosity to aid cell infiltration. Growth factor delivery using a thermoresponsive hydrogel within the scaffold functioned as a chemotactic stimulus to further enhance cell migration. The response of medially injected cells to dynamic culture conditions was determined using a custom built pulsatile flow bioreactor. Increased cell migration was evident in response to this stimulus. A new manufacturing protocol to create a means for the preservation and sterilisation of these scaffolds in a manner which can be easily adopted for use in a clinical environment is also described.

Bulk loading bio-therapeutics within a preserved, mechanically robust, customised decellularized scaffold creates a possible platform for enhanced *in vivo* performance by increased cell repopulation, suitable mechanical properties and reduced manufacturing times. This scaffold offers the potential to produce "off-the-shelf" patient specific tissue engineered grafts and bridge their translation to clinical use.

Acknowledgements

I have to start by thanking my two supervisors Dr Bruce Murphy and Dr Garry Duffy for the opportunity to pursue this research. Thanks for the guidance and support which made all this possible. I couldn't have hoped for two supervisors more honest and approachable, it's been a pleasure to work for you guys.

Secondly, a huge thank you to Prof Fergal O'Brien and all the members (past and present) of the Tissue Engineering Research Group in the Royal College of Surgeons in Ireland. Specifically, for their general help in the lab and answers to many, many questions, thanks to: Amos, Caroline, Conn, Cai, Erica, Johnny, Orlaith, Ryan, Tara, Tanya and special mention to my fellow vascular tissue engineer, Alan. I'd also like to thank all the members of the Trinity Centre for Bioengineering for any help over the last few years, particularly Henrique, Orna and Peter O'Reilly for his technical assistance.

I've had the pleasure of working with and around some fantastic people over the course of this journey. Thanks to all the Team Bruce members (Liam, Gar, Clive, Alan, Gill, Stephen, Eoin, Niamh and Karen) for their support and encouragement and my old office buddies, Gerard and Karl. Tea breaks and banter make everything a lot easier. To all my friends outside of Trinity, thanks for keeping me grounded and I promise this is the end of my student days.

A special thanks to my family, Mum, Dad, Denise, Elaine, Maurice and last but not least Lily! I couldn't have done it without you. In particular, my parents for instilling the value of education in me from day one.

Finally, I would like to acknowledge Enterprise Ireland and Trinity College Dublin for funding this study and James Anderson in Lislin Meats for generous access to his abattoir.

Publications

Journal Publications

SHERIDAN, W. S., DUFFY, G. P. & MURPHY, B. P. 2012. Injection techniques for bulk cell seeding decellularized vascular scaffolds. *International Journal of Nano and Biomaterials,* 4, 96-107.

SHERIDAN, W. S., DUFFY, G. P. & MURPHY, B. P. 2012. Mechanical characterization of a customized decellularized scaffold for vascular tissue engineering. *Journal of the Mechanical Behavior of Biomedical Materials*, 8, 58-70.

SHERIDAN, W. S., DUFFY, G. P. & MURPHY, B. P. 2013. Optimum Parameters for Freeze-Drying Decellularized Arterial Scaffolds. *Tissue Engineering: Part C Methods*, 19, 1-10.

SHERIDAN, W. S., Grant, O.B., DUFFY, G. P. & MURPHY, B.P. The Application of a Thermoresponsive Chitosan/β-GP Gel to Enhance Cell Repopulation of Decellularized Vascular Scaffolds. *Journal of Biomedical Materials Research Part B: Applied Biomaterials. Mar 25, 2014. [Epub ahead of print]*

The work contained in this thesis has been presented at the following national and international conferences:

International Conferences

Sheridan, WS, Grant, O, Lopez-Noriega, A, Duffy, GP, Murphy BP.

"Towards A Clinically Applicable Tissue Engineered Vascular Graft"

Proceedings of the American Society of Mechanical Engineers 2013 Summer Bioengineering Conference, Sunriver, Oregon, USA

Sheridan, WS, Duffy, GP, Murphy, BP.

"Customised Decellularized Vascular Scaffolds"

World Conference on Regenerative Medicine 2011, Leipzig, Germany

National Conferences

Sheridan, WS, Duffy, GP, Murphy, BP.

"Optimal Parameters for Freeze-drying Decellularized Arterial Scaffolds"

The 19th Annual Conference of the Section of Bioengineering of the Royal Academy of Medicine in Ireland 2013, Meath, Ireland

Sheridan, WS, Duffy, GP, Murphy, BP.

"Optimum Mechanical Properties and Cell Repopulation Techniques of a Decellularized Vascular Scaffold"

The 18th Annual Conference of the Section of Bioengineering of the Royal Academy of Medicine in Ireland 2012, Belfast, Ireland

Sheridan, WS, Duffy, GP, Murphy, BP.

"Quantification of the Mechanical Properties of Customised Decellularized Porcine Carotid Artery for use as a Vascular Scaffold" The 17th Annual Conference of the Section of Bioengineering of the Royal Academy of Medicine in Ireland 2011, Galway, Ireland

Awards

Nominated to present research findings at the Sir Bernard Crossland Symposium and Postgraduate Research Workshop 2012, entitled "Tissue Engineering Vascular Grafts Using Decellularized Porcine Arteries"

Shortlisted for the final of the Dublin Region Higher Education Alliance (DRHEA) Graduate Education Competition, "Future Voices: How Ireland's PhDs will enable National Recovery", talk entitled "Creation of an *in vitro* Test-bed for Vascular Medical Devices"

List of figures

Nomenclature

°C- Degrees Celsius

™- Trade Mark

2D- Two Dimensional

3D- Three Dimensional

bFGF- basic Fibroblast Growth Factor

BMC- Bone Marrow Derived Stem Cell

BSA- Bovine Serum Albumin

CABG – Coronary Artery Bypass Graft

CO2- Carbon Dioxide

CSCs- Cardiac Stem Cells

DAPI- 4',6-Diamidino-2-Phenylindole

dH_2O- Distilled Water

DMEM- Dulbecco's Modified Eagle's Medium

DMSO- Dimethyl sulfoxide

DNA- Deoxyribonucleic Acid

DPBS- Dulbecco's Phosphate Buffered Saline

dsDNA- Double Stranded Deoxyribonucleic Acid

ECs- Endothelial Cells

ECM- Extracellular Matrix

EDTA- Ethylenediaminetetraacetic acid

ELISA- Enzyme-linked immunosorbent assay

EPCs- Endothelial Progenitor Cells

ePTFE - expanded Polytetrafluoroethylene

FBS- Foetal Bovine Serum

GP- glycerophosphate

H&E- Haematoxylin and Eosin

HDPE- High Density Polyethylene

HGF- Hepatocyte Growth Factor

HIM- Helium Ion Microscopy

HUVECs- Human Umbilical Vein Endothelial Cells

IGF- Insulin-like Growth Factor

LDL- Low Density Lipoprotein

MHC- Major Histocompatibility Complex

min- minutes

MSC- Mesenchymal Stem Cell

NaOH- Sodium Hydroxide

OCT- Optimal Cutting Temperature

PDGF-BB- Platelet Derived Growth Factor-BB

PET- Polyethylene terephthalate

PEUU- Poly(ether Urethane Urea)

PLGA- poly(lactic-co-glycolic acid)

PLLA- Polylactic Acid

PVC- Polyvinyl Chloride

SD- Standard Deviation

SEM- Scanning Electron Microscopy

SMCs- Smooth Muscle Cells

rSMCs- Rat Smooth Muscle Cells

hSMCs- Human Smooth Muscle Cells

TEVG- Tissue Engineered Vascular Graft

T_f- Final Freezing Temperature

TGF-β- Transforming Growth Factor Beta

UTS- Ultimate Tensile Strength

VEGF- Vascular Endothelial Growth Factor

w/v- Weight/Volume

X- Magnification

M- Molar

mL- Millilitre ($x10^{-3}$)

µL- Microlitre ($x10^{-6}$)

N- Newtons

mm- Millimetre ($x10^{-3}$)

mmHg – Millimeters of Mercury

µm- Micrometre ($x10^{-6}$)

g- Grams

µg- Micrograms ($x10^{-6}$)

mTorr- Millitorr ($x10^{-3}$)

Contents

Chapter 1 Introduction

1.1 Background

The prevalence of vascular disease continues to increase worldwide (Roger et al., 2012). Obesity, smoking, unhealthy and unbalanced diets, lack of exercise, stress and diabetes are leading risk factors of vascular disease (Yusuf et al., 2004). All of these risk factors are widespread and increasing in every developed and developing society in the world (Gersh et al., 2010). Recent advances in catheter based treatment modalities such as balloon angioplasty and stenting have substantially increased the quality and range of treatments for vascular disease (Brar and Stone, 2009, Goodney et al., 2009). However, percutaneous interventions can be exhausted leaving diseased vessel replacement the gold standard treatment.

Coronary artery bypass grafts, lower limb bypass surgery and haemodialysis access grafts all require substitute vessel replacement. In 2007 in the US alone, over 416,000 bypass procedures were undertaken (Roger et al., 2012). Bypass grafting procedures largely utilise the saphenous vein or mammary artery for autologous grafting (Buxton et al., 2009). However, underlying vascular disease or previous vessel harvest often render these vessels unavailable (Salacinski et al., 2001, Gray et al., 2008). Success has been achieved in large diameter applications with the use of synthetic grafts, largely Dacron and ePTFE in cases where no autologous vessels are available. However, low patency and high failure rates have been associated with synthetic grafts for smaller diameter applications (<6mm diameter) (Walter and Magometschnigg, 2007). Subsequently in a large patient cohort this necessitates the need for a suitable alternative to autologous vessel grafting for small diameter applications.

Substantial progress has been made in the field of tissue engineering to address this clinical need (Niklason et al., 1999, L'Heureux et al., 2006, Zhao et al., 2010) but

there still remains some limitations to its progress: obtaining suitable architecture, appropriate mechanical properties, viable cell sources, inefficient cell seeding techniques and lengthy manufacturing times are still major challenges (Tranquillo, 2002, Yazdani et al., 2009, Villalona et al., 2010).

1.2 Arterial Wall Properties

The arterial wall's unique mechanical properties are obtained by the interaction between the two major extracellular matrix (ECM) proteins: collagen and elastin (Roach and Burton, 1957, Holzapfel et al., 2000). The medial lamellar unit is the basic structural component of the arterial wall, varying in number depending on location within the vascular tree. It consists of elastin fibers organised into fenestrated concentric sheets which contain circumferentially aligned SMCs embedded in small collagen fibers surrounded by a network of collagen fiber bundles (O'Connell et al., 2008). The elastin network provides elasticity to the vessel wall and is responsible for compliance, dictating the response of the vessel to hemodynamic stresses at low strains. Collagen acts as the primary load bearing element of the vessel wall. The collagen fibers are gradually recruited as the load is transferred from the elastin to the collagen, until the collagen bears the full load at high stress. Mimicking this complex interaction by attaining ECM components in sufficient quantities and levels of maturity within a construct is a crucial requirement of tissue engineering.

1.3 Tissue Engineered Vascular Grafts (TEVGs)

TEVG development has evolved substantially from the pioneering work of Weinberg and Bell, who combined a collagen gel with smooth muscle cells (SMCs) surrounded by fibroblasts, internally lined with endothelial cells (ECs) (Weinberg and Bell, 1986). This

was the first reported multilayered tissue engineered construct. However, the disorganised collagen resulted in weak mechanical properties unsuitable for use *in vivo*. Resorbable polymers, such as polyglycolic acid have been used as vascular scaffolds (Niklason et al., 1999). Non-thrombogenic durable constructs have been created *in vitro* by seeding SMCs onto these polymers and coating the inner lumen with ECs. Maturation of these seeded scaffolds *in vitro* by subjecting them to pulsatile flow conditions produced constructs with properties similar to that of native tissue that were suitable for *in vivo* use. However, this process is extremely time consuming (minimum 6 weeks), and balancing the rate of resorbtion of the polymer with tissue remodelling, to produce an ECM sufficiently robust for implantation, is a substantial challenge.

Another technique that has been developed involves culturing monolayers of vascular cells into sheets and rolling them around a mandrel to create a tubular construct (L'Heureux et al., 1998). This construct is then matured in a bioreactor under pulsatile flow to organise the sheets into layers and increase the mechanical integrity of the scaffold. These constructs have burst strengths higher than native tissue and have shown excellent remodelling and mechanical stability after 8 months *in vivo*. However, their fabrication is extremely time consuming involving up to 3 months of cell culture and construct maturation.

1.4 Decellularized Tissue

Decellularized tissue has been used extensively as a scaffold for TEVG development and may offer the ability to overcome some of the challenges facing current fabrication techniques (Schaner et al., 2004, Amiel et al., 2006, Zhu et al., 2008). These porous three-dimensional structures present the preformed complex architecture of the native vessel and are ideal for cell attachment and growth, while maintaining the mechanical

integrity of the native tissue (Gilbert et al., 2006). The disruption caused by removing the cellular material from the tissue can be minimized in order to create a stable and robust scaffold. A major drawback, however, is that the matrix that remains after decellularization is extremely dense and can prove difficult to infiltrate with cells. This is particularly the case with SMCs in the medial layer of the construct (Lu et al., 2004, Neff et al., 2011). A poorly infiltrated scaffold resulting in a lack of a fully quiescent contractile SMC medial layer has resulted in less than ideal mechanical properties and diminished *in vivo* performance (Yazdani et al., 2009). The highly dense nature of decellularized vascular tissue has also lead to excessive cell seeding and culture times to mature these constructs *in vitro*. These excessive maturation times are unfeasible if TEVGs are to have meaningful clinical success.

1.5 Study Aims

This research utilises decellularized exogenous tissue as a scaffold for the creation of a TEVG for small diameter vascular graft applications. The aim of this research is to manipulate decellularized scaffolds to advance them toward clinical applicability, in an attempt to overcome current deficiencies in TEVG development, while maintaining appropriate mechanical properties.

Chapter 2 Literature Review

2.1 Introduction

This chapter reviews previous work in the field of vascular tissue engineering. An understanding of the intricate structure-function relationship of the arterial wall is essential when contemplating tissue engineering a vascular graft. Therefore, Part 1 deals with an overview of the cardiovascular system, with particular emphasis on arteries, their composition, function and mechanical properties. The issue of vascular disease and the need for vascular grafts are discussed, focusing on the biological and mechanical requirements of a vascular graft. Following this in Part 2, a review of current tissue engineering techniques is described with particular emphasis on decellularized tissue. Different cell sources, seeding techniques and methods for maturing vascular constructs *in vitro* are detailed. Finally, a synopsis of the clinical success of TEVGs to date is outlined along with the future requirements to enable successful translation of vascular tissue engineering to a clinical setting.

2.2 Part 1 – The Cardiovascular System

2.2.1 Blood Vessels

The cardiovascular system comprises the heart and blood vessel network of arteries, veins and capillaries. The heart operates as a pump to force blood through this conduit network in order to supply the tissues and organs with nutrition and oxygen. The cardiovascular system also regulates pH levels, body temperature and cell salt and water content within the body. Furthermore, protection is provided by carrying white blood cells for defence against disease, infection and clotting factors to prevent blood loss after injury. Arteries are thick walled elastic vessels that carry high pressure oxygenated blood away from the heart to the capillary network where nutrient and waste exchange occurs within the tissues of every organ and returns to the heart via the low pressure venous circulation

(Fuster et al., 2011). This constant supply of blood is essential to the function of every tissue and organ in the body and must be maintained undisturbed at all times.

2.2.2 Arterial Wall Composition

The arterial wall is a composite structure consisting of three layers: tunica intima (inner layer), tunica media (central layer) and tunica adventitia (outer layer). A representation of these layers can be seen in Figure 2.1. The intima is the innermost layer on the lumen side of the vessel and comprises a monolayer of ECs. This monolayer is in direct contact with the blood flow and provides an anti-thrombotic and anti-coagulant barrier between the blood and vessel wall and helps maintain continuous laminar blood flow.

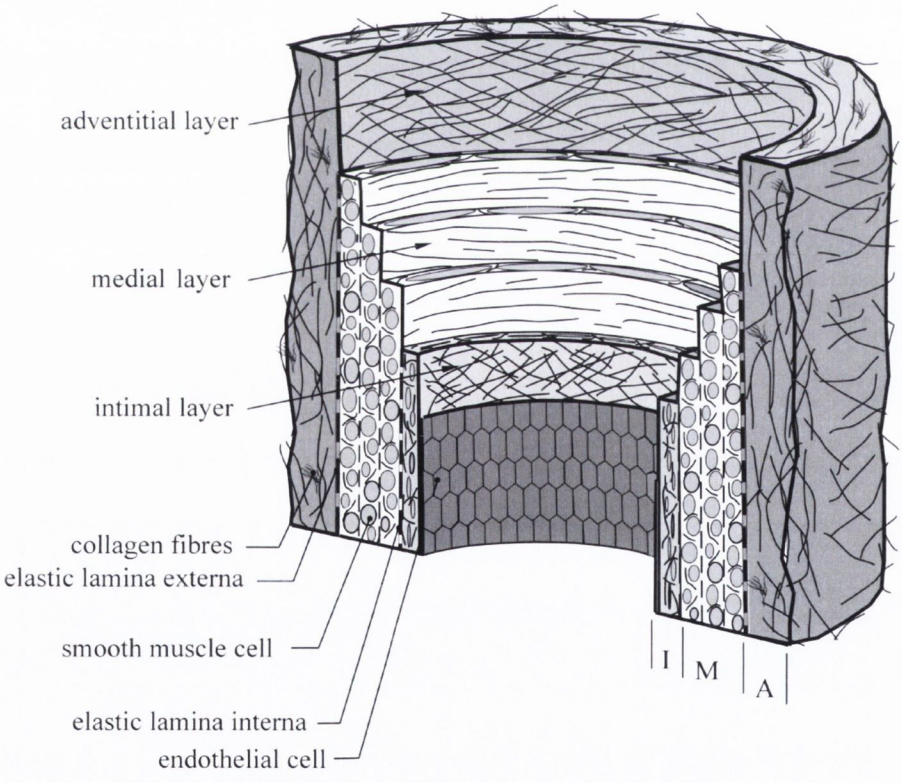

Figure 2.1 Arterial Wall Structure

The composite nature of the arterial wall is illustrated. The EC monolayer is visible on the lumen side of the vessel. The lamellar structure of the media is evident as shown by the layers of collagen and elastin fibers embedded in SMCs. (Holzapfel et al., 2000)

The endothelium is a complex mechanical signal transduction interface between flowing blood and the vessel wall. ECs release molecules that modulate coagulation, platelet aggregation, leukocyte adhesion and vascular tone. ECs allow the transport of substances across this barrier but prevent blood components contacting the highly thrombogenic sub-endothelial ECM. A basal lamina of type IV collagen, fibronectin and proteoglycans lie beneath the endothelial cells, acting as an adherent meshwork on which they can grow (Humphrey, 2002).

The intima and media are separated by an elastic membrane lining called the internal elastic lamina. This is a fenestrated sheet composed of elastin fibers and marks the beginning of the elastin network within the media. The elastin network is a series of concentric fenestrated sheets of elastin fibers that contain radial fiber struts interlinking these sheets. Elastin is a highly stable, inert insoluble fibrous polymer formed by the crosslinking of its soluble precursor, tropoelastin which is synthesised by SMCs (Rodgers and Weiss, 2005). It is highly crosslinked which contributes to its mechanical properties, insolubility and longevity (Wagenseil and Mecham, 2009). Elastin is primarily formed in fetal and post natal development (Davis, 1993, Bendeck et al., 1994). Potentially this may be regarded as a reason for minimal elastin formation in TEVGs. The gap between any two elastin sheets is known as a lamellar unit and constitutes the basic structural unit of the media (Wolinsky and Glagov, 1967). Figure 2.2 shows an illustration of the orientation of number of medial lamellar units. The number of medial lamellar units varies depending on the location of the artery within the vascular tree (an average 40 units in the human abdominal aortic media). A medial lamellar unit consists of SMCs circumferentially aligned between two elastin sheets. The SMCs are surrounded by a collagen membrane and other ECM components such as proteoglycans. The function of SMCs is to control the vasoactivity of the vessel wall in response to systemic or localised

biochemical and external biomechanical cues. The vasoactivity controls the dilation and contraction of the blood vessel wall to regulate blood pressure and flow. SMCs are also responsible for ECM synthesis.

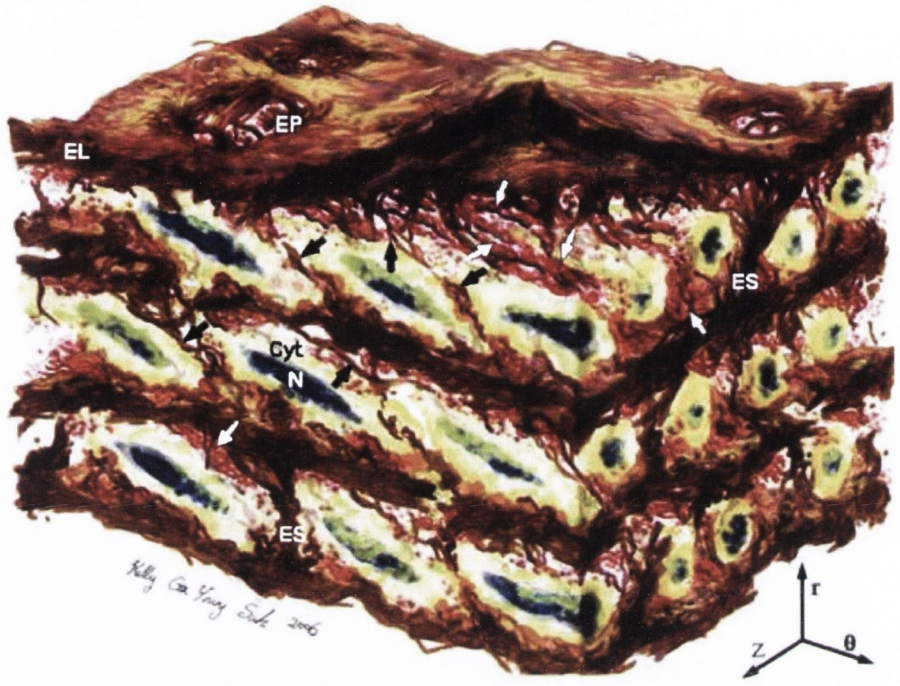

Figure 2.2 Schematic Representation of Three Lamellar Units

The composite interconnected nature of the SMCs and ECM components is illustrated. The elastin network is presented as layers of elastin fibers (EL), elastin pores (EP) and elastin struts (ES) which connect each layer and intralamellar elastin fibers (black arrows). Circumferentially aligned SMCs are present with nuclei (N) surrounded by cytoplasm (Cyt). Small and large collagen fibers are represented by white arrows. (r indicates radial direction, Z axial and θ circumferential). (O'Connell et al., 2008)

The collagen network within the medial layer is predominantly fibril forming collagen types I and III. Collagen is formed when SMCs secrete tropocollagen into the surrounding ECM which self assemble with 4 other tropocollagen which are crosslinked with glycosaminoglycans. These crosslinked tropocollagen aggregate to form micro-fibrils which then form sub-fibrils, and subsequently collagen fibrils, which are 50-500 nm in diameter (Freed and Doehring, 2005, Wagenseil and Mecham, 2009). Collagen fibrils

assemble into collagen fibers in wavy or crimped organisation around SMCs and between elastin sheets. Collagen fibers arrange into intralamellar bundles of fibers and are independent of the elastin and SMCs, receiving loads based on the overall medial lamellar unit state (O'Connell et al., 2008). These bundles of collagen fibers are crimped in their relaxed configuration at normal physiological pressure and straighten during tensile loading at higher pressures.

The adventitia is the outer most layer of the arterial wall and is mainly composed of thick dispersed collagen bundles, fibroblasts and small nerve fibers. The adventitia also contains the vaso vasorum, a network of capillaries supplying blood to the outer layer of large arteries. The adventitia's function is to encompass the rest of the vessel and anchor it to the surrounding structures and synthesise ECM components, it also acts as a source of stem cells and macrophages which play a key role in the pathophysiology of the arterial wall (Havelka and Kibbe, 2011).

2.2.3 Smooth Muscle Cells

SMCs are spindle or elliptically shaped and typically 100 μm long and 5 μm in diameter and orientate circumferentially within the vessel wall (Stegemann and Nerem, 2003). The function of SMCs is to control the vasoactivity of the vessel wall in response to external environmental cues. They are responsible for the dilation and contraction of the vessel wall in order to regulate blood pressure and flow. These environmental cues can be mechanical, such as the cyclic tensile stresses from the pulsatile pressure produced by the heart, or biochemical, such as ions, proteins and growth factors (Chan-Park et al., 2009). SMCs also synthesise proteins for the formation and maintenance of the ECM.

Mature healthy arteries subjected to normal blood flow conditions contain SMCs in the contractile phenotype. Contractile SMCs are spindle shaped and align

circumferentially, display little or no profileration, synthesise small amounts of ECM proteins and have high contractility (Stegemann et al., 2005, Rensen et al., 2007). It is in this quiescent state that SMCs are in full control of the vasoactive response of the vessel wall. In developmental and pathological conditions SMCs can differentiate to a synthetic phenotype. This differentiation sees a morphological change from a spindle shape to a more compacted, less elongated shape. A schematic of this differentiation is shown in Figure 2.3.

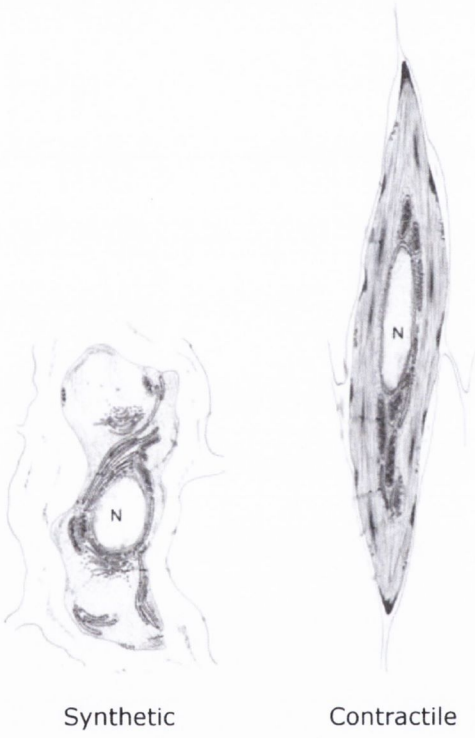

Figure 2.3 SMC Phenotype

The synthetic phenotype resembles a fibroblast-like morphology which is present in diseased vessels and in cells cultured in vitro, this phenotype proliferates rapidly producing large amounts of ECM. The contractile phenotype is a more spindle shape morphology and is present in native vessels with large contractile functionality. (N is nucleus). (Rensen et al., 2007)

This synthetic phenotype is associated with increased proliferation and migration and increased production of ECM components. The increased mobility of the synthetic SMCs

is combined with a huge reduction in contractile function. The ability of SMCs to modulate their phenotype is essential during the development of arteries, in such instances large cell numbers and ECM synthesis are required. Synthetic SMCs can proliferate quickly producing these numbers and laying down the foundations of the ECM. Differentiation to the contractile phenotype subsequently allows for the preservation of a stable arterial wall.

Phenotype modulation also plays a huge role in the pathophysiology of the arterial wall. Certain pathological conditions can induce a reverse phenotype transition from the normal contractile state to the proliferative synthetic cell which has grave consequences on vascular mechanics. This is particularly the case with restenosis following injury to the vessel wall after balloon angioplasty or stenting (Worth et al., 2001).

The phenotype modulation of SMCs is important in the isolation of vascular SMCs from native blood vessels for *in vitro* culture. SMCs switch to the synthetic phenotype when removed from their *in vivo* environment (Rzucidlo et al., 2007). The loss of contractile function combined with the increase in proliferation rate allows the cells to expand rapidly which is advantageous in preparing cells for use in research, but may also have associated disadvantages for vascular tissue engineering research.

2.2.4 Hemodynamic Forces on the Arterial Wall

The hemodynamic forces the arterial wall experiences *in vivo* are essential for blood vessel development in embryogenesis and in regulating healthy arteries. There are four main stresses acting on the arterial wall; radial stress, axial stress, circumferential stress and wall shear stress (see Figure 2.4). The radial stress is generated from the pressure of the pulsatile blood flow from the heart which is 120 mm Hg in systole and 80 mm Hg in diastole under normal healthy physiological conditions, and can increase substantially in a

hypertensive patient. The high pressure experienced by the arterial side of the circulation drives fluid flow and is distributed along the arterial tree, dropping to 35 mm Hg as blood enters the capillary system (Fuster et al., 2011). This pressure can directly influence ECs but more importantly it is responsible for creating the circumferential stress within the arterial wall. Subsequently, a circumferential strain is transmitted across the arterial wall to the SMCs within the medial layer which receive and regulate this biomechanical signal. A longitudinal strain of up to 70% is also maintained in the arterial wall, the specific value of this strain varies depending on the exact location within the arterial network (Wagenseil and Mecham, 2009).

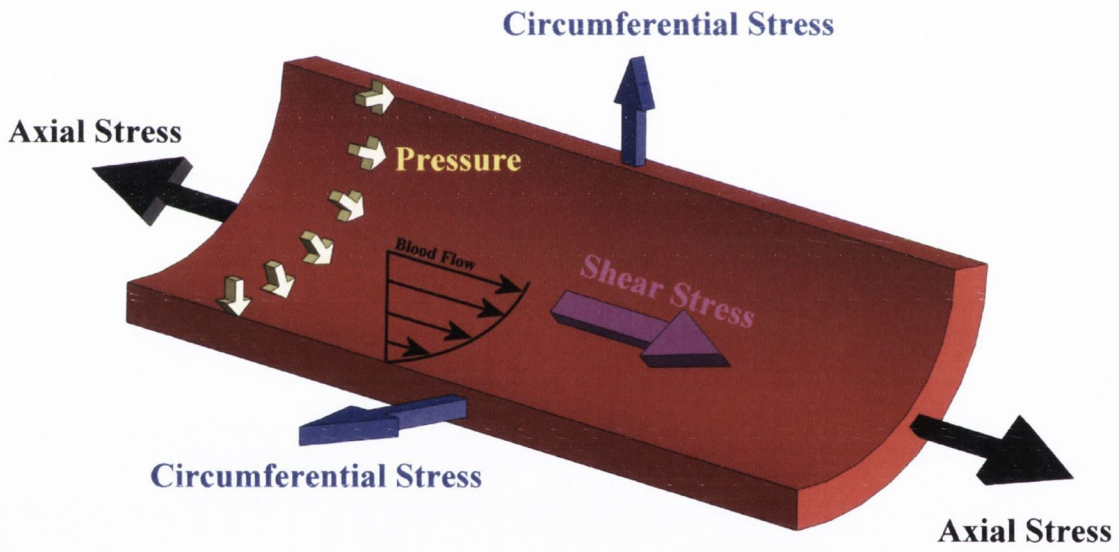

Figure 2.4 Hemodynamic Forces acting on the Arterial Wall

The principle hemodynamic forces acting on the arterial wall. Pressure due to the cardiac cycle is evenly distributed circumferentially and is shown with yellow arrows. The pressure causes a circumferential stress as indicated with blue arrows. The EC monolayer experience a wall shear stress as a result of the pulsatile blood flow (purple arrow). Arteries also experience an axial stress in the longitudinal direction.

Shear stress is also highly important in the mechanotransduction of biomechanical stimuli to the vascular cells, particularly ECs. Wall shear stress is the tangential drag force on the ECs caused by pulsatile blood flow and is responsible for EC function by regulating arterial diameter and gene expression (Laughlin et al., 2008). The EC monolayer is highly susceptible to fluctuations in this shear stress, creating signalling pathways which influence SMC proliferation and phenotype, which can lead to diseased states within the vasculature (Reneman et al., 2006, Johnson et al., 2011).

The individual ECM components and SMCs are normally in a pre-stressed state, such that there is no zero stress state of a blood vessel when removed from hemodynamic forces. Fung et al were the first to study this existence of residual stress in the arterial wall (Fung, 1991). The transmural residual stress exists to make the stress distribution more uniform under normal conditions and can change in response to injury or disease (Cardamone et al., 2009). Deviations from these normal conditions can affect the uniform stress distribution; however it is maintained throughout life by growth and remodelling.

2.2.5 Mechanical Properties of the Arterial Wall

The relationship between structure and function of the arterial wall is dictated by the unique interaction between the two major ECM proteins, collagen and elastin. Their composition and orientation are responsible for the non-linear mechanical response of the arterial wall (Roach and Burton, 1957, Holzapfel et al., 2000). Stress-strain curves generated from tensile tested arteries display a typical hyperelastic response of a biological soft tissue (Fung, 1993, Humphrey, 2002). The composite nature of the arterial wall produces a bi-phasic response due to the interaction between the collagen and elastin. A typical stress-strain response is shown in Figure 2.5 A. The highly elastic nature of the elastin sheets absorbs the initial load as it is applied to the arterial wall at the

same time the collagen fibers unravel. This corresponds to the initial toe region of the graph which relates to high strain levels for low stresses. As the load continues to increase and distend the elastin recruitment of the collagen fibers commences, corresponding to the transition region of the curve. Collagen is the primary load bearing constituent of the arterial wall, and as the load increases greater numbers of fibers align in the direction of the applied strain and uncrimp to receive the load as the tissue stiffens. This is evident in the upturning region of the stress-strain curve. A final linear response is seen when all the collagen has been recruited and the entire load is carried by the fully tensed straightened collagen fibers.

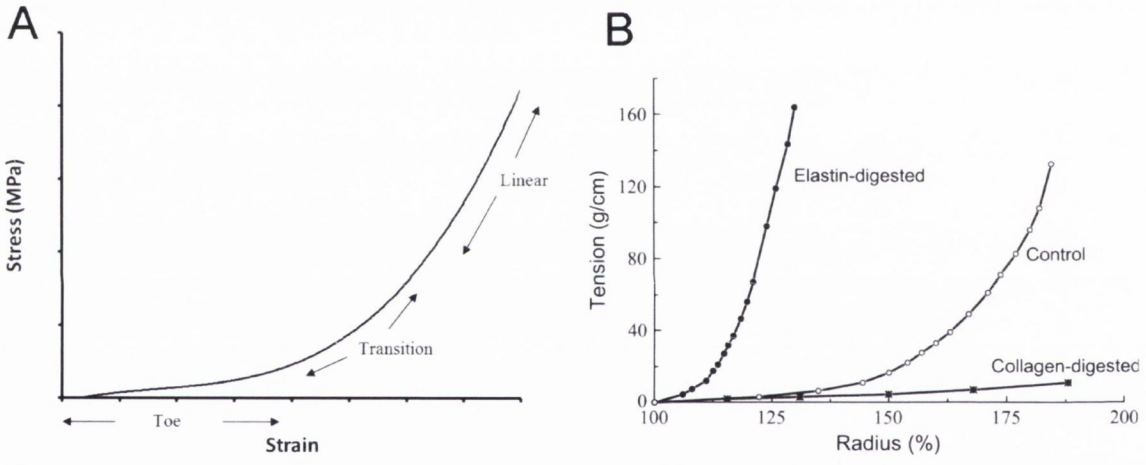

Figure 2.5 Tensile Response of Arterial Tissue

(A) Typical bi-phasic response of tensile tested arterial wall. The elastin is responsible for the low stress high strain toe region and collagen for the final linear response. (B) Individual ECM component digestion reveals the contribution of each component to the mechanical response. The elastin-digested sample displays low strain for high stresses due to the absence of an elastic component. In the collagen-digested sample strain is low due to the lack of stiff collagen fibers to bear the applied load. (Holzapfel, 2008)

The specific roles of the collagen and elastin can be more closely identified when they are individually digested from the artery and their mechanical response observed (Holzapfel, 2008), as shown in Figure 2.5 B. The elastin-digested sample comprising collagen only

shows high stress corresponding to low strains, essentially removing the toe region of the control sample that was attributed to the elastin. The slope of the final linear region of this sample is approximately the same as that of the control, further verifying that stiffness of the tissue in this region is directly attributed to the collagen fibers. Conversely, the collagen-digested sample consisting of elastin only has a similar stiffness to the toe region of the control sample representing the elasticity of the elastin. In this sample large strains are seen for small increases in stress. The absence of any collagen fibers to recruit and bear the tensile load results in an extremely low ultimate tensile strength compared to the control sample. This evidence further presents collagen as the predominant contributor to the tensile strength of arteries.

2.3 Vascular Disease

Vascular disease is associated with the heart and blood vessels and is responsible for more deaths worldwide than any other illness (Roger et al., 2012). This disease usually affects the heart (coronary artery disease), the brain (cerebrovascular disease or stroke) and the legs (peripheral vascular disease). Obesity, smoking, unhealthy and unbalanced diets, lack of exercise, stress, diabetes and genetic predisposition are all leading risk factors of vascular disease (Yusuf et al., 2004). Enhanced treatment modalities have reduced the mortality rates from vascular disease in the past 30 years, particularly in developed countries (O'Flaherty et al., 2013). However, the risk factors fuelling this disease continue to increase, specifically in developing countries, therefore the morbidity of the disease continues to rise (Gersh et al., 2010). The cost associated with treating vascular diseases was estimated to be $286 billion in 2007 in the US alone (Roger et al., 2011). The underlying process responsible for occlusive vascular disease is atherosclerosis and is described below.

2.3.1 Atherosclerosis

Atherosclerosis is a chronic inflammatory disease that mainly affects the medium and large arteries (Ross, 1999, Libby, 2002). It is an occlusive disorder which involves the build up of deposits within the arterial wall, forming plaques which narrow the vessel lumen, subsequently restricting blood. The main causes of death and debilitation associated with vascular disease; unstable angina, myocardial infarction and stroke can be directly attributed to atherosclerosis (Hansson, 2009). The mechanism of the development of one type of atherosclerotic lesion is illustrated in Figure 2.6.

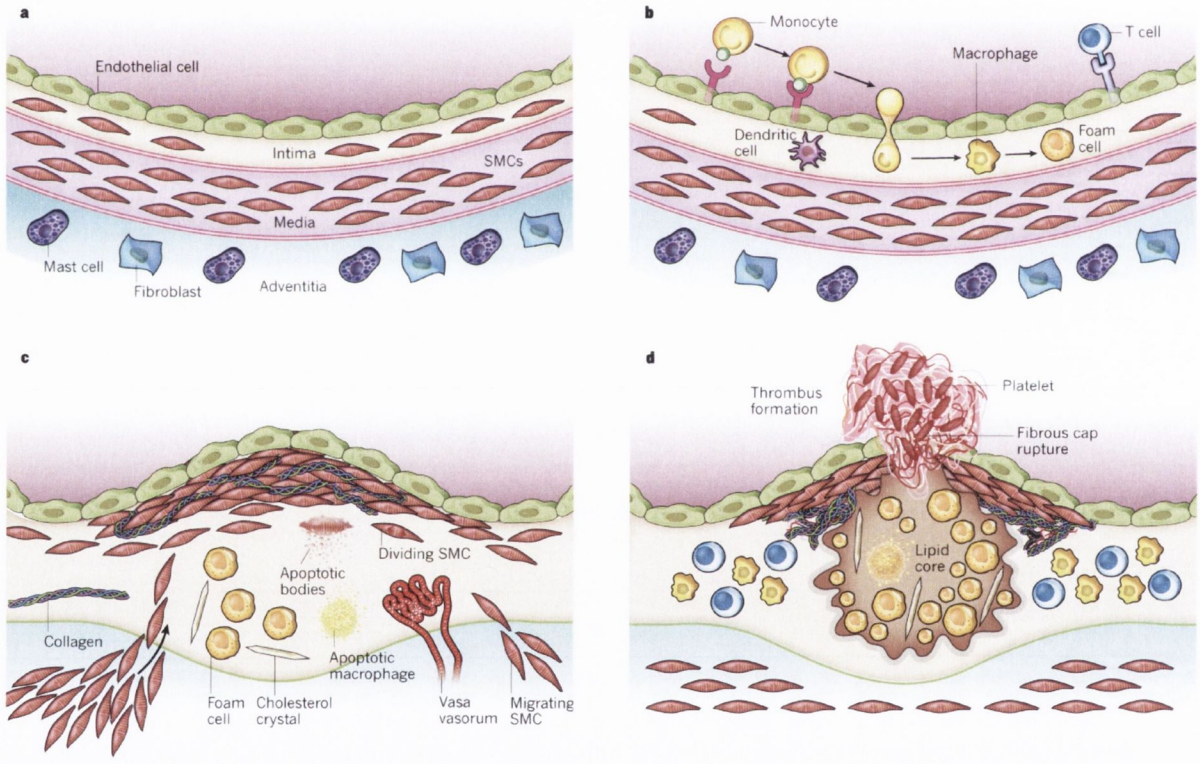

Figure 2.6 The Progression of Atherosclerosis

Early atherosclerosis develops from a healthy vessel wall gradually forming a plaque which can eventually lead to rupture of the thin fibrous cap. (Libby et al., 2011)

Figure 2.6 describes the basic mechanism of plaque formation, however, atherosclerosis is a complex slow forming disease that can result in the formation of a range of plaques.

These plaques can have varying characteristics which may not always cause bulging or blockage within the vessel lumen (Figure 2.7). These plaques are known as vulnerable plaques and range from rupture prone plaques to critically stenotic plaques and all contribute to acute cardiac events and sudden cardiac death (Naghavi et al., 2003).

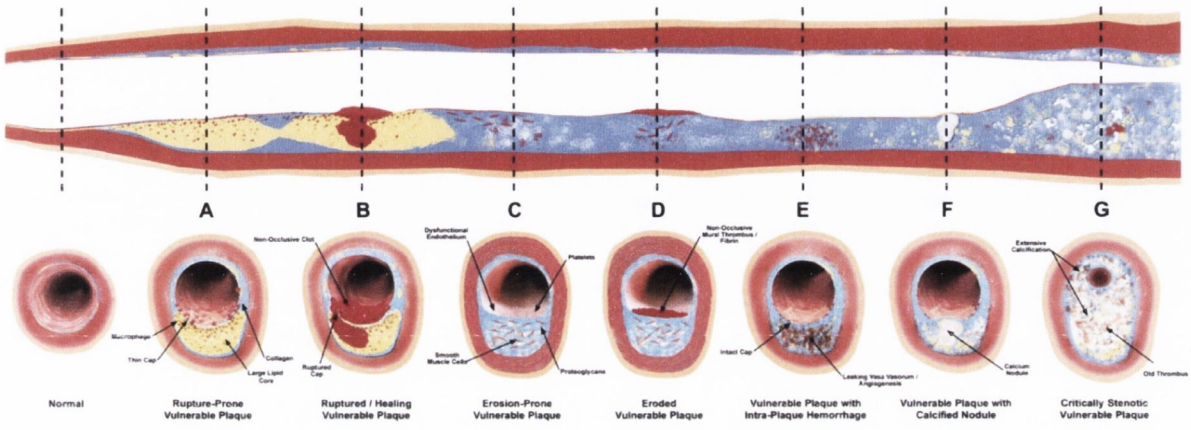

Figure 2.7 Different Types of Vulnerable Plaques

Atherosclerotic plaques do not always cause bulging and blockages of the vessel lumen and can vary greatly in their organisation while still carrying the risk of an acute cardiac event or sudden cardiac death. (Naghavi et al, 2003)

2.3.2 Catheter Based Treatment Modalities

Substantial progress has been made in the treatment of atherosclerotic plaques in the last two decades. The advent of percutaneous interventions particularly transluminal balloon angioplasty and stenting offered a radical non-invasive method of opening vessel occlusions and restoring blood flow (Grüntzig, 1978, Maillard et al., 2000). The introduction of drug eluting stents has further reduced restenosis rates (Morice et al., 2002). Complex lesions, multi-vessel disease and other underlying diseases limit the extent to which catheter based treatment modalities can be utilised. Heavily occluded arteries, bifurcation disease or diffuse disease can limit the success of percutaneous

interventions. When all these interventions have been exhausted bypass grafting may be utilised to restore blood to the infracted heart.

2.4 Bypass Grafting

Coronary artery bypass grafting involves the surgical insertion of a replacement conduit to bypasses an occluded vessel. The surgery necessitates a general anaesthesia, open heart surgery, and may utilise a heart lung machine. Consequently the procedure is complex, expensive and carries many risks. Bypass grafting is indicated for patients with left main coronary artery disease, triple vessel disease with depressed left ventricular function and diabetic patients with double or triple vessel disease (Schwartz and Galloway, 2004). The first coronary artery bypass graft (CABG) surgery was performed in the Cleveland Clinic by Dr Rene Favoloro in 1967 and since then has become one of the most common surgical procedures carried out worldwide. CABG constitutes the majority of bypass procedures, in 2009 in the US alone, 416,000 coronary bypass procedures were undertaken (Roger et al., 2012), however grafting of peripheral vessels is also common (Goodney et al., 2009).

2.4.1 Autologous Conduit Selection

There are a number of options for conduits for substitute vessel replacement within the vasculature. The utilisation of individual vessels for bypass grafts is largely patient specific. The optimum vessel of choice is the internal thoracic artery, which is associated with superior long term patency than any other substitute vessels. This is largely due to the excellent integrity of the intima of the substitute vessel and the requirement of a single anastomosis for connecting the vessel proximal to the occlusion (Cameron et al., 1996). However, most patients usually require more than one bypass graft per surgery to

complete revascularisation; therefore further substitute vessel harvesting is required. Other vessel substitutes include the saphenous vein, radial artery and the gastroepiploic artery, the saphenous vein being the most commonly used of these. An illustration of a heart with a treble bypass consisting of one internal thoracic artery and two saphenous vein grafts is shown in Figure 2.8.

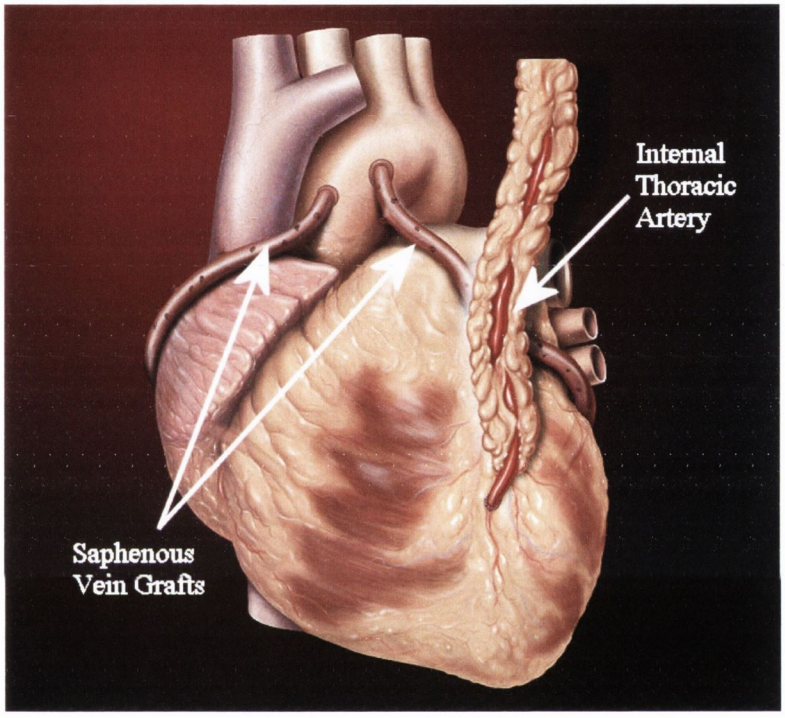

Figure 2.8 Schematic of a Heart Displaying CABG

There are three bypass grafts present, one internally mammary and two venous grafts bypassing the obstructed coronary arteries. (http://commons.wikimedia.org)

Saphenous vein grafts are associated with much lower long term patency rates, 60% at 10 years compared to internal thoracic arterial grafts, 85% at 15 years (Buxton et al., 2009) and early graft occlusion is common. Intimal hyperplasia and graft thrombosis are the main causes of graft failure. This is largely due to the compliance mismatch when using a vein as a replacement for an artery, additionally there is a large possibility of intima disruption and endothelium damage after vessel harvest (Manchio et al., 2005). The saphenous vein still remains the most commonly used autologous substitute vessel.

Previous vessel harvesting, co-existing vascular disease, venous thrombosis or varicose veins can limit the availability of the saphenous vein for harvesting as a bypass graft. In fact, autologous substitute vessels have been reported to only be available in up to 30% of patients (Veith et al., 1979, Salacinski et al., 2001, Desai et al., 2011).

2.4.2 Synthetic Grafts

Synthetic materials have been used as conduits for vascular applications. Success has been achieved in large diameter applications with the use of synthetic grafts, largely Dacron® and expanded polytetrafluoroethylene (ePTFE). Conduits constructed from these materials are used as substitute vessels in mainly high flow conditions such as the aorta and femoral arteries (Kannan et al., 2005). These materials perform well in such applications as they require high stiffness and strength to contend with the high pressure they experience from blood flow in such close proximity to the heart (Molina et al., 1995). Neo-intima formation is seen on these synthetic grafts, however, their cellular function is limited due to a lack of a viable medial layer (Walles et al., 2004).

In comparison, low patency and high failure rates have been associated with synthetic grafts for smaller diameter applications, namely <6mm diameter (Walter and Magometschnigg, 2007). Radial compliance as opposed to strength becomes the main issue with these small diameter synthetic grafts as they experience lower flow rates and are therefore predisposed to compliance mismatch problems (Salacinski et al., 2001). Thrombus formation within the conduit is common and there are major issues with intimal hyperplasia at the site of the anastomosis. In peripheral applications small diameter synthetic grafts are routinely used, usually composed of ePTFE. They have been shown to be suboptimal to autologous vein grafts and are only indicated for use if there is no suitable vein graft available (Klinkert et al., 2003).

2.4.3 Arteriovenous Grafts

Bypass grafts are also utilised in another application unrelated to vascular disease. Patients suffering from end stage renal disease (ESRD) undergo haemodialysis when their kidney function drops below 10% (Himmelfarb and Ikizler, 2010). Recently, a push toward creating natural arteriovenous fistulae rather than synthetic grafts for vascular access has been implemented. Natural fistula are optimum in most patients due to their longer life span and increased patency rates requiring less intervention (Wish, 2010) but are associated with high failure rates due to continuous needle puncture and the non physiological hemodynamics to which they are exposed. Furthermore, these are not available to all patients, with supply easily exhausted, and they can take excessive time for maturation and subsequent use (White et al., 2005). Synthetic grafts (largely ePTFE) have been widely used for this application but are associated with poor patency rates due to thrombosis and only have a 50% success rate after 3 years (Schwab, 2007). Autologous vessel grafting is another alternative for creating an arteriovenous graft. However, creating sufficient vascular access using autologous vessels increases the strain on an already limited supply of possible substitute vessels.

2.5 Part 2 - Tissue Engineered Vascular Grafts: A New Grafting Solution?

Tissue engineering is the combination of cells with a scaffold structure in order to create a tissue/organ substitute *in vitro*. The general approach to tissue engineering is described in Figure 2.9. Tissue engineering has gone some way to addressing many clinical needs (Ott et al., 2008, Harley et al., 2010, Haugh et al., 2010). In particular, the need for an alternative to autologous vessels for bypass grafting. Substantial progress has been made in this field to create a fully engineered arterial construct *in vitro* which can be implanted

for use as a vascular bypass graft (Niklason et al., 1999, L'Heureux et al., 2006, Zhao et al., 2010). Many different approaches have been applied to tissue engineering vascular grafts with many choices of cells and scaffolds available each with their individual challenges. These include developing a TEVG with appropriate ECM architecture and suitable mechanical properties which can remodel *in vivo*. However, to date, no research group/company has been able to achieve this goal and produce a regulatory approved TEVG for clinical use.

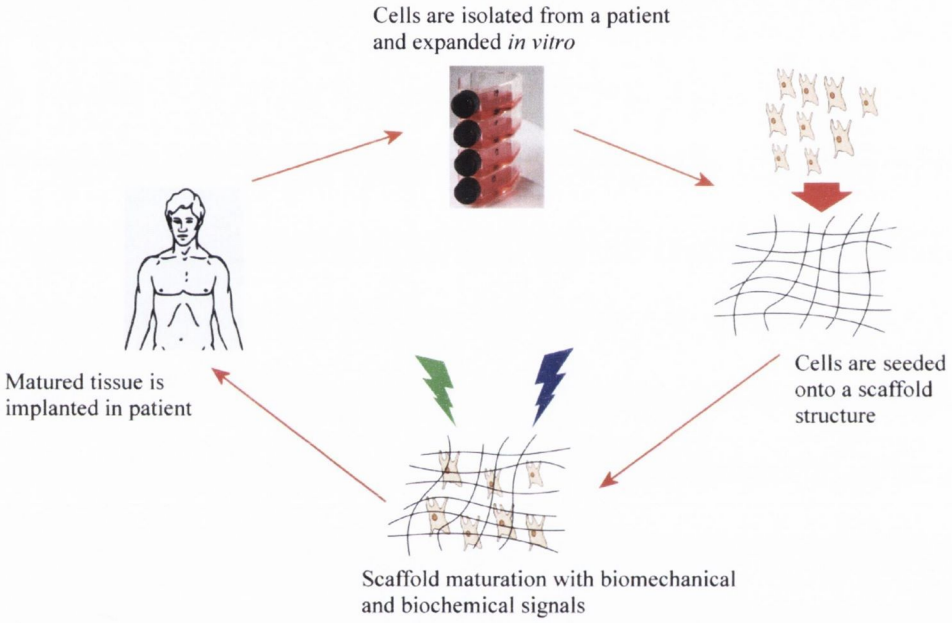

Figure 2.9 Tissue Engineering

The process of tissue engineering as applied to various tissue types such as bone, cartilage, arteries, lung and liver. The principal remains the same even though cell sources and type, scaffolds and signals may vary.

2.5.1 Requirements of a TEVG

There are a number of fundamental requirements which must be addressed when attempting to create a TEVG. The primary aim of a graft is to replace the function of a normal blood vessel; therefore at a minimum a TEVG must have sufficient suture

retention strength for implantation. Once surgically implanted the requirements of a TEVG are:

1. The ability to withstand physiological pressure which is at least in the 80-120 mm Hg range. Native arteries have a burst pressure of 5,000 mm Hg and saphenous vein has a burst pressure of 1,200 mm Hg which should be the minimum standard of any TEVG (Chan-Park et al., 2009).
2. Should be non-thrombogenic. The ability to create an EC monolayer on the lumen side of the TEVG is essential to prevent any thrombosis.
3. Compliance, the change in diameter of a cylindrical construct with respect to the internal pressure is also a key mechanical property for TEVGs. Compliance mismatch is a major cause of autologous graft failure and it is essential that any TEVG matches the compliance of native blood vessels (Abbott et al., 1987, Salacinski et al., 2001). This is particularly an issue around the anastomosis where a mismatch in compliance is most noticeable causing local flow disturbance resulting in the artery remodelling and possible intimal hyperplasia.
4. TEVGs must be flexible, elastic and kink resistant.
5. The ability to remodel *in vivo* will assist in matching the compliance of the host vessel. Full interaction within the implanted environment including the host cells is necessary to produce a fully stable bypass graft.

All these factors are desirable features and must combine for a TEVG to have appropriate vasoactive physiological properties, thus allowing the TEVG to function as a native vessel. Clinical and commercial translation of any TEVG has additional requirements:

1. Specifications for TEVGs will include a range of vessel diameters, lengths and wall thicknesses to suit a wide patient cohort.

2. Manufacturing TEVGs must be kept to minimum processing times using materials which are cost effective and readily available without the need for complicated storage or preparation procedures (Yow et al., 2006).
3. The materials used to achieve a clinically relevant TEVG must be non-inflammatory, non-toxic, non-immunogenic, resistant to infection and sterilisable (Kakisis et al., 2005).
4. Extended culture times associated with tissue engineering techniques (up to 5 months) are not feasible for use in a clinical setting, particularly in acute situations (Dahl et al., 2011).

All of the above conditions in some combination should be satisfied if TEVGs are to be used in a clinical setting. This will allow for subsequent regulatory approval, essentially functioning as any other medical device with an "off-the-shelf" capacity.

The first challenge in trying to accomplish the above ideal properties is in creating an appropriate ECM architecture. Scaffolds composed of varying materials have been utilised to achieve this architecture and will be further discussed below.

2.5.2 Protein Based Scaffolds

Pioneering work in the field of TEVGs began with the research of Weinberg and Bell in 1986. The TEVG produced by Weinberg and Bell was composed of a collagen scaffold and was the first three layered arterial construct fabricated *in vitro*. The basis of their construct consisted of a scaffold of isolated collagen formed into a gel. The collagen gel was then embedded with SMCs forming a solid matrix. The matrix was surrounded by fibroblasts and the inner lumen lined with ECs (Weinberg and Bell, 1986). A schematic representation of the construction of such a collagen based scaffold is illustrated in Figure 2.10. The disorganised collagen, aligned longitudinally, resulted in poor mechanical

properties unsuitable for *in vivo* use. The recorded burst pressure was only 90 mm Hg. However, this work was extremely important as it demonstrated that different isolated vascular cells could be individually recruited and cultured *in vitro* to produce a functional tissue. Further improvements in using collagen gels as scaffolds produced constructs approximating native vessels with slightly improved mechanical properties (L'Heureux et al., 1993). However, real advances using collagen scaffolds only came about with the introduction of a supporting sleeve to increase strength. This support sleeve or mesh, usually composed of Dacron™, granted sufficient strength to the cultured construct, allowing implantation and capacity to withstand *in vivo* pressures, subsequently demonstrating 65% patency at 6 months (Hirai and Matsuda, 1996).

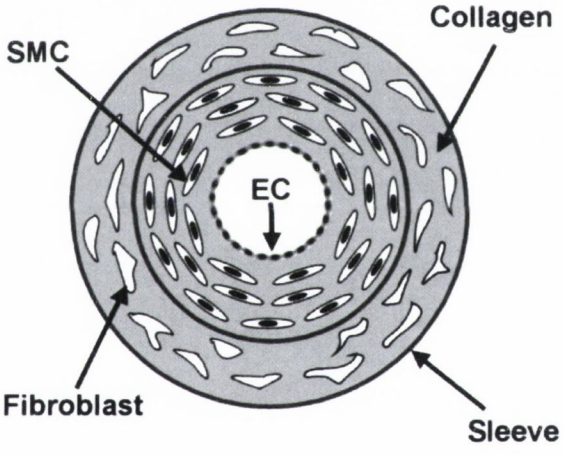

Figure 2.10 Collagen Based Vascular Construct

Collagen gel is embedded with SMCs and surrounded by collagen embedded fibroblasts. ECs seeded on the inner lumen form an anti-thrombogenic monolayer and an outer sleeve maintains the integrity of the construct. (Nerem and Seliktar, 2001)

The added mechanical advantages of a supporting sleeve are outweighed by the introduction of biocompatibility issues associated with the non-biological supporting material. The compliance mismatch and lack of full host integration, due to the presence of the synthetic support, results in a less than ideal solution to weak collagen scaffolds.

Further improvements in mechanical integrity using collagen based scaffold are achieved with: mechanical conditioning (Seliktar et al., 2000): electrospinning methods (Boland, 2004) or crosslinking techniques (Stegemann et al., 2007). Other protein-based natural materials such as fibrin have also been utilised in a similar manner to collagen scaffolds and have demonstrated similar problems with suboptimal mechanical properties (Tschoeke et al., 2008).

2.5.3 Biodegradable Synthetic Scaffolds

Bioresorbable polymers have been utilised in order to overcome the poor mechanical properties of protein based scaffolds. These synthetic materials provide the initial scaffold for cell seeding, offering increased strength for implantation, while gradually degrading *in vivo* as the seeded construct begins to remodel. A schematic representation of this process of using polymer scaffolds is shown in Figure 2.11. This process allows enhanced integration into the surrounding host tissue producing a stable and robust graft. Prior to their investigation for use as scaffolds for TEVGs these materials were used and clinically validated in surgery, mostly as sutures. They include materials such as: polylactic acid, polyglycolic acid, polyurethane and polyethylene terephthalate. Niklason et al reported the first *in vivo* use of a TEVG comprised of polyglyolic acid seeded with SMCs (Niklason et al., 1999).

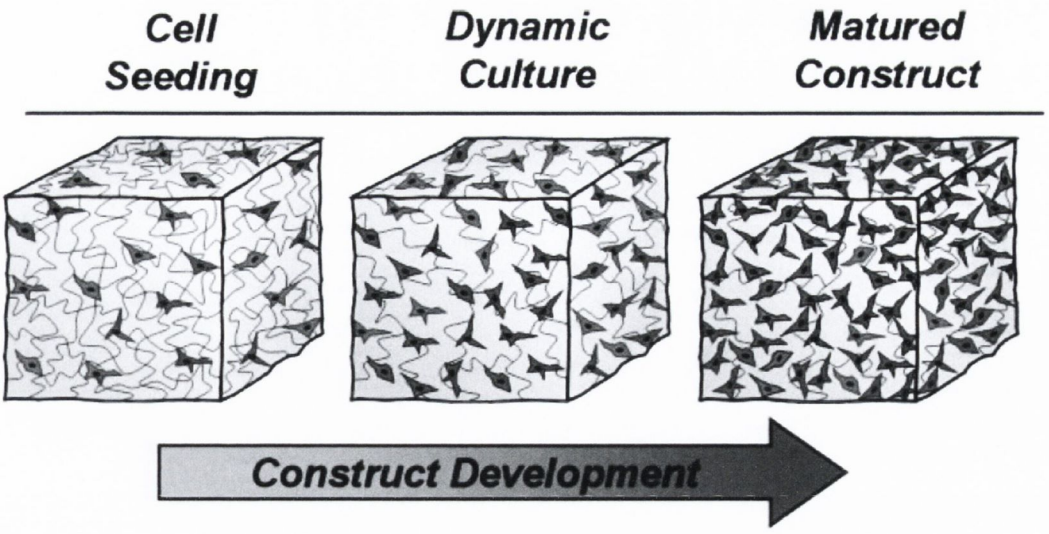

Figure 2.11 Schematic of Polymer Based Vascular Scaffold Development

The polymer scaffold is seeded with cells and subjected to dynamic culture conditions. Cell proliferation and ECM organisation matures the scaffold as the polymer degrades. (Nerem and Seliktar, 2001)

The seeded construct was matured *in vitro* by subjecting it to a pulsatile flow, the resulting cyclic strain matched fetal development in large mammals (5% strain at 165 beats/min). These conditions encourage the synthesis of ECM components by the seeded SMCs. After 8 weeks maturation the polymer scaffold was largely degraded while ECM remains. EC seeding of the lumen and further maturation resulted in a construct suitable for implantation. Histologically, the construct appeared physiologically relevant with a populated media of SMCs and burst pressures in excess of 2,000 mm Hg were recorded. The construct remained patent for up to four weeks in an *in vivo* animal model.

Progress with the use of bioresorbable polymers have produced stable constructs that display vasoactivity and demonstrate increased *in vivo* performance. New combinations of polymers with varying degradation rates and cell attachment characteristics, combined with optimised bioreactor conditioning techniques, have improved the performance of these constructs (Opitz et al., 2004b, Hoerstrup et al., 2006,

Crapo et al., 2008, Tschoeke et al., 2009). Balancing the rate of resorption of the polymer with tissue remodelling to produce an ECM sufficiently robust for implantation, which subsequently does not create a compliance mismatch, is a substantial challenge. Furthermore, residual polymer debris from the degradation of the scaffold can exist within the tissue, which may prevent full tissue integration or at worst toxicity leading to an inflammatory response within the vessel wall (Nerem and Seliktar, 2001).

Bioreactor conditioning of polymer based constructs produces an ECM that is sufficiently strong for implantation with large amounts of collagen (Niklason et al., 1999, Quint et al., 2011). This collagen, which is circumferentially aligned, is directly responsible for the high burst pressures achieved by these constructs. However, the natural intricate structure of the elastic lamellae of the native artery and its interaction with collagen and SMCs has resulted in few constructs expressing mature elastin in its native configuration (Patel et al., 2006, Dahl et al., 2007, Crapo and Wang, 2010). This is a major limitation of bioabsorbable polymers as scaffolds for TEVGs, as low levels of elastin leads to compliance mismatch *in vivo,* which is one of the main failure modes for these implanted constructs (Opitz et al., 2004a, Kakisis et al., 2005).

The processes associated with the manufacture of these constructs are extremely time consuming. The maturation times of bioreactor conditioning are not yet clinically viable. The polymers used in these scaffolds offer the advantage of being easy to manufacture, cheap and reproducible. However, the excessive maturation times will lead to inflated costs. Producing large scale numbers for a general population with the current methods would be logistically difficult and extremely expensive.

Various polymer scaffolds created by numerous techniques continue to be investigated for use as vascular scaffolds. In one such study by Quint et al the fabrication method of Niklason et al, described above, is utilised to create a TEVG from banked

allogenic porcine SMCs by maturation in a bio-mimetic environment for 10 weeks (Niklason et al., 1999, Quint et al., 2011). These constructs consist of the seeded cells and newly formed ECM after degradation of the polymer and are subsequently rendered acellular by the removal of the SMCs to leave a stable robust ECM. This acellular construct is then seeded with ECs and implanted *in vivo* performing adequately as an end-to-side bypass graft in a porcine carotid artery for 30 days. Although this fabrication method still remains cumbersome and time consuming it does allow for the production and banking of constructs that can be used quickly in clinical applications, removing the excessive fabrication time as the limiting factor in its clinical use. However, there are still cost implications with this manufacturing protocol. There still remain many issues regarding the *in vivo* performance of these grafts, as the ECM that remains after removing the SMCs is immature and not as robust as native arterial ECM, particularly with regard to elastin content. Nevertheless, this is an important development in the use of biodegradable synthetic scaffolds and it is an extremely promising attempt to bridge the gap to clinical translation by developing novel methods to tackle the issue of excessive fabrication times.

2.5.4 Sheet Rolling

An alternative technique for fabricating a TEVG which does not rely on a scaffold is a process known as "sheet rolling" developed by L'Heureux et al. This novel technique is based entirely on cultured human cells. Harvested fibroblasts from skin and human umbilical vein SMCs are independently cultured for 4 weeks. These cultures form organized sheets of cells and ECM which can be removed intact from culture flasks. Rolling these sheets around a mandrel creates a tubular construct which can be further matured under pulsatile flow conditions. ECs are seeded onto the lumen of this construct

resulting in a three layered, organised arterial construct with circumferentially aligned cells resembling native arterial tissue (L'Heureux et al., 1998). The process is represented in Figure 2.12.

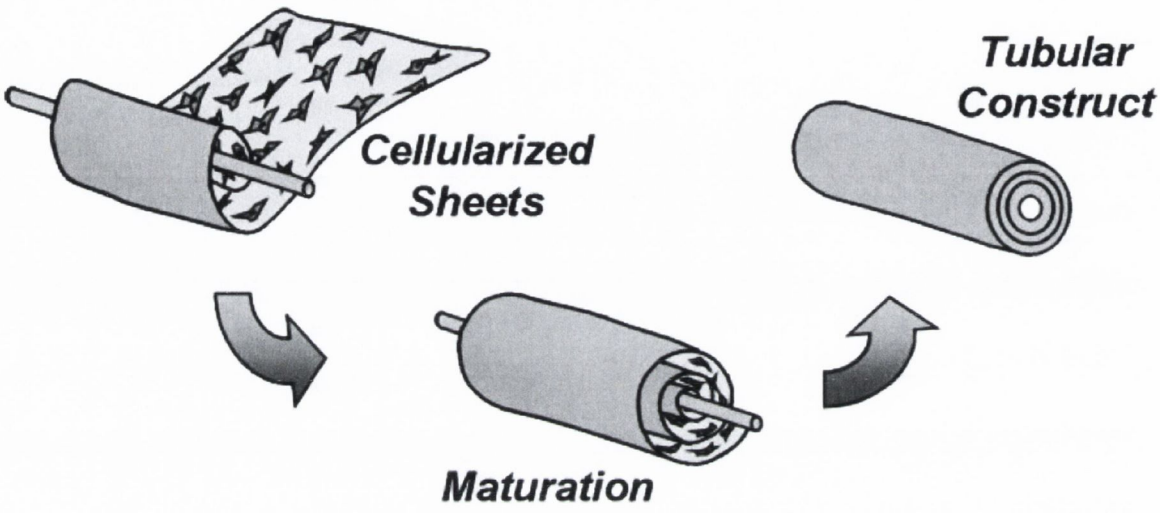

Figure 2.12 Creation of a Vascular Construct by the Sheet Rolling Technique
Harvested fibroblasts are cultured into cell sheets and rolled around a mandrel. These layers of rolled sheets are matured in dynamic culture conditions to create a stable layered tubular construct. This process takes at least 5 months. (Nerem and Seliktar, 2001)

These constructs have high burst strengths (2500 mm Hg) and have shown excellent remodelling and mechanical stability after 8 months *in vivo* (Konig et al., 2009). However, their fabrication is extremely time consuming involving up to 5 months of cell culture and construct maturation, with considerable cost and expertise necessary for their creation. Similar to the polymer scaffolds, exhibiting high burst pressure does not signify ideal mechanical properties, as this layered structure does not contain significant amounts of elastin, further highlighting the major limitation of *in vitro* elastin synthesis. The significant progress which has been made using each type of scaffold and a summary of their individual properties is shown below in Table 2.1.

Table 2.1 ***Summary of Materials Used as Scaffolds in Vascular Tissue Engineering***

Material	Scaffold Type	Advantages	Disadvantages
Natural polymers	Collagen Collagen Gel	Natural component of native vessel Good cell attachment and signalling	Poor mechanical properties
Synthetic polymer	PGA PLA PU PET	Cheap, accessible, reproducible material with biocompatible record Sufficient mechanical properties for implantation Good host tissue integration	Possible toxicity from degraded debris Inadequate and time consuming cell seeding. Slow to mature *in vitro* Lack of optimum elastin for compliance
Sheet rolling	Cell layers no scaffold	Good mechanical properties Reproducible Non invasive cell source Capability of remodelling *in vivo*	Expensive and impractical production times (> 5 months) ECM equivalent is not physiologically relevant (no elastin)
Decellularized exogenous tissue	Porcine carotid artery etc	Cheap and readily available Natural vessel ECM architecture and mechanical properties Good cell attachment	Cell seeding and migration difficulty due to dense matrix

2.6 Decellularized Scaffolds

Decellularization is the process of removing all the cellular components from a tissue or an organ leaving the complex architecture of the ECM remaining. Figure 2.13 displays histology of native and decellularized porcine arterial tissue. The highly cellular native tissue is transformed into a porous architecture, consisting of undisrupted ECM with the absence of any cells. The scanning electron micrograph (SEM) image (Figure 2.13 C)

highlights the dense porous consistent nature of the remaining matrix. The use of decellularized tissue as a scaffold for tissue engineering has had significant success to date. The relative ease of decellularization and widespread availability of exogenous tissue make it a particularly attractive alternative to other vascular scaffolds. Recent success with whole organ decellularization has highlighted the advantages of this technique for a wide variety of tissue substitutes (Ott et al., 2008, Petersen et al., 2010, Zhou et al., 2010).

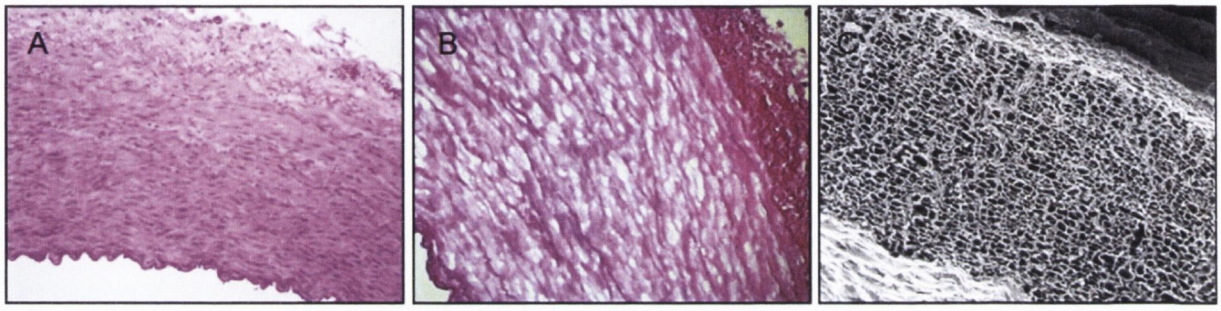

Figure 2.13 Decellularized Arterial Tissue

(A) H&E stain of native tissue displays high cellularity and surrounding dense ECM structure. (B) After decellularization no evidence of cells is visible with a porous matrix remaining with largely undisrupted ECM. (C) SEM of decellularized artery shows the porous nature of the scaffold and the consistency of the matrix across the arterial wall. (Yazdani et al., 2010)

Decellularized tissue has been used extensively as a scaffold for TEVGs and may offer the ability to overcome some of the challenges facing current fabrication techniques. There are many different methods of decellularization and the process has been applied to various types of tissue across many species for multiple applications (Schaner et al., 2004, Amiel et al., 2006, Derham et al., 2008, Zhu et al., 2008, Crapo et al., 2011). These methods are summarised in Table 2.2. The composition and ultrastructure of the remaining ECM varies according to the processes employed and can have significant implications on the mechanical properties of the decellularized tissue.

Table 2.2 Processes Utilised in Decellularization of Vascular Tissues

Method	Action	Affects on ECM	Reference
Physical			
Mechanical agitation	Rollers, rotators, sonication etc can cause cell lysis	Excessive mechanical forces required to fully remove cellular material can damage ECM, hence mainly used to increase chemical exposure	(McFetridge et al., 2004b, Roy et al., 2005)
Hydrostatic Pressure	Disruption of cell membrane	Non-denaturing if temperature is controlled, still require debris removal	(Funamoto et al., 2010)
Chemical			
Triton X-100	Disrupts lipid-lipid and lipid protein interactions	Protein-protein interactions unaffected leaving ECM structure intact. Removes GAGs	(Yazdani et al., 2009, Amiel et al., 2006)
Sodium dodecyl sulphate (SDS)	Solubilises cytoplasmic and nuclear cellular membranes	Over exposure can denature protein. Mostly used in combination with other detergents	(Gui et al., 2009, Schaner et al., 2004)
Solvents	Lipid extraction	Can degrade collagen	(McFetridge et al., 2004b)
Enzymatic			
Trypsin	Cleaves peptide bonds	Can disrupt ECM with long exposure removes laminin, elastin and GAGs	(Teebken et al., 2000, Liu et al., 2008)
Nucleases	Hydrolize bonds of ribonucleotide and deoxyribonucleotides	Will not efficiently remove cell material alone and can be difficult to remove from tissue	(Rieder et al., 2004, Roy et al., 2005)

Methods of decellularization include physical disruption to the tissue (freezing, pressure, agitation, sonication), chemical methods (alkaline/acid, detergents, chelating agents, protease inhibitors) and the use of enzymes (Gilbert et al., 2006). Often a combination of these treatments are utilised to ensure complete removal of all cellular components. The actual process of decellularization by its very nature will cause disturbance to the native

three-dimensional architecture of the ECM. In order to expose the cells to the denaturing agents the ECM components must be disrupted to some extent, this disruption may be minimised by selecting the most suitable protocol for the specific tissue being decellularized. However, at a minimum all cells must be exposed to the denaturing agents and a path must be available for the removal of all cellular material after this exposure.

Porcine arterial tissue is a commonly sourced tissue for decellularization for use as a TEVG (Teebken et al., 2000, Amiel et al., 2006, McFetridge et al., 2007, Zhu et al., 2008, Yazdani et al., 2009) due its close physiological similarity to human vasculature. Other sources include canine arteries (Cho et al., 2005), human femoral arteries (Wilshaw et al., 2012), human vein (Schaner et al., 2004, Martin et al., 2005), ureters (Narita et al., 2008, Derham et al., 2008) and urinary umbilical matrix and small intestinal sub-mucosa (Badylak, 2007, Gilbert et al., 2008).

The protocols for decellularizing porcine tissue vary among research groups but commonly used protocols combine enzymatic digestion and detergent extraction with physical agitation. Physical agitation, such as freezing, high pressure and rotational forces cause lysis of the cell membrane leaving the cytoplasm susceptible to enzyme digestion. Trypsin is the most widely used enzyme for protein digestion. Trypsin cleaves the peptide bonds on the carbon side of arginine and lysine if the next residue is not proline (Gilbert et al., 2006). Separation of the exposed cellular components occurs in the presence of trypsin; however, prolonged exposure will degrade the elastin component of the tissue. Non-ionic detergents such as Triton X-100 or ionic detergents such as sodium dodecyl sulphate (SDS) are often utilised. Non-ionic detergents disrupt lipid-lipid and lipid-protein interactions but do not affect protein-protein interactions (Seddon et al., 2004), thus leaving the structural ECM components fully intact. The exposure to detergents causes the solubilisation of the cytoplasmic and nuclear cellular components that have

been separated by enzymatic digestion. The removal of all the cellular debris and nucleic acids is undertaken by the continued washing and physical agitation of the tissue. A final wash sequence is commonly implemented to ensure removal of all residual chemicals used in the decellularization process.

It should be noted that there is no such thing as the optimum decellularization protocol for all biological tissues. Factors such as species, tissue type, tissue source, chemicals, concentrations and agitation methods will all influence the degree of decellularization and preservation of ECM components. Therefore, it is essential to tailor a decellularization protocol to a specific application ensuring the process is optimised to guarantee its efficacy.

2.6.1 Mechanical Properties of Decellularized Arterial Tissue

The successful decellularization of arterial tissue produces a porous ECM with a reduced wall thickness and increased diameter. The removal of the SMCs and resulting compaction of the tissue is responsible for the geometric alterations. Mechanical testing of decellularized tissue has been carried out to determine how the process affects the mechanical response of the tissue. A number of methods have been detailed to determine this mechanical response; Figure 2.14 shows the mechanical response from two different mechanical tests. Some research groups have tensile tested rectangular or dumb-bell shaped specimens cut from the opened strips of tissue and determined the tensile response to failure in both the axial and circumferential directions (Amiel et al., 2006, Yazdani et al., 2009, Funamoto et al., 2010). Cutting the arterial wall open releases residual stresses, particularly from the elastin network and may not truly reflect the interaction of the collagen and elastin within the arterial wall when tested, prompting research groups to keep specimens intact by tensile testing ring section of arteries (Seliktar et al., 2000,

McFetridge et al., 2004b, Venkatasubramanian et al., 2006). Inflation tests have also been used to analyse the mechanical response by producing pressure-diameter curves (Roy et al., 2005, Dahl et al., 2007, Williams et al., 2009).

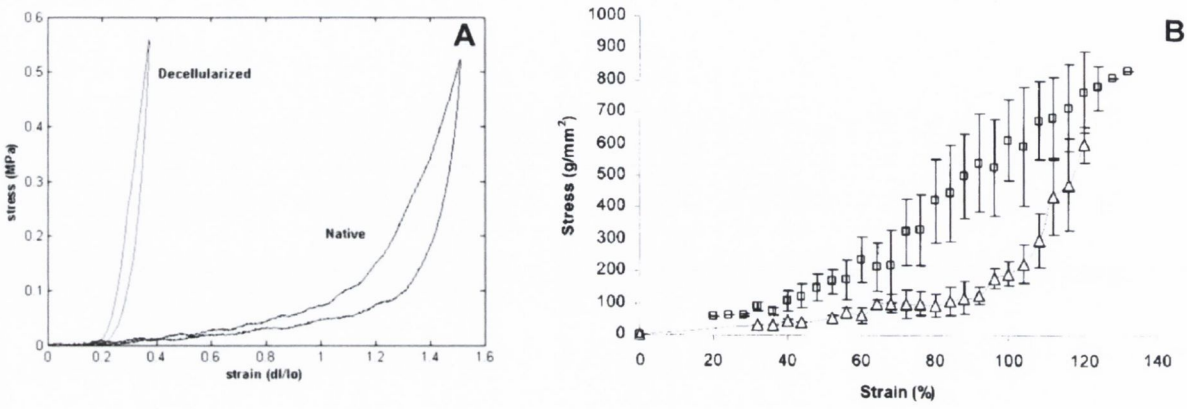

Figure 2.14 Mechanical Response of Tensile Tested Decellularized Tissue

(A) Stress-strain curve for cut rectangular decellularized carotid arteries tested in the axial direction. The decellularized tissue is noticeably stiffer in the final collagen region of the curve and significantly less extension is evident in the tissue. (B) A similar response is seen with intact ring sections. Increased stiffness is seen in the decellularized tissue (□) compared to the native tissue (⌂). (Williams et al., 2009, McFetridge et al., 2004)

The consensus from these tests is that the matrix that remains after decellularization is much stiffer and less distensible than the native arterial tissue from which it's derived. The increase in modulus of decellularized tissue is evident in both the circumferential and axial directions as well as whole intact ring specimens. This stiffening is directly attributed to the uncrimping of collagen fibers and hence their ease of recruitment in the direction of the applied strain and overall early fiber engagement. In the absence of SMCs the bundles of collagen fibers are more free to fully engage and bear the full applied load resulting in a higher stiffness. A higher ultimate tensile strength was also evident from these tests, which is again due to the full fiber engagement at high stresses. It should be noted that the above tests were carried out on multiple tissue types and sources and were decellularized by varying protocols and tested under various parameters. As a result of

this, direct comparison of recorded results across different studies may not be accurate. However, the overall response and general trends of the mechanical test results can be relied upon, as the aim of all decellularization protocols is to maintain the ECM undisrupted.

2.6.2 Current Limitations of Decellularized Tissue as a Vascular Scaffold

A major drawback in utilising decellularized tissue as a vascular scaffold is that the matrix which remains after decellularization is extremely dense and can prove difficult to infiltrate with cells both *in vitro* and *in vivo*. This is most evident with SMCs in the medial layer of the construct (Lu et al., 2004, Neff et al., 2011). A poorly infiltrated scaffold resulting in a lack of a fully quiescent contractile SMC medial layer may result in less than ideal mechanical properties. The highly dense nature of decellularized vascular tissue has also lead to excessive cell seeding and culture times to mature these constructs *in vitro* (Yazdani et al., 2009). Figure 2.15 shows DAPI stained histological sections of a SMC seeded decellularized porcine arterial tissue by Yazdani et al. The limited penetration within the scaffold is typical of abluminally cell-seeded decellularized scaffolds. A capsule effect of an accumulation of cells at the site of seeding in close proximity to the nutrient supply is commonly seen. The clear increase in cell number due to the proliferation of cells on the scaffold confirms the effectiveness of decellularized tissue for cell attachment and growth. However, the density of the decellularized tissue matrix prevents the full repopulation of a quiescent SMC medial layer and poses a significant hurdle in its use as a scaffold.

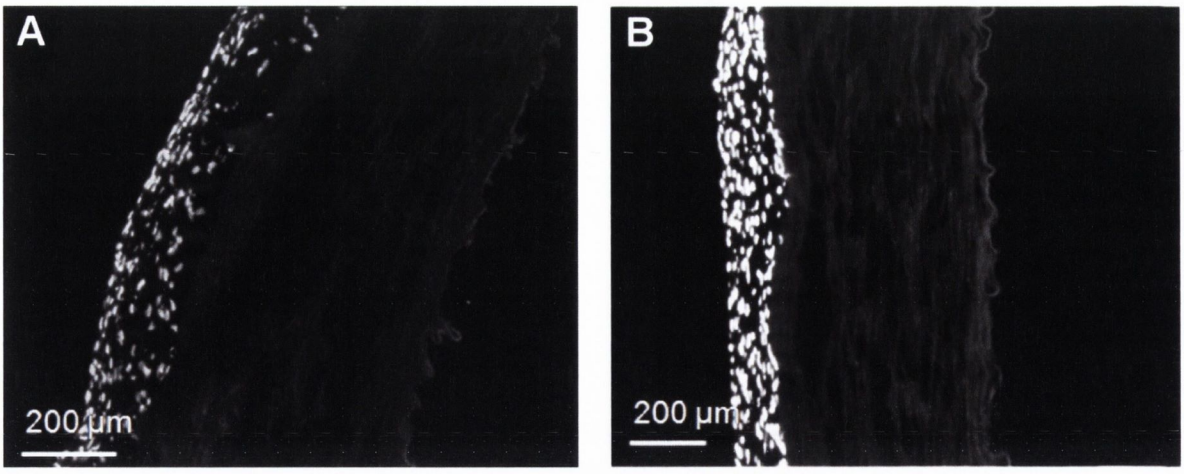

Figure 2.15 Poor Cell Infiltration of a Decellularized Vascular Scaffold

(A) DAPI stained section of decellularized porcine tissue seeded with SMCs (fluorescing white) after 7 days in vitro culture. (B) After 14 days culture. The SMCs readily attach to the abluminal side of the scaffold after seeding and proliferate well. However, an increase in cell number is visible after 14 days with little or no further infiltration into the scaffold. (Yazdani et al., 2009)

A similar capsule effect was evident in another study by McFetridge et al using decellularized porcine carotid arteries (Figure 2.16). Once more cell infiltration is limited to the adventitia and there is no evidence of cells within the medial layer after two weeks static culture or a further three weeks dynamic culture in a pulsatile flow bio-mimetic environment (McFetridge et al., 2007). However, in the same study a decellularized artery was cut open in the radial direction and placed on a cell culture flask with the cut surface contacting the cells, and cultured under static conditions for five weeks. Interestingly, the cells freely migrated within the medial layer of the scaffold (Figure 2.16 C) along the axis of the radially cut fibers. This further highlights the high density limitation of decellularized vascular scaffolds. Although they contain pores, it appears that the elastin sheets provide a tough barrier for cells to migrate through. In the McFetridge et al study they concluded that this limited cell migration was not due to mass transfer issues, as the

seeded cells expressed enzymes indicative of remodelling which would allow them to migrate easily within the elastin layers given a suitable incentive.

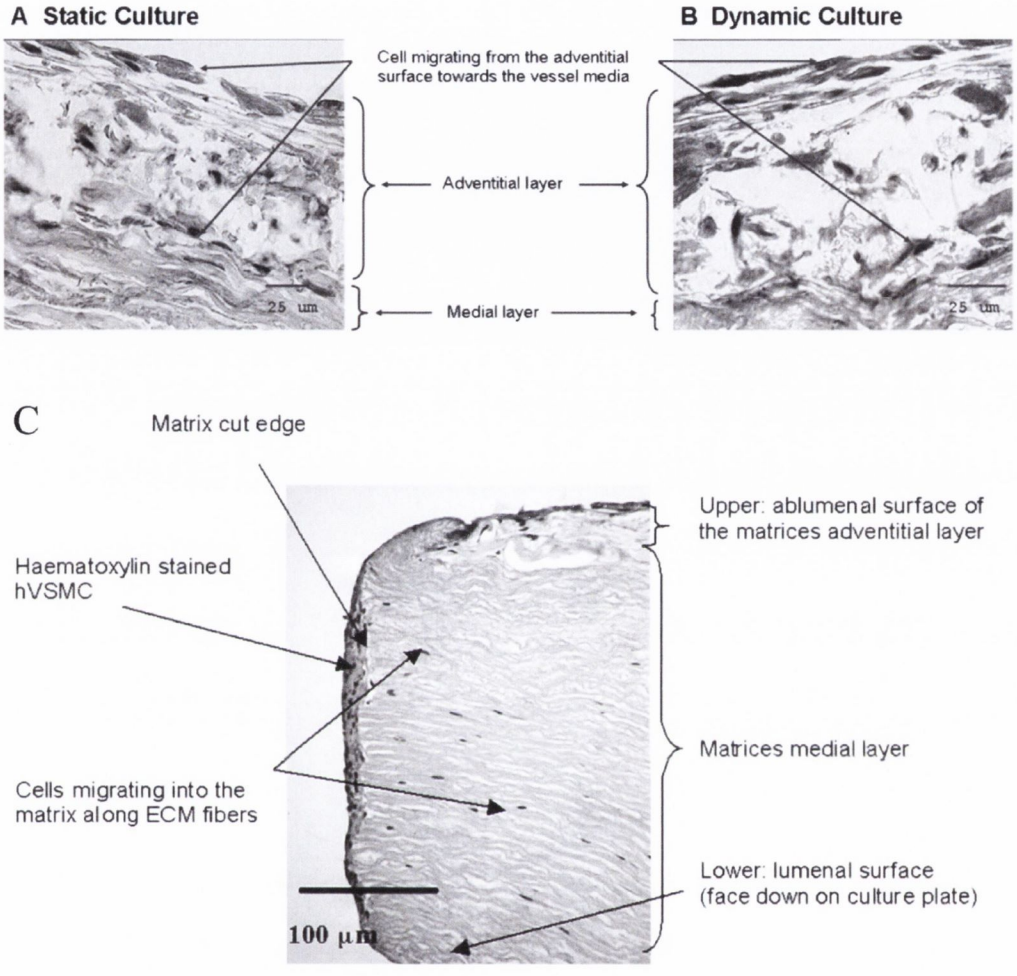

Figure 2.16 Cell Migration within Decellularized Vascular Scaffolds

(A) Abluminally seeded cells after two weeks of static culture migrate through the adventitia to the medial surface. (B) A further three weeks dynamic culture sees no further migration of these cells within the media. (C) Cell migration throughout the medial layer is evident when cells have direct access across radially cut ECM fibers (elastin layers). (McFetridge et al 2007)

This capsulation effect of cells remaining in close proximity to a nutrient supply is common in tissue engineering and it is a particular problem with decellularized scaffolds due to the highly dense nature of the scaffold.

Autologous vein harvesting for CABG occurs immediately prior to the bypass surgery and it is within this time frame that TEVGs must compete. The commercial demand for TEVGs will require their availability at short notice. The logistics of CABG will mean maturation times of weeks or months will be unpractical, particularly for emergency situations. Decellularized tissue offers the advantage of readily available scaffolds in varying geometries and dimensions without the necessity for extended cultivation times to create a stable ECM. However, the poor cell infiltration of the matrix must be overcome in order to harness the full potential of decellularized tissue as a vascular scaffold.

2.7 Cell Sources

A further factor limiting the clinical development of all TEVGs is the harvest and propagation of autologous cells. The two main vascular cell types required (SMCs and ECs) are not available by minimally invasive harvesting from a patient prior to the requirement for a TEVG. Arterial or venous biopsies must be harvested from a patient in order to generate a primary culture for both these vascular cells. Ideally TEVG fabrication would utilise these native vascular cell types. Researchers have strived to locate other sources of cells to produce TEVGs which involve less invasive harvesting techniques with reduced patient discomfort while minimising procedural time and costs (Yow et al., 2006).

Endothelial Progenitor Cells (EPCs) are a potential source of mature ECs. EPCs are a subset of hematopoietic stem cells that were first isolated by Asahara et al in 1997. They are located in circulating blood and possess the ability to migrate, proliferate and differentiate into endothelial cell lineages but have not yet acquired characteristics of mature ECs (Asahara et al., 1997, Kawamoto and Asahara, 2007). The feasibility of using

EPCs has been demonstrated by isolating them from peripheral blood, expanding them *ex vivo* and seeding them onto decellularized porcine tissue (Kaushal et al., 2001). In this study the construct was pre-conditioned and subsequently implanted, maintaining patency for 130 days. Similarly, EPCs have been used in conjunction with biodegradable elastomeric scaffolds, obtaining successful results *in vitro* (Gao et al., 2008). The EPCs provided a non-thrombogenic stable luminal surface similar to a native EC monolayer. Further studies with EPCs have displayed the potential for differentiation not only into ECs but also SMCs which can be further manipulated to express a contractile phenotype (Krenning et al., 2008).

Another potential autologous cell source is bone marrow derived stem cells (BMCs). These adult stem cells can be isolated from bone marrow of individual patients, expanded rapidly *in vitro* and re-implanted without the risk of immune rejection or need for long term immunosuppression. Matsumura et al were the first group to prove the feasibility of constructing TEVGs comprised of BMCs. Polymer scaffolds were seeded directly with BMCs harvested from pigs with subsequent autologous implantation (Matsumura et al., 2003b). Large numbers of BMCs can be harvested; therefore they do not require any *ex vivo* expansion, reducing the time to fabricate the TEVG. Implantation for up to 8 weeks revealed fully patent vessels which were fully endothelialised and contained SMCs within the media with expression of a contractile phenotype. These results have been repeated by different groups using assorted scaffolds and seeding techniques (Roh et al., 2007a, Liu et al., 2007, Brennan et al., 2008). Positive results were obtained by seeding decellularized tissue with BMCs which were differentiated in culture into endothelial-like cells and smooth muscle-like cells prior to seeding and demonstrated good patency after 8 weeks *in vivo* (Cho et al., 2005). BMCs provide an obvious choice in

the creation of TEVGs, offering an easily accessible source, minimal *in vitro* handling and excellent differentiation potential into both vascular cell types.

Mesenchymal stem cells (MSCs) are a cell type that has been widely used in regenerative medicine (Macchiarini et al., 2008, George, 2010). MSCs can be found in a range of sources including bone marrow, fat, blood, liver and spleen with bone marrow derived MSCs being the most widely studied. MSCs are an adherent cell type which contribute to the non-adherent hematopoeitic stem cell niche with the ability to differentiate into a number of cell types such as osteoblasts, chondrocytes, adipocytes and tenocytes and can be quickly expanded with ease in culture. MSCs have particularly attractive characteristics for vascular tissue engineering as they have an inherent anti-thrombogenicity (Huang and Li, 2008), a capacity to differentiate both *in vitro* and *in vivo* into endothelial cells and/or smooth muscle cells, (Silva et al., 2005, Mirza et al., 2008, Zhao et al., 2010) an ability to secrete signalling molecules to recruit other cell types, (Meyerrose et al., 2010) and to modulate the immune response (Da Silva Meirelles et al., 2009, Bajpai and Andreadis, 2012). They also lack major histocompatibility complex (MHC) II markers on their surfaces, and so are allogenically tolerated by host immune systems (Krawiec and Vorp, 2012). For these reasons MSCs have been widely used in the creation of TEVGs (Dong et al., 2009, O'Cearbhaill et al., 2010). Gong et al demonstrated that differentiating human MSCs toward a SMC lineage by both culture conditions and dynamic mechanical conditioning in a three-dimensional bio-mimetic environment produced a more stable and physiologically relevant construct after 8 weeks of maturation (Gong and Niklason, 2008). Furthermore, canine MSCs have been seeded onto electrospun PLGA scaffolds for seven days static culture and then implanted as canine abdominal aorta bypass grafts for 24 weeks. The explanted grafts showed excellent patency with no thrombosis and good *in vivo* remodelling with a confluent EC

monolayer and SMCs located in the media (Zhang et al., 2008). Zhao et al have also successfully demonstrated the utilisation of ovine MSCs using a decellularized vascular scaffold by differentiating MSCs into both ECs and SMCs in culture prior to scaffold seeding, see Figure 2.17.

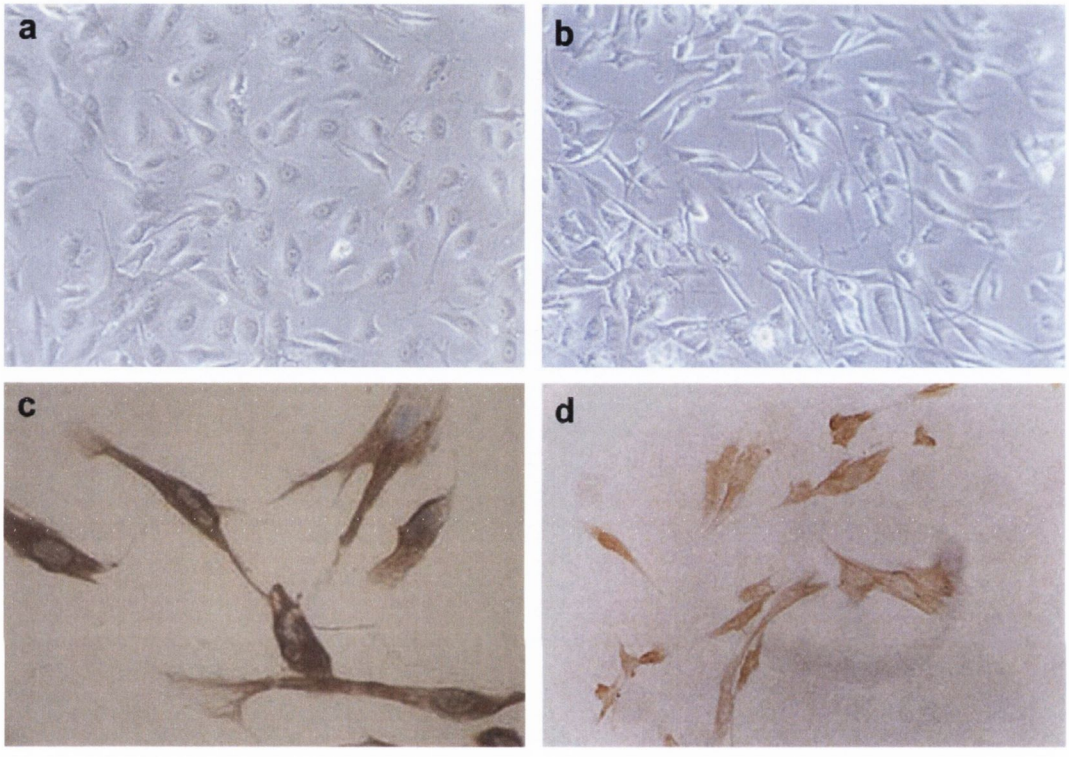

Figure 2.17 Human MSC Differentiation Toward EC and SMC lineages

(A) Typical cobblestone morphology of ECs after differentiation in culture toward EC-like cells. (B) Differentiation of the same MSC source toward SMCs. (C) ECs test positive for Van Wilebrand factor, an EC immunohistochemical marker. (D) SMCs test positive for alpha smooth muscle actin, a SMC immunohistochemical marker. (Zhao et al 2010)

This cell culture took 2 weeks for EC differentiation and 1 week for SMC differentiation. After 1 week of static culture these seeded constructs were implanted as ovine carotid grafts for 5 months and showed excellent patency and mechanical stability with a confluent EC monolayer and SMC populated medial layer (Zhao et al., 2010). The seeded MSCs were fluorescently labelled for tracking with some cells still present in the

construct after 2 months, demonstrating that the MSCs survived until this time point and contributed to the remodelling of the vascular tissue.

Other less common cell types that have been investigated and have shown potential as a cell sources for TEVGs include adipose derived stem cells (DiMuzio and Tulenko, 2007) and muscle derived stem cells (Nieponice et al., 2008) and pericytes (He et al., 2010).

An interesting and recently investigated potential source of cells for TEVGs are cardiac stem cells (CSCs). Located within the heart wall, CSCs can be harvested by biopsy of the myocardium of the heart and expanded *in vitro* (Bearzi et al., 2007). Differentiation into a number of cell types are possible with CSCs, such as cardiomyocytes, ECs, SMCs and fibroblasts (Barile et al., 2007). While these cells are being investigated largely for cardiac repair, (Smith et al., 2007) there is clear potential for their exploitation for TEVG applications. Most of this initial research with human CSCs has been carried out on explants from hearts taken during open heart procedures, therefore there still remains some challenges to overcome to achieve a non-invasive method of explant biopsy.

2.7.1 Seeding Techniques

There are a number of methods for seeding vascular cells onto scaffolds for TEVG fabrication. The most basic seeding technique is static seeding. This involves simply applying cells directly onto the scaffold allowing gravitational forces to adhere cells to the scaffold surface. This is usually performed by pipetting a cell concentration resuspended in culture medium on the abluminal surface or within the lumen of the scaffold. Constant rotation of the scaffold or rotation after a certain duration permits cell attachment and ideally results in a uniform distribution of cells on the scaffold surface

(Hsu et al., 2005, Quint et al., 2011, Yazdani et al., 2010, Isenberg et al., 2006). While this technique is widely used it can be time consuming, can result in non-homogenous cell distribution and poor cell morphology resulting in unstable cell monolayers (ECs) which can lead to cell loss when exposed to blood flow (McFetridge et al., 2004a, Villalona et al., 2010). This usually requires further maturation in static culture or by exposing the EC monolayer to shear stress from pulsatile flow conditions *in vitro* adding further excessive fabrication times and contamination risks. This allows the cells to align with the flow, take on more elongated morphology and overall strengthen their adherence to the scaffold to resist physiological flow rates and shear stress (Pawlowski et al., 2004). Coatings, such as fibronectin, laminin and collagen on scaffold surfaces can improve adherence but may also lead to increase risk of thrombosis (Wu et al., 2008, Villalona et al., 2010, Zhao et al., 2010). ECs are commonly seeded in this manner as they require just a monolayer on the lumen side surface of the scaffold. The cell numbers for seeding, culture medium volume, rotational speeds and times all vary depending on the scaffold and cell type utilised, with research groups usually determining the optimum parameters to fit their individual requirements (Niklason et al., 1999, Cho et al., 2005, Hoerstrup et al., 2006, Wu et al., 2008, Tillman et al., 2012). Cell seeding for the medial layer is usually carried out with abluminal static seeding techniques. These methods only allow for accumulation of cells on the scaffold surface with limited infiltration within the scaffold to the medial layer without any additional biomechanical or biochemical cues (Yazdani et al., 2009).

Dynamic seeding of cells has been utilised to increase the efficiency of cell seeding. Dynamic methods include rotational seeding whereby a scaffold is rotated in a cell suspension in a spinner flask to enhance exposure of the cells to the scaffold. This aims to increase cell adhesion density while minimising stresses on the cells (Hsu et al.,

2005). Rotational methods are also associated with excessive seeding times and require large cell concentrations for efficient seeding. Centrifugal seeding uses similar methods but at much higher rotational speeds to force cells into scaffolds (Godbey et al., 2004, Roh et al., 2007b). A bar chart of the increase in cellular activity within a scaffold after seeding with three techniques is shown in Figure 2.18.

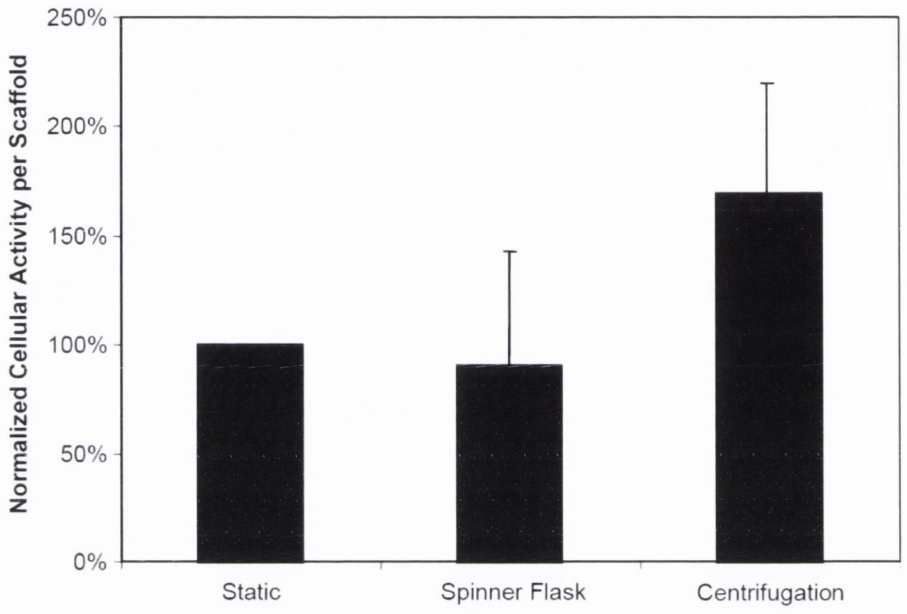

Figure 2.18 Dynamic Cell Seeding Efficiency

PGA scaffold seeded with human bladder SMCs by centrifugation returned higher seeding efficiencies than static or spinner flask seeding. The high cellular activity was also homogenous throughout the scaffold. (Godbey et al., 2004)

The aim of using centrifugal seeding in this study was not only to retain higher cell numbers within the scaffold but also to produce a more homogenous distribution of cells (Godbey et al., 2004). While cell viability is maintained under the high centrifugal forces, there may be undesired changes to cell morphology.

The shortcomings of most seeding techniques are largely the excessive time frames associated with repopulating scaffolds or no cell infiltration of the medial layer. Attempts have been made to bulk cell seed scaffolds i.e. produce a uniform distribution of

cells throughout the scaffold in a rapid manner. A vacuum seeding technique has been successful in achieving this in an efficient manner with poly(ester urethane)urea (PEUU) scaffolds (Soletti et al., 2006). The vacuum seeding method by Soletti et al is shown in Figure 2.19. The scaffold is infused with a cell suspension and the vacuum applied to the outside of the scaffold draws the cells outward toward the abluminal side.

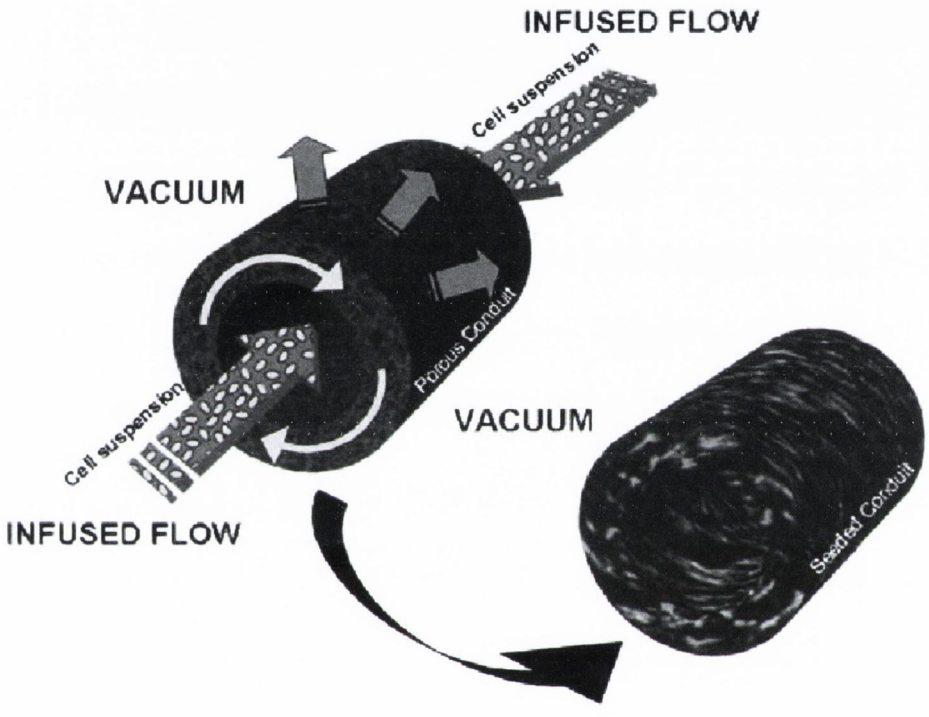

Figure 2.19 Vacuum Seeding Technique

Cell suspension is infused within the scaffold and the cells are pulled through the porous scaffold. This produces a fast, reproducible method of uniformly repopulating the scaffold. (Soletti et al., 2006)

Optimisation of the vacuuming produces a uniform distribution of cells across the entire scaffold and scaffolds seeded in this manner have been successfully tested *in vivo* (He et al., 2011). Cell morphology and viability appeared unaffected by the vacuum process, however, the process is limited to scaffolds with similar porosity and certainly isn't viable for highly dense heterogeneous decellularized scaffolds.

Other dynamic seeding techniques largely rely on the use of pulsatile flow bioreactors which provide a biomechanical stimulus to mature constructs *in vitro* (see Section 2.8). These bio-mimetic environments are usually self contained units in which the constructs are secured in place for the duration to minimise handling and reduce contamination. Williams et al describe a perfusion bioreactor system whereby a syringe pump reciprocally pumps a cell suspension within the lumen of a PGA scaffold for 24 hours, (Williams and Wick, 2004), while Zhao et al utilise a peristaltic pump to perfuse a cell suspension in culture media through the wall of a PET scaffold by blocking the flow distal to the scaffold (Zhao and Ma, 2005). The advantages of these perfusion techniques are high seeding efficiencies and minimal handling of the scaffolds, which is particularly advantageous in terms of creating the EC monolayer. However, they are limited to use with certain scaffold types and are associated with prolonged culture times, extending the already timely fabrication process while increasing contamination risks. Furthermore, the bioreactor systems are complex and may be difficult to scale up for large scale production for clinical use.

Other novel cell seeding techniques that have been utilised for creating TEVGs include the use of cells labelled with magnetic nanoparticles seeded onto a decellularized scaffold under magnetic force, (Perea et al., 2006, Shimizu et al., 2007) and also electro spinning cells directly into the scaffold during the fabrication process (Stankus et al., 2007). Most research groups use a combination of static and dynamic seeding techniques, usually incorporating the seeding process into a bioreactor setup. The main challenge for cell seeding is producing a fully repopulated scaffold, quickly, with an even distribution of cells, particularly within the medial layer.

2.7.2 Novel Seeding Techniques for Decellularized Scaffolds

The low porosity and highly dense nature of decellularized tissue can prove difficult to infiltrate with the standard cell seeding techniques described above. The capsulation of cells on the surface of these scaffolds and minimal medial layer infiltration has warranted the development of some novel scaffold modifications and alternative seeding techniques. Bergmeister et al attempted to improve cell infiltration of a decellularized scaffold by increasing the inherent low porosity, see Figure 2.20. In this study the decellularized tissue was radially perforated with 50μm holes using a laser at a concentration of 50 holes/cm^2 (Bergmeister et al., 2005). After implantation as a carotid artery bypass grafts for 6 months a higher and faster level of cell repopulation was noted in the laser cut scaffolds compared to the non-laser cut controls. Overall, laser cutting the scaffold demonstrated significantly better remodelling due to the increased porosity, however, no mechanical quantification was undertaken to assess the effects on the mechanical properties of the scaffold caused by these laser cut alterations and one graft did fail due to neo-intimal hyperplasia.

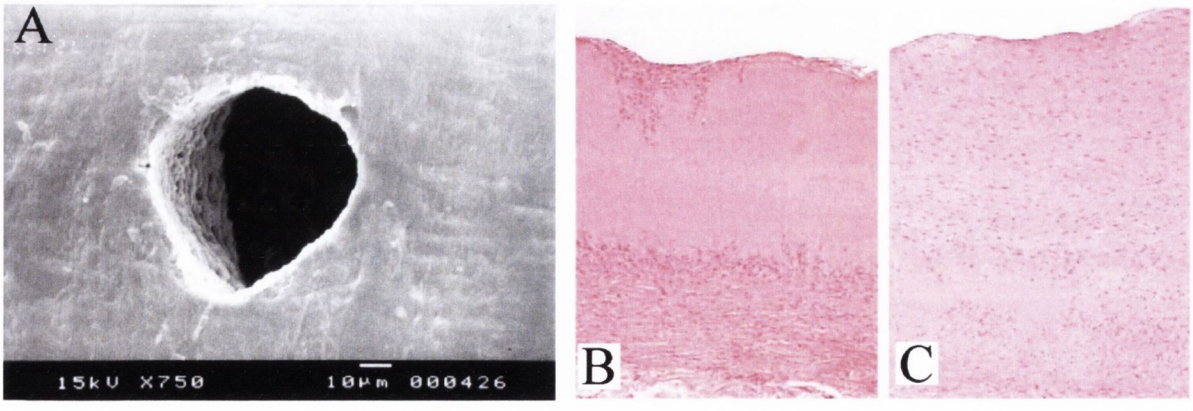

Figure 2.20 Laser Cutting Decellularized Scaffold and in vivo Repopulation

(A) 50μm diameter hole laser cut into decellularized tissue shows minimal disruption to the surrounding matrix. (B) 6 weeks in vivo shows some infiltration of host cells. (C) After 6 months almost complete repopulation is evident. (Bergmeister et al 2005)

A similar method of laser cutting an acellular scaffold was carried out by Ksayanov et al. The laser perforation was combined with centrifugal casting in order to maximise the seeding efficiency (Kasyanov et al., 2009). Figure 2.21 shows the method of casting, whereby the laser cut holes were filled with cells encapsulated in a hyaluronan-based hydrogel and a high magnification fluorescent microscopy image of a high density seeded laser cut hole. The process demonstrated excellent cell retention within the scaffold and no significant difference to the ultimate stress or strain values and good perfusion characteristics. This is a highly promising technique for quickly and efficiently seeding the medial layer of an acellular scaffold. However, the performance of the scaffold *in vivo* was not demonstrated. Aggressively manipulating the tissue in this manner may have implications on the *in vivo* mechanical response of the construct. Furthermore, the release profile of the cells from the hydrogel is not detailed in this study and warrants investigation to ensure sufficient cell numbers are released in suitable time frames.

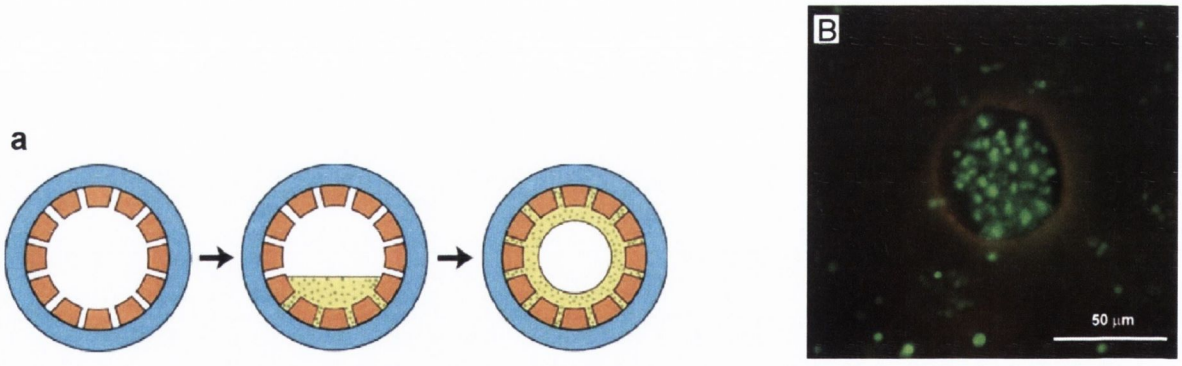

Figure 2.21 Centrifugal Casting of Laser Perforated Scaffold

(a) Decellularized small-intestinal submucosa containing laser cut micro-pores are filled with a cell encapsulated hydrogel solution and rotated. (b) Fluorescent microscopy of labelled cells show the high cell retention within the laser cut hole. (Kasyanov et al 2009)

Further attempts to reduce the density of decellularized scaffolds to aid cell infiltration have been demonstrated by the use of pure collagen and pure elastin scaffolds (Lu et al.,

2004, Simionescu et al., 2006, Kurane et al., 2007, Chuang et al., 2009). Simionescu et al showed that the complete removal of these individual ECM components demonstrated a higher infiltration of cells in the elastin only scaffolds *in vivo.* A further increase in repopulation with scaffolds loaded with basic fibroblast growth factor (bFGF) was also demonstrated. Subdermal implantation of these scaffolds not only showed increased host cell infiltration but demonstrated new ECM synthesis within the scaffold (Simionescu et al., 2006). The benefit of the reduced porosity of these scaffolds and the utilisation of bFGF is shown in Figure 2.22. The collagen and elastin only scaffolds both outperformed the decellularized and crosslinked decellularized controls. The addition of bFGF clearly aided the infiltration of host fibroblasts in both scaffold types.

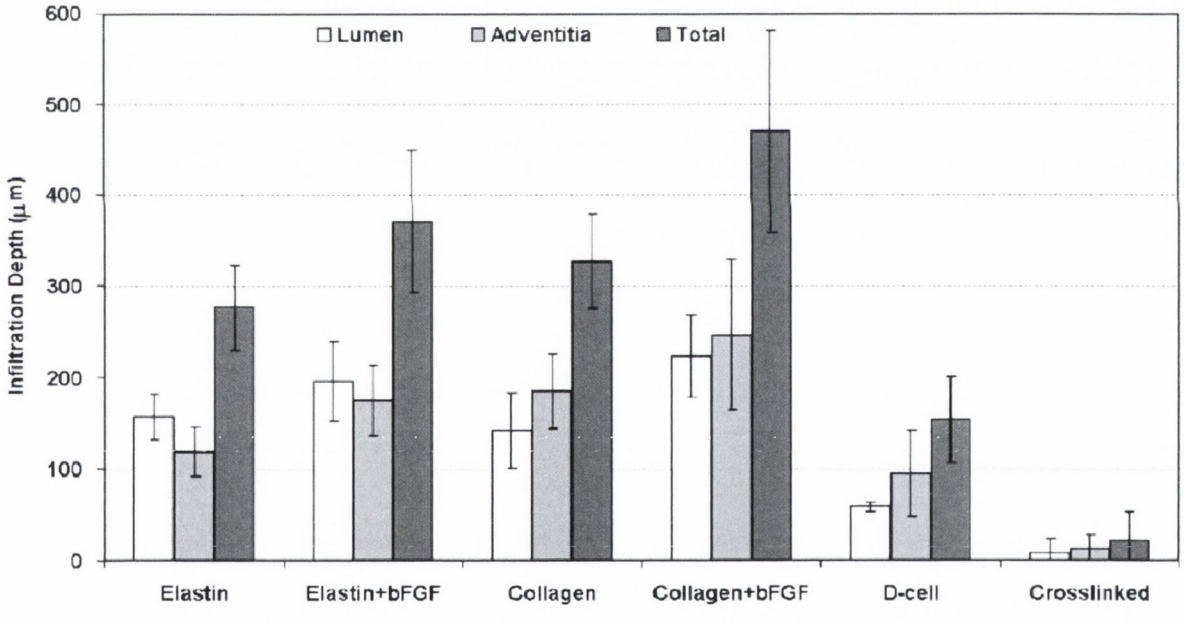

Figure 2.22 Infiltration Depths of Implanted Collagen and Elastin Scaffolds

Subdermal implantation after 28 days showed that the collagen + bFGF scaffold had the greatest infiltration of host cells. The collagen only and elastin only scaffold both displayed increased repopulation compared to the decellularized and crosslinked scaffolds with better performance evident with the addition of bFGF in both scaffolds. (Simionescu et al., 2006)

This interesting result shows the restriction of decellularized scaffolds for host cell integration. This study additionally highlights that under adequate conditions cells will effectively repopulate these scaffolds. This study underlines the potential for these scaffolds but has a number of limitations, namely, subdermal implantation is not representative of the actual *in vivo* environment and associated hemodynamic forces a TEVG will experience. Also the added benefit of using a growth factor to promote migration is promising and has been demonstrated elsewhere. Vascular endothelial growth factor (VEFG) and bFGF have been coated onto decellularized scaffolds to enhance re-endothelialisation, (Conklin et al., 2004, Zhou et al., 2009). However, utilising bFGF in the same manner as the Siminonescu et al study will be limited as it was loaded in an agarose gel and sealed within the lumen before implantation, thus an immediately functioning vessel will not be achieved with this approach. An alternative loading technique may reproduce these results and allow this graft to function in a hemodynamic environment.

The benefits of increasing the porosity to aid cell infiltration are clear but require a fine balancing act between removing ECM components and not adversely affecting the mechanical properties of the scaffold and ultimately *in vivo* performance.

2.8 Construct Maturation

The hemodynamic forces that act on native arteries *in vivo* have been discussed above. These forces act both locally and holistically on the arterial wall by the translation of these forces to vascular cells. As stated above gene expression, vessel tone and chronic remodelling are regulated by the response of ECs to shear stress caused by pulsatile flow, (Davies, 1995, Laughlin et al., 2008). The endothelium acts as a signal transduction interface for these hemodynamic forces. Similarly, SMCs responded directly to the cyclic

stretch on the arterial wall caused by the pressure generated by the pulsatile blood flow (Osol, 1995). This cyclic strain is transferred to the SMCs and in combination with local and systemic biochemical stimuli the SMCs control the vasoactivity of the blood vessel wall.

Investigations with vascular cells and subsequently the development of the vascular tissue engineering field led to the simulation of these hemodynamic forces locally to vascular cells and constructs. Early research by Leung et al showed that mechanical strain can regulate SMC protein synthesis (Leung et al., 1976). Similarly Kim et al were among the first researchers to demonstrate an increase in ECM gene expression and organisation and thus mechanical properties of a tissue engineered construct by exposing seeded SMCs to cyclic strain *in vitro* (Kim et al., 1999). Additionally SMC morphology, alignment and phenotype modulation has been shown to be a function of cyclic mechanical strain (Kanda et al., 1993, Seliktar et al., 2000, Kurpinski et al., 2006). Pulsatile flow bioreactors are the most common methods of simulating these hemodynamic forces for TEVG conditioning. Bioreactors have been routinely used to apply this cyclic mechanical strain and shear stress in order to mature constructs *in vitro* (Barron et al., 2003, Williams and Wick, 2004, Bilodeau et al., 2005, Hahn et al., 2007). A typical bioreactor setup is seen below Figure 2.23. Subjecting a seeded construct to physiologically relevant hemodynamic conditions allows the seeded cells to experience the cyclic mechanical strain necessary to produce cell migration, proliferation, differentiation, ECM synthesis and phenotype modulation while simultaneously providing a consistent nutrient supply to the cells. This method of maturation has been successfully applied to all types of scaffold and cell sources described above. Bioreactor setups vary widely between research groups in relation to scaffold and cell type, seeding techniques and duration.

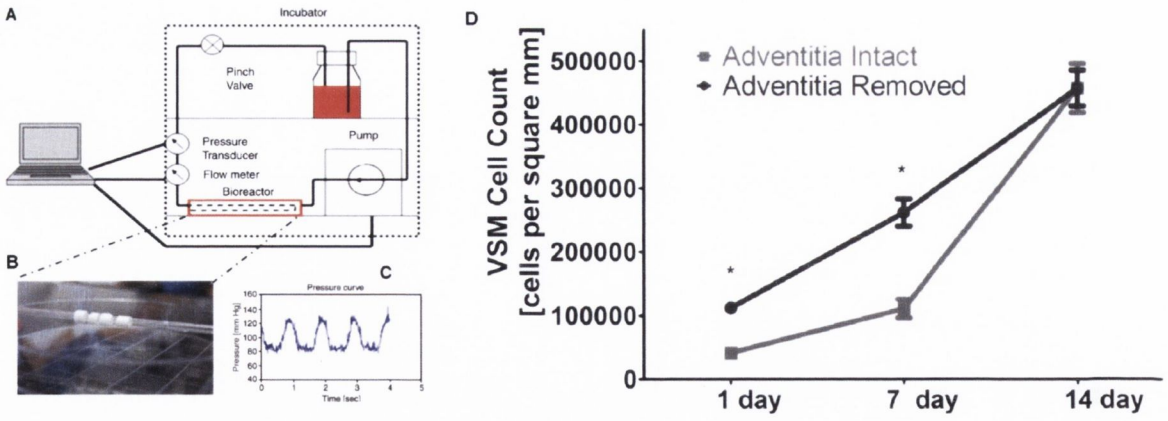

Figure 2.23 Bioreactor Setup

(A) Schematic of the bio-mimetic environment, a peristaltic pump provides pulsatile flow from a culture medium reservoir to the mounted constructs, the entire system is contained within a standard incubator and pressure and flow rates are monitored from an external PC. (B) Constructs are mounted on a polymer tube to receive cyclic strain (C) Pressure profile of pulsatile flow. (D) SMCs numbers increase with time exposed to the cyclic strain for both adventitia intact and removed decellularized vascular scaffolds. (Yazdani et al 2009)

However, the principle of applying physiologically relevant hemodynamic conditions to condition a TEVG and the successful maturation of these constructs in response to these forces is consistent across all research groups. The specific requirements, design features and instrumentation for these bioreactors will be further discussed and investigated in Chapter 6.

Chemical stimuli have also been used to aid cell recruitment and modulate SMC phenotype and hence mature TEVGs *in vitro*. Growth factors such as platelet derived growth factor-BB (PGDF-BB) and VEGF has been shown to promote cell proliferation and migration in attempts to promote angiogenesis *in vivo* (Carmeliet and Conway, 2001, Owens et al., 2004), while TGF-β1 has been shown to inhibit proliferation and promote migration and upregulate SMC contractile proteins (Chan-Park et al., 2009). Fibroblast growth factor has also been proven to aid cell infiltration and promote the maturation of

construct *in vitro* (Kurane et al., 2007). Often these biochemical stimuli are utilised in combination with the mechanical means mentioned above to develop a matured robust TEVG.

2.9 Toward Clinical Applicability

The field of vascular tissue engineering has progressed substantially from the seminal work of Weinberg and Bell in 1986. The processes discussed above, namely the advancement of diverse biomaterials for scaffolds, refinement of bio-mimetic environments, exciting new cell sources and novel seeding techniques have driven the evolution of TEVG development. However, no research group has created a regulatory approved TEVG which demonstrates long term patency rates similar to autologous vessel grafts, produced with clinically relevant times and costs that meets regulatory standards. The incentive of an "off-the-shelf" TEVG for a large patient cohort that is implemented as a standard medical device is the ultimate goal of vascular tissue engineering.

The development of the non-invasive percutaneous catheter based treatment modalities detailed in Section 2.3.2 has proffered new approaches to revascularisation therapies. The continuous development of these technologies has significantly reduced the incidences of death and myocardial infarction with overall improved outcomes (Grines et al., 1993, Serruys et al., 1994, Moses et al., 2003). Nevertheless, the SYNTAX trial investigating the long term outcomes of percutaneous interventions versus CABG have shown that CABG should remain the standard of care for patients with complex lesions (Mohr et al., 2013). Similarly, the FREEDOM trial concluded that for patients with diabetes and advanced coronary artery disease, CABG was superior to percutaneous interventions (Farkouh et al., 2012). The primary outcome in the FREEDOM trial was a combination of death from any cause, nonfatal myocardial infarction, or nonfatal stroke.

Evidently, percutaneous interventions play an integral role in revascularisation therapies with the added advantages of being minimally invasive with reduced costs and quick recovery times. However, the long term preservation of myocardial function and reduction in mortality rates using CABG cannot be overlooked and ensures the prolonged use of coronary bypass grafts well into the future. This further highlights the motivation and clinical need to translate TEVGs from the laboratory to the bedside.

2.9.1 Clinical Success to date

The potential for long term clinical use of a TEVG was first demonstrated by Shin'oka et al in Tokyo in 1999 with the first in man use of a TEVG. The scaffold utilised was a polycaprolactone-polylactic acid copolymer reinforced with woven polyglycolic acid seeded with autologous vascular cells harvested from a peripheral vein (Shin'oka et al., 2001). The 10 mm diameter construct was matured *in vitro* for ten days prior to transplantation to reconstruct a pulmonary artery occlusion in a 4 year old girl with a single ventricle and pulmonary atresia. After 7 months there were no thrombogenic complications, stenosis or obstruction of the TEVG. Although this was a larger diameter conduit of short length used in a low pressure application it is of high significance, as it demonstrates a proof of principle for the clinical translation of tissue engineering techniques. This strategy was repeated with similarly successful results in 22 patients with various congenital heart defects involving single ventricle physiology (Matsumura et al., 2003a). Further patient trials utilised bone marrow cells as a less invasive cell source for scaffold seeding which could be harvested and expanded quicker without the use of xenoserum and was expanded to 42 patients (Shin'oka et al., 2005). After 32 months these patients had fully patent grafts after evaluation for aneurysm or calcification

using cineangiography or computed tomography. Figure 2.24 A-B displays pulmonary angiogram of a patient pre-implantation and six month follow up.

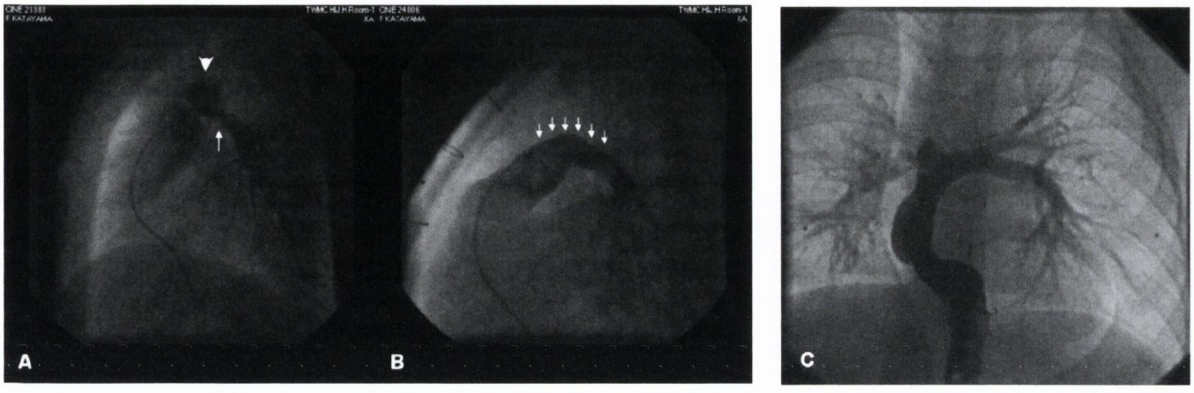

Figure 2.24 Angiograms of Mid and Late Term Follow ups of TEVGs

(A) Pre-implantation stenosis and aneurysm formation is clear (white arrows). (B) TEVG implantation restores blood flow at 6 months. (C) 5 year follow up (different patient) shows no sign of stenosis or aneurysm and a fully patent vessel present. (Shin'oka et al, Hibino et al)

There was one patient death unrelated to the TEVG. The potential for growth, repair and remodelling is evident with these TEVGs with another follow up after 5 years (Figure 2.24 C) with no graft related mortality, aneurysm, calcification, rupture or infection (Hibino et al., 2010). One patient had mural thrombosis (treated with warfarin) and four patients underwent successful angioplasty for stenosis. It should be noted that these patients were predominantly paediatric and therefore had high concentrations of stem cells which may not be as equal in an older patient cohort.

L'Heureux et al have reported on the use of their Liveline™ TEVG created using their completely autologous sheet rolling technique (described in Section 2.5.4), in the formation of an arteriovenous fistula in six patients receiving hemodialysis (L'Heureux et al., 2007). All patients suffered from end stage renal disease and had failing natural arteriovenous fistula after long term hemodialysis. The primary outcome of the study was a patent graft at 3 months after which the graft would be utilised for hemodialysis access.

Patients were evaluated at 3-20 months with mixed results as shown in Figure 2.25 (McAllister et al., 2009).

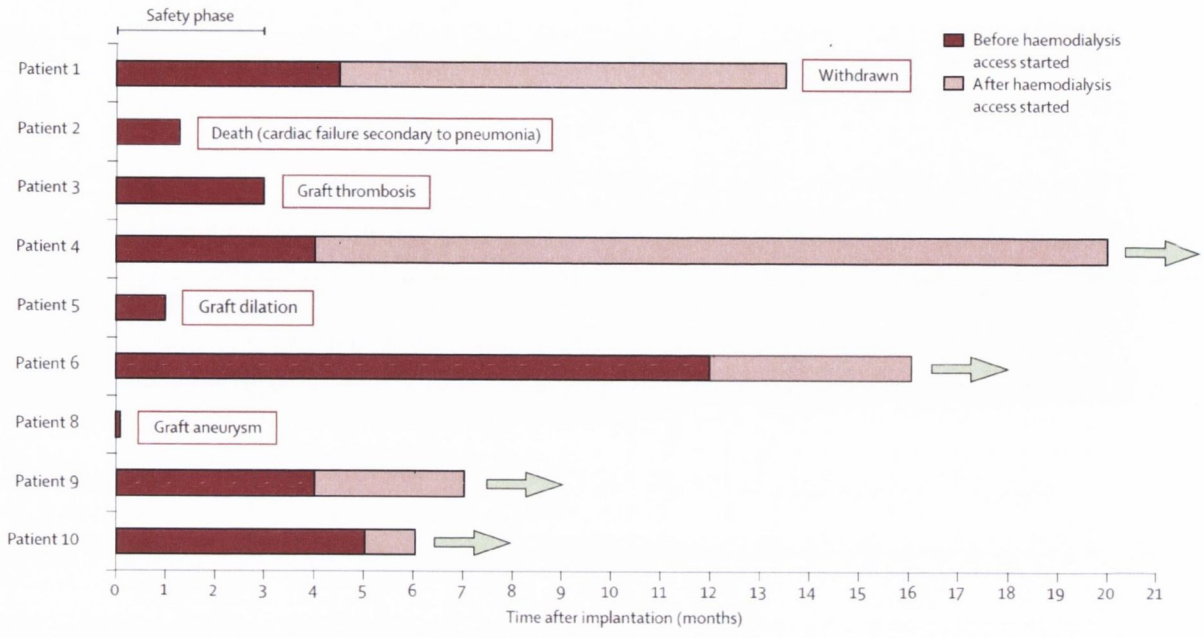

Figure 2.25 Clinical Evaluation of Sheet Based TEVG

Ten patients received sheet rolled TEVGs cultured from autologous cells for use as an arteriovenous fistula for hemodialysis access. (L'Heuruex et al)

One patient was withdrawn immediately prior to implantation due to surgical complications, one patient died from unrelated causes and three patients had graft failure (thrombosis, dilation and aneurysm formation) prior to 3 months. The remaining five patients had functioning grafts at 6-20 months with a total of 68 patient months of patency, (78% primary patency in 7 patients). The results reported by McAllister et al are extremely promising, the three graft failures within three months are consistent with the creation of natural arteriovenous fistulas as the particular patient subgroup is extremely high risk (previously failed dialysis-access grafts, diabetes, controlled hypertension and obesity). The performance of the Lifeline™ vascular graft was successful in an extremely difficult high risk patient subgroup, however the main limitation of the TEVG was the excessive lead times associated with its manufacturing (> 5 months). In an effort to

overcome this limitation the TEVG was recently used in a patient after freezing and devitalisation (Wystrychowski et al., 2011). This allowed for simple storage and transportation of the TEVG and use after only 5 days to endothelialise the lumen surface. The TEVG was implanted as an arteriovenous graft and was functional and patent after 8 weeks. The studies utilising the Lifeline™ graft further highlight the clinical relevance of implementing a TEVG in the clinical setting, however, its performance as an actual bypass graft experiencing physiologic hemodynamics needs to be fully evaluated.

Olausson et al have recently described the clinical use of a TEVG fabricated by repopulating a decellularized vein scaffold with autologous cells (Olausson et al., 2012). Bone marrow stems cells were differentiated into SMCs and EC and seeded onto a decellularized allogenic donor iliac vein, matured in a bioreactor for 2 weeks and subsequently implanted as meso Rex bypass graft for an extrahepatic portal vein obstruction in a 10 year old girl. The graft immediately restored blood flow, see Figure 2.26. Ultrasound examination after 9 months showed sufficient blood supplies, however at 1 year blood flow significantly reduced and although still patent the TEVG was narrowed due to a mechanical obstruction of tissue in the mesocolon.

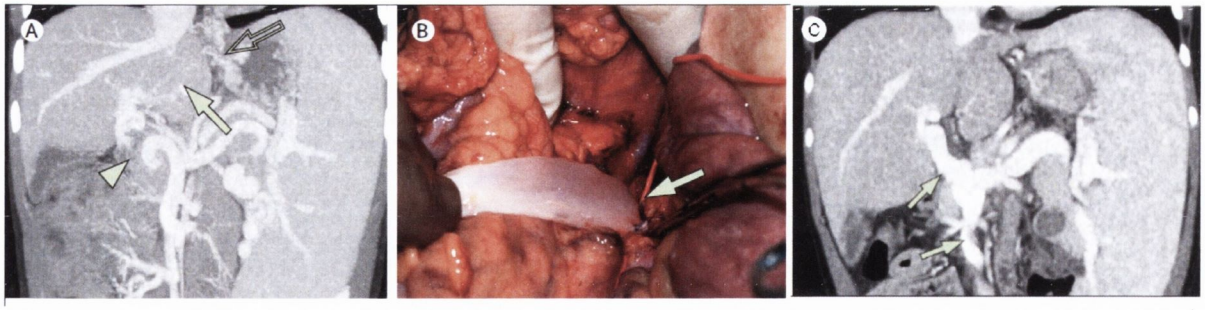

Figure 2.26 Implantation of an Autologous Cell Seeded Decellularized Scaffold
(A) Arrows indicated the extrahepatic portal vein obstruction prior to surgery. (B) TEVG sutured into position. (C) Angiography of TEVG after 1 week showing restoration of blood flow. (Olausson et al)

A second TEVG was subsequently implanted to extend the original length of the graft and prevent further compression. This successfully restored blood flow levels and normal liver function resumed.

Another successful clinical use of decellularized tissue as a scaffold for tissue engineering was reported by Macchiarini et al in the fabrication of replacement trachea for a patient with end-stage bronchomalacia (Macchiarini et al., 2008). Epithelial and MSC derived chondrocytes were seeded onto a decellularized human donor trachea and implanted as a replacement left main bronchus. The graft was fully functional and mechanically stable after 4 months. While the construction of a trachea is obviously very different than any vascular tissue engineering, this study further demonstrates the clinical applicability of utilising decellularized tissue with autologous cell sources.

The above studies clearly demonstrate that tissue engineering techniques for small diameter graft applications can be successfully translated to a clinical setting. However, while these studies were landmark investigations in their fields, fully translating these techniques to a clinical environment still remains some way off. These studies represent proof of concept of the clinical feasibility of TEVG but major hurdles still remain in their full clinical translation. The challenges, limitations and requirements for full clinical translation of TEVG are discussed below.

2.9.2 Requirements for Clinical Translation

Clinical translation of TEVG from the laboratory will require regulatory approval from the relevant regulatory bodies. The path to regulatory approval will vary depending on the jurisdiction, the production method and specific application of the TEVG. Designation may be as a biological device, minimally manipulated tissue or combination device or Class III advanced therapy medicinal product. Nevertheless, TEVGs will have to prove

efficacy and safety in animal models and early clinical trials before approval. Assuming a potential TEVG has demonstrated safety and efficacy i.e. mechanical integrity, immunogenicity and patency rates equal to synthetic grafts, ideally the following requirements will have to be met for the scale up to wide spread clinical use:

1. *Manufacturing Times*

   The use of TEVG for arteriovenous fistulas, peripheral bypass grafts or coronary bypass grafts will require the minimum amount of patient wait time. Fabrication methods of weeks and months are simply not clinically viable, particularly for acute cases of myocardial infarction. Complex manufacturing processes involving autologous cell harvesting and expansion will ultimately be impractical to translate to a hospital setting.

2. *Storage/Shipping/Shelf Life*

   Ideally a TEVG would function similar to any medical device or synthetic graft material in that it can be shipped to and stored in a hospital without any special requirements adding complexity to the process. Room temperature or 4°C storage is the minimum requirement of these products. Handling of the TEVG must not require any additional intricacy. Preferably, TEVGs would not require any special shipping or handling techniques allowing for a realistic shelf life. Furthermore, TEVG regardless of the manufacturing process must be fully sterilisable to allow for packaging and transport and eventual use in an aseptic environment.

3. *Geometric Variations*

   A range of geometric variations must be sufficiently fabricated to manufacture products for a large patient cohort. All bypass grafts will vary in diameter and length and must be sized appropriately to ensure size mismatch doesn't occur.

4. *Quality Control*

Fabrication processes may involve complex techniques of material manipulation or construct maturation, these processes must be reproducible and subjected to full validation to ensure repeatability in quality across all TEVGs.

5. *Viable Cell Sources*

   A feasible cell source that does not add to patient discomfort or require extended expansion time *in vitro* is preferable for clinical translation. Ideally an allogenic cell source should be utilised to eliminate cell harvesting which increases the complexity of the process for autologous cell sources. Also, any cells used in the fabrication process would ideally be cultured without the use of xenoserum which is in widespread use currently for cell culture, as it has been associated with rare immune responses and transmission of diseases such as bovine spongiform encephalopathy (Mogues et al., 2005, Peck et al., 2012).

6. *Economic Feasibility*

   The most important factor in the clinical translation of TEVG is the cost associated with their fabrication. Taking all of the above factors into consideration the overall cost of creating a TEVG must be kept to a minimum. This will make many of the current fabrication techniques redundant as it is difficult to imagine excessive manufacturing times (months) being economically viable. Reimbursement potential of a TEVG will be dependent on the efficacy and cost-effectiveness of the treatment in comparison to other options. Current costs of CABG in the United States is roughly US$20,000 per surgery (Eisenberg et al., 2005) and PTFE grafts for hemodialysis access currently cost US$6700 more to maintain than native vein fistulas (McAllister et al., 2008). These figures establish the market within which TEVGs must perform to demonstrate economic feasibility within healthcare systems.

2.10 Conclusion

The literature discussed in this review has detailed the structure-function relationship between vascular cells and the individual ECM components of the native arterial wall and the hemodynamic forces which they experience *in vivo*. Understanding these forces and the interaction of these components, in both healthy and diseased states is essential in attempting to fabricate a TEVG.

A number of differing and successful techniques have been developed to create TEVGs, however no research group/company has yet succeeded in translating these techniques to a regulatory approved clinical setting. The importance of stable and mature ECM components has been highlighted, particularly the elastin network which has been a notable pitfall in the *in vitro* production of TEVGs to date. Viable cell sources, inefficient seeding techniques, lengthy manufacturing times, sustainable shelf life and high costs have been underlined as the limiting factors in preventing clinical translation of TEVGs.

The application of decellularized exogenous tissue offers an attractive alternative to other vascular scaffolds as it already contains a relevant ECM. The main challenge in utilising a decellularized arterial scaffold is the high tissue density which results in inefficient cell repopulation. Techniques to overcome this hurdle have proved positive with further physical manipulation to increase porosity and the combination of growth factors to increase cell infiltration. Refining these techniques to fully overcome these issues could potentially see decellularized tissue become the scaffold of choice for TEVGs. The readily available, multi dimensional characteristics and ideal mechanical properties offers decellularized tissue the potential to produce "off-the-shelf" patient specific TEVGs and bridge the translation to clinical use.

Chapter 3 Customisation and Mechanical Quantification of Decellularized Porcine Arterial Tissue

The results in this chapter have been published as the following papers:

SHERIDAN, W. S., DUFFY, G. P. & MURPHY, B. P. 2012. Injection techniques for bulk cell seeding decellularized vascular scaffolds. *International Journal of Nano and Biomaterials,* 4, 96-107.

SHERIDAN, W. S., DUFFY, G. P. & MURPHY, B. P. 2012. Mechanical characterization of a customized decellularized scaffold for vascular tissue engineering. *Journal of the Mechanical Behavior of Biomedical Materials*, 8, 58-70.

3.1 Introduction

Substantial progress has been made in the field of tissue engineering to address the clinical need, (as highlighted in Chapter 2) for a TEVG for small diameter applications (Niklason et al., 1999, L'Heureux et al., 2006, Zhao et al., 2010). Decellularized exogenous tissue demonstrates promise for use as a vascular scaffold for the reasons discussed in Chapter 2. A major drawback of decellularized tissue remains; namely the matrix that is left behind after decellularization is extremely dense and can prove difficult to infiltrate with cells, particularly SMCs in the medial layer (Lu et al., 2004, Neff et al., 2011). Poorly repopulated scaffolds have resulted in less than ideal mechanical properties and diminished *in vivo* performance (Cho et al., 2005, Villalona et al., 2010). Furthermore, the highly dense nature of decellularized tissue has lead to excessive cell seeding and culture times to mature these constructs *in vitro*, which is not a tenable solution for successful clinical translation.

The aim of this chapter is to modify and mechanically characterise decellularized porcine arterial tissue for use as a scaffold for the creation of a TEVG. To overcome the major limitation of slow repopulation a novel method of directly injecting cells within the medial layer of the decellularized scaffold was investigated. This injection technique involves inserting needles into the wall of the native tissue prior to and during the decellularization process, allowing a means of rapidly bulk seeding the scaffold with cells. In conjunction with this, reducing the overall density of the scaffold to aid cell infiltration upon repopulation was also examined. Owing to the importance of the elastin network and its implication on mechanical properties such as compliance, collagen was chosen to be digested from the scaffold in order to reduce the scaffold density. These modifications will ideally maintain scaffold integrity and potentially overcome current

tissue engineering shortcomings of unsuitable mechanical properties, incomplete cell seeding and excessive cell seeding times.

3.2 Material and methods

3.2.1 Tissue Harvest

Carotid arteries were freshly harvested from 70-90kg pigs in a local abattoir (Lislin Meats Ltd, Mullagh, Co. Cavan, Ireland). Common carotid arteries 5-7 mm in diameter were extracted from each pig using sterile instruments and subsequently rinsed in phosphate buffered saline (PBS). All arteries were returned to the laboratory stored in PBS on ice. Samples were prepared by removing excess connective and adventitial tissue and cut into approximately 30mm long lengths (Figure 3.1 A-B). All samples were then frozen in PBS for later use as it has been previously shown frozen storage does not significantly affect artery mechanics (Stemper et al., 2007).

3.2.2 Decellularization

The method used to decellularize the arterial tissue was adapted from a protocol described in the literature (Amiel et al., 2006). The protocol consists of an enzymatic digestion and detergent extraction. Firstly, samples were immersed in de-ionized water for 24 h at 4°C. Samples were then incubated in 0.05% Trypsin with 0.02% EDTA (Sigma-Aldrich, Ireland) for 1 h at 37°C. After a short rinse in PBS to remove excess trypsin, the samples were placed in a solution of 2% Triton X-100 and 0.8% ammonium hydroxide (Sigma-Aldrich, Ireland) in de-ionized water for 72 h at 4°C. To ensure the elimination of all disrupted cellular material this solution was changed every 24 h. A final wash sequence of 48 h in de-ionized water with a change after 24 h was carried out to remove all residual chemicals used in the decellularization process. Each step in the above protocol (except

trypsin incubation) was carried out under constant rotational agitation to maximize chemical exposure to the tissue (Figure 3.1 B).

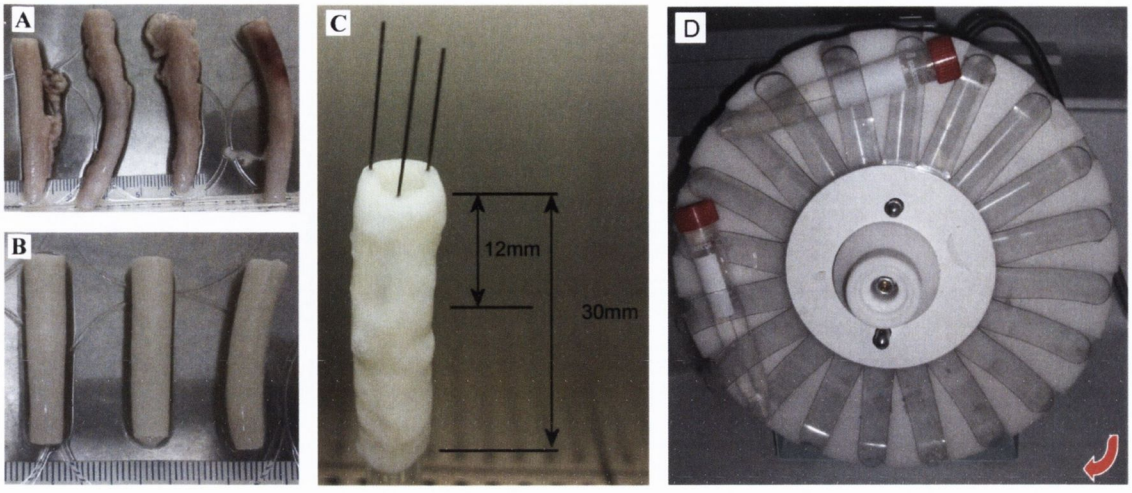

Figure 3.1 Injection Channel Creation with Micro-Needles

(A) Freshly harvested native tissue (B) Native tissue is cleaned of excess connective and adventitial tissue and cut to 30 mm sections. (C) Three micro-needles are inserted into the transverse wall of the native tissue prior to decellularization and remain in situ for the entire duration of decellularization. (B) Decellularization occurs under rotational agitation within 15 ml Falcon tubes

3.2.3 Decellularized Tissue with Micro-needles/Injection Channels

A method was developed to create an injection channel within the scaffold which provides an entry point or route for cell injection within the intact medial layer. This was undertaken with further tissue manipulation by the insertion of three small bore micro-needles (300μm outer diameter, 190 μm inner diameter) into the transverse section of the native tissue. These needles were inserted at approximately 120° circumferentially to each other into the arterial wall and directed longitudinally along the sample within the medial layer to a distance of 12 mm from the insertion point (Figure 3.1 C). The samples were then subjected to the same decellularization protocol as described above. Samples were maintained in their natural cylindrical configuration, with the three micro-needles within the media at all stages of the decellularization protocol.

3.2.4 Collagen Digested Tissue

To investigate reducing the density of the decellularized tissue further customisation was carried out by removing varying amounts of collagen after the decellularization process. Sodium hydroxide (NaOH) was used to digest the collagen. NaOH has been used previously to digest collagen in preparation of samples for scanning electron microscopy (Crissman, 1987). The above decellularization protocol was followed with one additional step of subjecting the samples to sonication in 0.5M NaOH prior to the final wash sequence. Two groups were subjected to sonication for 15 mins and 90 mins respectively. A third group was sonicated for 120 mins combined with mechanical agitation in 0.1M NaOH for 24 h at room temperature.

3.2.5 Scanning Electron Microscopy (SEM)

Native tissue and collagen digested decellularized scaffolds with injection channels were examined by SEM. Native tissue and decellularized scaffolds were fixed in 2.5% buffered glutaraldehyde for 24 h. These samples were maintained in their cylindrical configuration and the needles were maintained in situ throughout. Needles were then removed and the samples were washed separately three times in PBS for 15 mins. Then, each section was subjected to sequential washes of 30%, 50%, 70%, 90% and 100% ethanol for 15 mins with the final wash performed three times. The dried samples were mounted on an aluminium stub and sputter coated with gold. SEM (Zeiss Ultra Plus, Germany) was used to view the ultrastructure of the medial layer of the native and decellularized samples and specifically the injection channels.

3.2.6 Scaffold Cytotoxicity

In order to assess if any residual chemicals remain within the scaffold after decellularization, which could lead to scaffold cytotoxicity, an MTT Cell Growth Assay (Millipore ™, Ireland) was performed. This assay is based on the conversion of MTT into formazan crystals by living cells, which determines mitochondrial activity. 4,000 Rat mesenchymal stem cells (rMSCs) were seeded into the wells of a 96 well plate and cultured for 24 h in 100µl rMSC culture medium (DMEM, formulation D5671, Sigma-Aldrich, Ireland) supplemented with 10% foetal bovine serum (FBS, Biosera), 2% penicillin/streptomycin (Sigma), 1% L-glutamine (Sigma), 1% GlutaMAX (Gibco BioSciences) and 1% non-essential amino acids (Gibco BioSciences)). Native tissue, decellularized scaffold, collagen digested scaffold, a sample of Polyvinyl chloride (PVC) and high density polyethylene (HDPE) were soaked in culture medium for 24 h. The PVC was selected as a positive control as it is a known cytotoxic material and HDPE as the negative control as it is a known non-cytotoxic material. After 24 h the medium of the cultured rMSCs was replaced with an extract of medium from the soaked samples which was cultured for a further 24 h at 37°C. Three extracts were taken for each material and performed in duplicate. 10 µl of MTT reagent was then added to each well with 90 µl of medium and mixed by gentle tapping of the tray. After incubation for an additional 4 h at 37°C the MTT reaction medium was removed and blue formazan was solubilised by 100 µl dimethylsulfoxide (DMSO). Absorbance was measured at 570 nm with a reference wavelength of 630 nm with the HDPE seeded cells serving as a 100% viability control.

3.2.7 DNA Quantification

The residual DNA content of the decellularized scaffold was determined using a Quant-iT™ PicoGreen dsDNA kit (Invitrogen, Biosciences, Dublin, Ireland) in accordance with

the manufacturer's instructions. Briefly, samples of native tissue and decellularized scaffolds were lyophilized, weighed, and digested in papain (125mg/ml) in 0.1 M sodium acetate, 5 mM cysteine HCl, 0.05 M EDTA, pH 6.0 (all from Sigma-Aldrich, Ireland) at 60°C under constant rotation for 18 hours. The papain sample solution was diluted with TE buffer (10 mM Tris-HCl, 1 mM EDTA, pH 7.5, Invitrogen) and incubated with an equal volume of Picogreen™ working solution. Sample fluorescence was measured (excitation 480 nm, emission 538 nm), DNA concentration deduced using a standard curve and average values expressed as μg DNA/mg dry weight (n=3).

3.2.8 Mechanical Testing

Uniaxial tensile tests were carried out to determine the mechanical response of the native tissue and decellularized scaffolds using a Zwick tensile testing machine (Zwick Z005, Roell, Germany). The following groups (n=10 each) were tested:

1. Native tissue.
2. Decellularized Scaffold.
3. Decellularized Scaffold with injection channels.
4. Collagen digested tissue
    a) 15 mins sonication.
    b) 15 mins sonication with injection channels.
    c) 90 mins sonication.
    d) 120 mins sonication and 24 h mechanical agitation.

Two ring sections 4mm long were cut from each specimen and tensile tested to failure using a 100N load cell. Custom made grips were machined which contained 1mm diameter protruding stainless steel rods which aligned parallel for mounting the ring

sections. The tests were undertaken at a constant displacement rate of 2mm/min in a PBS bath at room temperature. All samples were preconditioned to a crosshead displacement of 0.1mm (corresponding to ~10% strain). Tissue displacement was determined by the use of video extensometer tracking of dots, which were applied to the transverse wall of the ring section. These dots (approximately 1 mm diameter) were applied with red permanent marker to the wall section roughly 1mm apart. Two dots were applied on each side of the sample wall in this manner and aligned parallel when placed on the bars of the grips of the tensile testing machine (Figure 3.2). The video was triggered at the commencement of movement of the crosshead and a custom frame grabbing program recorded images of the test at a rate of 1frame/second with a time stamp embedded in the recorded file name.

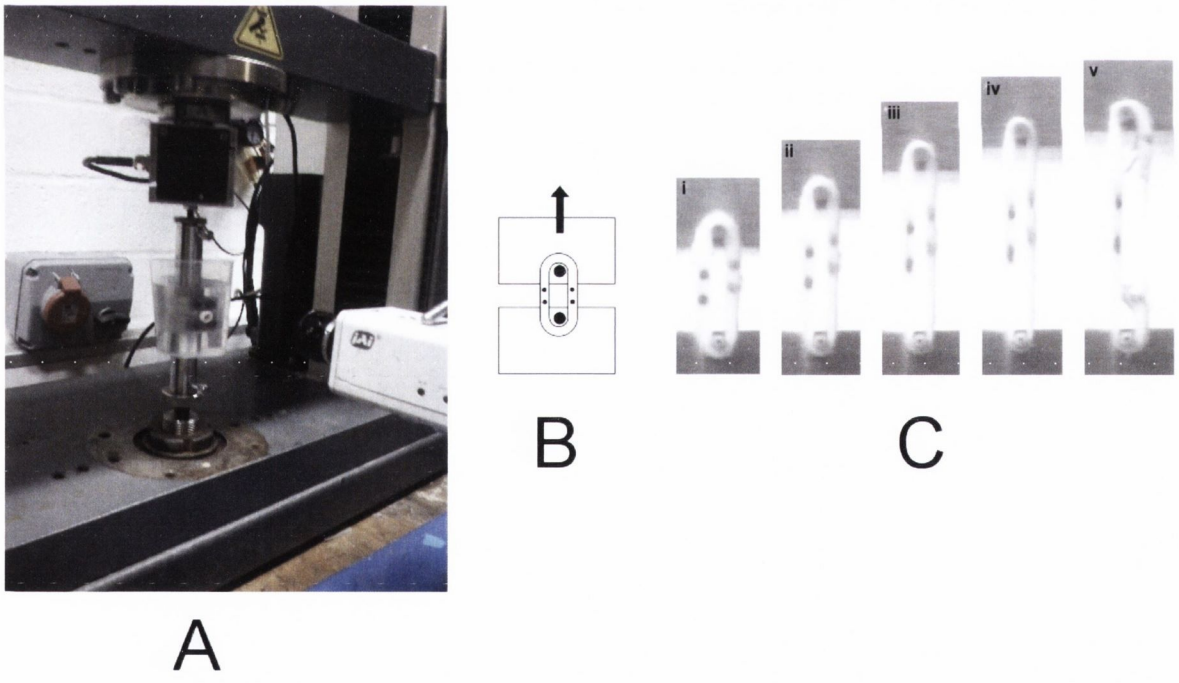

Figure 3.2 Mechanical Test Setup

(A) 4 mm ring section marked with dots is mounted on protruding 1 mm rods on custom built grips and tensile tested at 2mm/min. The entire test is captured for video extensometer tracking. (B) Illustration of loaded sample on grips. (C) Image sequence of a typical test showing sample extension and dot movement to failure.

This allowed for the tracking of the dots on the tissue, and the calculation of their relative displacement by analysing the recorded images. ImageJ software (US National Institutes of Health) was used to determine the centroid of each dot for each individual frame and hence calculate the relative displacement.

True stress (σ) and true strain (ε) were calculated using the following formulae:

$$\sigma = \frac{F(t)}{A_0 \frac{L_0}{L(t)}} \qquad \text{(Eqn 3.1)}$$

$$\varepsilon = \ln\left(\frac{L(t)}{L_0}\right) \qquad \text{(Eqn 3.2)}$$

Where F(t) is the measured force at time t, A_0 is the initial cross-sectional area, L_0 is the initial displacement (distance between two vertical dots in the first frame) and L(t) is the displacement at time t. L_0 is determined after the preconditioning cycle by manually moving the crosshead until the dots align vertically and parallel to the central axis of the test machine. The test commenced once the force was zeroed in this position. L_0 was determined in this manner due to the variability within samples in the small strain region of the stress-strain curve. This variability is largely due to the dimension variations (diameters, wall thickness and collagen content may vary slightly between samples). The displacement between the dots is measured by calculating the vertical distance between the centroid of each dot.

The mechanical response of the tested samples was observed by generating the stress-strain curves from the tensile test data (Figure 3.3). All data was averaged for the applied 3rd order fitted polynomial equation to the test data at strain intervals up to the maximum strain at failure for each group. For each group described above the strain at

failure and ultimate tensile strength (UTS) was also recorded. The slope of the fitted linear responses to the first third and last third of the stress strain data defined the moduli for the collagen and elastin dominant phases (see Figure 3.3 B for an example of determining the moduli of the two regions).

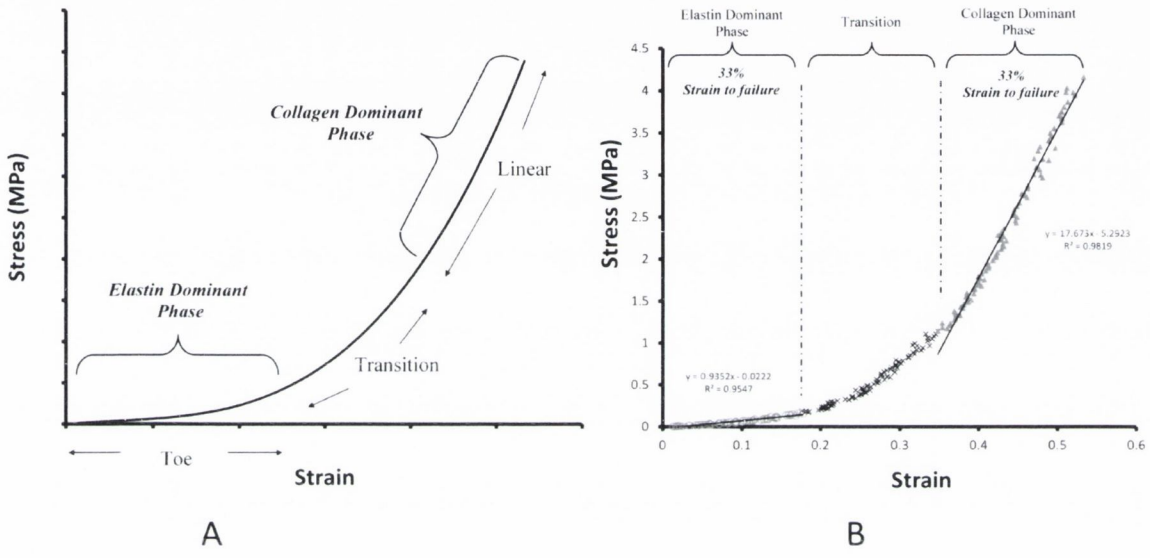

Figure 3.3 Typical Mechanical Response of Tensile Testing Ring Specimen

(A) Typical bi-phasic tensile response of arterial tissue displaying the elastin dominant phase (toe region) and collagen dominant phase (final linear region). (B) Sample response of a tested specimen with linear responses fitted to the first and last 33% of the curve marking the elastin dominant phase and collagen dominant phase respectively.

3.2.9 Scaffold Repopulation with SMCs

Initial scaffold repopulation was carried out to determine the feasibility of using the injection channels as a means of bulk cell seeding the decellularized scaffold. This was undertaken with the non-collagen digested scaffolds which were prepared as described in Section 3.2.3. The micro-needles were flushed and soaked for 1 h in 100% ethanol and prior to insertion within the native tissue they were flushed with PBS to remove all

ethanol to ensure there was no affect on cell viability at injection. This was carried out under sterile conditions in a class II safety cabinet. Furthermore, all PBS and trypsin used in the decellularization process was maintained in sterile conditions and the decellularization solution and de-ionized water was passed through a 0.2 μm filter to ensure no contamination occurred. Rat SMCs (ECACC, Salisbury, UK) were used for this initial investigation into the feasibility of the injection channels. The rat aortic SMCs were expanded initially in Rat Smooth Muscle Growth Medium (same source) and then in low-glucose Dulbecco's modified Eagle Medium (D6046 formulation, Sigma-Aldrich, Ireland) supplemented with 10% foetal bovine serum and 2 % penicillin/streptomycin.

The rSMCs were cultured in an incubator at 37°C, 5% CO2, and 95% relative humidity. The cells used for seeding experiments were between passages 5 and 9. Four different cell injections were carried out. The injections (n=3 each) consisted of:

Group I 500,000 cells in 0.1ml solution examined at time points of 2 h and 24 h.

Group II 2×10^6 cells in 0.1ml solution examined at time points of 2 h and 24 h.

Group III 4×10^6 cells in 0.1ml solution examined at time points of 2 h and 24 h.

Group IV 3×10^6 cells in 0.1ml solution with high pressure injection examined at time points of 2 h and 24 h.

The 2 h time point was chosen for an initial investigation, to determine the outcome of the cells immediately after injection. The longer time point was chosen to demonstrate that the cells were stable and viable after 24 h, and to determine if there was any movement of cells away from the injection site toward the nutrient supply.

Cells were fluorescently labelled using PKH26 Red Fluorescent Cell Linker Kit (Sigma-Aldrich, Inc). Labelling was carried out according to the manufacturers' instructions. This product is for general cell membrane labelling that incorporates a

fluorescent dye with long aliphatic tails (PKH26) into lipid regions of the cell membrane. All cell injections were carried out within a class II safety cabinet in a fully aseptic environment. The desired cell concentration was measured and drawn into a standard 1ml Luer lock syringe, which was subsequently connected directly to the needle within the scaffold, allowing for cell delivery from the syringe with minimal handling of the scaffold. One needle was injected on each scaffold, with the other two non-injected needles removed after the removal of the first needle, the non-injected needles act as controls on each scaffold. Once the syringe was connected to the *in situ* needle, the needle was gradually retracted as the plunger on the syringe was pressed gently; this allowed for a gradual smooth delivery of the cells as the needle itself was removed. Once injected each construct was left standing vertically for 30 mins to allow for cells to settle and to begin adhesion to the scaffold. After 30 mins tissue culture media was added and the constructs were incubated for 2 h and 24 h respectively. Group (IV) scaffolds were injected at much higher pressure, instead of allowing a gradual removal of cells from the syringe the plunger was forced to expel the cell solution quickly at high pressure.

3.2.10 Scaffold Repopulation with Human SMCs

A second set of repopulation experiments was under taken using hSMCs in order to demonstrate the feasibility of bulk cell seeding the decellularized scaffolds using the injection channels with a human cell source. The collagen digested scaffolds were also repopulated with hSMCs to investigate if a reduction in scaffold density increased cell infiltration. hSMCs were cultured in standard tissue culture flasks using Dulbecco's Modified Eagle Medium (D6046 formulation, Sigma-Aldrich, Ireland) supplemented with 10% foetal bovine serum, 1% L-glutamine and 2% penicillin/streptomycin. Media was changed every 3 days and cells were removed from flasks using trypsin-EDTA solution.

Cells were expanded and all seeding experiments were undertaken between passages 6-10. Cell number was calculated using a haemocytometer.

The following groups were investigated for repopulation (n = 2 each):

Group I Decellularized scaffold at 2 h time point.

Group II Collagen digested scaffold with 15 mins sonication in NaOH at 2 h time point.

Group III Collagen digested scaffold with 90 mins sonication in NaOH at 2 h time point.

Group IV Collagen digested scaffold with 90 mins sonication in NaOH at 24 h time point.

Groups I, II & III consisted of scaffolds 10 mm in length while Group IV scaffolds were 30 mm long. Decellularization of porcine carotid arteries and injection channel creation was carried out as described above; the only alteration that occurred was that all processing steps were carried out under sterile conditions. Two hours before cell injection the scaffolds were soaked in sterile cell culture media and incubated at 37° C with 5 % CO_2.

The 10 mm long constructs were injected at a concentration of 500,000 cells/0.05ml media in each needle. The needles were removed from the tissue as the cells were simultaneously injected through the medial cavities. Injected scaffolds were left standing vertically for 30 mins to allow for cells to settle and to begin adhesion to the scaffold. After 30 mins cell culture media was added and the constructs were incubated for 2 h. The 30 mm long scaffolds were injected with 1 X 10^6 cells/0.1ml media in each needle in the same manner. After 30 mins the injected scaffolds were incubated for 24 h.

3.2.11 Histology

5mm ring segments were taken from each tested sample group for histological analysis. Samples were embedded in paraffin wax in an automatic tissue processor (ASP300, Leica, Germany). The needles were removed from samples before processing of the decellularized tissue with injection channels. All samples were sectioned longitudinally using a rotary microtome (Leica microtome, Leica, Germany). 7μm sections were cut and collected on glass slides and subsequently washed through a graded series of ethanol from 100 to 70% (v/v). Samples of native and decellularized tissue were stained using Hematoxylin and Eosin (H&E), Masson's Trichrome and Picrosirius Red. To further verify cell removal, sections were stained with diamidino-2-phenylindole (DAPI). Sections were dehydrated and cleaned in ascending concentrations of ethanol and xylene before coverslips were mounted (DPX mountant, BDH).

The cell injected scaffolds were removed from the incubator at each time point, embedded in OCT compound (Tissue Tek) and snap frozen in liquid nitrogen for cryostat sectioning. The constructs were maintained in their vertical configuration throughout. Cryostat sectioning was utilised as the PKH26 dye added to the cells is eliminated by the paraffin embedding process. After snap freezing the samples were stored at -80°C until sectioning. All samples were sectioned longitudinally using a rotary cryostat (Leica microtome, Leica, Germany). 7μm sections were cut and collected on glass slides. Slides were washed in PBS to remove excess OCT compound and mounted in Vectashield Mounting Media with DAPI. Observation under light and fluorescent microscopy and digital image acquisition was carried out with an inverted microscope (Olympus IX 71) for both the wax embedded and cryosectioned samples. DAPI stained sections had excitation at 360nm and emission at 460 nm and the PKH26 labelled sections had excitation at 551nm and emission at 567nm.

3.2.12 Statistics

Results are presented as mean ± standard deviation for the mechanical testing. A Student's T-test was used to test significance between specific cases, results were considered significantly different at $p < 0.05$. For each group tested the mechanical tests comprised 5 specimens with two ring sections tested from each sample. This accounts for n=5, however, similar trends were witnessed from both ring sections on each specimen, resulting in an effective n=10 for each group.

3.3 Results

3.3.1 Decellularization

Histological examination of both native arterial tissue and tissue subjected to the decellularization process is shown in Figure 3.4. H&E staining of the native tissue displayed the characteristic medial lamellar units of SMCs surrounded by collagen fibers within concentric layers of elastin (ECM stains pink, cells black). Decellularized tissue confirmed complete removal of native vascular cells, with an intact porous matrix of multiple concentric layers of collagen and elastin remaining (Figure 3.4 A-B). The wall thickness decreased with removal of cells. Masson's Trichrome stain further verified cell removal by the absence of stained cytoplasm in the decellularized tissue (cytoplasm stains pink and collagen blue). The morphology of the matrix is more visible with this collagen specific stain, the bundles of collagen fibers are seen tightly packed in the native tissue. The absence of SMCs in the decellularized tissue allows the collagen fibers to loosen but still maintain their circumferential orientation (Figure 3.4 C-D).

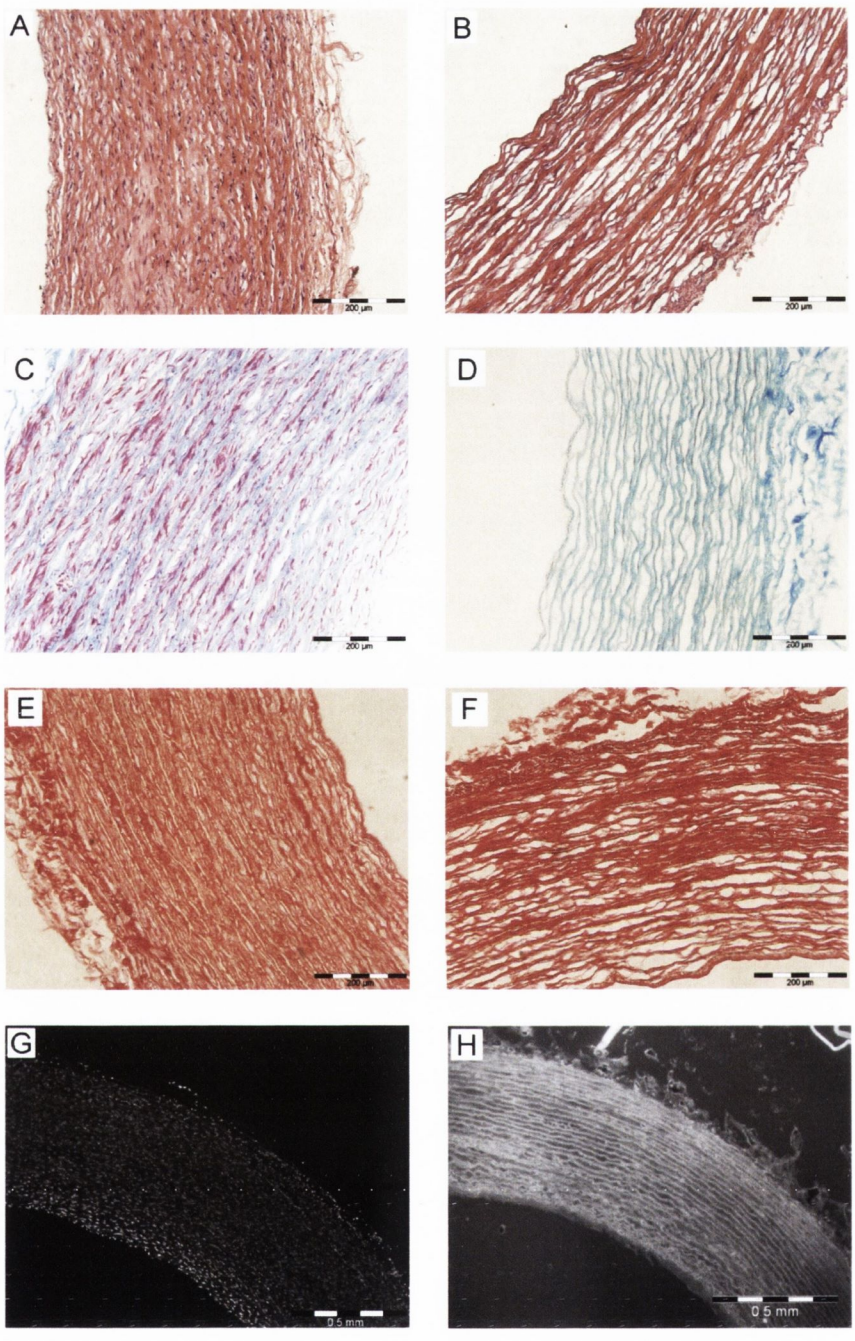

Figure 3.4 Decellularization of Porcine Carotid Arteries

Histology of porcine carotid arterial tissue before (A,C,E,G) and after (B,D,F,H) decellularization. (A) H&E stained native artery showing cell configuration and structure of ECM components. (B) Decellularization shows removal of cells and remaining porous ECM. (C) Masson's Trichrome stain displays high cell density embedded in collagenous ECM. (D) Complete cell removal and remaining undisrupted collagen fiber network. (E) Picrosirius Red stain of native tissue shows dense collagen content. (F) After decellularization a porous collagen structure remains. (G) DAPI stain shows highly cellular native tissue. (H) After decellularization DAPI reveals no cells or cell remnants.

Closer examination of the collagen after decellularization by Picrosirius Red staining showed the presence of smaller collagen fibers (collagen stains red) not visible with the Masson's Trichrome stain. The native tissue once again displayed the tight packing of the collageneous ECM (Figure 3.4 E-F). The pores created by the removal of the cells are seen to contain small collagen fibers resulting in a porous but highly dense matrix after decellularization. DAPI staining was used to further verify the removal of all cells and cell remnants. The circumferential alignment and orientation of the SMCs nuclei was visible in the native tissue with no visible fluorescent material in the decellularized tissue (Figure 3.4 G-H).

3.3.2 Decellularized Scaffold with Injection Channels

In this part of the study three 300μm diameter nitinol needles were successfully inserted into the wall of the native tissue prior to decellularization. None of the needles penetrated the vessel wall. The needles were inserted at approximately 120° circumferentially to each other. The addition of the needles did not hinder the process of decellularization as can be seen in Figure 3.5. H & E staining confirmed the removal of all cells from the tissue and this was additionally verified with DAPI staining (Figure 3.5 C). The ultrastructure of the tissue did not appear altered by the addition of the needles. The concentric layers of collagen and elastin were visible in the same configuration as the decellularized tissue without needles (Figure 3.5 A).

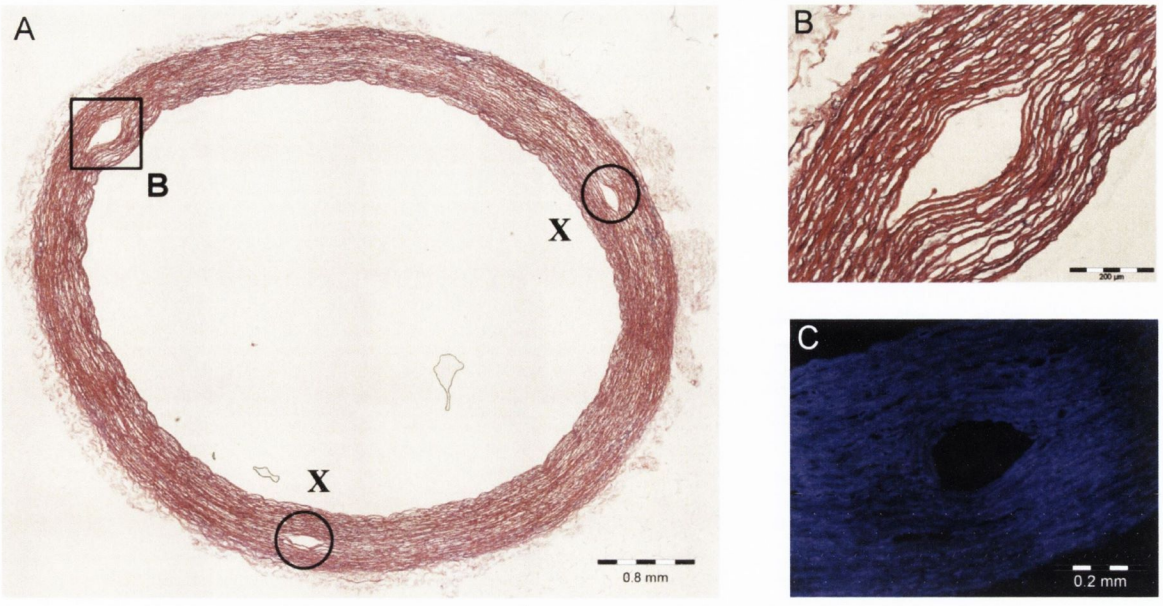

Figure 3.5 Injection Channel Creation

(A) H&E stain of entire scaffold section showing ECM structure and three injection channels. X denotes injection channels (B) Higher magnification H& E stain of an individual injection channel showing an elliptical structure with minimal localized ECM disruption and separation of elastin sheets. (C) DAPI stained section of an injection channel showing no affect on decellularization process due to incorporation of an injection channel.

Three cavities or channels were evident at the locations of the inserted needles in the medial layer. These channels were elliptical in shape with major axis of approximately 275μm and a minor axis of 125μm. The channels displayed minimal damage to the ECM components along the length of the tissue, and maintained their open configuration upon needle removal. The needles were inserted within a lamellar unit and appeared to spread or widen this layer as they were inserted further down the length of the tissue. The channel expanded the surrounding tissue without cutting or shearing any of the bundles of collagen fibers or elastin sheets, resulting in extremely localized and minimal matrix disruption (Figure 3.5 B).

3.3.3 Collagen Digested Scaffolds

Picrosirius Red staining of the four collagen digested groups described above is shown in Figure 3.6 and reveals the highly dense nature of the collagen network in the native tissue. After decellularization a porous 3-D network of collagen remained. Collagen digested scaffolds subjected to 15 mins sonication in NaOH created a more porous scaffold. A great deal of the small collagen fibers were digested and removed from the tissue which created a matrix with an obvious increase in porosity (Figure 3.6 C). Digestion of the large collagen fibers was not apparent and the overall collagen network appeared fully intact. Decellularized scaffolds with injection channels subjected to 15 mins sonication in NaOH had a similar increase in porosity as a result of the collagen digestion. The injection channels created by the needles appeared identical to those in the decellularized scaffold, causing minimal disruption to the surrounding ECM (Figure 3.6 D). The trend of increasing porosity with collagen digestion continued in the 90 mins sonication group. Small collagen fibers are almost entirely removed from these samples and a major increase in the overall porosity of the scaffold is apparent. The large collagen fibers appear slightly reduced in diameter and stained much weaker, however the overall collagen network remained intact (Figure 3.6 E).

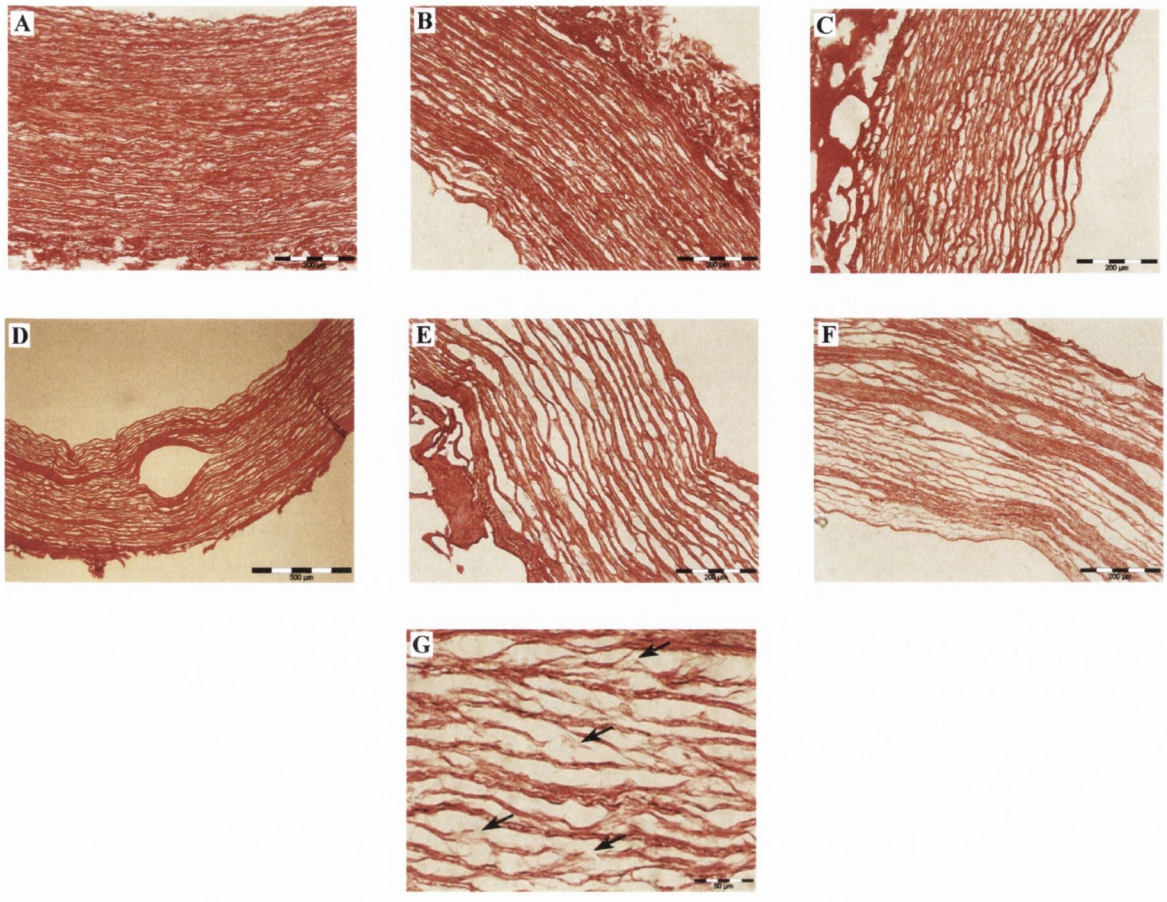

Figure 3.6 Collagen Digestion of Native Tissue and Decellularized Scaffolds

(A) Native tissue displaying highly dense collagenous ECM. (B) Decellularization reveals a porous architecture and dense collagen network. (C) 15 mins sonication in NaOH showing increased porosity with digestion and removal of small collagen fibers evident. (D) Creation of injection channel does not affect mechanism of collagen digestion (E) 90 mins sonication in NaOH shows removal of all small collagen fibers with the collagen fiber bundle network intact. (F) Samples digested with 120 mins sonication & 24 h agitation in NaOH showed weak staining and a disrupted collagen fiber bundle network. (G) High magnification highlights this disrupted collagen network and breakdown of collagen fiber bundles after 120 mins sonication and 24 h agitation in NaOH, arrows indicate collagen fiber bundle rupture.

Large scale disruption was evident in the final group which were subjected to 120 mins sonication in NaOH and 24 h mechanical agitation. The remaining collagen in these samples stained very weakly and there was an obvious large scale reduction in the diameter of the collagen fiber network which was consistent across the scaffold wall

(Figure 3.6 F). Rupture of the collagen fiber network was visible throughout the scaffold. This is particularly evident when the stained sections are viewed at a higher magnification. At numerous locations across the scaffold the disintegration of the collagen fiber network was noticeable with the unravelling of bundles of collagen and actual rupture of fibers as indicated with arrows (Figure 3.6 G).

3.3.4 Scanning Electron Microscopy (SEM)

The SEM images further confirmed the decellularization process. Individual cells cannot be identified in the native tissue; however, the highly dense, compacted nature of the ECM components was evident (Figure 3.7 A). The porous nature of the decellularized scaffold due to the removal of cells after decellularization was clear (Figure 3.7 B).

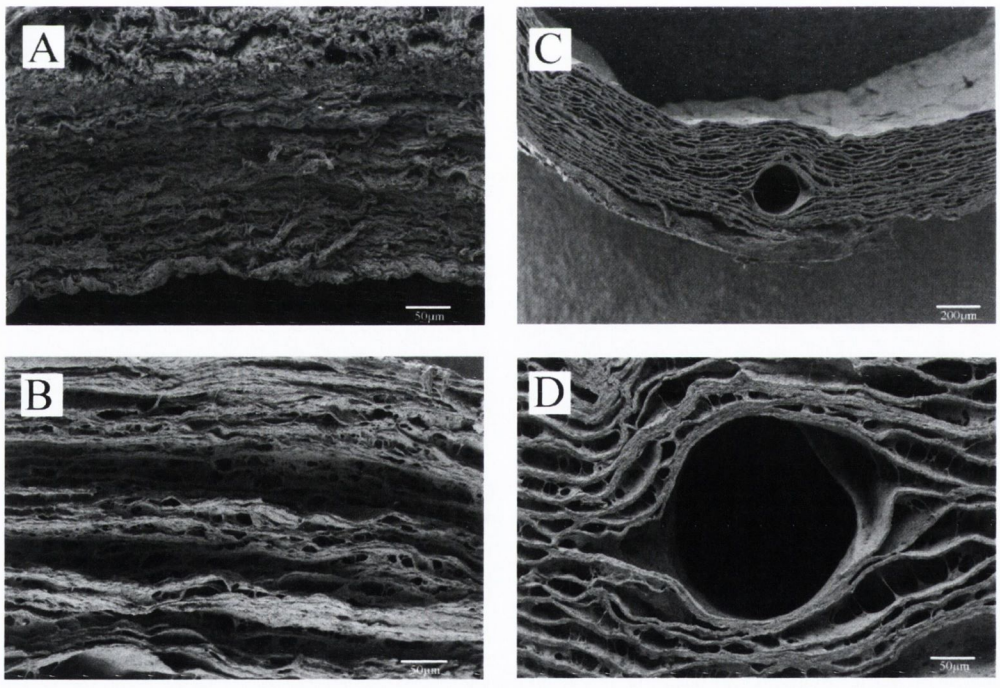

Figure 3.7 SEM of Native and Collagen Digested Scaffold

(A) Compacted layered structure of native tissue. (B) Porous architecture after cell removal shows high scaffold density. (C) Injection channel creation displays minimal ECM disruption. (D) Detailed view of channel demonstrates how needle insertion separates elastin layers without shearing or rupture of elastin sheets or collagen fibers.

The creation of the injection channels correlated with the histology identifying minimal ECM disruption present (Figure 3.7 C). A higher magnification view of the injection channel alone (Figure 3.7 D) further highlighted the exact interaction between ECM components and the needle, confirming separated elastin sheets and no shearing or rupture.

3.3.5 MTT Assay

The metabolic activity as determined using the MTT assay, showed similar levels of activity for native tissue, decellularized scaffolds, collagen digested scaffolds and the negative control (HDPE). While a significant difference to the positive control (PVC) was evident for each tested group. The results are displayed as a percentage of metabolic activity normalised to the negative control, HDPE (Figure 3.8).

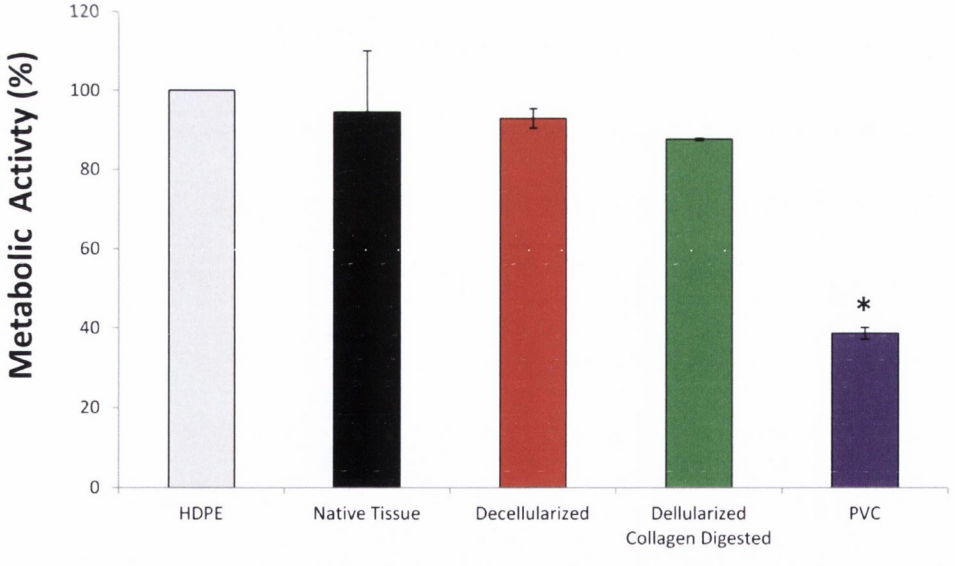

Figure 3.8 MTT Assay Results

Decellularized and collagen digested scaffolds displayed similar levels of metabolic activity as native tissue and HDPE and were significantly different to PVC. This demonstrates no cytotoxic residual chemicals from the decellularization process remain within the scaffolds. * denotes statistical significance to all the other groups,* $p < 0.05$.

3.3.6 DNA Quantification

Residual DNA within the decellularized scaffold was quantified using a Quant-iT™ PicoGreen dsDNA kit. The native tissue contained 3.41 ± 0.72 μg DNA/mg dry weight and the decellularized scaffold 0.13 ± 0.005 μg DNA/mg dry weight (Figure 3.9). This corresponds to ~4% remaining DNA in the scaffold compared to the native tissue.

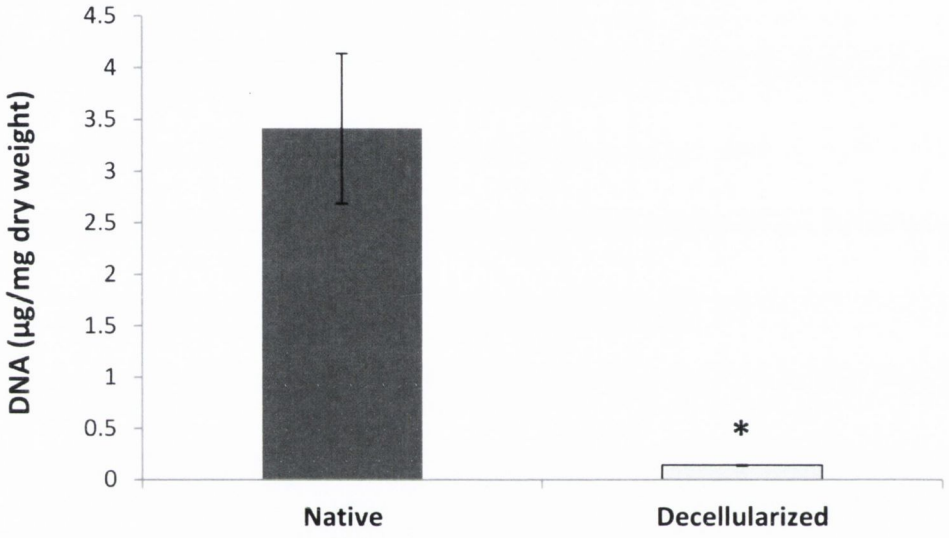

Figure 3.9 DNA Quantification

*Average DNA content per dry weight for native tissue and decellularized scaffolds. The DNA content is significantly reduced after the decellularization process to ~4% of the native tissue, * $p<0.05$*

3.3.7 Mechanical Testing

The averaged stress-strain curves (n=10 each) are shown in Figure 3.10 and Figure 3.11, and a summary of the mechanical properties can been seen in Table 3.1. Decellularized scaffolds produced an overall similar mechanical response to that of the native tissue; however, there were some noticeable differences to individual properties.

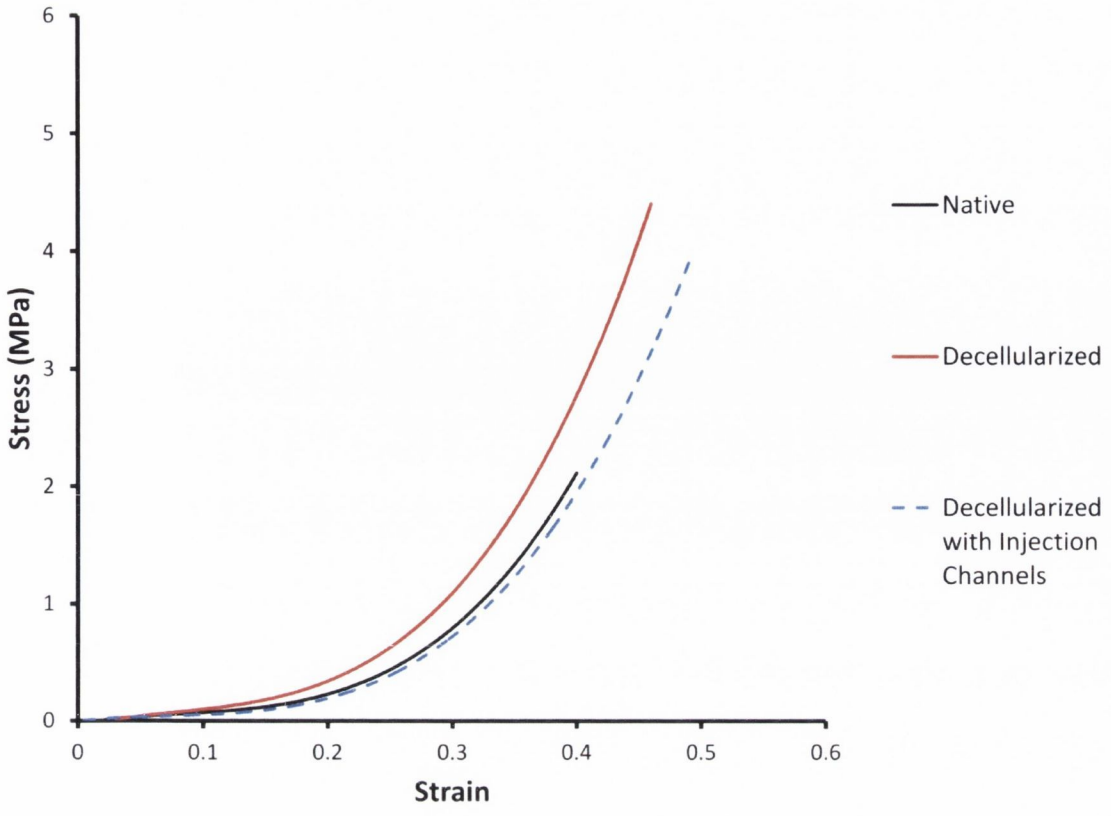

Figure 3.10 Tensile Response of Native Tissue, Decellularized Scaffold and Decellularized Scaffold with Injection Channels

A similar mechanical response is seen in each tissue group. The decellularized tissue is stiffer and less distensible than the native tissue. The creation of the injection channels produces a stiffer response than the native tissue but less stiff than the decellularized tissue and has an increase in distensiblility.

The modulus of the elastin dominant phase was significantly higher with much less extension resulting in an earlier advent of the collagen region of the curve. The decellularized tissue failed at much higher UTS, was significantly stiffer in the collagen dominant phase and also demonstrated a higher strain at failure (Figure 3.12). The creation of the injection channels maintained a similar response to the native tissue and decellularized scaffolds (Figure 3.10). The modulus of the collagen dominant phase was higher than the native tissue but was slightly decreased from that of the decellularized scaffolds.

Collagen digestion caused notable changes to the mechanical properties of the scaffold. After 15 mins sonication in NaOH the scaffold still displayed the bi-phasic mechanical response as seen in Figure 3.11. The distension of the elastin dominant phase was apparent with much higher strains noted at the transition region of the graph. However, the UTS was similar to that of the decellularized tissue.

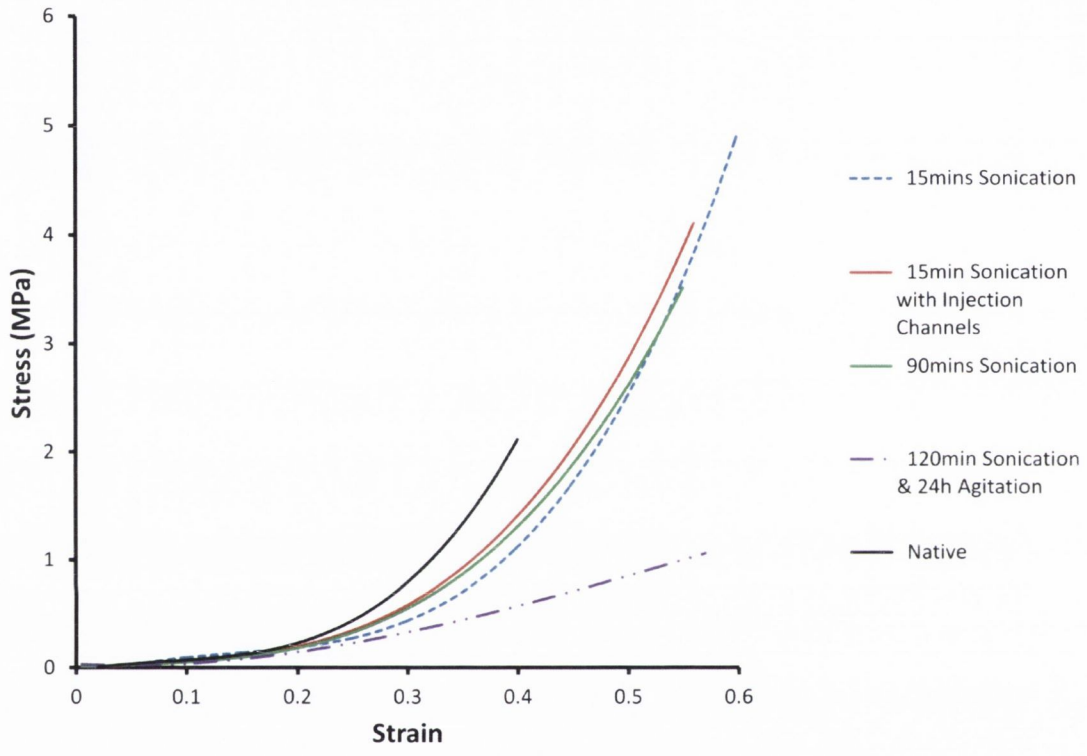

Figure 3.11 Tensile Response of Native Tissue and Collagen Digested Scaffolds

Collagen digested scaffolds were more distensible than the native tissue. Similar mechanical response is seen after 15 mins and 90 mins sonication. Injection channel creation did not affect the tensile response. Excessive collagen digestion grossly altered the tensile response.

Following 90 mins sonication in NaOH a very similar response to the 15 mins sonication group was seen; the main difference was a lower modulus in the collagen dominant phase, a lower UTS and higher strain at failure. The final group subjected to 120 mins sonication and 24 h agitation in NaOH displayed a significantly different response. The

samples were visibly weaker and more translucent prior to the commencement of the tensile test. The modulus of the collagen dominant phase and UTS was extremely low. The modulus of the elastin dominant phase and strain at failure was similar to the other groups (Figure 3.12).

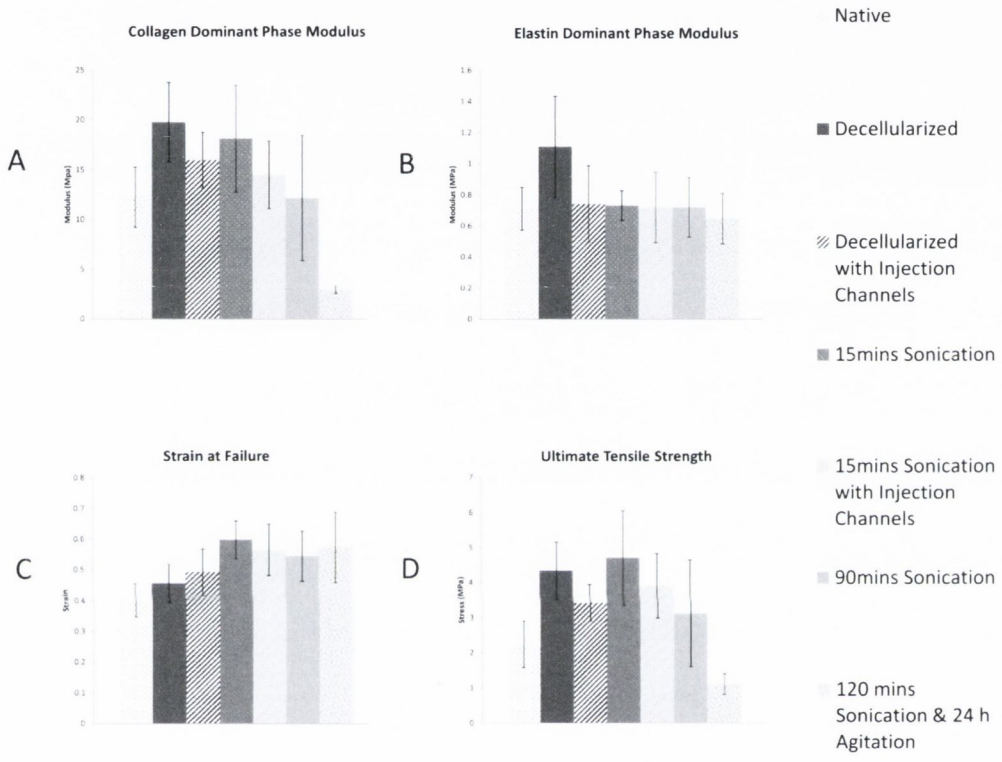

Figure 3.12 Comparison of Mechanical Properties of Tensile Tested Groups

(A) Modulus of the collagen dominant phase increases after decellularization and decreases with collagen digestion. A drop in modulus is seen with creation of injection channels. (B) Elastin dominant phase modulus varies significantly after decellularization and is reduced by injection channel creation and collagen digestion, returning the modulus value toward native tissue. This indicates that the elastin network is fully functioning and undisturbed. (C) Strain at failure is seen to increase after decellularization due to cell removal and increased collagen fiber mobility and uncrimping of collagen fibers. A further increase is seen after further scaffold customization due to injection channel creation and collagen digestion. (D) UTS increases significantly after decellularization and a reduction is seen with injection channel creation. 15 mins sonication maintains the same UTS but decreases with further collagen digestion, with a dramatic reduction after 120 mins sonication & 24 h agitation.

Table 3.1 Mechanical properties of native and decellularized porcine carotid arteries

	Elastin Dominant Phase Modulus (MPa)	Collagen Dominant Phase Modulus (MPa)	Strain at Failure	UTS (MPa)
Native	0.71 ± 0.14^{b}	12.26 ± 3.04	0.40 ± 0.05	2.24 ± 0.67
Decellularized	1.11 ± 0.32	19.81 ± 3.97^{a}	0.46 ± 0.06	4.34 ± 0.82^{a}
Decellularized with IC	0.74 ± 0.24^{b}	16 ± 2.78^{a}	0.49 ± 0.08^{a}	$3.43 \pm 0.52^{a,b}$
15mins Sonication	0.73 ± 0.1^{b}	18.15 ± 5.35^{a}	$0.6 \pm 0.06^{a,b}$	4.71 ± 1.35^{a}
15mins Sonication with IC	0.72 ± 0.23^{b}	14.50 ± 3.4	0.57 ± 0.08^{a}	$3.91 \pm 0.92^{a,b}$
90mins Sonication	0.72 ± 0.19^{b}	12.19 ± 6.3^{b}	$0.55 \pm 0.08^{a,b}$	3.13 ± 1.52^{b}
120mins Sonication &24h Agitation	0.65 ± 0.16^{b}	$2.97 \pm 0.38^{a,b}$	$0.57 \pm 0.11^{a,b}$	$1.11 \pm 0.29^{a,b}$

[a] Significant difference from native

[b] Significant difference from decellularized

IC = Injection Channel

3.3.8 rSMC Scaffold Repopulation

The low cell concentration of Group I (500,000 cells) proved ineffective at repopulating the decellularized scaffold. At the 2 h time point few cells were visible within the scaffold, (see Figure 3.13 A). There were no visible cells on or in the scaffold after 24 h. Group II injections (2 X 10^6 cells) displayed higher levels of repopulation (Figure 3.13 B). At 2 h there was widespread evidence of circumferential dispersion of cells within the tissue. The PKH26 labelled cells show this dispersion clearly, with a large concentration of cells at the site of the injection (Figure 3.13 B). It is also clear that the cells are largely located within the lamellar units in the same region of the injection channel. The rSMCs were still present within the scaffold at 24 h, however, the cell numbers did appear reduced (Figure 3.13 C). Variation in the amount of cell retention was evident across scaffolds and also varied distally along the length of the scaffolds.

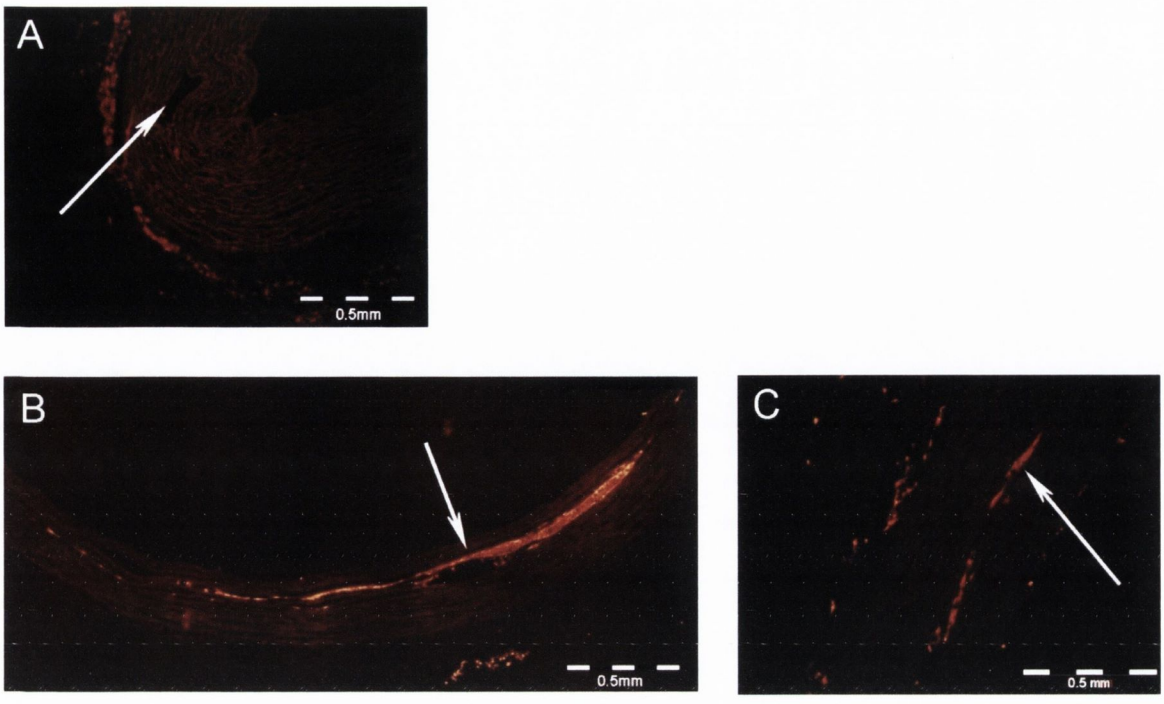

Figure 3.13 Non-Collagen Digested Scaffold Repopulation with rSMCs

(A) Group I injections with low cell number displayed poor cell retention (PKH26 labelled cells fluoresce red). (B) Group II injections at higher concentration showed cell dispersal at 2 h. (C) After 24 h cell retention is low. White arrows indicate injection site.

Group III displayed successful repopulation of the scaffold away from the injection site (Figure 3.14). The high concentration of 4 X 10^6 rSMCs resulted in a significant circumferential dispersion of cells away from the injection site after 24 h. The DAPI staining reveals a high number of cells present at the 24 h time point. Closer examination of the injected cells by DAPI staining (at high magnification) shows that the cells have migrated between a number of lamellar units (Figure 3.14 B). Cell retention varied across scaffolds, as shown by PKH26 cell labelling in Figure 3.14 C.

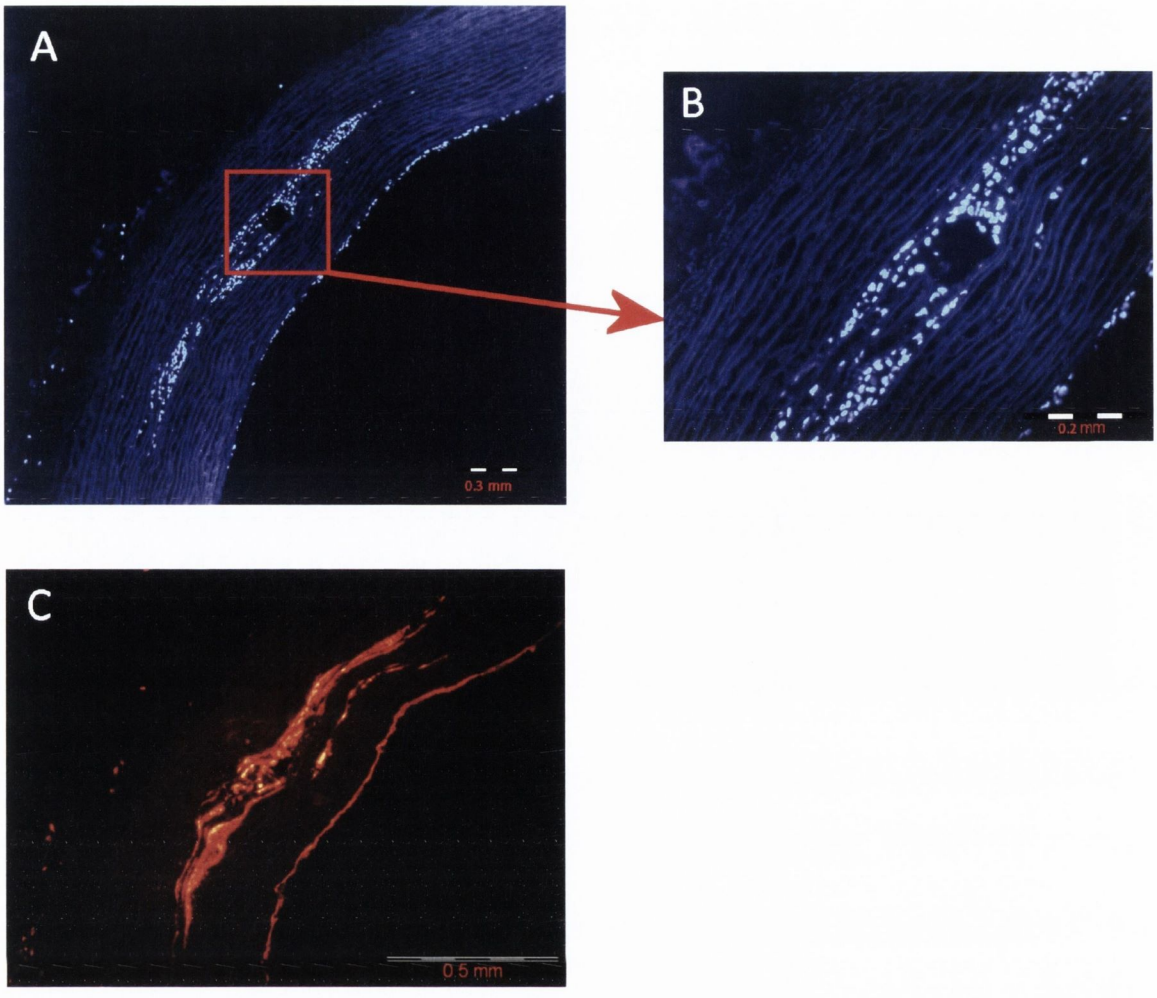

Figure 3.14 High Concentration rSMC Injection

(A) DAPI stained section showing significant cell dispersion from injection channel. (B) Higher magnification shows the channel surrounded by cells. (C) PKH26 dyed cells highlights inconsistency in scaffold repopulation..

The high pressure cell injection of Group IV proved to cause excessive damage to the ECM of the scaffold, see Figure 3.15. The high pressure caused the lamellar unit of the collagen and elastin networks to tear and separate at the site of the injection channel. This tearing resulted in a bulge of the tissue toward the inner lumen as the bulge was filled with the injected cells.

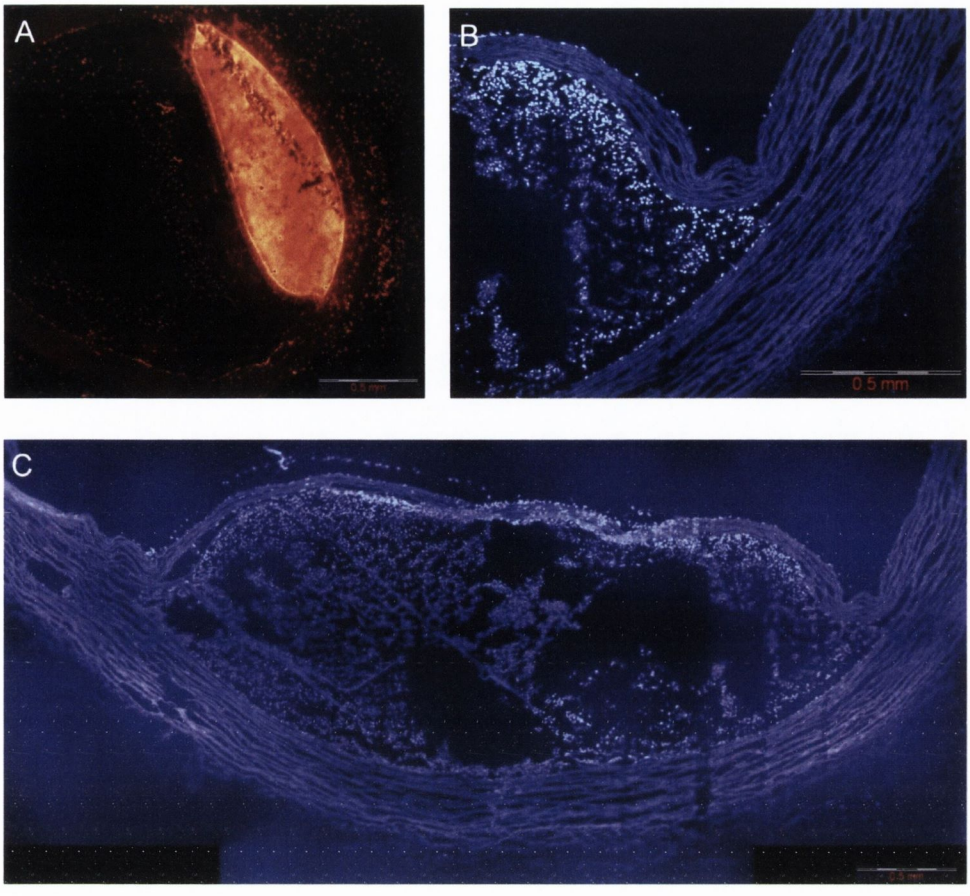

Figure 3.15 High Pressure rSMCs Injection of Decellularized Scaffolds

(A) PKH26 labelled cells displayed within damaged ECM due to high pressure injection. (B) High magnification DAPI stain showing damage to ECM. (C) After 24 h cell numbers are high, damage to the ECM is detrimental but the scaffold wall is intact.

The integrity of the scaffold still remained as the vessel wall itself did not burst. The high concentration of cells that were injected filled the bulge (Figure 3.15 A). DAPI staining revealed the individual cells lacked penetration within the scaffold. The cells are all located together within the bulging disrupted tissue and not within the structurally intact ECM (Figure 3.15 B). The scale of the disruption was widespread across the tissue forming a large bulge and was still evident after 24 h static culture, though cell numbers appear smaller after 24 h.

3.3.9 hSMC Scaffold Repopulation

The results of the hSMC injections are shown in Figure 3.16. Penetration of the non-collagen digested decellularized tissue proved ineffective by injecting hSMCs through the medial injection channels. Phalloidin stained section (cytoplasm stains green) shows cells were present within the cavity, filling up this channel but were not visible within the tissue away from the injection site (Figure 3.16 A). This was consistent throughout the length of the injected scaffold. DAPI staining of the injected scaffolds sonicated for 15 mins in NaOH displayed a filling of the channel with cells; however, some infiltration within the surrounding tissue was also evident (Figure 3.16 B). Cell nuclei were visible outside the injection channel between a number of elastin layers. Examination of the injected 90 mins sonicated scaffold revealed a much higher rate of cell infiltration away from the injection channel (Figure 3.16 C). Cells were present outside of the channels showing increased circumferential dispersion compared to the other scaffolds. The higher cell concentration and longer seeding times of the 30 mm long scaffolds showed much higher levels of cell repopulation. Figure 3.16 D-E exhibit increased circumferential dispersion of cells away from the injection site. Large numbers of cells are retained within the medial layer after the 24 h of static culture. These cells are located across a number of elastin layers and extend circumferentially in both directions away from the injection site (Figure 3.16 F), and are present along the length of the injected scaffold. This circumferential dispersion is seen at each injected channel.

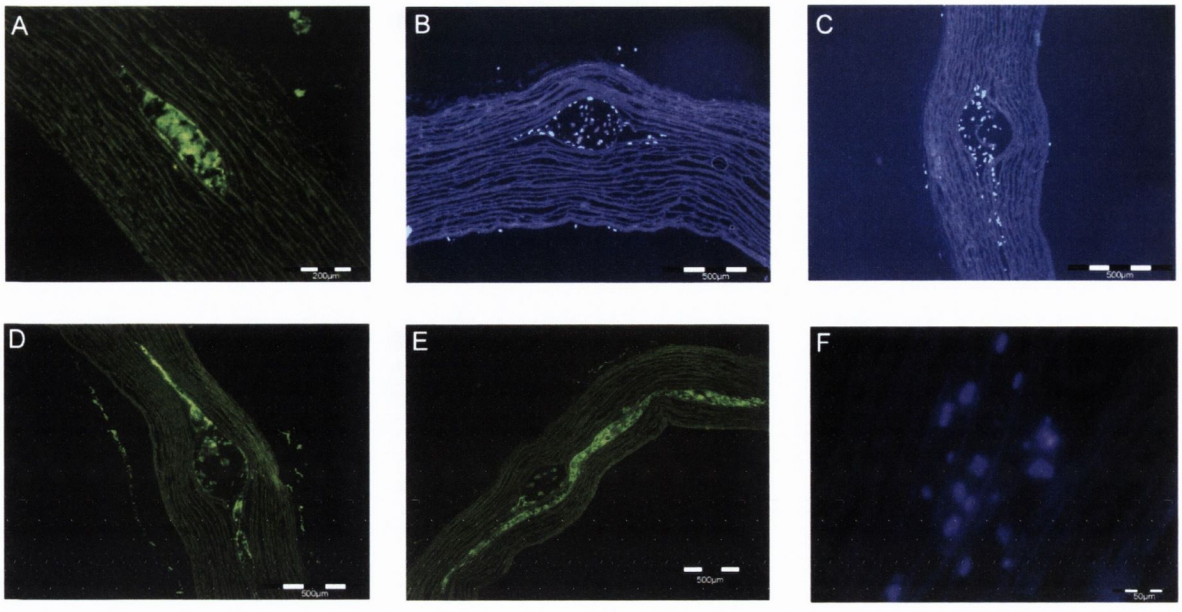

Figure 3.16 hSMC Repopulation of Decellularized and Collagen Digested Scaffolds

(A) 10mm long decellularized scaffold injected with 500,000 hSMCs displays no infiltration outside of the injection channel. (B) DAPI stained section of a scaffold digested by 15 mins sonication to increase porosity shows some cell infiltration away from the injection channel. (C) Cell infiltration away from the site of injection is seen across scaffolds after 15 mins sonication. (D) Phalloidin stain of a 90 mins sonicated 30 mm long scaffold injected with 1 X 10^6 hSMC per injection channel displayed a much greater increase in the circumferential dispersal of cells away from the injection site. (E) Each injection channel on the 90 mins sonicated scaffold displayed similar successful repopulation away from the injection site. (F) High magnification of a DAPI stained section reveals cells infiltrate between elastin layers.

3.4 Discussion

One of the remaining goals of vascular tissue engineering is the realisation of a fully populated contractile SMC medial layer, created within realistic culture times using a physiologically relevant scaffold. If this goal can be achieved the probability of translating the technology to large scale clinical application will be significantly improved. Attempts have been made to overcome this problem within synthetic scaffolds for vascular applications using rotational vacuum techniques (Godbey et al., 2004, Soletti

et al., 2006, Nieponice et al., 2008, Kasyanov et al., 2009, Soletti et al., 2010), the high porosity and large pore size make these synthetic scaffolds easier to seed with large cell numbers in short time periods. While in the case of dense decellularized scaffolds bulk seeding the medial layer has not been successfully achieved. This chapter aimed to address this by customising the properties of decellularized porcine carotid arteries by creating a method for bulk seeding cells into the medial layer while not sacrificing the mechanical integrity of the scaffold.

The creation of channels within scaffolds for tissue engineering has been utilised to increase cell infiltration (Rose et al., 2004, Radisic et al., 2006, Durham et al., 2013), but this has not yet been achieved longitudinally within the medial layer of decellularized vascular scaffolds. There have been previous attempts to increase the porosity in decellularized tissue (Bergmeister et al., 2005). Axial perforation of the decellularized tissue with 50μm holes using a laser noted a higher level of cell repopulation *in vivo*. Pure collagen and pure elastin scaffolds have been studied (Lu et al., 2004, Kurane et al., 2007, Chuang et al., 2009). Completely removing these individual ECM components resulted in a higher infiltration of cells in the elastin scaffolds in-vivo. Subdermal implantation of these scaffolds not only showed increased host cell infiltration but demonstrated new ECM synthesis within the scaffold (Simionescu et al., 2006). The benefits of increasing the porosity to aid cell infiltration are clear, but require a fine balancing act between removing ECM components and not adversely affecting the mechanical properties of the scaffold. Although both collagen and elastin contribute to the mechanical response of the tissue (Holzapfel, 2008), collagen was chosen for digestion. The more complex elastin network is difficult to synthesise from scratch and a lack of elastin is a leading cause of graft failure *in vivo* due to compliance mismatch (Greenwald and Berry, 2000, Patel et al., 2006, Lee et al., 2011). A scaffold without an elastin network would not provide the

elastic response necessary to match a native artery and it is therefore essential for any vascular graft to strive to replicate a matured elastin network (Lee et al., 2011, Fonck et al., 2007, Stekelenburg et al., 2009).

The decellularization protocol utilised here produced a fully acellular scaffold with no trace of intact cells or cell remnants, based on histological analysis, while maintaining the ultrastructure of the ECM fully intact (Figure 3.4). DNA analysis confirmed histology results showing ~4% of DNA content as compared to native carotid arterial tissue. Small collagen fibers were most notably affected by the NaOH protocol resulting in a progressively more porous scaffold in response to duration of sonication. Sonication for 90 mins proved the most efficient sonication duration, removing the majority of the small collagen fibers while not affecting the collagen fiber bundle network. Excessive digestion in NaOH for 120 mins sonication and 24 h agitation resulted in the breakdown of this collagen fiber bundle network. These results showed that successful digestion of collagen fibers in a controlled manner can be utilised to modify or tailor the collagen density of the scaffold. The MTT assay demonstrated no cytotoxic residual chemicals remained within the scaffolds, proving that the decellularization chemicals and protocol did not affect cell viability.

Mechanical testing of these manipulated scaffolds was carried out to determine the effect on the overall mechanical response of the scaffolds. Decellularizing the native arterial tissue produced a stiffer less distensible scaffold which matches the results obtained elsewhere in the literature (Conklin et al., 2002, Roy et al., 2005, Williams et al., 2009). The stiffening of the tissue and reduction of the elastin dominant phase of the stress-strain curve is attributed to the loosening of the tissue due to cell removal, and uncrimping of collagen fibers. This causes an earlier than normal engagement of the collagen fibers in the direction of the applied strain (Williams et al., 2009) hence the early

upturn in the transition region of the graph, and the increase in modulus of the collagen dominant phase. This increased fiber mobility is due to the increased porosity and less compacted nature of the decellularized tissue resulting in easier recruitment and reorientation in the direction of the applied strain of the collagen fibers.

The creation of injection channels within the tissue also produced a stiffer scaffold; whereby the modulus of the collagen dominant phase is significantly higher than the native tissue. This can again be accounted for by the loosening and uncrimping of the collagen fibers. The reduction in modulus from the decellularized scaffold may be accounted for by the local deformation created by the needle insertion delaying full collagen recruitment in this final linear region. The increase in distensiblity in the elastin dominant phase is combined with a significant decrease in the modulus compared to the decellularized scaffold Figure 3.12. This noticeable change in the response of the tissue must be as a result of the needle insertion. Two possible explanations for this are: (i) the localised disruption created by the injection channel may hinder collagen fiber recruitment resulting in a slight delay in collagen fiber engagement hence extending the elastin dominant phase, (ii) the needle disruption affects elastin struts and a small number of elastin sheets locally, reducing the effectiveness of the elastin network and also reducing the elastin dominant phase stiffness, hence delaying the transfer of the load to the collagen fibers. It is important to note that while these results signify disruption to the ECM, the overall function of the elastin remains intact and combines with the collagen network to produce a comparable mechanical response to the native tissue.

Customisation of the tissue by collagen digestion demonstrated that the tensile response of manipulated decellularized scaffolds can be tuned to closely mimic the response of native tissue. The digestion of the small collagen fibers and not the collagen fiber bundles ensures that the tissue maintains sufficient UTS, and mirrors the stiffness of

native tissue. The collagen digestion protocol that delivers potentially the optimum result involves NaOH digestion and 90 mins sonication. This protocol ensures that the elastin and collagen region stiffness's match the native tissue, and the overall strength of the tissue is not compromised. The addition of injection channels to this experimental protocol reduces the stiffness and the strength (Figure 3.11), demonstrating that some damage has been initiated in the ECM components. However this damage is not sufficient to cause significant adverse effects on the tensile response of the scaffold. The strain to failure increases in all the collagen digested groups, and the mechanism for this may be due to the removal of the small collagen fibers, which leads to fewer uncrimped fibers available for early recruitment, which delays the collagen engagement and load transfer from the elastin. The final group subjected to 120 mins sonication and 24 h agitation in NaOH displayed a markedly different response (Figure 3.11) indicating that the collagen fiber bundle network was significantly affected by the NaOH digestion, supported by the histology data showing complete fiber breakdown (Figure 3.6). The elastin dominant phase modulus and strain at failure was similar to the other groups signifying that the elastin structure remains undisrupted by the collagen digestion. This demonstrates that only collagen is affected by our customisation techniques suggesting explanation (ii) above is unlikely to be responsible for the noted changes in mechanical properties.

Scaffold repopulation with rSMCs were undertaken to access the feasibility of using the injection channels for bulk scaffold seeding. The low concentration Group I injections proved unsuccessful in repopulating the scaffold, with no cells present within the medial layer. The cell number was clearly too low to make a significant impact on repopulating the scaffold. A possible explanation for this is due to the lower cell numbers not infiltrating the tissue immediately upon injection. Since the cells are present mainly within the injection channel, few cells would have attached during the 30 mins adhesion

time, allowing for run off when placed in the media within the incubator. This is evident when the cell number was increased fourfold, resulting in significant cell numbers retained within the ECM in Group II (Figure 3.13). Increasing the cell concentration clearly demonstrated improved scaffold infiltration. Circumferential dispersion showed a successful media repopulation. The increase in concentration between Groups II and III showed greater cell retention injection with 4×10^6 injected cells in a solution of 0.1ml cell culture media. Increasing the volume higher than 0.1ml per injection would result in increased spillage. The high cell numbers visible after 24 h in Group III demonstrates the potential of this novel bulk seeding method to retain cells within the scaffold.

The injection protocol relies heavily on circumferential dispersion throughout the scaffold, and this is limited to some extent, particularly cross lamellar infiltration of cells. The small volume of the injection channels allows them to function as an entry point as opposed to a reservoir for the cells. The highly dense ECM is still an issue in preventing cross lamellar infiltration. Another issue which this initial injection study highlighted is a lack of consistency with the injection technique. Figure 3.14 displays the successful medial repopulation, while cells were present within each injected scaffold the cell number and distance of circumferential migration varied across scaffolds and longitudinally within individual scaffolds. The issue of inconsistent and lack of radial repopulation warranted the investigation of reducing scaffold porosity and the second scaffold repopulation cell study with hSMCs.

The lack of cross lamellar infiltration was further evidenced by the high pressure injections of Group IV which proved unsuccessful (Figure 3.15). While these high pressure injections failed to increase infiltration efficiency and only resulted in ECM disruption, it should be noted that although this damage was severe it did not result in bursting of the vessel wall of the scaffold, its integrity remained. This is important to note

as it shows that an ideal injection pressure can be achieved that does not put excess strain on the ECM components while still allowing cell repopulation.

The second scaffold repopulation study utilised hSMC to investigate the effects of collagen digestion on cell infiltration with a physiologically relevant cell source. The results further indicate that the injection channels are a suitable method of repopulating the medial layer with hSMCs. The higher cell concentration of 1 X 10^6 cells per needle injected within the 90 mins sonicated scaffold showed the most optimum results. Poor cell infiltration is seen in the undigested and 15 mins sonicated scaffolds, with the majority of cells filling the injection channel (Figure 3.16 A-B). The NaOH digestion of the small collagen fibers increase the porosity of the scaffold and aids the efficient infiltration of cells away from the channel after injection which is clearly seen by the circumferential distribution of cells in the 90 mins sonicated scaffold (Figure 3.16 D-E). The creation of the injection channel provides a sufficient access route for cell infiltration and bulk seeding of the scaffold in a short time frame.

3.5 Conclusion

This chapter demonstrated that the combination of decellularization and manipulation of porcine arterial tissue could potentially provide a novel scaffold with adequate strength, stiffness and porosity to enable successful bulk cell seeding of the medial layer with SMCs. The formation of injection channels running the length of the scaffold creates an ideal access route for seeding SMCs. Digesting collagen increases the scaffold porosity. These alterations have the potential to significantly reduce cell seeding and culture times. Customising decellularized tissue in this manner was shown to cause minimal localised disruption to the ECM components and does not have a detrimental effect on the overall mechanical response of the tissue. The feasibility of using the injection channels as an

entry point for cells was successfully demonstrated by injecting rSMCs and hSMCs into the medial layer of the decellularized scaffolds. The more porous collagen digested scaffold demonstrated the highest repeatable level of cell infiltration.

Chapter 4 Lyophilisation of Decellularized Arterial Tissue

The results in this chapter have been published as the following paper:

SHERIDAN, W. S., DUFFY, G. P. & MURPHY, B. P. 2013. Optimum Parameters for Freeze-Drying Decellularized Arterial Scaffolds. *Tissue Engineering: Part C Methods*, 19, 1-10.

4.1 Introduction

Chapter 3 described a means of bulk cell seeding the medial layer of customised decellularized scaffolds. This technique has the potential to greatly reduce manufacturing times; however, the issues of sterilisation and long term preservation were not addressed in the Chapter 3 study. The successful translation of TEVGs to a clinical environment will require new methods for long term preservation to produce a reasonable shelf life and appropriate sterilisation techniques. Lyophilisation (freeze-drying) offers a potential solution to these issues, as it produces a completely dry stable scaffold, which can be easily sterilised with ethylene oxide or gamma radiation (Nakamura et al., 2004, Tillman et al., 2012, Wang et al., 2012a). While freeze-drying is incorporated into the manufacturing of a number of commercially available acellular biological devices (Badylak, 2007, Badylak et al., 2009), there is little information available on the effects of freeze-drying on decellularized vascular scaffolds. Furthermore, many decellularization protocols in the literature use freeze-drying as part of the decellularization process, (Amiel et al., 2006, Yazdani et al., 2009, Zhao et al., 2010) without any quantification of how this may alter scaffold mechanics.

Controlling the crystal nucleation rate and crystal size is necessary when freeze-drying biological tissues, as excessive crystal growth and size can disrupt ECM components and create tissue heterogeneity (O'Brien et al., 2005, Nail et al., 2002). The importance of determining the ideal freeze-drying parameters to preserve the ECM has been demonstrated for other biological tissues such as decellularized heart valves (Wang et al., 2012a), and bovine pericardium (Polak and Pitombo, 2011) but not for decellularized vascular scaffolds.

This chapter focuses on determining the effects of the freeze-drying process on the mechanical integrity of decellularized porcine carotid arteries with the main hypothesis

being that altering the freeze-drying parameters, namely freezing rate and final temperature may disrupt the ECM resulting in altered scaffold mechanical properties.

4.2 Methods and Materials

4.2.1 Decellularization

Carotid arteries were freshly harvested from 70-90kg pigs in a local abattoir in the same manner as described in Chapter 3. Common carotid arteries 5-7 mm in diameter were returned to the laboratory with a warm ischemic time of less than 5 h before freezing at -20°C. Decellularization was also carried out as per the protocol described in Chapter 3. Two scaffold groups were prepared:

Group 1: *Standard Scaffold*

A "so called" standard decellularization protocol was used, as it produces an unaltered ECM, the protocol has similarities to most decellularization methods and has been used by a number of research groups (Amiel et al., 2006, Cho et al., 2005, Yazdani et al., 2009). Briefly, samples were immersed in de ionized water for 24 h at 4°C under rotational agitation and subsequently incubated in 0.05% Trypsin with 0.02% EDTA for 1 h at 37°C. Samples were then placed in a solution of 2% Triton X-100 and 0.8% ammonium hydroxide in de-ionized water for 72 h at 4°C with a daily solution change and a final wash sequence of 48 h in de-ionized water, all under rotational agitation.

Group 2: *Customised Scaffold*

The second group of scaffolds were prepared as described in Chapter 3, this was a manipulated scaffold created to reduce porosity and increase cell infiltration. The protocol was exactly as described above for the standard scaffold group but with the additional

step of selectively decreasing collagen content by sodium hydroxide (NaOH) digestion. This occurred after the 72 h of agitation in the decellularization solution. The samples were immersed in 0.5 M NaOH and sonicated for 90 minutes at room temperature. All samples from both groups were frozen in PBS at -20°C immediately after decellularization.

4.2.2 Freeze-drying Cycles

Three different freeze-drying cycles were investigated (see Figure 4.1):

1. **T_f = -10°C**

   A constant cooling rate during freezing of 1°C/min to a final temperature of -10°C, followed by a 60 min hold at this temperature. A 4 h ramp to 0°C under vacuum of 200mTorr and 17 h at 0°C and secondary drying at 20°C at the same pressure.

2. **T_f = -40°C**

   The same protocol as T_f = -10°C above, except a final temperature of -40°C was reached.

3. ***SF* T_f = -40°C**

   Same protocol as T_f = -40°C except the freeze-dryer shelf was pre-cooled to -60°C prior to commencement of the cycle.

Prior to freeze-drying all samples were thawed rapidly in a water bath at 37°C and then incubated at room temperature for > 1 h in the PBS in which they were originally frozen. Each sample, for cycles T_f = -10°C and T_f = -40°C, was positioned on a stainless steel mandrel, suspended on a stainless steel tray and placed on the shelves of the freeze dryer (Virtis Genesis 25EL, Biopharma, Winchester, UK). Samples for *SF* T_f = -40°C were

removed from PBS, air dried for 1 min to remove excess fluid, placed in tubes and snap frozen in liquid nitrogen. Prior to placement within the freeze-drier the mandrels, tray and tweezers used to mount the samples were cooled to -60°C for 1 h. Each freeze-drying cycle was applied to both the standard decellularized and customised scaffolds.

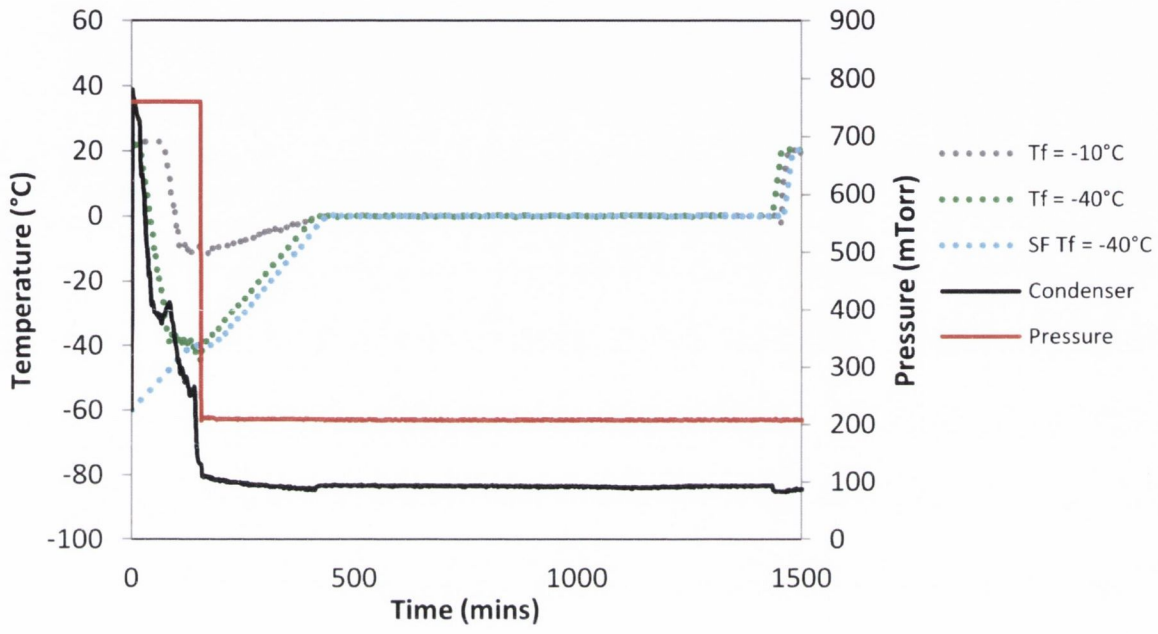

Figure 4.1 Freeze-drying Cycles

(A) Three freeze-drying protocols were investigated, T_f = -10°C, T_f = -40°C and snap frozen samples in a pre-cooled -60°C chamber to T_f = -40°C.

4.2.3 Histology

5mm ring segments were taken from each group for histological analysis. Samples were embedded in paraffin wax in an automatic tissue processor (ASP300, Leica, Germany). Samples were sectioned longitudinally using a rotary microtome (Leica microtome, Leica, Germany). 7µm sections were cut and collected on glass slides and subsequently washed through a graded series of ethanol from 100 to 70% (v/v). Native and decellularized tissue was stained using Hematoxylin and Eosin (H&E) and Veorhoff Van Geison. Sections were dehydrated and cleaned in ascending concentrations of ethanol and

xylene before coverslips were mounted (DPX mountant, BDH). Observation under light microscopy and digital image acquisition was carried out with an inverted microscope (Olympus IX 71).

4.2.4 Mechanical Testing

4.2.4.1 Tensile Tests

Uniaxial tensile tests were carried out on scaffolds subjected to each of the freeze-drying cycles for both the standard decellularized and customised scaffolds. Non freeze-dried native tissue, standard decellularized scaffolds and customised scaffolds were also tested as controls. The tests were performed using a Zwick tensile testing machine (Zwick Z005, Roell, Germany). Freeze-dried samples were re-hydrated in PBS for > 1 h and intact ring sections 4 mm long were cut from each sample (n=10), mounted on custom made grips and tensile tested to failure in the same manner described in Chapter 3.

4.2.4.2 Opening Angle Measurement

Opening angle measurements were undertaken to determine the effects of freeze-drying on the residual stress within the scaffold wall. Ring sections 2-3 mm in length were cut from re-hydrated freeze-dried samples. Each sample was placed in a well of a 24 well plate and submerged in PBS at room temperature. After 30 mins the sample was removed, placed on a chopping board and cut open by a single radial cut. The sample was returned to the well plate to equilibrate for 30 mins after which an image was recorded. The opening angle was defined as the angle (θ) formed from the midpoint of the inner circumference to the end points of the inner circumference (Figure 4.2). ImageJ software (US National Institutes of Health) was used to determine this angle from the raw image.

In the case of large recoil in the sample θ was measured in the same manner but given a negative value (Figure 4.2 D), n=10 for all groups.

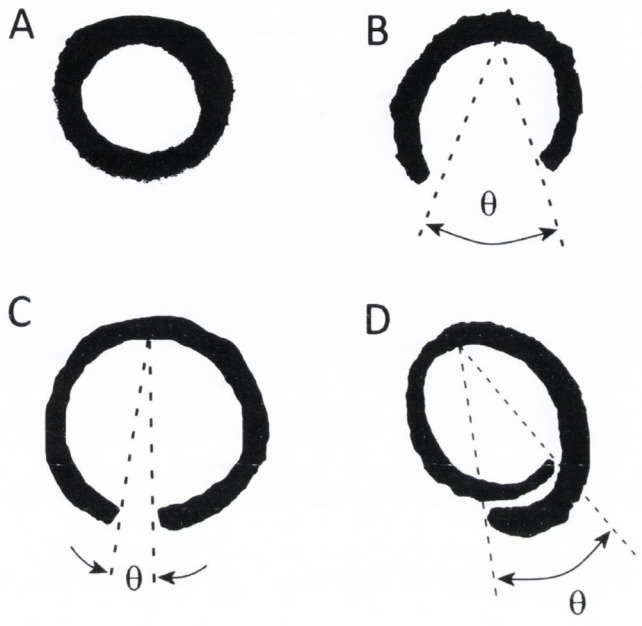

Figure 4.2 Opening Angle Measurement

(A) Intact scaffold in stressed state. (B) Native tissue in zero stress state achieved by radial cut of ring section producing an opening angle θ. (C) Decellularized scaffolds displayed a reduced value for θ compared to native scaffolds. (D) Customised scaffolds revealed an excessive reduction in θ to the extent that the scaffold recoiled beyond the diameter of the zero stress state. These θ values are taken as negative.

4.2.4.3 Suture Retention Strength

Suture retention strength was determined at room temperature. Freeze-dried samples were re-hydrated in PBS for > 1 h prior to testing (n=6). The sample was secured in the bottom of the test machine using a custom built grip which allowed uniform clamping. A single suture (3-0 Tevdek® II, Teleflex Medical) was inserted 5 mm from the scaffold edge, passed through a hook in the top grip and securely fastened. The suture was pulled from the tissue at a rate of 10mm/min until rupture and the maximum force reached was recorded as the suture retention strength.

4.2.5 Cell Repopulation of Freeze-dried Scaffolds

In order to demonstrate that the freeze-drying process does not affect the cytocompatibility of decellularized scaffolds, the optimum freeze-drying cycle determined from the results of the biomechanical testing was selected for a cell repopulation analysis. Injection channels were created by the insertion of micro-needles into the wall of native arterial tissue prior to customised decellularization as described in Chapter 3. The scaffold was then injected with rMSCs within the medial layer of the scaffold, also as described in Chapter 3 after 2 h re-hydration in cell culture medium (as above). The cell seeded scaffolds (n=3) were then cultured in static conditions for 7 days with a medium change every two days. At this time point the scaffolds were snap frozen in OCT compound, cryosectioned and DAPI stained as described in Chapter 3.

4.2.6 Statistics

Box plots were used to present the distributions of the data. Each box displays interquartile range (IQR) with median and outliers (defined as median ± 1.5*IQR) are shown with individual dots. A students T-test was used to test significance between each group separately, and results with $p < 0.05$ were considered statistically significant.

4.3 Results

4.3.1 Freeze-drying

Freeze-drying in all scaffold groups produced a uniformly dried, brittle scaffold which conformed well to the stainless steel mandrel (Figure 4.3 A). Scaffolds slid off the mandrel with minimal force to reveal an intact, dried scaffold with a reduced wall thickness due to removal of solute (Figure 4.3 B).

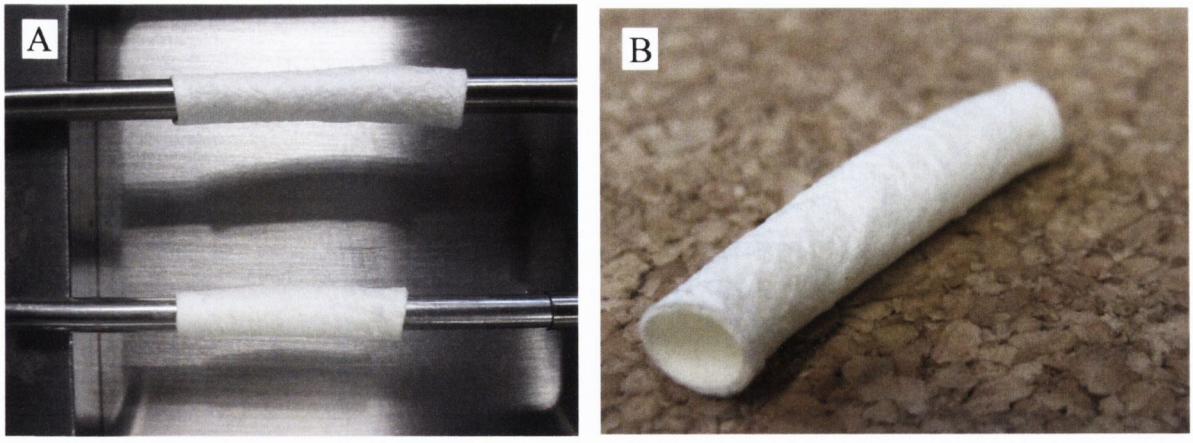

Figure 4.3 Freeze Dried Scaffolds

(A) Freeze-dried scaffold on stainless steel mandrels placed on raised stainless steel trays within the freeze-drier. (B) After freeze-drying the scaffold are easily removed from the mandrel producing a fully dried, stable scaffold.

Figure 4.4 shows the sample results of H&E staining for all groups. The T_f = -10°C groups displayed inconsistent and uneven drying across the scaffold wall (Figure 4.4 D). The porous nature of the scaffold in the wall centre contained separated collagen fiber bundles, which are not apparent at the scaffold edges where collagen fiber bundles are compressed together. There was also evidence of disruption of the collagen fiber network within the centre of the scaffold wall.

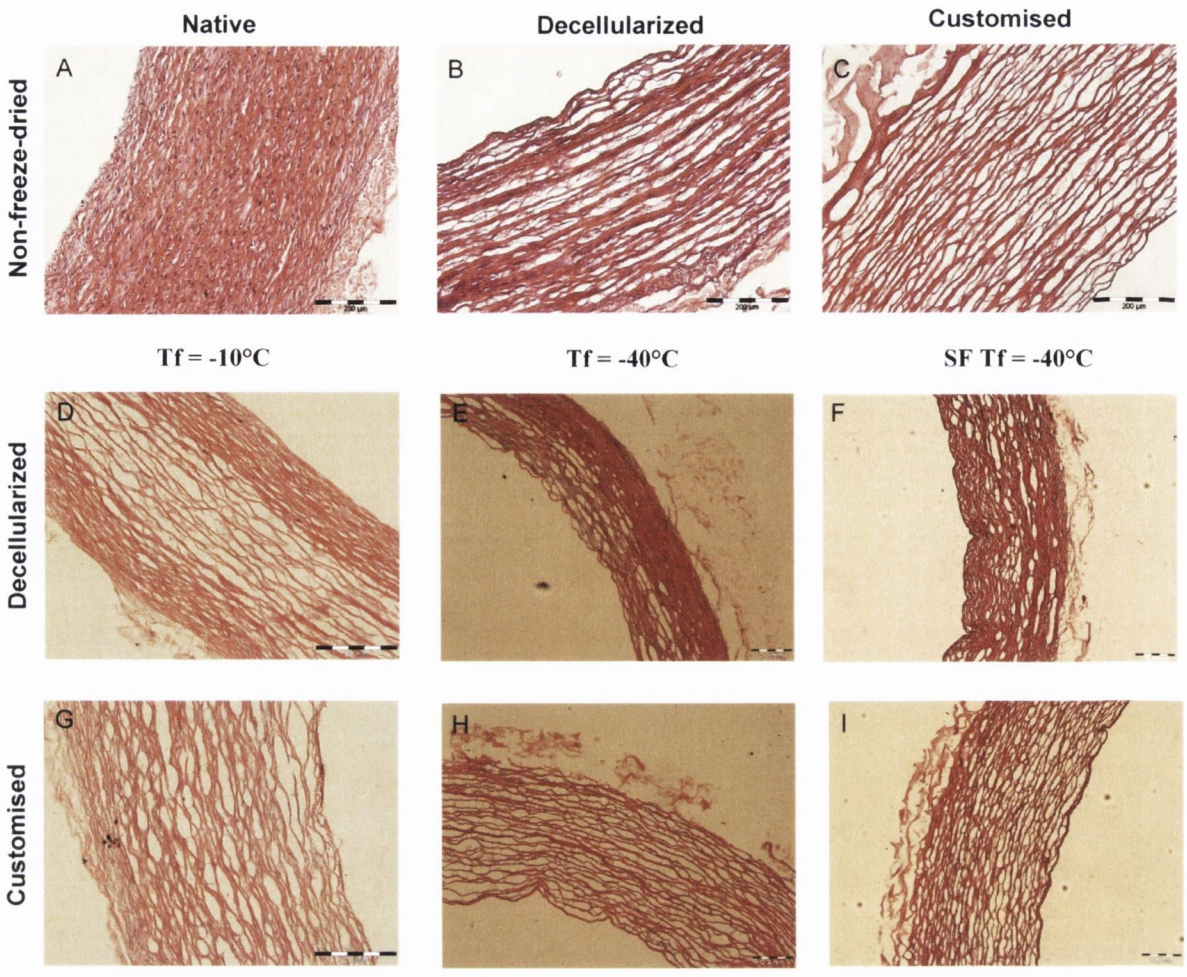

Figure 4.4 H&E Stain Displaying Effects of Freeze-drying on Scaffolds

(A) Highly cellular non freeze-dried native tissue. (B) Cell removal reveals a porous intact ECM after decellularization. (C) Decreased matrix density is evident after customisation. (D) Decellularized scaffolds in the T_f = -10°C group displays a non-homogenous matrix with fiber rupture within the wall centre. (E) T_f =-40°C shows markedly less fiber disruption than T_f = -10°C. (F) SF T_f = -40°C produced a homogenous structure with minimal ECM disruption for the decellularized scaffolds. (G) The T_f = -10°C customised scaffold showed evidence of fiber disruption but not as severe as the decellularized scaffold. (H) Fiber damage was visible for the customised scaffolds in the Tf = -40°C group with consistent drying. (I) SF T_f = -40°C customised scaffolds resembled the non freeze-dried scaffolds with homogenous drying. All scale bars indicate 200μm.

Figure 4.5 details the disruption to the ECM after freeze-drying, with native and decellularized tissue displayed for comparison. The intact undulating collagen fibers were

apparent in the native tissue and maintained after decellularization (Figure 4.5 A-B). Rupture of a large number of collagen fiber bundles was clear and highlighted in Figure 4.5 C (black arrows). The customised scaffold also showed evidence of fiber disruption (Figure 4.4 G) but this damage is less severe than the decellularized scaffold (Figure 4.5 D). The drying process appears more consistent for the customised scaffolds and evenly distributed across the scaffold wall. T_f = -40°C displayed markedly less fiber disruption than T_f = -10°C. For standard decellularized scaffolds (Figure 4.4 E) the collagen fiber bundles were clearly intact, however inconsistent drying appears across the scaffold wall particularly on the luminal side where loosening of the ECM was evident. Veorhoff Van Geison staining further revealed disruption to the elastin network which was not immediately obvious from the H&E staining. Elastin fibers are stained black by this stain, and fragmentation of the elastin sheets was clear within the decellularized scaffolds subjected to T_f = -40°C (Figure 4.5 F). Minor collagen fiber damage was seen in the customised scaffolds with the same freeze-drying cycle (Figure 4.4 H), while homogenous drying was seen across the scaffold wall. All scaffolds subjected to SF T_f = -40°C produced a homogenous structure with minimal ECM disruption (Figure 4.4 F,I). Minimal fiber disruption was observed under high magnification (Figure 4.5 E), where the ECM after freeze drying appears comparable to non freeze-dried scaffolds.

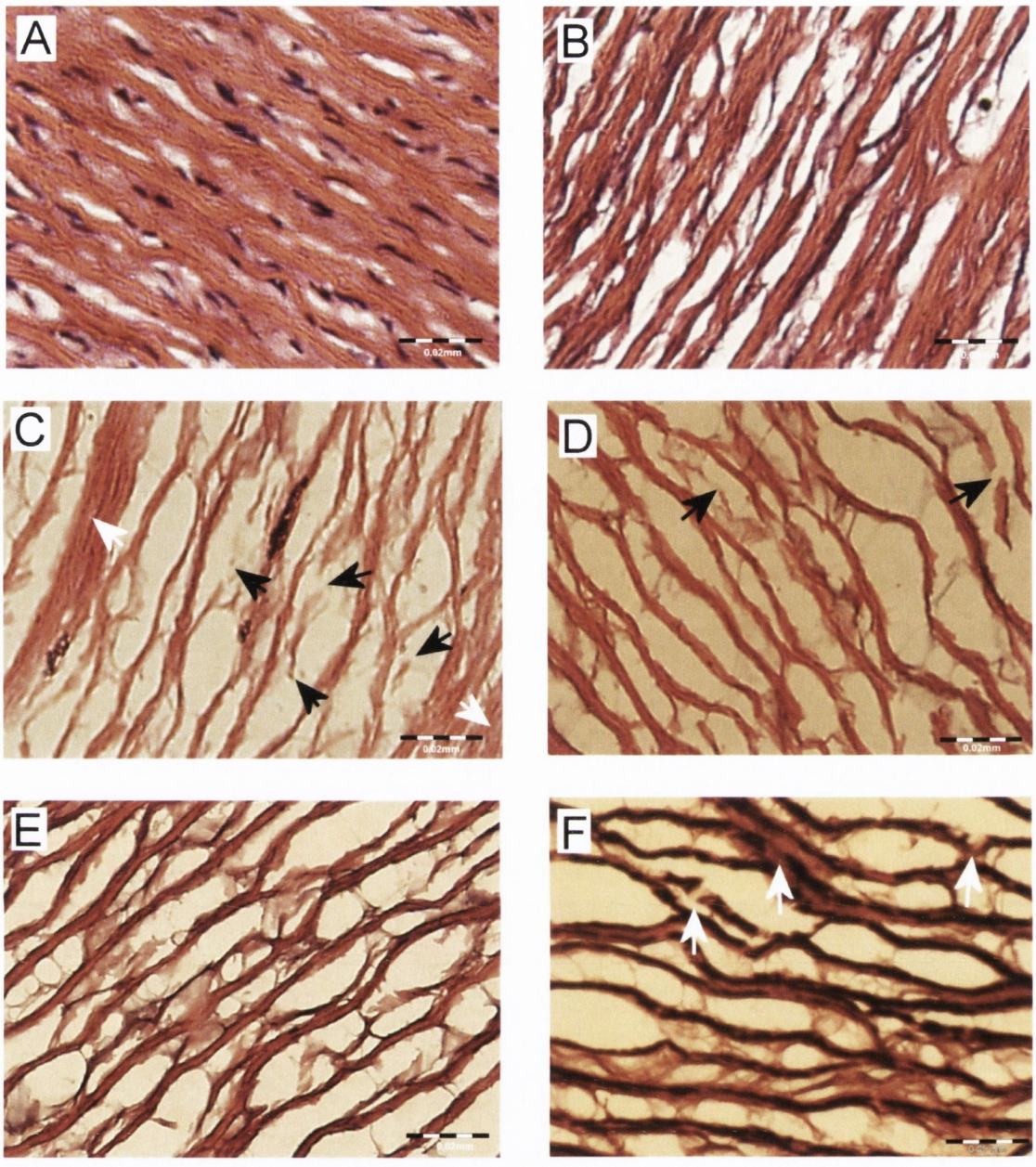

Figure 4.5 ECM disruption due to Freeze-drying

A) H&E staining of native tissue reveals highly dense undisrupted nature of collagen fibers. (B) Decellularization does not disrupt fibers (C) H&E staining shows T_f = -10°C causes major collagen fiber disruption in decellularized scaffolds, black arrows indicate fully ruptured fibers and white arrows display areas of non-uniform drying where. (D) Less fiber damage was visible in T_f = -40°C decellularized scaffolds. (E) SF T_f = -40°C customised scaffolds retained similar ECM configuration. (F) Verhoff Van Gieson staining of decellularized scaffold in the T_f = -40°C group displayed disruption of the elastin network (elastin fibers stain black). Fragmentation of the elastin sheets was visible (white arrows). Scale bars in A-C indicate 20μm and 50μm in D

4.3.2 Mechanical Test Results

4.3.2.1 Tensile Tests

The stress-strain curves of all of the scaffolds tested displayed a hyperelastic response typical of a biological soft tissue (Fung, 1993, Humphrey, 2002). The standard scaffold T_f = -10°C group produced a much reduced elastin region and short transition leading to a stiffer collagen region (Figure 4.6 A).

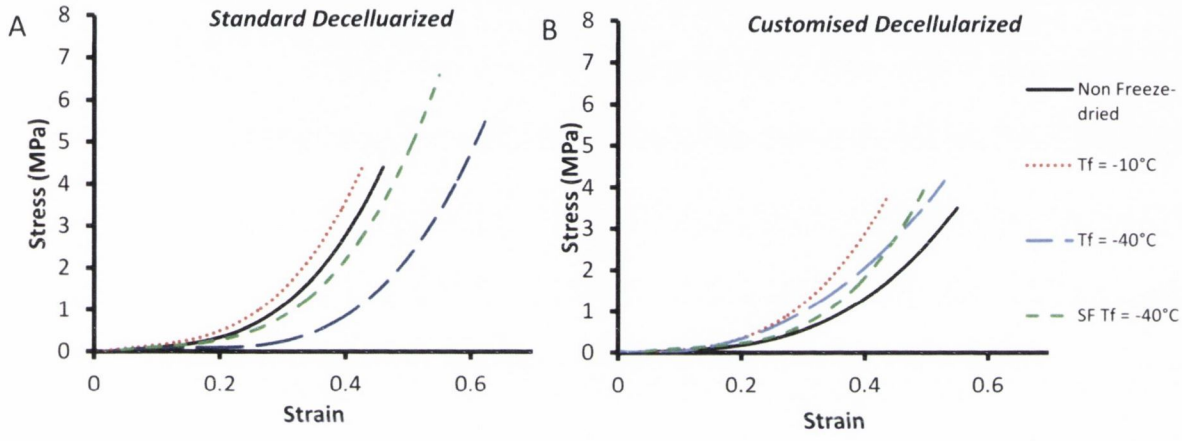

Figure 4.6 Mechanical Response of Tested Scaffolds

(A) Decellularized scaffolds for T_f = -10°C produced a stiffer less distensible response with an earlier than normal transition to the collagen region. T_f = -40°C displays a markedly different response with a large shift in the transition region of the graph extending the elastin dominant phase. SF Tf = -40°C matches closely the response of the non freeze-dried scaffolds particularly in the elastin dominant phase. (B) Customised scaffolds for T_f = -10°C produced a stiffer response with a much earlier transition region, similarly for T_f = -40°C an earlier transition region was seen with a less stiff collagen region. SF T_f = -40°C matched the response of the non freeze-dried scaffolds for the elastin region but an altered stiffer response was evident in the collagen phase.

T_f = -40°C displayed a different response with a much extended elastin region shifting the transition region to much higher strain values and ending with a normal collagen phase. Moreover, a significant reduction in the modulus of the elastin phase and similar collagen

phase modulus was observed in this group in comparison to the standard decellularized group (Figure 4.7 A). There is no significant difference between the collagen phase modulus and the non freeze-dried scaffolds for SF T_f = -40°C except for the customised scaffolds. While there was a significant reduction for the T_f =-40°C protocol versus the standard decellularized group (Figure 4.7 B).

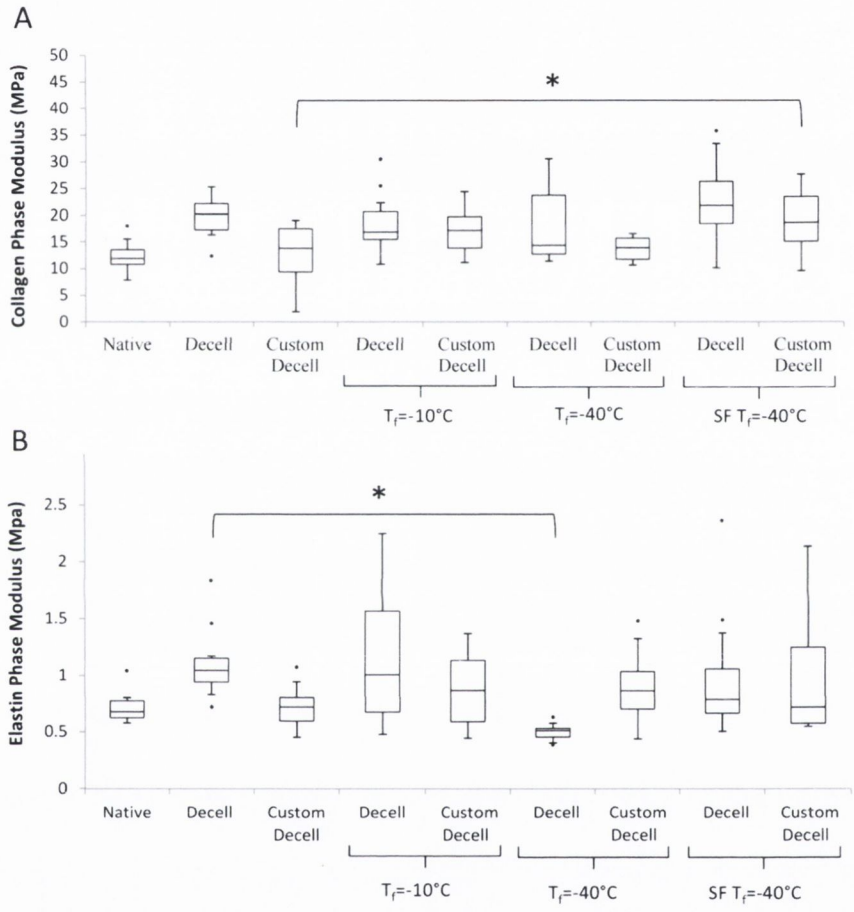

Figure 4.7 Collagen and Elastin Dominant Phase Moduli

*(A) Decellularization does not alter the collagen phase modulus while customisation does. Freeze-drying did not significantly affect the collagen modulus except for customised SF T_f = -40°C. (B) Decellularization increases the elastin phase modulus while customisation reverses it toward the native modulus. T_f = -40°C significantly reduces the elastin phase modulus for decellularized tissue, below both the native and decellularized moduli. While SF Tf = -40°C maintains the elastin modulus for both decellularized and customised decellularized scaffolds. Statistical significance is indicated as *$p<0.05$.*

The customised scaffolds exhibit some alterations in the mechanical response after freeze drying (Figure 4.6 B). T_f = -10°C produced a less distensible response with a reduced toe region and early transition region. Similarly, for T_f = -40°C an earlier transition region was observed which was stiffer than the non freeze-dried scaffolds. The SF T_f = -40°C scaffolds matched closely the response of the non freeze-dried scaffolds with a comparable elastin and transition region while the collagen phase was noticeably stiffer on the curve and the collagen phase modulus was significantly different (Figure 4.7 A). The elastin phase moduli for both the decellularized and customised scaffolds were not significantly altered after freeze-drying.

4.3.2.2 Opening Angle Measurement

Native tissue displayed the largest opening angle upon release of the residual stress; while the customised scaffolds had a significantly lower opening angle than decellularized scaffolds and native tissue specimens with recoil extending below the original diameter (Figure 4.8). Decellularized scaffolds displayed a reduction in residual stress for each of the freeze-drying cycles with no statistical significant difference for any cycle. Customised scaffolds had a statistically significant decrease in opening angle for each freeze-drying cycle in comparison to native tissue.

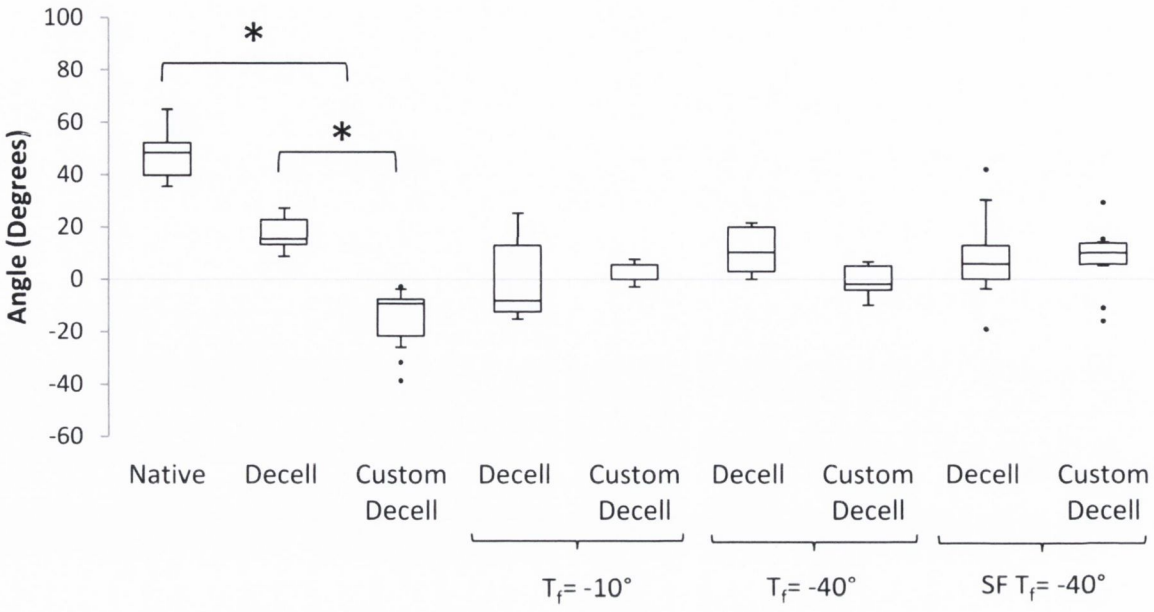

Figure 4.8 Opening Angles

*Decellularized scaffolds display a significant reduction in θ compared to the native tissue. Customised scaffolds see a significant decrease in θ due to collagen digestion, compared to both native tissue and decellularized scaffolds. Freeze-drying reduces the opening angle for the decellularized scaffolds and increases for each of the customised scaffolds which can be attributed to collagen fiber damage and scaffold heterogeneity. SF T_f = -40°C scaffolds are reverted back toward that of the native tissue. *$p<0.05$.*

4.3.2.3 Suture Retention Strength

The maximum force to pull a suture through a scaffold wall to failure for each of the groups tested is shown in Figure 4.9. The maximum average forces for native tissue, decellularized and customised decellularized scaffolds were 1.8 N ± 0.41, 1.8 N ± 0.42 and 1.9 N ± 0.49 respectively. The suture retention strength was similar across all freeze-drying cycles to these controls, except T_f = -40°C for decellularized scaffolds. There was a significant difference compared to the native and decellularized controls for T_f = -40°C.

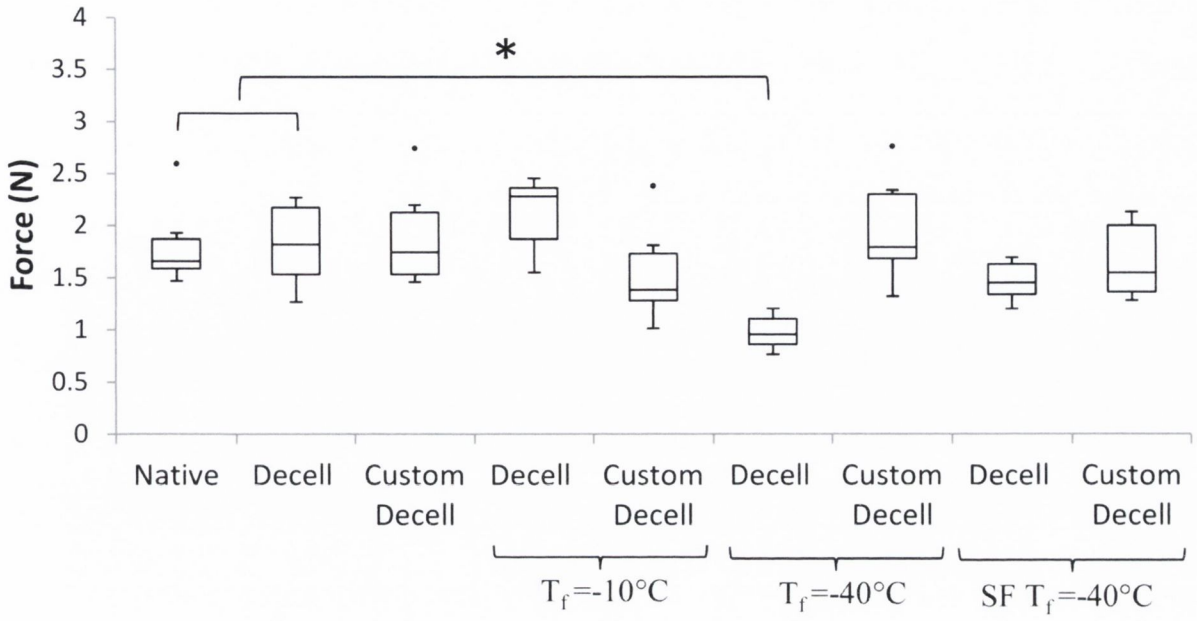

Figure 4.9 Suture Retention Strength

*Suture retention strength for native tissue and decellularized scaffolds. Decellularization, customisation and freeze-drying had little effect on the suture retention strength. T_f = -40°C for decellularized scaffolds produced a significant drop in suture retention strength. Statistical significance is indicated as *$p<0.05$.*

4.3.3 Scaffold Repopulation

The optimum freeze-drying cycle for customised decellularized scaffolds was determined to be the SF T_f = -40°C and was utilised to freeze-dry scaffolds for repopulation with rMSCs. The insertion of the needles within the scaffold did not have any detrimental effects on the freeze-drying process, the scaffold was easily mounted on the mandrel and removed after freeze-drying (see Figure 4.10 A-B). The needles were situated within the centre of the medial layer, and caused minimal damage to the scaffold architecture during freeze-drying. Figure 4.10 B shows how no further disruption was caused to the scaffold as a result of the needle insertion. After 2 h incubation in tissue culture medium the scaffold was sufficiently hydrated and resembled exactly the non freeze-dried scaffolds used in Chapter 3 and the cell injection process was undertaken without any complication

as a result of freeze-drying. After 7 days of static culture the injected rMSCs were present and viable within the medial layer of the scaffold with some circumferential migration away from the injection site (see Figure 4.10 C).

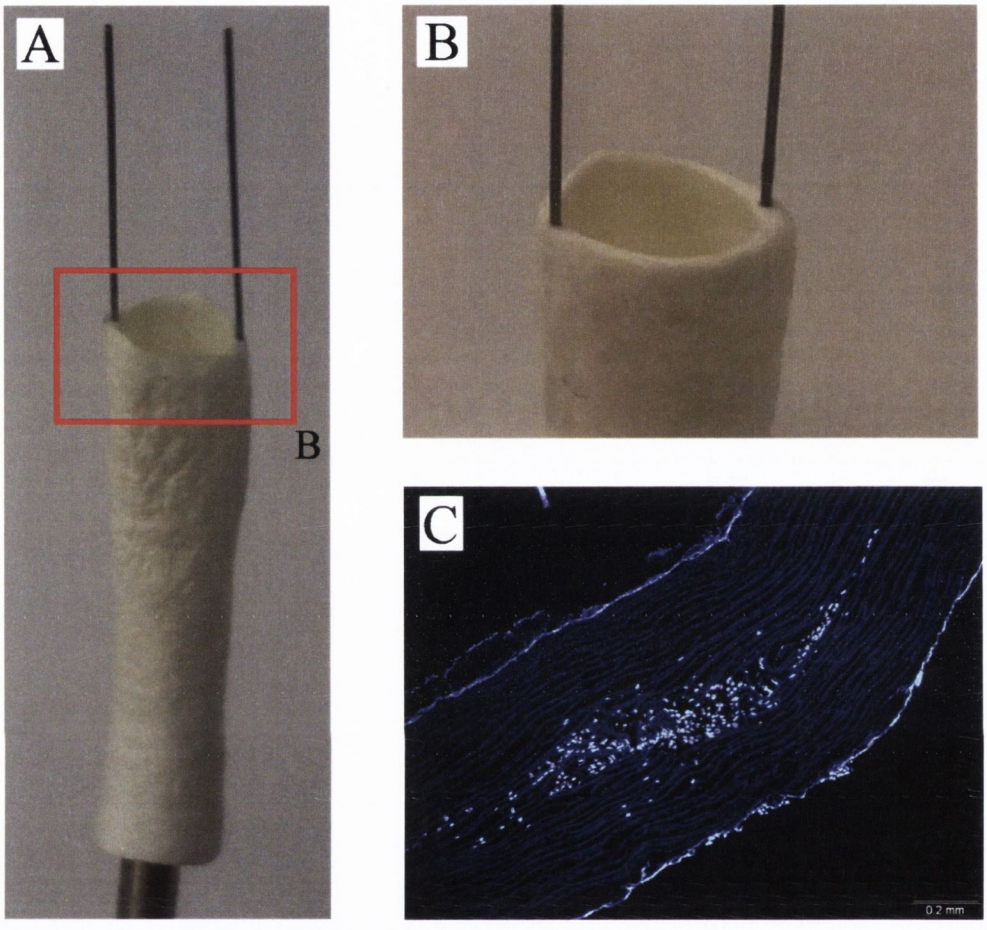

Figure 4.10 Repopulation of Freeze-dried Scaffolds

(A) Needle insertion did not affect the freeze-drying process. (B) Needles remain within the centre of the medial layer in the dried configuration with no excessive damage to the scaffold architecture. (C) Medial injection through the in situ needles repopulated the medial layer of the scaffold with rMSCs (DAPI stained cell nuclei fluoresce).

4.4 Discussion

There are currently a number of vascular tissue engineering techniques obtaining impressive *in vivo* results, which have the potential to advance towards routine clinical use (McAllister et al., 2009, Olausson et al., 2012). Regardless of the technique utilised

however, there are certain criteria any TEVG must meet such as having a means of long term preservation for simple storage and transport, adequate sterilisation techniques and overall ease of use.

To incorporate shelf life concerns and sterilisation protocols this chapter investigated a number of freeze-drying protocols. It has previously been shown that ethylene oxide (Atala et al., 2006, Zhao et al., 2010, Tillman et al., 2012) and gamma radiation (Gajiwala and Gajiwala, 2004, Nakamura et al., 2004, Cornwell et al., 2009) are suitable methods for sterilizing freeze-dried biological tissue for eventual use *in vivo*. However, no freeze-drying protocols have been investigated to determine the optimum parameters that will maintain the micro-architecture and mechanical properties of a decellularized vascular scaffold.

Decellularized vascular tissue comprises a compacted highly dense layered structure. The sublimation of ice crystals from within the layered structure and orientation of the collagen and elastin networks will not merit the formation of pores in the traditional sense in homogenous solutions, but may manifest as damage to the ECM components due to their intricate, interlinked orientations.

T_f = -10°C was the least effective freeze-drying cycle producing a non-homogenous structure for both the standard decellularized and customised scaffolds. Evidence of uneven drying in the decellularized scaffolds was apparent in the histology, whereby ice crystal growth was clearly larger in the centre of the scaffold wall, this subsequently led to collagen fiber disruption (Figure 4.4 D). Although more homogenous drying was evident for customised scaffolds, fiber damage was still visible (Figure 4.4 G). The consequence of this uneven drying was also seen in the mechanical response of the tissue. T_f = -10°C scaffolds were stiffer and less distensible with earlier engagement of collagen fibers, observed by the shortened toe region and early transition region on the

stress-strain curve (Figure 4.6 A-B). The mechanical response of the freeze-dried customised scaffolds more closely matches the response of their non freeze-dried controls; this is in comparison to the decellularized scaffolds which see increased deviations from their non freeze-dried controls. The slightly improved result seen in the customised scaffolds may indicate that the increased solute within the tissue, due to the decreased density, allows more homogenous nucleation and ice crystal growth.

Overall in the T_f = -40°C group, less damage was visible with H&E staining. However, uneven drying was evident in the decellularized scaffolds. Upon further investigation the tensile tests reveal that there was a large change in the mechanical response of these scaffolds. The greatly extended toe region of the graph signifies elastin damage (Figure 4.6 A) which was confirmed with Verhoff Van Geison staining (Figure 4.5 F) and the significant difference between the elastin region modulus and non freeze-dried control. The customised scaffolds produced an altered shift in the mechanical response, with an earlier than normal transition to the collagen phase, however, this altered response was much less severe than the decellularized scaffold. Fiber damage was visible from the histology but less drastic than the customised scaffolds in the T_f = -10°C group. The excessive disruption within the decellularized group may be a result of the higher density of the matrix. The tightly packed matrix has less solute space and will result in non-uniform nucleation throughout the wall causing less contiguous, more numerous and less evenly distributed crystal growth. The non-uniform nucleation and growth of these smaller ice crystals will reduce sublimation and heat transfer efficiency which results in the visible uneven drying as seen in the scaffold heterogeneity. It is postulated that the less dense nature of the customised scaffold will negate this non-uniform nucleation resulting in contiguous more evenly distributed ice crystals. For this reason, scaffold heterogeneity is not seen in the histology (Figure 4.4 H) and the

mechanical response of the customised scaffold does not display excessive elastin network disruption.

The SF T_f = -40°C cycle initiated instant uniform nucleation and small crystal growth throughout the scaffolds. The freeze-drier shelf was pre-cooled to -60°C to ensure the scaffolds remain at the lowest temperature possible (≤ -60°C). The SF T_f = -40°C cycle produced the overall optimum results with minimal fiber damage, which was evident from the histology for both the decellularized and customised scaffolds (Figure 4.4 F,I), and the mechanical response of both scaffolds closely matched that of their controls (Figure 4.6 A-B). In particular the elastin phase and transition region are both comparable to the controls, indicating an undisrupted elastin network; moreover there was no significant difference in the modulus for the elastin phase for each of the scaffolds. The process of snap freezing the scaffolds in liquid nitrogen creates extremely small ice crystals. Small ice crystals are usually less thermodynamically stable due to the reduction in surface area/volume. However, since the pre-cooled shelf was at -60°C, and the first step of the freeze-drying cycle allows for heating to -40°C, small ice crystals are encouraged to re-crystallise to produce bigger more contiguous crystals which are more stable and allow for more efficient sublimation (Searles et al., 2001). This is effectively an annealing step that guarantees more uniform distribution of stable ice crystals resulting in even drying and no disruption of the ECM components. The SF T_f = -40°C freeze-drying technique is even more effective in the customised scaffolds as ice crystal distribution is more homogenous to begin with as the less dense scaffold has more space to promote uniform nucleation. These results further highlight the suitability of our customised scaffold for use in vascular tissue engineering.

Transmural residual stress exists to ensure uniform stress distributions under normal conditions and can change in response to injury or disease (Fung, 1993,

Humphrey, 2002). The opening angle test relieves the transmural residual stress (Figure 4.2). It has been shown that the individual constituents of the ECM are responsible for the value of θ, with elastin having a residual tension and collagen a residual compression (Zeller and Skalak, 1998). Decellularization is known to cause a reduction in opening angle (Williams et al., 2009). Our results confirm this effect was observed in the decellularized scaffolds compared to native, but also a significant difference between the decellularized and customised scaffolds. Here an excessive compressive component of the scaffold is expressing itself as the scaffold sections recoiled to a lesser degree than the intact diameter. Freeze-drying further altered the residual stress as a reduction in opening angle was seen across the decellularized freeze-dried scaffolds, this may be due to the collagen fiber disruption in T_f = -10°C and SF T_f = -40°C and the elastin damage in the T_f = -40°C. Opening angles for customised scaffolds were significantly increased for each freeze-drying cycle, which reverted the opening angle back toward that of native tissue.

The suture retention tests further verify that the SF T_f = -40°C technique for freeze-drying was the most effective. This is a vital test in terms of clinical applicability, as suturing a TEVG correctly in place with industry standard sutures is an essential measure for *in vivo* graft performance. The results from these tests indicate that freeze-drying does not significantly alter the suture retention strengths of the decellularized or customised scaffolds, except for decellularized scaffolds in the T_f = -40°C group. Potentially, the elastin disruption due to freeze-drying as described above has also significantly reduced the suture retention strength further verifying that this freeze-drying cycle is unsuitable for use with decellularized scaffolds. The SF T_f = -40°C scaffolds were not significantly different further demonstrating the techniques' applicability for both decellularized and customised scaffolds.

The results of the biomechanical testing and histology clearly indicate that the SF T_f= -40°C freeze-drying cycle for the customised scaffolds preformed best overall in terms of maintaining the ECM undisrupted after freeze-drying. For this reason this cycle was utilised for cell repopulation. Freeze-drying a scaffold with *in situ* needles did not alter the scaffold properties and injection with rMSCs in the manner preformed in Chapter 3 was successfully undertaken. The rMSCs were present and viable after 7 days demonstrating no negative effects on the scaffold from freeze-drying.

4.5 Conclusion

A new freeze drying protocol for both "standard" decellularized porcine carotid arteries and customised collagen digested decellularized porcine carotid arteries has been described. This technique involves snap freezing the scaffolds in liquid nitrogen prior to insertion into a pre-cooled freeze-drier below the T_f at which primary drying occurs. This protocol produces a homogeneous scaffold with undisrupted ECM components and minimal alteration to the overall mechanical properties of the scaffold. This protocol allows for the creation and perseveration of injection channels within the medial layer of the scaffold which permit rapid scaffold repopulation by direction injection. The optimum freeze-drying protocol described in this chapter did not affect the cytocompatibility of the scaffold. This new manufacturing protocol creates the means for the preservation and sterilisation of decellularized arterial scaffolds in a manner which can be easily adopted for use in a clinical environment.

Chapter 5 Enhanced Scaffold Repopulation Using a Chemotactic Stimulus

The use of the chitosan/β-GP as a tool for protein delivery was carried out in conjunction with Orna Grant (Trinity Centre for Bioengineering).

The results in this chapter have been pubished as the following paper:

SHERIDAN, W. S., Grant, O.B., DUFFY, G. P. & MURPHY, B.P. The Application of a Thermoresponsive Chitosan/β-GP Gel to Enhance Cell Repopulation of Decellularized Vascular Scaffolds. *Journal of Biomedical Materials Research Part B: Applied Biomaterials. Mar 25, 2014. [Epub ahead of print.*

5.1 Introduction

Chapter 3 and Chapter 4 have evaluated novel alterations to decellularized vascular scaffolds for the creation of TEVGs. These alterations were primarily to propel the scaffolds toward clinical use by addressing some of the limitations in using decellularized scaffolds. However, full cell migration throughout the scaffold is still limited by the highly dense matrix that remains after decellularization and any increase in cell numbers and more uniform distribution of cells prior to implantation will increase the possibility of better *in vivo* host integration. To this end, the hypothesis of this chapter is that embedding a biochemical stimulus within the scaffold may aid cell repopulation.

Growth factors have been widely used to promote cell proliferation, migration and recruitment, as well as modulating cell differentiation, phenotype and promoting angiogenesis (Stegemann and Nerem, 2003, Forte et al., 2006). The benefits of growth factors in regenerative medicine are extensive (Segers and Lee, 2010), however they have some limitations such as short half-lives, expense, relatively large size and possible side effects at supraphysiological concentrations; therefore their delivery must be carefully controlled and efficient (Babensee et al., 2000, Tayalia and Mooney, 2009). This warrants the use of a vehicle/carrier for their successful delivery.

Temperature-responsive hydrogels represent a promising vehicle to deliver cells/proteins by direct injection; they can undergo a reversible phase transition at body temperature, allow fast gelation and controlled degradation while providing a protective environment for encapsulated cells and/or a reservoir for protein delivery (VandeVord et al., 2002, Borden et al., 2010, Van Vlierberghe et al., 2011). Chitosan is a natural, biocompatible, biodegradable, non-toxic, antimicrobial cationic polysaccharide the applications of which in tissue engineering and drug delivery have been widely studied (Nettles et al., 2002, Van Vlierberghe et al., 2011, Bernkop-Schnürch and Dünnhaupt,

2012). Like other hydrogels, chitosan gels have a large aqueous component; this mimics the consistency of natural tissue and is advantageous for nutrient exchange and cell viability. In addition, certain chitosan hydrogels particularly chitosan/β-GP hydrogels are thermosensitive, whereby the thermoresponse can be manipulated to create suitable injectable gels for *in vivo* use (Chenite et al., 2001). Similarly, chitosan gel properties can be tailored to allow sustained local release of cells, small-molecule drugs (Ruel-Gariépy et al., 2000, Hastings et al., 2012), and proteins such as growth factors (Wang et al., 2010, Faikrua et al., 2013), making it an ideal vehicle for bio-therapeutic delivery.

The aim of this chapter is to further advance our customised decellularized arterial scaffold toward clinical applicability by direct injection of a clinically relevant cell type and/or proteins to enhance cell repopulation within the scaffold. A thermoresponsive injectable chitosan/β-GP hydrogel was used as a delivery vehicle for rMSCs and/or murine hepatocyte growth factor (HGF). HGF and MSCs are utilised due to their therapeutic potential (Da Silva Meirelles et al., 2009, Segers and Lee, 2010). MSCs express HGF receptors, (Neuss et al., 2004) and HGF exerts a very strong chemotactic stimulus on MSCs which has been shown to promote the migration of MSCs (Forte et al., 2006). It is hypothesised that the chitosan hydrogel provides a suitable vehicle for cell delivery and will allow for controlled and sustained release of the growth factor in order to enhance cell migration within the scaffold.

5.2 Methods and Materials

5.2.1 Decellularization

Decellularization was carried out as described in Chapter 3 for the customised decellularized scaffold creation which included the NaOH collagen digestion step. These decellularized scaffolds were used for the Group 1 statically seeded controls (see below).

Scaffolds were also created with injection channels within the medial layer also as described above. Three nitinol micro-needles (300μm outer diameter, 190μm inner diameter) were inserted into the transverse section of the arterial wall 120° apart and extended to a depth of approximately 12 mm (Figure 5.1 A).

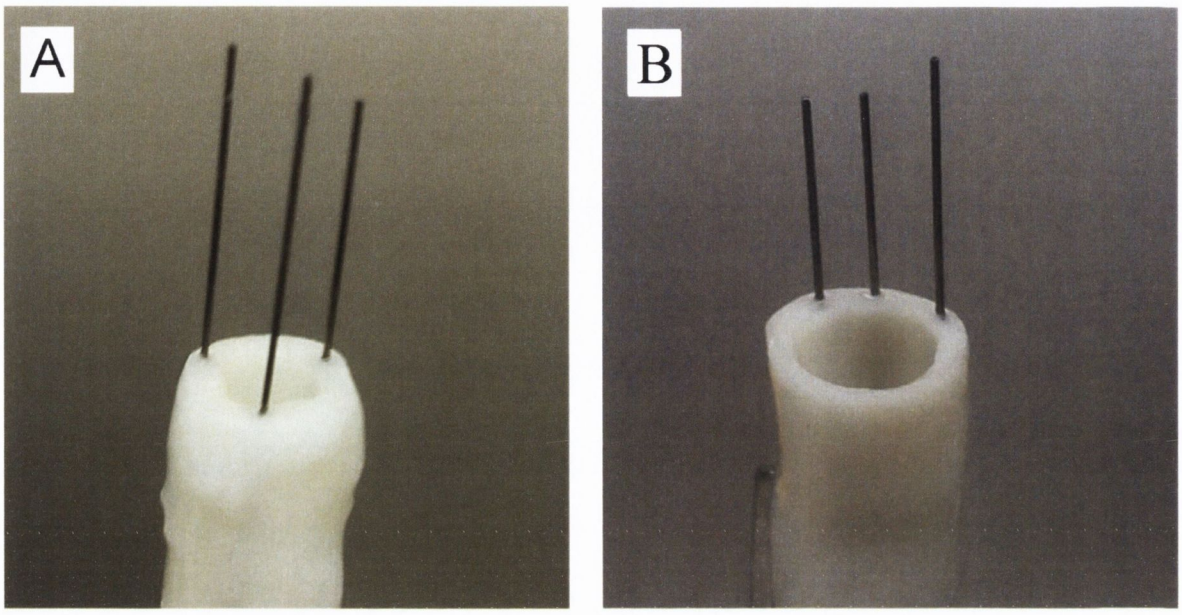

Figure 5.1 Micro-needle Insertion within Scaffold

(A) Three micro-needles inserted 120° apart prior to decellularization. (B) Three micro-needles 60° apart.

These scaffolds were then subjected to the same decellularization protocol as above, with the needles remaining in situ for the entire duration. A second set of scaffolds containing mico-needles were created (Group 5, described below). These scaffolds were fabricated in the same manner as above except the needles were inserted closer together, approximately 60° apart, corresponding to approximately 4-6 mm circumferential distance between needle centre points (see Figure 5.1 B).

5.2.2 Helium Ion Microscopy

Decellularized scaffolds containing injection channels were prepared for observation using helium ion microscopy (HIM). The decellularized scaffolds were fixed in 2.5% buffered glutaraldehyde for 24 h. These samples were maintained in their cylindrical configuration and the needles were maintained in situ throughout. Needles were then removed and the samples were washed separately three times in PBS for 15 mins. Subsequently, each section was subjected to sequential washes of 30%, 50%, 70%, 90% and 100% ethanol for 15 mins with the final wash performed three times. HIM was performed on specimen/substrate with a Zeiss Orion Plus to view the ultrastructure of the medial layer of the decellularized scaffolds, specifically the injection channels. Image resolution of the microscope is manufacture specified at 0.35 nm. The working distance was 10 mm and a 10 μm aperture was used. The beam current was 0.8 pA with a tilt angle of 15 degrees. Charge compensation was enabled using an electron beam flood gun. No additional conductive coating of the specimens was employed.

5.2.3 Gel Formulation

A 2% w/v chitosan, 7% w/v β-glycerophosphate (β-GP) solution was prepared in a similar manner as previously described (Hastings et al., 2012). The gel formulation was created using ultra-pure chitosan (UP CL214 from Pronova Biomedical, Oslo, Norway) with a degree of deacetylation >95%. 100mg of chitosan was dissolved in 4.5ml of deionised water at pH 8-9. 350mg of β-GP was dissolved in 0.5ml of deionised water at pH 8-9. A homogenous gel was achieved by adding the β-GP solution to the chitosan solution drop by drop while stirring on ice. Gels were stored on ice until further use.

A chitosan/β-GP gel containing HGF (R&D Systems, UK) was also formulated in a similar manner. The gel formulation process was as described above except a HGF

solution was added drop by drop to the chitosan while stirring for a final concentration of 0.0005% w/v HGF (5μg/ml HGF). A homogenous gel was achieved by adding the β-GP solution to the chitosan/HGF solution drop by drop while stirring on ice. This concentration was chosen based on published release data for small molecule drugs, (Hastings et al., 2012) preliminary release studies using bovine serum albumin (data not shown), and on a desired local concentration of at least 20ng/ml, previously shown to promote the migration of MSCs (Forte et al., 2006). The HGF solution used was a 0.001% w/v HGF, 0.1% w/v BSA (Sigma-Aldrich, Ireland) solution in PBS, prepared in accordance with the manufacturer's protocol for freezing.

5.2.4 Rheological Testing of Protein-Loaded Chitosan/β-GP Gel

Rheological testing of the chitosan/β-GP gel was undertaken in order to determine whether the addition of HGF affects the thermoresponsive profile of the gel. This was performed on protein-loaded samples. The gel was prepared as described above for the HGF loaded gel, but using BSA as a surrogate for HGF. A 0.101% BSA solution in PBS (representing the HGF as well as its carrier BSA) was mixed with the water added to the chitosan to give a final concentration of 0.0505% w/v BSA. An oscillatory temperature sweep was then performed using an AR-1000 cone and plate rheometer (TA Instruments). The thermoresponsive profile of the gel was assessed as a function of temperature over time, using the measured storage modulus as an indicator of gel structure. A temperature sweep mode over a range of 20°C to 50°C with a 1°C per minute increase was utilised, with an oscillatory stress of 10 MPa at a frequency of 1 Hz. Data were collected from three independent gels. Similar rheological testing was not performed for chitosan/β-GP encapsulated rMSCs as it has previously been shown that the addition of human MSCs to this gel did not alter the thermoresponse (Hastings et al., 2012).

5.2.5 HGF Release from chitosan / β-GP

Approximately 500mg of chitosan/β-GP HGF gel was placed into each of three sterile glass vials. Approximately 500mg of control chitosan/β-GP gel was placed into another sterile vial. These gels were then allowed to gel by incubation for one hour in a water bath at 37°C. 1ml of cell culture medium (as below) was then placed into each vial. This culture medium was collected and replaced at time points of 4 h, 24 h, 3, 5, 7 and 28 days. At each time point, culture medium was collected from each vial for concentration analysis by ELISA (murine HGF ELISA kit, R&D Systems, UK).

5.2.6 Cell Preparation and Seeding

Sprague Dawley rat mesenchymal stem cells (rMSCs) were cultured in standard tissue culture flasks using Dulbecco's Modified Eagle Medium (DMEM, formulation D5671, Sigma-Aldrich, Ireland) supplemented with 10% foetal bovine serum (FBS, Biosera), 2% penicillin/streptomycin (Sigma), 1% L-glutamine (Sigma), 1% GlutaMAX (Gibco BioSciences) and 1% non-essential amino acids (Gibco BioSciences). Cells were maintained as sub-confluent monolayers in T175 flasks under standard conditions (37°C, 5% CO2). All seeding experiments were undertaken between passages 6–10.

Five groups using decellularized scaffolds were selected for investigation (n=3 each):

Group 1. *Static abluminal seeding*

rMSCs cells were trypsinized, centrifuged and resuspended in fresh culture medium at a concentration of 20 X 10^6 cells/mL. Approximately 2 X 10^6 cells suspended in 100µl culture medium were pipetted on the abluminal surface of the scaffold and allowed to adhere for 30 mins. This was

repeated twice after rotation of the scaffold by 120° each time to ensure a homogenous circumferential cell distribution. This seeding technique mirrors routinely used methods (Niklason et al., 1999, Yazdani et al., 2009, Zhao et al., 2010).

Group 2. *Medial injection of cells only*

2 X 10^6 rMSCs suspended in 100µl of fresh culture medium were injected through each of the in situ needles within the medial layer of the scaffold as the needle itself was removed.

Group 3. *Medial injection of cells encapsulated in chitosan/β-GP*

rMSCs cells were trypsinized and centrifuged and the cell pellet was resuspended in the chitosan/β-GP gel at a concentration of 20 X 10^6 cells/mL. This gel/cell combination was then injected within the medial layer of the scaffold as in Group 2.

Group 4. *Medial injection of chitosan/β-GP HGF gel with abluminal cell seeding*

In order to enhance migration radially through the medial layer the chitosan/β-GP HGF gel was medially injected through the in situ needles 120° apart. The gel loaded scaffolds were incubated at 37°C for > 45mins to allow for gelation. Subsequently 6 X 10^6 rMSCs were abluminally seeded.

Group 5. *Medial injection of cells and chitosan/β-GP HGF gel*

The chitosan/β-GP HGF gel was medially injected in a single needle followed by > 45mins incubation at 37°C. rMSCs were subsequently injected in the needles located 60° either side of the injected gel in the same manner as Group 2.

All scaffolds were immersed in culture medium and placed in an incubator at 37°C in separate T-25 tissue culture flasks. Groups 1-3 were cultured for each time period of 1, 3 and 7 days, Groups 4 & 5 were cultured for 7 days only. All cells were fluorescently labelled using PKH26 (Sigma-Aldrich, Ireland) according to the manufacturer's instructions.

5.2.7 Histology and Migration Quantification

Native tissue and decellularized scaffolds were fixed in 10% formalin and paraffin embedded using an automatic tissue processor (ASP300, Leica, Germany). All samples were sectioned longitudinally in 7μm sections using a rotary microtome (Leica microtome, Leica, Germany). All samples were stained using Hematoxylin and Eosin (H&E) and Picrosirius Red and to further verify cell removal sections were also stained with DAPI. Sections were dehydrated and cleaned in ascending concentrations of ethanol and xylene before coverslips were mounted (DPX mountant, BDH).

All rMSCs were labelled with PKH26 membrane labelling prior to seeding, according to the manufacturer's protocol. Scaffolds were removed from the incubator at each time point, embedded in OCT compound (Tissue Tek) and snap frozen in liquid nitrogen for cryostat sectioning (Leica microtome, Leica, Germany). Slides were washed in PBS to remove excess OCT compound, stained for 15 mins with Alexa Flour®488 Phalloidin (Invitrogen) and mounted in Vectashield Mounting Media with DAPI. Observation under light and fluorescent microscopy and digital image acquisition was carried out with an inverted microscope (Olympus IX 71). Scaffold sections were scaled using ImageJ and the maximum cell migration in both directions away from each injection site was measured at 300μm intervals over the length of the injected scaffold.

5.3 Results

5.3.1 Decellularization

Histological examination by H&E staining of the native artery displayed an extremely cellular tissue embedded with a highly organized ECM architecture of collagen and elastin (Figure 5.2 A).

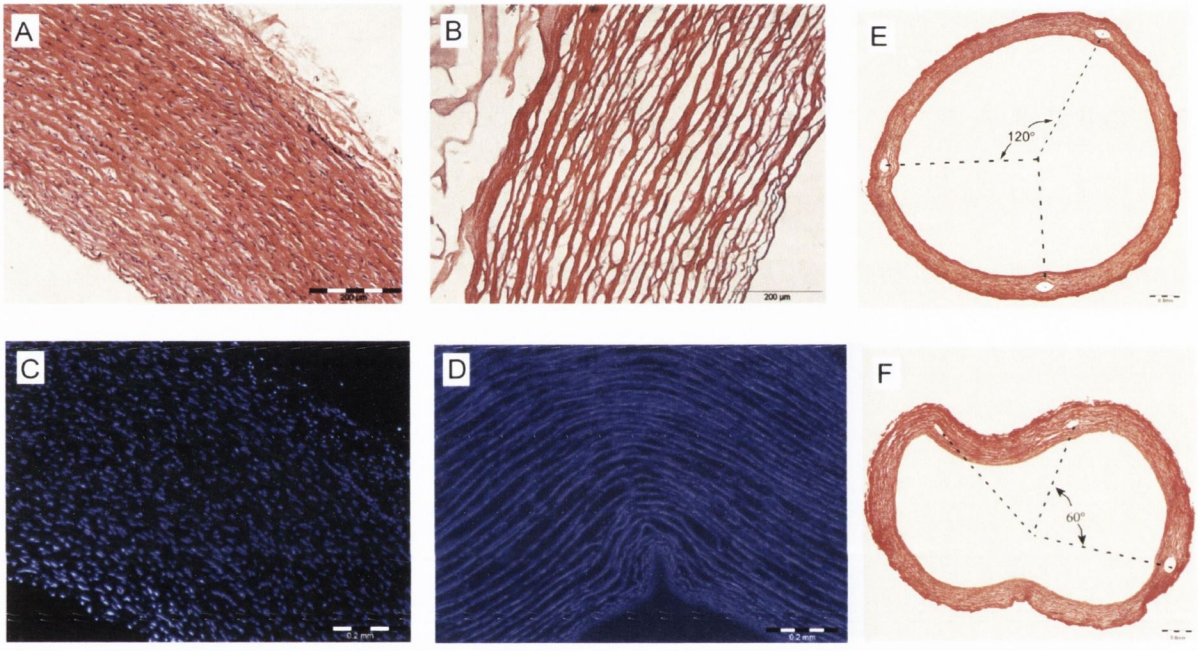

Figure 5.2 Decellularization and Injection Channel Creation

(A) H&E stained native artery displaying high cellularity and ECM density. (B) H&E stain shows cell removal after decellularization with porous undisrupted ECM architecture remaining. (C) Cells fluoresce in DAPI stained section. (D) No fluorescence after decellularization due to removal of cells and cell remnants. (E) Pircrosirius red stain of entire scaffold section. Injection channels created 120° apart with no effect on decellularization or major ECM disruption. (H) Injection channels 60° apart.

In comparison the decellularized scaffolds showed no evidence of cells, and an ECM consisting of undisrupted collagen and elastin networks was retained (Figure 5.2 B). DAPI staining confirmed the complete removal of all cellular components and remnants with no fluorescent nuclear material visible after decellularization (Figure 5.2 C-D).

Medial injection cavities were successfully created within the scaffold by the inclusion of the small bore needles within the medial layer throughout the decellularization process (Figure 5.2 E-F). Minimal ECM disruption was visible around the site of the needle insertion, the collagen fiber bundles and elastin layers were separated by the presence of the needle on the plane in which it was inserted, however there was no evidence of fiber rupture or shearing due to the needle insertion. The remaining cavities were approximately 250μm in diameter, located in the centre of the media, and were consistent along the length of the inserted needle.

The HIM images further confirmed the decellularization process as no cells were visible within the decellularized scaffold within the highly dense and compacted nature ECM components (Figure 5.3). The porous nature of the decellularized scaffold due to the removal of cells after decellularization was clear (Figure 5.3 A-C). The creation of the injection channels correlated with the histology with minimal ECM disruption (Figure 5.3 D). Higher magnification views of the injection channel alone (Figure 5.3 E-F) further highlighted the exact interaction between ECM components and the needle confirming separated elastin sheets and no shearing or rupture. The injection channel was cut open to view the extent of the disruption to the individual elastin layers which the needle separated (Figure 5.3 G-I). Minimal damage was seen along the length of the injection channel, with a smooth inner surface visible over the majority of the channel. Some areas of disruption were visible from the interaction of the needle with the elastin sheets. High magnification view of these areas show only surface level interruption with no visible fiber damage or protrusion from other lamellar layers.

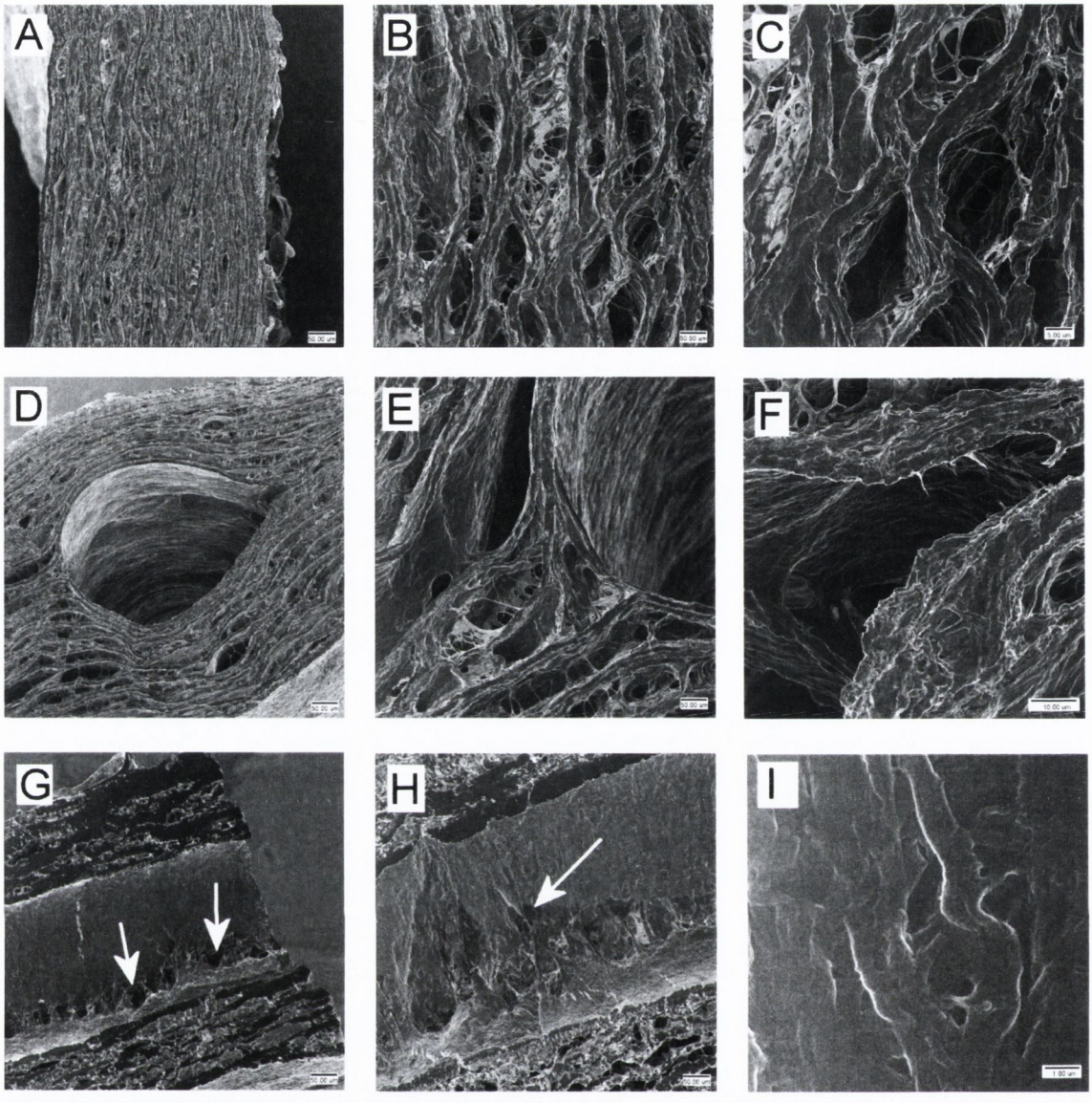

Figure 5.3 Helium Ion Microscopy

(A) View of highly dense entire scaffold wall. (B) Higher magnification clearly displays the porous nature of the scaffold. (C) Individual pores due to cell removal were evident. (D) Entire wall with injection channel shows minimal disruption. (E) High magnification view of the channel/scaffold interface shows no evidence of sheet shearing or rupture. (F) The separation of the sheets of elastin at the site of needle insertion was evident. (G) Cross section of an injection channel revealed minimal ECM disruption (white arrows). (H) Some surface disruption was present (white arrow). (I) High magnification view of this disruption shows no evidence of excessive fiber rupture.

5.3.2 Chitosan/β-GP gel bulk properties

The gel formulation produced a viscous fully injectable gel before solidification. The gel took ~30 minutes for gelation. The chitosan/β-GP gel was dyed for preliminary investigation to determine the injectable nature of the gel within the injection channels. Figure 5.4 displays an injected scaffold with dye added to the chitosan/β-GP gel to emphasise the manner in which the gel was injected within the injection channel. It is clear from this image that the gel was easily injected and suitably filled the injection channel, with some local dispersion into the surrounding media. The presence of the gel was consistent along the entire length of the injection channel. The viscosity of the gel was suitable for injection through the 300 μm diameter small bore needles in a controlled stable manner.

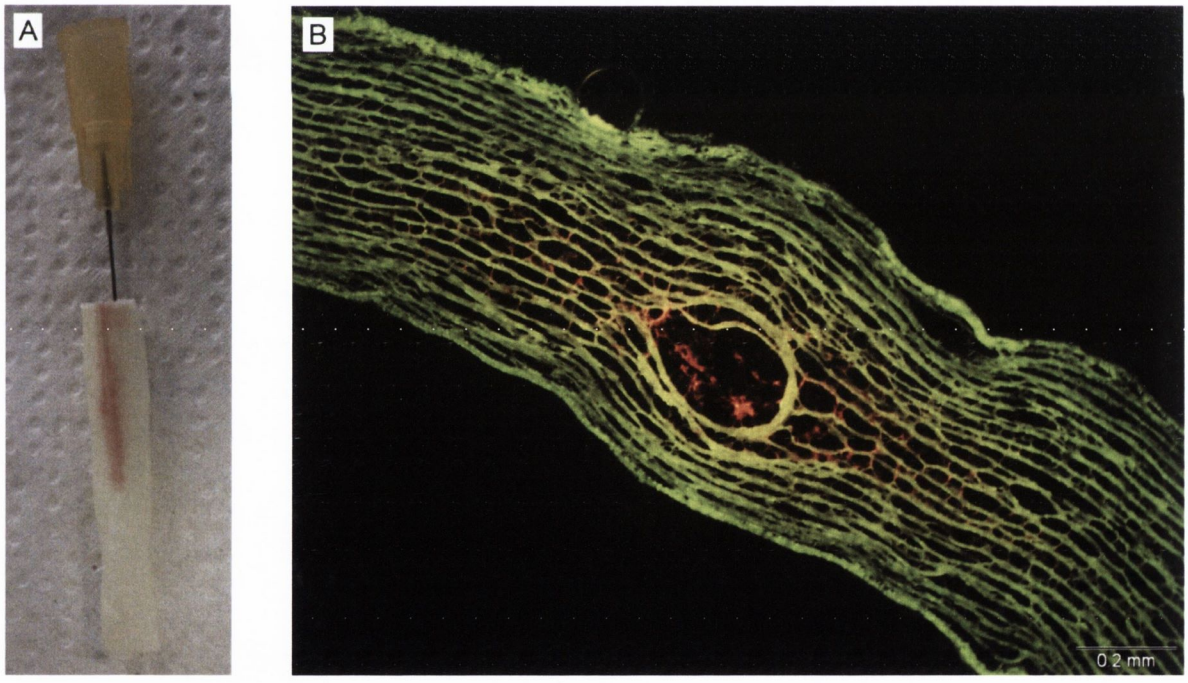

Figure 5.4 Food Dyed Chitosan/β-GP Gel Injection

(A) Red dyed chitosan/β-GP gel injected through injection channel showed filling of the channel and some dispersal within the scaffold. (B) Cyrosection of injected dyed gel displayed a reservoir within the injection channel and some circumferential dispersion.

5.3.3 Rheological testing of chitosan/β-GP gel

Overall, the protein-loaded gel exhibited behaviour similar to the control gel (Figure 5.5). Gelation is represented by an increase in storage modulus; for the protein-loaded gel, this occurred at approximately 30°C. This was slightly lower than the gelation temperature of the control gel (approximately 33°C). Up to around 42°C, the protein-loaded gel maintained a higher storage modulus than the control gel, indicating that the protein-loaded gel had a more solid structure at these temperatures.

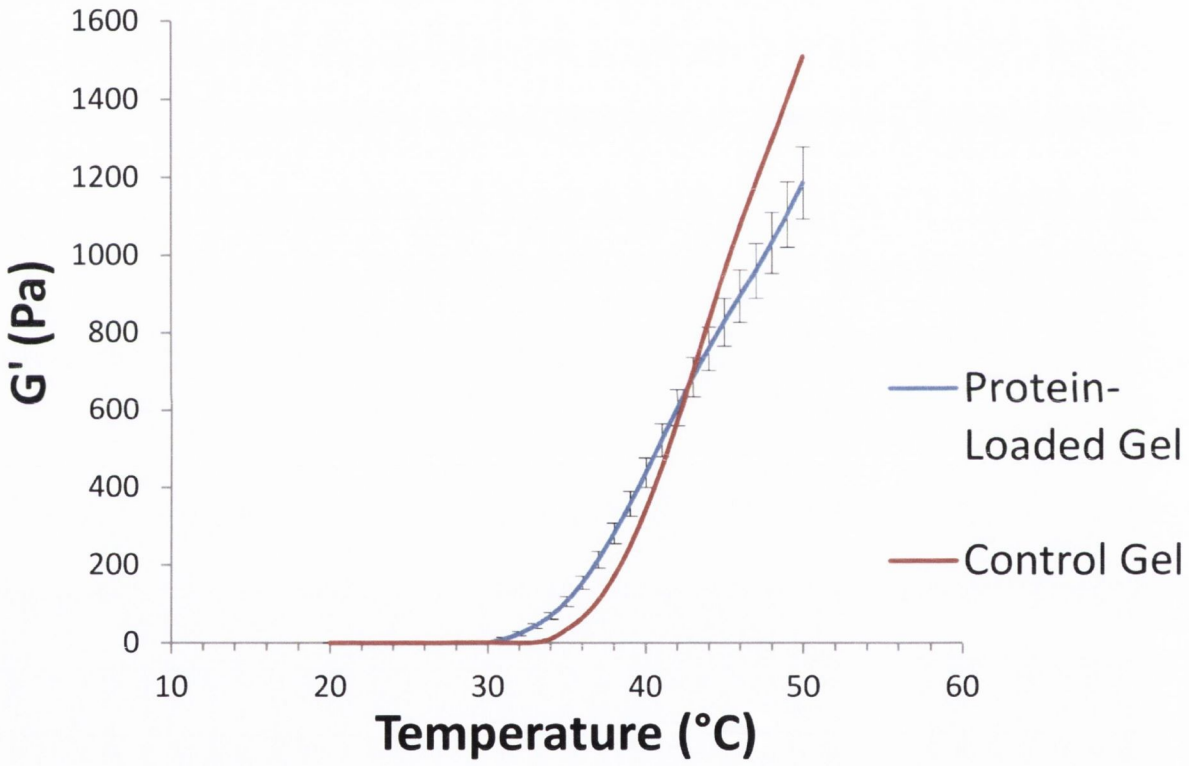

Figure 5.5 Thermoresponse of Chitosan/β-GP Gel

The storage modulus of the protein loaded gel matches closely that of the control with gelation at 30°C (n=3).

5.3.4 HGF release from chitosan/β-GP HGF gel

Chitosan/β-GP gel with a concentration of 5μg/ml HGF was used for release studies. HGF released from 500ml of this gel was studied over 28 days at 37°C. The release profile from the chitosan/β-GP HGF gel displayed a burst release of HGF occurring over the first 24 h, followed by a decreased but sustained release up to seven days. The release then tapered off to full release at 28 days (Figure 5.6). In total, the gel released approximately 58% of its original HGF load over the first 7 days.

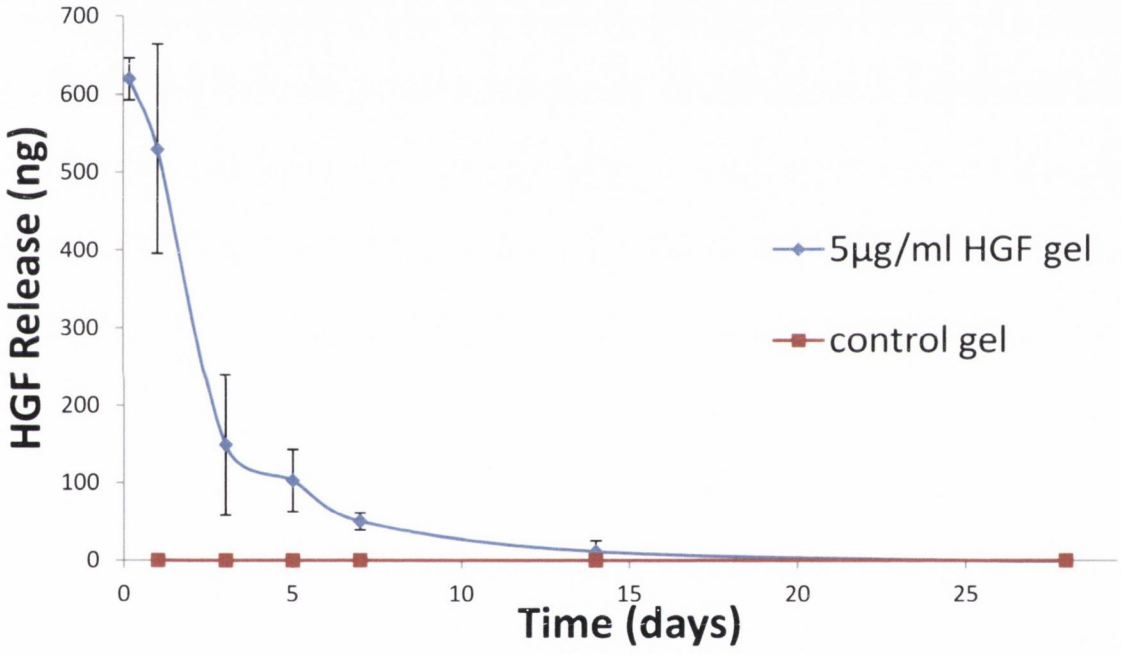

Figure 5.6 HGF Release from Chitosan/β-GP Gel

Sustained release of HGF is visible up to 28 days with 58% release at 7 days (n=3).

5.3.5 Scaffold Repopulation

Group 1

All scaffolds in Group 1 were abluminally statically seeded. Seeded cells were present and viable at all time points. The static cell seeding produced a homogenous distribution

of cells on the abluminal surface (Figure 5.7 A-C). The circumferential distribution of cells was evident from the histology. The cells were also evenly distributed along the entire length of the scaffolds. After 24 h cells were present with high cell retention after seeding (Figure 5.7 A). A similar distribution of cells was visible at 3 days while the fluorescence and cell number appeared reduced after 7 days (Figure 5.7 A-C). All cells at each time point adhered well to the abluminal surface, noticeably; there was no evidence of cell migration into the medial layer of the scaffold.

Group 2

Scaffolds in Group 2 were directly injected through the medial injection channels. Cells were present and viable within the medial layer of all scaffolds at all time points. At 24 h cells were mostly present within the injection channel throughout the length of the channel (Figure 5.7 D). Cells were also present away from the injection site within the media but limited to the distal end of the channel. Migration away from the injection site at 24 h was minimal. At 3 days cells appeared within the channel and also within the media (Figure 5.7 E). Movement away from the injection channel was also evident at 7 days; however, there was a degree of variability across samples in regard to cell number and distance of migration within the media Figure 5.7 F.

Group 3

Scaffolds in Group 3 were injected with chitosan/β-GP encapsulated rMSCs directly within the medial layer of the scaffold. Successful repopulation of the injection channels with cells was evident at each time point. After 24 h cells were largely maintained within the gel located within the channel (Figure 5.7 G). Some cells are visible within the lamellar units away from the injection site. Similarly, at 3 & 7 days repopulation of the

scaffold with cells/gel was confined to within the injection channels (Figure 5.7 H-I). This was consistent across all scaffolds and over the length of the injection channel.

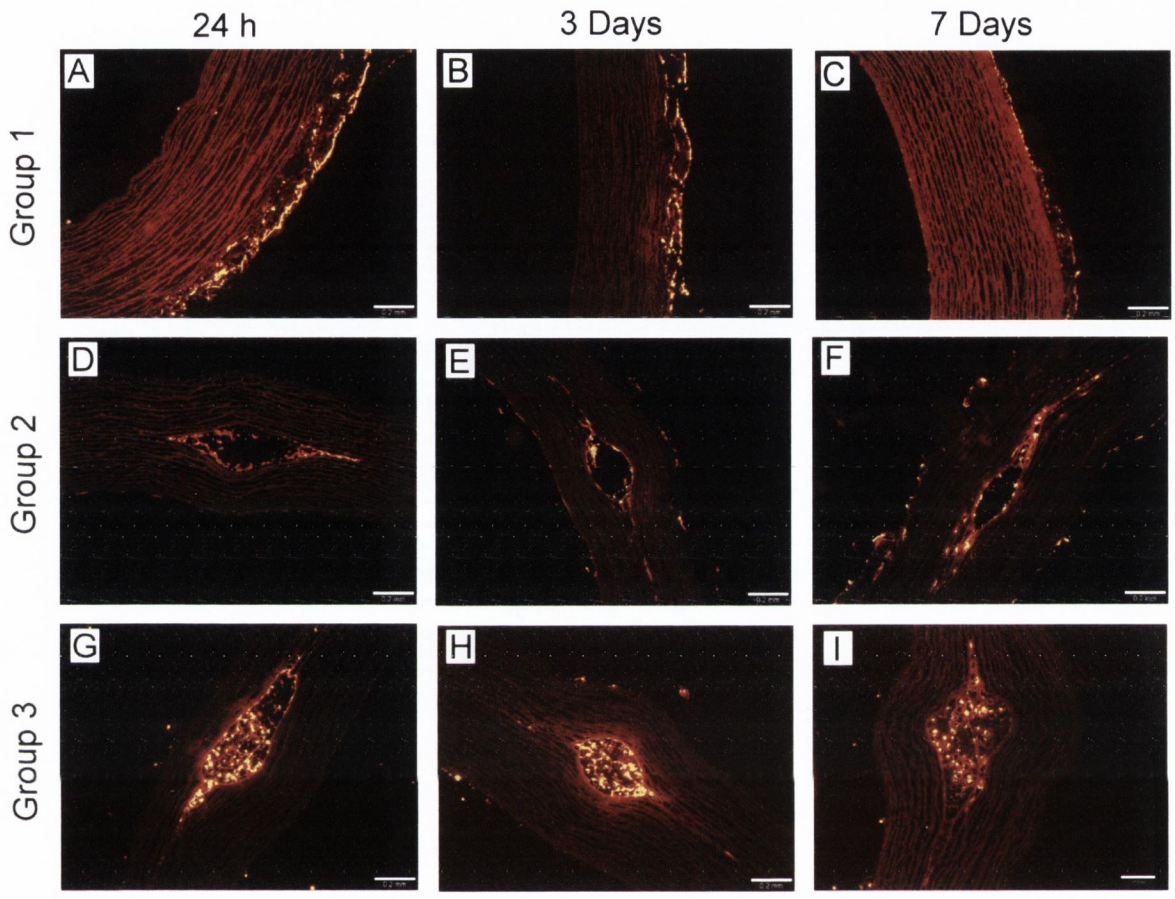

Figure 5.7 PKH26 labelled Cell repopulation

(A) Group 1 static seeding of rMSCs on abluminal surface shows high cell adherence at 24 h. (B) Cell retention is good at 3 days but no scaffold infiltration is visible. (C) Cells are present at 7 days but in reduced numbers. (D) Group 2 direct medial injection of cells without a carrier show cell retention within injection channel at 24 h. (E) Migration and proliferation of cells is visible at 3 days but variable across scaffolds. (F) At 7 days cells have migrated away from injection site within the elastin layers which they were injected. (G) Group 3 gel encapsulated cells were delivered consistently within the injection channels. (H). Cells were present and viable at 3 days with limited migration from the gel. (I) Cells were still encapsulated at 7 days. All scale bars are 200μm.

Group 4

Chitosan/β-GP HGF gel was directly injected within the medial layer of scaffolds in Group 4 and the scaffolds were subsequently abluminally seeded. There was no evidence of any medial repopulation at 7 days. Cells were present and viable but limited to the abluminal surface; there was no evidence of migration of cells radially toward the growth factor in the injection channel (Figure 5.8 A-B). A homogenous distribution of cells away from the injection channels was present on the abluminal surface over the length of the scaffold (Figure 5.8 B).

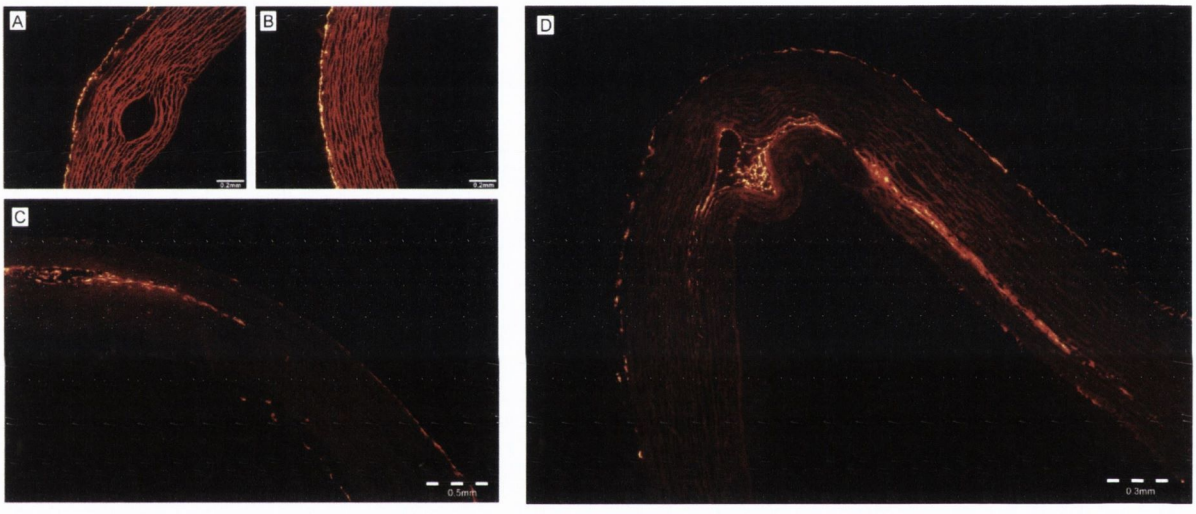

Figure 5.8 Incorporation of Chitosan/β-GP HGF Gel Within Injection Channels

(A) Direct medial injection of HGF showed no promotion of PKH26 labelled cell migration within medial layer after 7 days. Capsulation of cells is evident on the abluminal surface. (D) This capsulation effect was consistent across the scaffold as homogenous cell adherence was visible on the surface only. (C) Directional migration of rMSCs was visible in response to medially injected chitosan/β- GP HGF gel. This was consistent in the direction of the released HGF at each injection channel. (D) The distance of this circumferential migration varied over the length of the scaffold and was confined to the elastin layers separated at the injection site.

Group 5

The scaffolds in Group 5 were injected with both the chitosan/β-GP HGF gel and rMSCs. Cell migration was evident within these scaffolds after 7 days (Figure 5.8 C-D). The migration was seen across all scaffolds and was consistent in the direction of the injected chitosan/β-GP HGF gel. The magnitude of this directional migration varied over the length of the injection channel with the maximum migration evident at the distal end (Figure 5.8 D). The cell migration was limited to the circumferential lamellar units at the injection sites, minimal radial migration was observed. Migration distance toward the released HGF was statistically significant for each scaffold in Group 5 (Figure 5.9 A).

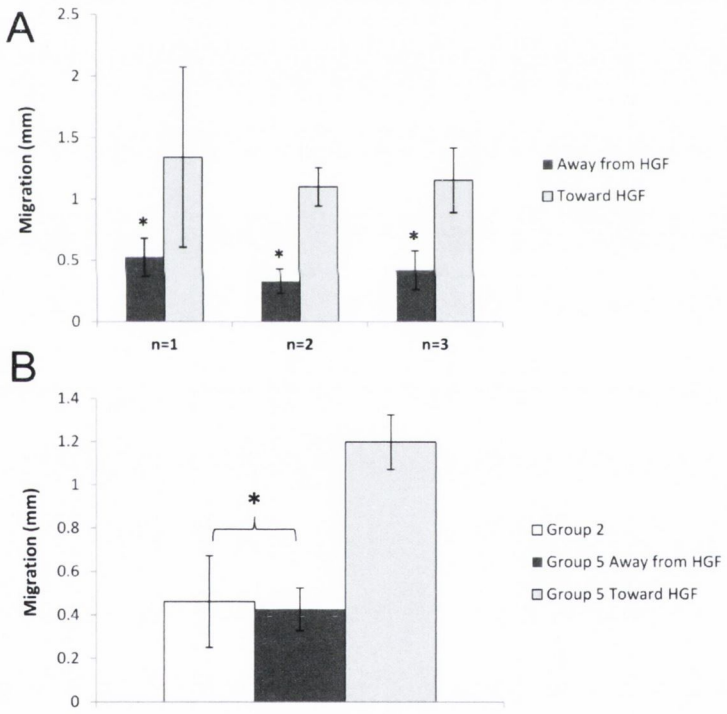

Figure 5.9 Quantification of Cell Migration

(A) Migration toward the released HGF was statistically significant for each scaffold in Group 5. (B) The average migration in Group 2 and migration away from the HGF was significantly different to the average migration toward the HGF.

The average migration in Group 2 and migration away from the HGF was significantly different to the average migration toward the HGF (Figure 5.9 B). The maximum circumferential migration was 3 mm (Figure 5.10 A).

A degree of autofluorescence from the released HGF allowed for visualisation of the injected chitosan/β-GP HGF gel within the scaffold on the DAPI stained sections. This made distinguishing cells from the gel difficult as both fluoresce blue (Figure 5.10 B). However, the PKH26 labelled cells (Figure 5.10 C) allowed for the identification and subsequent removal and thresholding of the cells from the DAPI stained sections so a merged image overlapping the chitosan/β-GP HGF gel onto the PKH26 labelled section was created using ImageJ software. This allowed for the visualisation of the migration path of the rMSCs toward the chitosan/β-GP HGF gel (Figure 5.10 D). The chitosan/β GP HGF gel and cells are all contained within the elastin layers at the injection site.

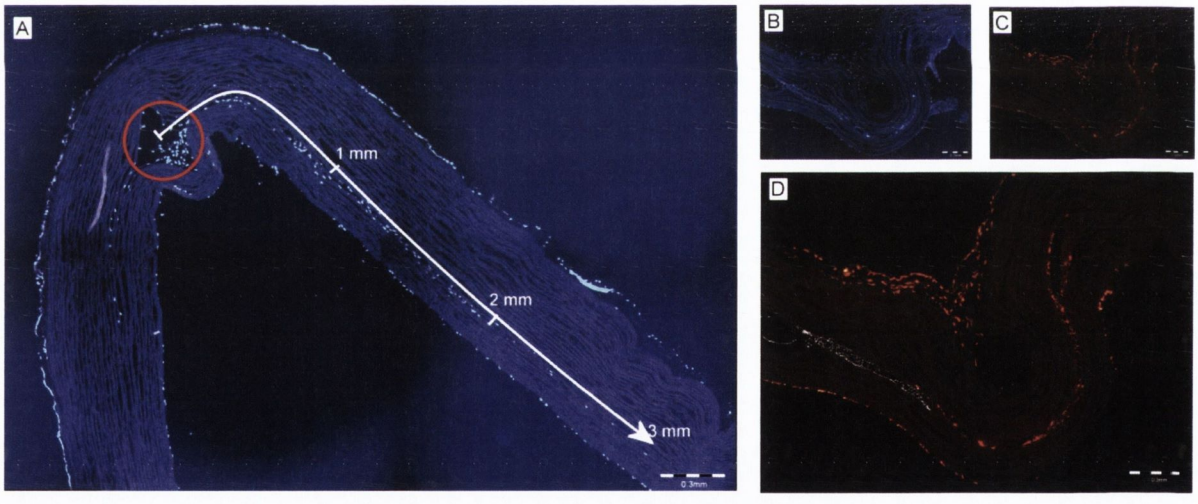

Figure 5.10 Directional Migration in Response to Released HGF

(A) DAPI staining allowed identification of individual cell migration and showed a maximum circumferential migration of 3 mm. (B) DAPI stained section caused released HGF to fluoresce. (C) PKH26 labelled cells fluorescence of the same section. (D) A threshold and overlay of (B) & (C) portrays the migration of the rMSCs toward the released HGF. The injected HGF is constrained within the elastin layer and likewise the injected migrated cells are contained within these same layers.

5.4 Discussion

The clinical translation of TEVG will require grafts with short manufacturing times, produced in a repeatable manner with a suitable geometry for a wide patient cohort. Decellularized arterial scaffolds, unlike other vascular scaffolds, already exhibit the mechanical integrity for direct implantation as vascular grafts (Borschel et al., 2005, Bergmeister et al., 2008). However, this benefit may be negated by the excessive culture times associated with cell seeding these scaffolds, as the remaining matrix is highly dense and has proven difficult to infiltrate with current cell seeding techniques (McFetridge et al., 2007, Yazdani et al., 2009). The fate of seeded cells after implantation and their exact role in remodelling has not yet been fully understood. The ability of seeded cells to secrete signalling molecules to recruit other cell types has been shown to enhance host cell infiltration and remodelling *in vivo*, and may be as important as their potential at fulfilling a functional role after engraftment and differentiation (Iso et al., 2007, Wang et al., 2012b).

Keeping in theme with the customisation techniques for the scaffold described above a more clinically relevant cell source was adopted for the optimisation of cell seeding in this chapter, rMSCs. MSCs are an attractive cell type due to their inherent allogenicity, their capacity to differentiate *in vivo* into endothelial cells and/or SMCs, (Silva et al., 2005, Gong and Niklason, 2008, Mirza et al., 2008) and their ability to secrete signalling molecules to recruit other cell types and modulate the immune response (Da Silva Meirelles et al., 2009, Bajpai and Andreadis, 2012). MSCs have been shown to provide a therapeutic benefit despite migration away from the delivery site after 3 weeks post implantation in infarcted hearts (Iso et al., 2007). Furthermore, they secrete various bioactive molecules which aid tissue regeneration and remodelling, (Da Silva Meirelles et al., 2009) so they can function as a renewable source for these molecules. Zhao et al

successfully differentiated ovine MSCs in culture into both endothelial cells and SMCs before seeding onto a decellularized scaffold and subsequent implantation as a carotid artery bypass graft (Zhao et al., 2010). The grafts were patent and stable after 5 months with no thrombus formation, however, the seeded MSCs which were labelled for tracking were detectable after 2 months but not after 5 months. This further highlights that MSCs may have more of a therapeutic benefit than a functional role in scaffold integration.

The aim of this chapter was to enhance cell migration within the customised decellularized scaffold in order to achieve a more uniform cell distribution within the scaffold. A fully repopulated medial layer may improve the *in vivo* performance by allowing faster remodelling and better integration with the host tissue. Growth factors, if delivered effectively in sufficient concentrations have also been shown to aid cell infiltration and remodelling both *in vitro* and *in vivo* (Tayalia and Mooney, 2009). HGF was utilised as it has been shown to promote the migration of MSCs, (Forte et al., 2006) and chitosan gel as it has been previously employed as a delivery vehicle for cells and proteins (Kasyanov et al., 2009, Wang et al., 2010, Hastings et al., 2012, Faikrua et al., 2013). In this chapter a quick, efficient and repeatable method of combining these therapeutics within a customised decellularized scaffold has been identified.

The decellularization protocol produced a fully acellular porous scaffold ideal for cell attachment and growth (Figure 5.2 A-F). The addition of the needles prior to decellularization created the injection channels within the scaffolds in an organised and repeatable manner with minimal ECM disruption (Figure 5.2 E-F). HIM further highlighted this localised ECM disruption with particular emphasis on the minimal fiber damage within the channel itself (Figure 5.3 G-I). The 30 minute gelation of the chitosan/β-GP gel is ideal for this application. While rapid gelation is preferable to prevent dispersion into surrounding tissue and loss of a concentrated reservoir, there are

no external forces acting on the scaffold immediately after injection, therefore 30 minute gelation is suitable for this purpose. The addition of HGF did not alter the handling properties or thermoresponse of the gel as a similar response to the non protein loaded control was visible (Figure 5.5).

The HGF release profile (Figure 5.6) showed that this gel is capable of sustained HGF release. There was an initial burst release in 24 h with 58% release at 7 days and further sustained release until ~20 days. This is a desirable release profile for the local biochemical stimulation of either cells seeded in conjunction with the HGF within the scaffold or for the recruitment of host cells post implantation. In comparison to other techniques used for growth factor delivery the chitosan/β-GP HGF loaded gel demonstrates excellent delivery efficiency. Coating techniques such as soak loading can result in loosely attached molecules and non-homogenous distribution of the protein on the scaffold which can potentially be lost due to handling during implantation. Kurane et al showed that encapsulating bFGF in agarose gel loaded within the lumen significantly enhanced repopulation of a decellularized scaffold after subdermal implantation (Kurane et al., 2007). Similarly, VEFG and bFGF have been coated onto decellularized scaffolds to enhance re-endothelialisation (Conklin et al., 2004, Zhou et al., 2009). These studies establish that growth factors can aid cell seeding and repopulation, however cell migration in response to a growth factor has not previously been demonstrated within the medial layer of decellularized scaffolds.

Cell adherence and retention was high with the standard abluminal seeding technique used in Group 1, however capsulation of seeded cells is an issue with this technique (Yazdani et al., 2009, Villalona et al., 2010, Neff et al., 2011). This is evident as no cells were present within the medial layer at any time point showing only abluminal surface integration with the scaffold. Group 2 scaffolds were directly injected with

rMSCs, in Chapter 3 successful repopulation of the medial layer using these injection techniques was demonstrated, however this had not been undertaken with rMSCs or extended to a 7 day study. Cells were present and viable within the medial layer at each time point, however, the distribution and cell quantity was variable across scaffolds. This demonstrated that while the medial injection technique was successful, it may be limited and difficult to standardise. Clinical translation of such a technique would require high levels of reproducibility and the elimination of any variability to gain regulatory approval. In this instance direct injection without the use of a cell carrier/vehicle may not be the optimum injection mechanism if no further maturation is undertaken. In contrast, in Group 3 the encapsulation of rMSCs within the chitosan/β-GP gel provided an ideal vector for the quick, consistent and efficient delivery of cells to the medial layer. Hydrolgels used successfully as cell carriers have been largely used for delivery to targeted sites such as infracted hearts or in critical limb ischemia with the principal benefit being the retention of cells at the target site, preventing reflux after injection (Hua et al., 2003, Borden et al., 2010). However, reflux in this application is not an issue as cell injection was *in vitro* in a quiescent environment, therefore the primary benefit of cell encapsulation was repeatable and consistent cell delivery.

Medial repopulation in Group 4 proved entirely unsuccessful as there were no cells present within the medial layer after 7 days of static culture (Figure 5.8 A-B). This 7 day time point coincides with the majority of HGF release from the chitosan/β-GP and it was hypothesised that a sufficient release of HGF would promote a degree of radial migration through the lamellar layers. The lack of cell migration was likely due to the highly dense nature of the decellularized matrix architecture (Figure 5.3 C). Radial cell migration is nonexistent notwithstanding the reduction in density of the scaffold due to collagen digestion. As shown in Chapter 3 the digestion of small collagen fibers improves

cell dispersal upon medial injection, but this was largely limited to the circumferential direction. Although, the concentric sheets of elastin that constitute the arterial wall contain pores, (O'Connell et al., 2008) evidently these sheets are too dense for cells to easily migrate through. A capsulation effect on the abluminal surface which was in direct contact with the nutrient supply was seen similar to the Group 1 statically seeded controls. This result further highlights the inefficiency of abluminal seeding for decellularized scaffolds. Some research groups claim migration of cells up to 200μm upon further in vitro maturation under dynamic bio-mimetic conditions after abluminal static seeding (Yazdani et al., 2009), however this may be due to ECM synthesis by the seeded cells rather than actual infiltration of the dense scaffold.

In contrast, migration was visible toward the released HGF after 7 days in Group 5. Circumferential migration in the direction of the injected chitosan/β-GP HGF was evident at each cell injection site (Figure 5.8 C-D). The distance of circumferential migration varied distally along the injection channel, with a maximum cell migration of 3mm (Figure 5.10 A). The migrated cells were contained within the elastin layers that were disrupted by the creation of the injection channels with no further radial migration of cells evident. This appears to be a novel result as it demonstrates a large amount of cell migration within the medial layer of a decellularized scaffold in a short time period. Cell migration in static culture of $> 200\mu m$ was shown by McFetridge et al whereby a decellularized porcine artery was cut open radially and left in culture with the cut surface facing down which allowed human SMCs to migrate circumferentially through the elastin layers and collagen fibers (McFetridge et al., 2007). In addition, abluminally seeded cells in the same study displayed no radial infiltration within the medial layer after two weeks static culture and three weeks dynamic culture in a perfusion bioreactor. While this clearly demonstrates the ability of cells to migrate circumferentially within decellularized

tissue, the 3 mm migration demonstrated here is significantly higher and is achieved without cutting the scaffold wall open. Furthermore, the migration is consistent across scaffolds. There was a statistically significant difference in the distance of cell migration toward the released HGF in each scaffold in Group 5. The overall average migration toward the HGF was also significantly different to both the migration away from the HGF, and the average migration achieved without the HGF stimulus in Group 2. This further highlights the consistent benefit of utilising a growth factor stimulus to increase cell migration within the medial layer.

The overlay of the PKH26 labelled cells and DAPI stained cells (Figure 5.10 B-D) highlighted the mechanism of cell migration. The HGF is white in this image while the migrated cells fluoresce red. This clearly underlines how the dense elastin sheets prevent the radial migration of cells and similarly how the released HGF is constrained within these layers. The HIM images further highlight the dense elastin layers and how the spreading of these sheets at the injection channels acted as the entry point for the injected cells to begin their circumferential migration while the same elastin sheets prevent radial migration (Figure 5.3 D-F).

It is envisioned that other growth factors will have similar release profiles from the chitosan/β-GP gel and can therefore be incorporated within our scaffold in the same manner as the HGF. Proteins such as IGF, VEGF and bFGF can further enhance host cell recruitment, proliferation and differentiation and ultimately faster and superior scaffold integration and tissue remodelling. The creation of multiple injection channels within our customised decellularized scaffold is possible which can allow for the loading of multiple gel encapsulated bioactive molecules and/or gel encapsulated MSCs and their sustained controlled release.

5.5 Conclusion

The results described in this chapter demonstrate the use of a bioactive customised decellularized vascular scaffold. The use of a chitosan/β-GP gel allowed for the controlled and sustained release of growth factors within this scaffold. The clinically relevant cell source of rMSCs were implemented successfully within the customised decellularized scaffold. Encapsulation of rMSCs in the chitosan/β-GP delivers a reproducible consistent concentrated cell reservoir within the medial layer. Cell migration within the medial layer of this scaffold due to released HGF demonstrates the feasibility of releasing bio-active molecules to the medial layer to accelerate scaffold repopulation.

Chapter 6 Bioreactor Design and Validation

All bioreactor design and validation was carried out in conjunction with Alan Ryan (Royal College of Surgeons in Ireland).

6.1 Introduction

As discussed in Chapter 2, bio-mimetic environments which match the arterial hemodynamic forces experienced *in vivo* are utilised to dynamically condition TEVGs *in vitro*. This is undertaken to augment mechanical properties by increased ECM synthesis and pre-condition seeded cells prior to implantation. The benefits of applying shear stress and cyclic strain to vascular cells was initially determined in two-dimensional systems (Breen et al., 2006), and these displayed how cells respond to varying flow regimes by changes in gene expression patterns and cell differentiation (Davies, 1995). These systems are ideal for investigations relating to cell monolayers, in particular EC seeded substrates. However, for TEVG development a three dimensional dynamic system is required. The replication of an accurate physiological microenvironment is usually undertaken with pulsatile flow bioreactors. The pulsatile flow has the ability to emulate the hemodynamic forces in a controlled system, with a basal pressure created by the reservoir of pulsed medium, combined with the pulsatile nature of the flow, causes a cyclic strain on the construct. The pulsatile flow also creates shear stress on the luminal surface of the construct. Alteration of the working length of the construct by manipulating mounting of the construct within the system creates an axial strain within the construct. These controllable parameters contained within a single bioreactor system account for all the hemodynamic forces acting on the arterial wall *in vivo* (Figure 2.4).

Pulsatile flow bioreactors are utilised across all types of tissue engineering techniques, regardless of the scaffold type (Williams and Wick, 2005, Hoerstrup et al., 2006, L'Heureux et al., 2006, Yazdani et al., 2009). The primary aims of applying simulated hemodynamic forces to constructs are: cell migration, proliferation, morphology change and alignment, ECM synthesis, cell differentiation and phenotype modulation. In general, decellularized scaffolds do not rely on ECM synthesis as the pre-

formed ECM architecture already exists, however bioreactors are integral for repopulating decellularized scaffolds by promoting cell migration and differentiation toward SMCs if non native cell sources are utilised. Furthermore, for both native SMCs and differentiated SMCs the switch in phenotype from synthetic to contractile is of utmost importance for the creation of a quiescent medial layer and can be controlled through the use of bioreactor systems (Nerem and Seliktar, 2001, Chan-Park et al., 2009).

The use of a pulsatile flow bioreactor system is an ideal method to determine the potential *in vivo* response of medially injected MSCs. The aim of this chapter is to design and validate such a system that will allow the transduction of hemodynamic forces to MSCs within the medial layer of a customised decellularized scaffold, while also allowing for the creation of a luminal cell monolayer. In order to develop a customised bioreactor system for this specific application the following design criteria must be met:

- The ability to manipulate flow rate and pressure to achieve physiological levels of cyclic strain.
- The entire system must fit and operate within a standard incubator to provide 5% CO_2, 100% humidity to the seeded constructs.
- The bioreactor must accommodate 3 or more isolated constructs at one time.
- A method of seeding a uniform distribution of ECs within the lumen of the constructs without unnecessary extra construct handling.
- Components must be fully sterilisable and contained within a leak free system.
- Overall ease of assembly in an aseptic environment.
- Ability to adjust the axial strain on the construct.
- Reproducibility across constructs.

6.2 Materials and Methods

6.2.1 Bioreactor Layout

Simplicity is the key focus in the layout and design of this custom built pulsatile flow bioreactor. Different methods for providing the pulsatile flow within such a system have been used in the literature, namely compressed air (Hoerstrup et al., 2001), syringe pumps (Syedain et al., 2011), peristaltic pumps (Tschoeke et al., 2008) or a combination of these (Niklason et al., 1999). A peristaltic pump is utilised here as it easily provides the desired pulsatile flow pattern and accommodates a range of tubing sizes to allow variation of flow rates. The height of the reservoir of culture media that is pulsed through these tubes determines the overall basal pressure of the system. The main method of utilising a peristaltic pump to provide cyclic strain to three constructs simultaneously is shown in Figure 6.1.

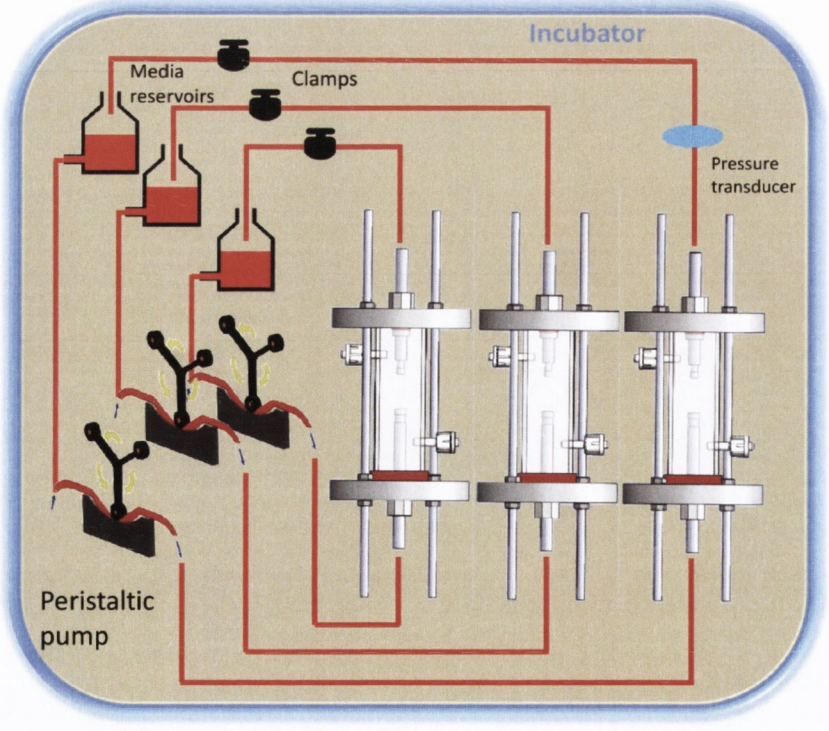

Figure 6.1 Bioreactor Layout

Parallel flow configuration with individual medium reservoirs and flow circuits.

The pressure and cyclic distension is controlled by altering the medium reservoir height and constriction of the tubing with a pinch valve distal to the chamber. Medium is pulsed through each chamber from an individual reservoir and the entire system can fit within a standard incubator. Individual flow circuits reduce the risk of contamination, as the medium reservoirs are not shared.

A multi-channel three headed roller peristaltic pump that can incorporate up to four tubing circuits was sourced. This peristaltic pump (FH100 M, Thermo Scientific) allows for the attachment of multiple cassettes on the pump head containing tubing of suitable dimensions to pulse the medium through the individual chambers at suitable flow rates (Figure 6.2). The pump head rotation is fully controllable and set to 20 rpm, as it is a three headed roll this provides a pulse frequency of 1 Hz which is equivalent to physiological conditions of 60 beats/min.

Figure 6.2 Multi-channel Peristaltic Roller Pump

The multi-channel pump can provide pulsatile flow to four chambers simultaneously, reducing contamination risk and adding reproducibility. (www.thermoscientific.com)

6.2.2 Chamber Design

The design inputs for the chamber are:

1. Ease of assembly with minimal handling to reduce contamination risk.
2. Easily mounted, leak proof scaffold.
3. Adjustable scaffold working length.
4. Fully sealed system.
5. EC seeding capability.

A "step up" assembly approach was utilised to create a simple means of loading the scaffold and assembling the surrounding chamber. This consisted of the gradual building of the individual components, allowing for minimal scaffold contact, and is depicted via the numbered steps in Figure 6.3, as follows:

(1) The first step in the assembly process is to place the silicone seals onto the stainless steel scaffold holders.

(2) The scaffold is then mounted onto the stainless steel holders, using sutures to create a tight leak proof seal.

(3) The outer polycarbonate casing is placed over the scaffolds and the holders are inserted through the polycarbonate plates, which are then compressed to form a tight leak proof seal.

(4) The entire chamber unit is then compressed and tightened with nuts on threaded stainless steel bars.

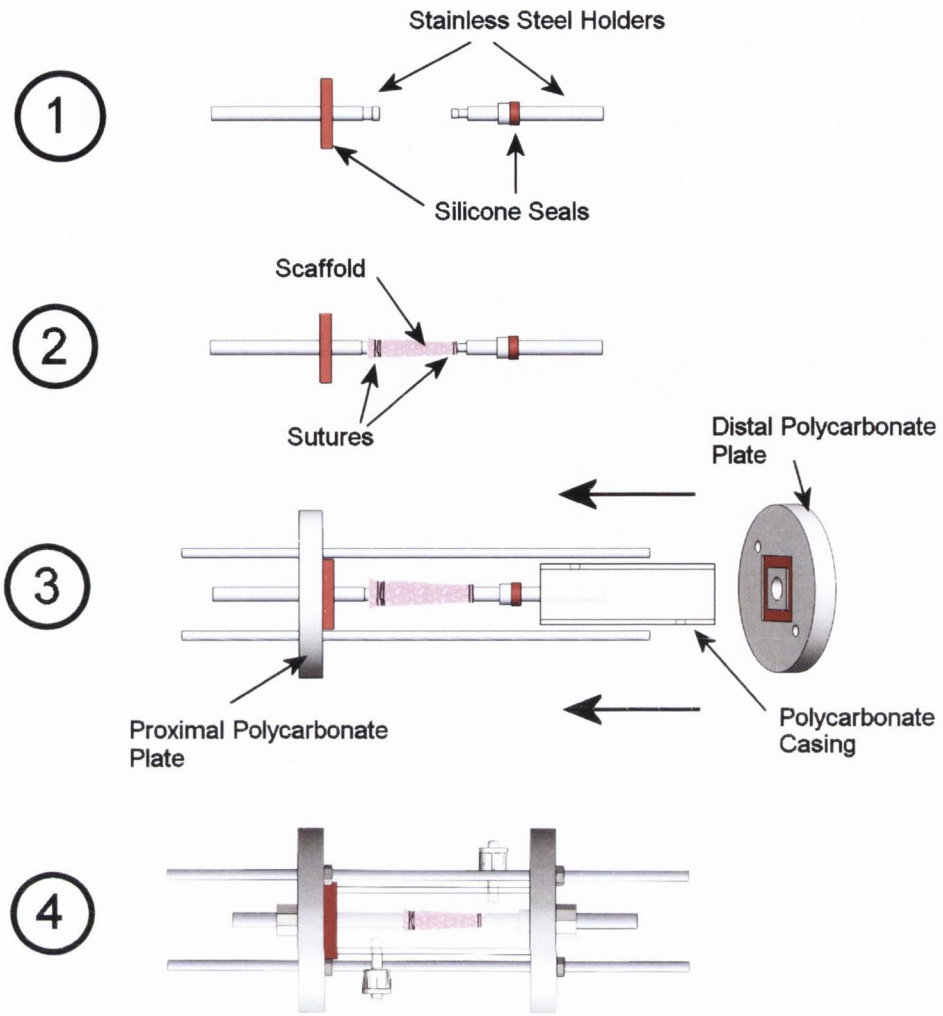

Figure 6.3 Chamber Design

A "step up" assembly approach was utilised for bioreactor assembly. (1) Silicone seals are placed on the stainless steel holders. (2) The scaffold is mounted on the holders using sutures. (3) The polycarbonate casing is placed over the scaffold and compressed between the silicone seals and polycarbonate plates. (4) The entire chamber unit is fully sealed using nuts on threaded stainless steel bars.

The outer casing contains luer lock connectors which allow for the attachment of 0.2μm filters for gas exchange Figure 6.4 A. The polycarbonate plates are circular in profile to allow EC seeding of the lumen surface. An EC suspension can be injected within the scaffold lumen and the entire chamber can be rotated at low speed to achieve a uniform cell distribution on the lumen surface. The proximal silicone seal allows for the

adjustment of the scaffold holder which subsequently can change the working length of the scaffold until the desired axial stretch of ~20% is achieved (Figure 6.4 B).

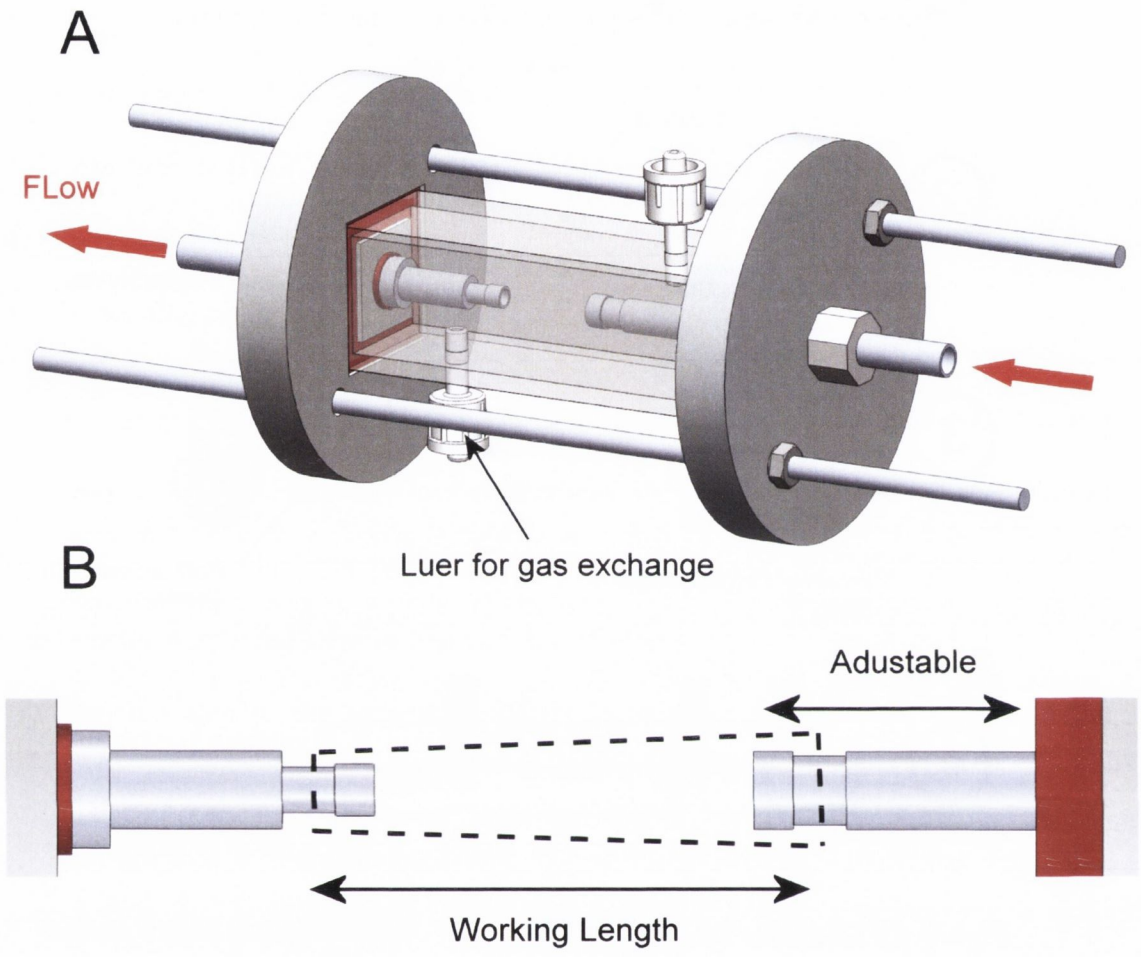

Figure 6.4 Assembled Bioreactor Chamber

(A) Isometric view of chamber showing flow direction with red arrows. (B) Detailed view of stainless steel holders for construct mounting, the non-fixed holder is adjustable to alter the working length of the construct applying an axial stress.

The individual chamber units were connected to 6.4 mm diameter silicone tubing (ThermoScientific General-Purpose BioPharm Silicone Tubing) by press fitting to the stainless steel holders. Glass beakers with an inlet and outlet ports were used as reservoirs and attached to a retort stand to the maximum height available within the incubator.

6.2.3 Cytotoxicity Tests

Extraction tests were performed on all materials that come into contact with tissue culture medium within the bioreactor system. These tests were performed in accordance with ISO Standards (ISO 10993-5 Biological evaluation of medical devices - Part 5: Tests for in vitro cytotoxicity). These tests determine the lysis of cells and/or the inhibition of cell growth caused by extracts from the materials used within tissue culture medium. Materials were submerged in rMSC tissue culture medium, (as described in Chapter 5) with a ratio of surface area per extraction volume of 6 cm^2/ml for 24 h at 37°C. The following materials were tested:

- Polycarbonate Chamber
- Polycarbonate Plates
- 316L Stainless Steel Holder
- Silicone Seal
- Thermo Scientific General-Purpose BioPharm Silicone Tubing
- Polyvinyl chloride (PVC)
- Polystyrene (tissue culture plastic)
- Assembled Bioreactor System

The PVC was selected as a positive control as it is a known cytotoxic material and polystyrene as the negative control as it is a known non-cytotoxic material. The effect of sterilisation methods on the materials were considered in the preparation for the extraction test with materials subjected to both autoclave sterilisation and ethanol sterilisation by soaking for > 30 mins. The entire bioreactor system was assembled and/or flushed with ethanol for > 30 mins. The ethanol was then removed and the entire system

flushed in sterile PBS for another 30 mins. The PBS was then removed and culture medium pulsed through the system within the incubator for 24 h.

In order to access cell viability an extract MTT Cell Growth Assay (Millipore ™, Ireland) was performed as described in Section 3.2.6. DNA quantification was performed using a Quant-iT™ PicoGreen dsDNA kit (Invitrogen, Biosciences, Dublin, Ireland) in accordance with manufacturer's instructions. 20,000 rMSCs were seeded onto 6 well plates and cultured for 24 h. The medium was then replaced with extract medium for each material and cultured for an additional 24 h. Cells were lysed in 0.2 M carbonate buffer and 1% Triton X-100 and subjected to three freeze thaw cycles. Samples were incubated in Picogreen™ working solution. Sample fluorescence was measured (excitation 480 nm, emission 538 nm) and DNA concentration deduced using a standard curve.

6.2.4 Validation

Cyclic Strain

Cyclic strain on the scaffold wall is primarily regulated via a pinch valve attached to the silicone tubing downstream of the chamber unit (Figure 6.5 A). As the pinch valve is closed it creates a restriction in the tubing, thus increasing the pressure upstream to the valve and subsequently increasing the expansion of the scaffold wall. To confirm the magnitude of the deformation, video extensometer tracking was utilised, so the level of cyclic strain applied to the construct by the pulsatile flow could be calculated. Images were taken using a USB microscope camera system (Dinolite, The Netherlands) at a magnification of 20 X. The mounted constructs' working length was adjusted to 20% axial stretch, prior to connection to the bioreactor system.

The next step involved connecting the chamber with the chamber unit to the rest of the bioreactor system. At this position the diameter of the unloaded construct was

determined by image capture (Figure 6.5 B). This image included a section of the stainless steel holder which was used to dimensionally calibrate the image. Pulsatile flow was then initiated within the incubator; this pressurised the system and initiated cyclic strain within the construct. After the system had equilibrated a one minute video was recorded of the pulsing construct using the USB microscope camera with the incubator door open. The recorded video was split into individual frames and calibrated using the dimensions of the stainless steel holder. Using ImageJ (US National Institutes of Health) the individual frames were thresholded to produce the expanded and relaxed construct wall diameter, and the average diameter was measured for each frame over three locations along the construct (see Figure 6.5 D).

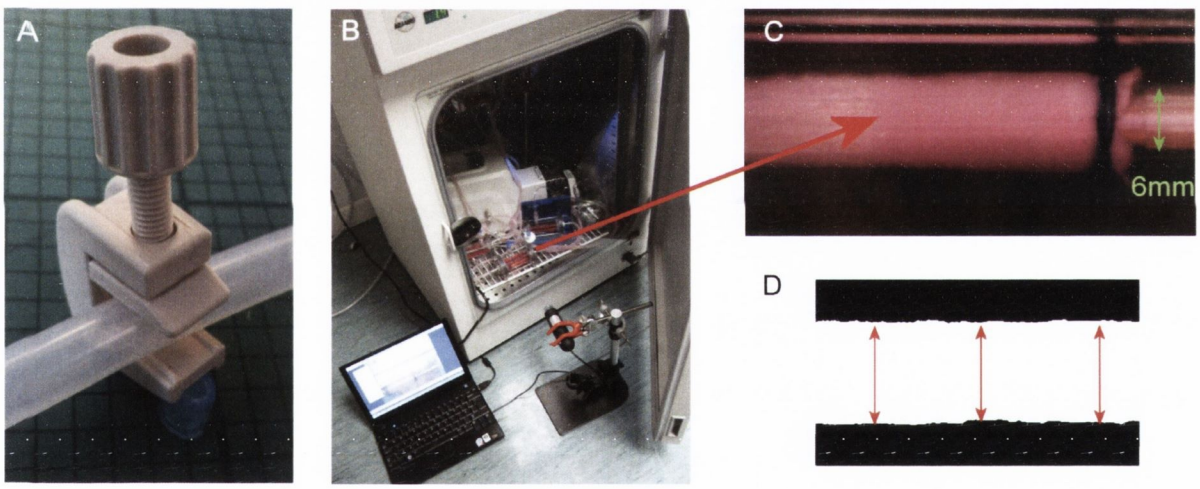

Figure 6.5 Cyclic Strain Measurement

(A) Clamp allows constriction of tubing distal to the bioreactor chamber. (B) Video capture of pulsing construct. (C) Captured frame of diastole with reference dimension for calibration. (D) Thresholded image with multiple diameter measurements.

The amount of constriction on the tubing was altered and further video captured until a desired level of ~5% cyclic strain was obtained. The pressure was measured distal to the chamber using a digital manometer (Digitron, Farnell, Ireland) to determine the peak systole and peak diastole pressures across the system.

Shear Stress

The bioreactor system has been designed to match the key features of arterial flow, namely; the flow rate, Reynolds number, shear rate, and shear stress. In order to study the dynamic flow characteristics of the system a number of assumptions are necessary.

- The vessels are assumed to be straight, rigid tubes with a smooth luminal surface and a non-porous wall.
- The flow is assumed to be steady state and entrance effects are neglected.

In order to determine whether the flow is of a laminar or turbulent nature inside the construct, it is necessary to calculate the Reynolds number (Re). Reynolds number is a dimensionless number which quantifies the relationship between inertial and viscous components in a flow system via the following formula:

$$Re = \frac{d * \bar{V} * \rho}{\mu} \qquad \text{(Eqn. 6.1)}$$

Where d is the internal vessel diameter (0.5cm), ρ is the fluid density (1.05g/cm^3), μ is the fluid viscosity, which is approximately 1 centipoise (1 mPa.s) at 37°C for supplemented tissue culture medium, and $\bar{V}$ is the mean velocity which can be calculated from the experimentally determined flow rate φ (60mls/min) by equation 6.2, below:

$$\bar{V} = \frac{4 * \varphi}{\pi * d^2} \qquad \text{(Eqn 6.2)}$$

The mean wall shear stress, τ_{shear}, can be calculated using the Hagen-Poiseuille equation, below:

$$\tau_{shear} = \frac{4 * \mu * \varphi}{\pi * r^3} \qquad \text{(Eqn 6.3)}$$

Where r is the internal radius.

6.3 Results

6.3.1 Bioreactor System

The bioreactor system was successful in providing a pulsatile flow and subsequent cyclic strain to the mounted scaffolds with the following key advantages:

- The stainless steel holders proved successful at maintaining the construct in position, additionally no leakage occurred in the system once pressurised (Figure 6.6 A).
- The suture attachment proved to be a simple and quick method of mounting the scaffold and was undertaken with minimal handling (Figure 6.6 B).
- The chamber design and step up assembly process also allowed for quick assembly with minimum time out of culture medium for the cell loaded scaffold.
- The silicone sealing system was leak proof and tested beyond the range of the physiologic pressures experienced in this application (>200 mm Hg).
- The luer lock connectors attached easily to 0.2 μm filters to allow for sufficient gas exchange for the culture medium located within the chamber and can be easily removed and replaced without disrupting the flow regime (Figure 6.6 C).
- The entire assembled unit fit easily within an incubator allowing for a reservoir height of 60cm. This generated a basal pressure with a peak systole of ~70 mm Hg and peak diastole pressure of ~40 mm Hg, using 6.4 mm outer diameter tubing, with a volumetric flow rate of 60 ml/min.
- The Reynolds Number was calculated as 268 and the mean wall shear stress was 0.84 dynes/cm^2.

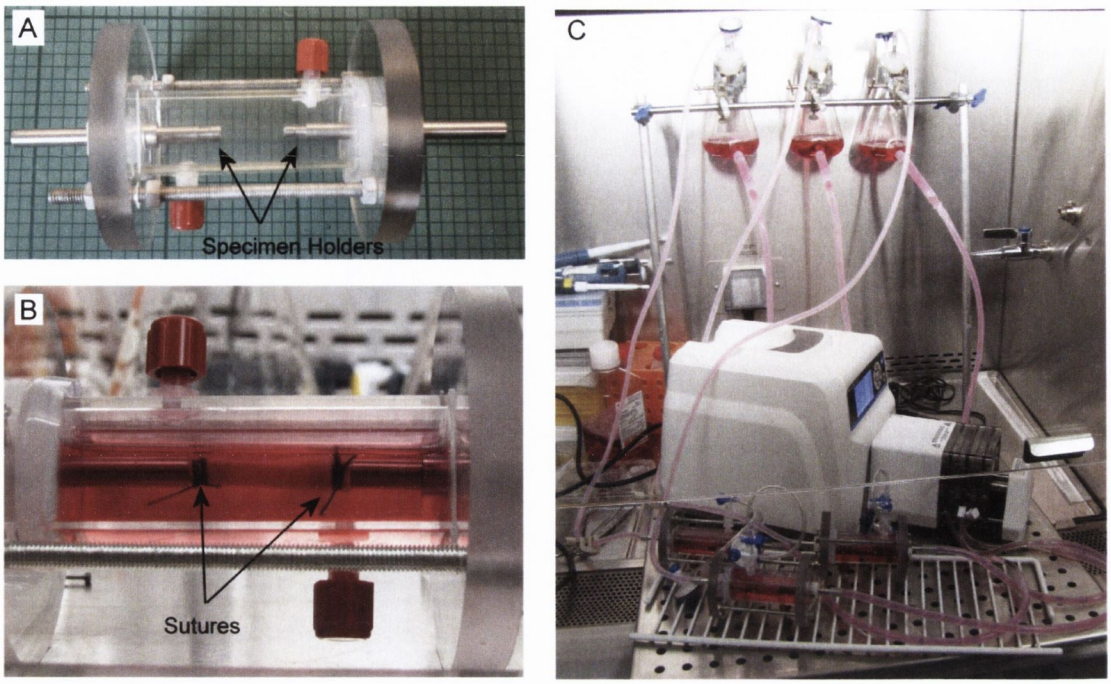

Figure 6.6 Assembled Bioreactor System

(A) Chamber assembly with inlet and outlet for gas exchange and waste media removal. (B) Suture attachment of construct. (C) Entire assembled bioreactor.

6.3.2 Cytotoxicity

The extraction tests on the materials used to construct the bioreactor and the bioreactor system itself were not cytotoxic to rMSCs. The metabolic activity as determined using the MTT assay showed similar levels of activity for each material compared to the negative control (polystyrene) and a significant difference to the positive control (PVC) was evident for each material. The bioreactor system was also significantly different to the positive control (Figure 6.7).

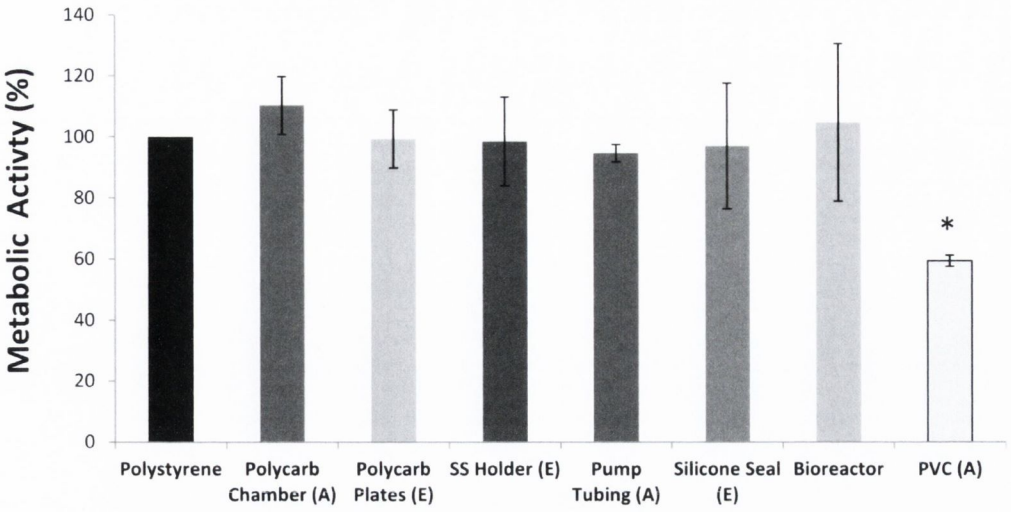

Figure 6.7 MTT Assay Cytotoxicity Results

*Each of the bioreactor components and the bioreactor system performed similarly to the negative control polystyrene and were significantly different to the positive control PVC. A denotes autoclave sterilisation while E denotes ethanol sterilisation. Results are normalised to polystyrene negative control expressed as 100% metabolic activity, *p < 0.05 vs positive control.*

Similar results were obtained for the DNA quantification assay used to determine the effect of the extracted medium on rMSC proliferation. The Quant-iT™ PicoGreen dsDNA assay showed similar levels of cell proliferation after 24 h for each of the bioreactor components and the bioreactor system to the negative control. A significant difference was seen for each of the groups compared to the positive control.

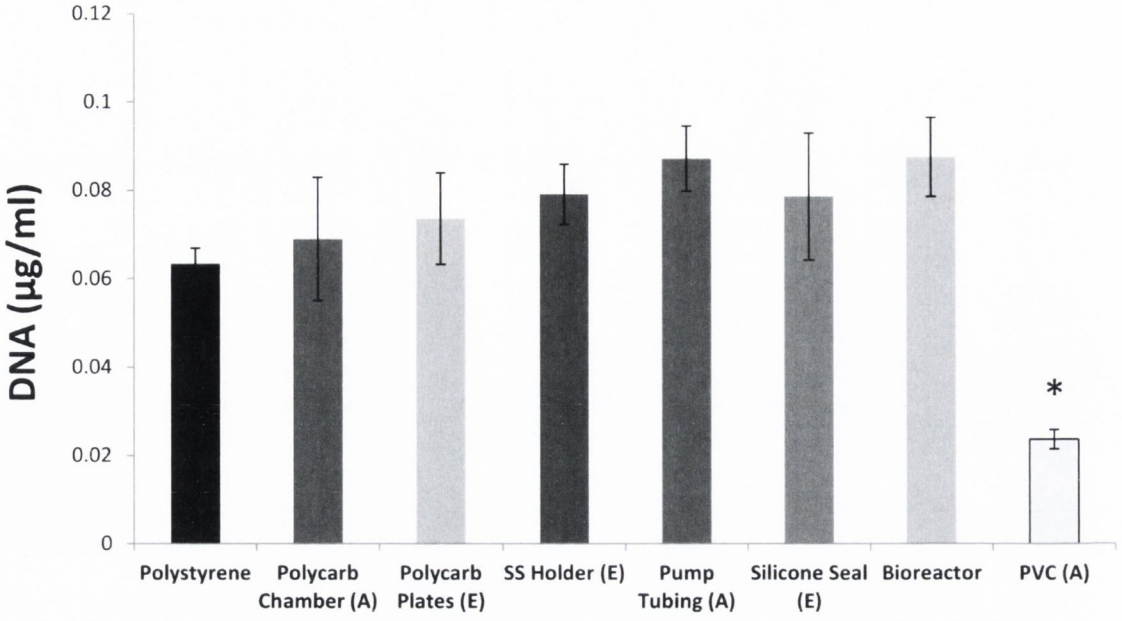

Figure 6.8 PicoGreen Cytotoxicity Results

*Similar levels of cell proliferation were seen for each of the components of the bioreactor and the entire system to the negative control and a significant difference was seen in comparison to the positive control. A denotes autoclave sterilisation and E denotes ethanol sterilisation. Average DNA ± standard deviation *p< 0.05 v positive control.*

6.3.3 Cyclic Strain

Altering the level of constriction of the tubing distal to the chamber, using the pinch valve, caused an increase in pressure and corresponding increase in the amplitude of the cyclic strain on the construct. The video extensometer tracking of this distention allowed for refinement of the level of constriction to produce ~5% strain. The basal pressure in the system caused a pre-strain on the construct, while the pulsatile pressure waveform generated the cyclic strain waveform (Figure 6.9).

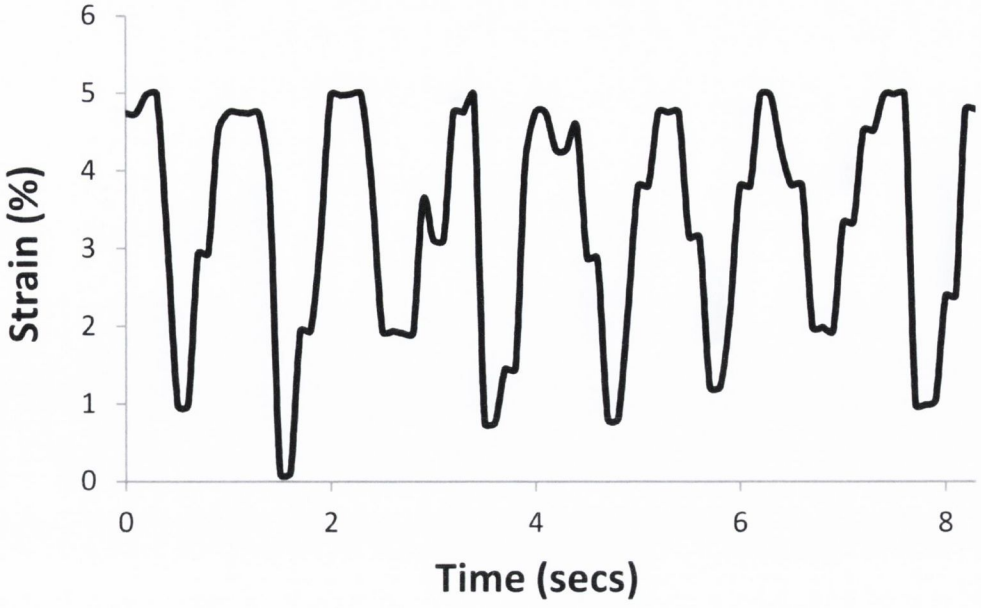

Figure 6.9 Cyclic Strain Measurement

Graph of cyclic strain experienced by a scaffold over time as determined by videoextensometer tracking. 0% strain represents the diameter due to prestrain from the basal pressure.

6.4 Discussion

The aim of this chapter was to design, build, and validate a novel pulsatile flow bioreactor for the *in vitro* culture of decellularized scaffolds. The bioreactor system designed was successful in applying *in vivo* hemodynamic forces, thereby addressing the design criteria discussed at the start of this chapter.

The peristaltic pump, tubing selection and distal constriction of the flow, combined to generate a cyclic strain of ~5%. Cyclic strain was the primary physiologic parameter that the bioreactor system aimed to replicate. Arterial cyclic strain *in vivo* has been reported in the 3-10% range, depending on the vessel location and subject age (Salacinski et al., 2001, Stekelenburg et al., 2009). The recorded strain within the bioreactor falls within this range, and is similar to what is seen in the carotid artery *in vivo*, which is of similar dimensions to the decellularized scaffold utilised here (Yang et

al., 2011). Furthermore, 5% cyclic strain has been utilised in the maturation of TEVGs, and has demonstrated increased cell migration, profileration and ECM synthesis (Niklason et al., 1999, Yazdani et al., 2009, Couet et al., 2012).

At a flow rate of 60mls/min and frequency of 1 Hz the Reynolds number was found to be 268. This indicates that the flow is laminar, as it is below the generally accepted threshold of <2000, for fully developed laminar flow. This value is similar to what has been measured for arteries *in vivo*, where Reynolds number ranges from 100-1000 depending on vessel location (Ku, 1997, Vennemann et al., 2007, Caro et al., 1978). The average wall shear stress determined from the bioreactor system was 0.84 dynes/cm^2. This value is much lower than that measured *in vivo*, which ranges from 3-12 dynes/cm^2, depending on subject age and artery location (Reneman et al., 2006). The main reason for the low wall shear stress is due to the viscosity of the cell culture medium. The viscosity of blood ranges from 3.5-10 centipoise, depending on flow conditions and vessel geometries, while the viscosity of cell culture medium is approximately 1 centipoise. Low wall shear stresses are known to be a contributor to atherosclerotic plaque formation via altered EC function and phenotype (Reneman et al., 2006, Libby et al., 2011). However, low wall shear stress has also been shown to increase proliferation of ECs and has been effectively used to generate endothelialised TEVGs *in vitro* (Kaushal et al., 2001). This can allow for EC adhesion and acclimation and possibly a beneficial proliferative response, until the wall shear stress can be increased by increasing the flow rate.

The basal pressure within the bioreactor was recorded as ~70/40 mm Hg. This average pressure across the system of 55 mm Hg is approximately half the value of average physiologic blood pressure. This is a limitation of the system, and could be overcome by increasing the reservoir height, or by pressurising the reservoir. However, it should be noted that this low basal pressure did not affect achieving the desired cyclic

strain on the scaffold, which is the principle physiologic parameter the bioreactor strived to replicate. Also, the pressure pulse amplitude of 30 mm Hg is comparable to the normal physiological pulse amplitude of 40 mm Hg.

The entire assembled bioreactor system, including the peristaltic pump fitted and operated within a standard incubator. The system does not hinder the gas exchange of the medium to the external environmental conditions of the incubator. The parallel circuit arrangement allowed for up to four independent constructs to be conditioned at once, with independent culture medium reservoirs to reduce contamination. The novel circular chamber profile allows the ability to remove the chamber unit and utilise it for rotational EC seeding, without removing the construct (this will be addressed further in Chapter 7).

The results of the extraction tests for cytotoxicity indicate that all materials utilised in the construction of the bioreactor were cytocompatible and did not elicit a cytotoxic response. This was determined by non-significant changes in metabolic activity (Figure 6.7), and cell number (Figure 6.8), after 24 hours versus the negative control, polystyrene. The individual components were sterilised prior to cytotoxicity testing via autoclaving or ethanol soaking. Overall, these results indicate that the bioreactor system is non-cytotoxic and can be fully sterilised with no adverse effects to the inherent cytocompatibility of the materials from which the bioreactor is constructed.

In keeping with the practicality of assembling the system in aseptic conditions and minimising scaffold handling, the step up assembly approach proved successful. These custom moulded silicone seals not only constituted a useful method of ensuring a leak proof system but also incorporate the manipulation of the working length of the scaffold without any extra handling. Furthermore, the simplicity of the system allows for reproducibility across samples as the exact parameters for loading are identical across

each circuit and the manner of the construct mounting incorporates the dimensional variations amongst decellularized arterial scaffolds.

6.5 Conclusion

A bio-mimetic system that can be housed within a standard incubator, that subjects physiologically relevant dynamic conditions to decellularized arterial constructs has been described. The use of the bioreactor potentially will provide a means of identifying any limitations to the medial cell seeding technique while also determining the dynamic performance of this customised scaffold. The system also allows for the simple application of a luminal cell monolayer to the scaffold in conjunction with the bulk seeded medial layer. The simulation of dynamic hemodynamic forces should provide the rMSCs with a suitable environment for proliferation, migration and differentiation. The response of rMSCs to this bio-mimetic environment will be addressed in the next chapter.

Chapter 7 Initial Investigation into the Behaviour of Medially Injected rMSCs in a Bio-mimetic Environment

7.1 Introduction

The response of cells seeded on vascular scaffolds to dynamic conditions has been widely studied, and detailed in Chapter 2. The principle benefits of exposing these constructs to a bio-mimetic environment are increased cell proliferation, migration and differentiation (Niklason et al., 1999, Crapo et al., 2008, Gong and Niklason, 2008). The full benefits of dynamic bioreactor conditioning may not be realised in decellularized scaffolds due to the inadequate, non-medial layer cell infiltration. However, now this issue of successfully seeding cells within the medial layer of decellularized scaffolds has been addressed to some degree (see Chapter 3). Furthermore, using a biochemical stimulus to increase the degree of cell migration within the medial layer has been described in Chapter 5. Both of these manipulations of decellularized scaffolds were successful in enhancing medial cell repopulation in static culture. However, in order to determine if complete cell repopulation is possible *in vitro*, these customised scaffolds must be assessed within a physiologically relevant three dimensional bio-mimetic environment (as described in Chapter 6). The response of medially injected rMSCs within this pulsatile flow bioreactor system will also ascertain the potential *in vivo* performance of these scaffolds and identify any shortcomings in the medial injection technique.

A fully functioning TEVG will also require an EC monolayer. The importance of this monolayer has been discussed in Chapter 2. Thus far, EC seeding has not been addressed in this thesis, as the primary focus has been on producing a robust scaffold and improving the limited medial layer cell infiltration associated with decellularized scaffolds. This EC monolayer is not only essential for providing a thromboresistant barrier but is integral to the behaviour of medial cells and TEVG development (McFetridge et al., 2004a, Quint et al., 2011). Success has been achieved with seeding endothelial progenitor cells, isolated from circulating peripheral blood (Krenning et al.,

2008, Kaushal et al., 2001). MSCs have been successfully differentiated into ECs and endothelial-like cells in both static and dynamic culture conditions (Zhao et al., 2010, Duffy et al., 2011, Krawiec and Vorp, 2012). This ability to differentiate, combined with their allogenicity, make MSCs an attractive cell source for endothelialisation of TEVGs.

The aim of this chapter is to apply physiologically relevant conditions to medially seeded decellularized scaffolds and HGF loaded decellularized scaffolds within a pulsatile flow bioreactor system. Increased migration of cells within the medial layer of these scaffolds is the primary objective of utilising this system. Furthermore, seeding of rMSCs and HUVECs was undertaken to determine the feasibility of EC adhesion to the inner lumen of this customised decellularized scaffold.

7.2 Methods

7.2.1 Scaffold Preparation

Two scaffolds were selected for investigation within the bioreactor system:

Group 1. Collagen digested decellularized scaffold with three injection channels located 120° apart. These scaffolds were prepared as described in Chapter 3 (n=3).

Group 2. Chitosan/β-GP HGF gel loaded scaffold with 3 needles 60° apart. The chitosan/β-GP, HGF concentration and scaffolds were prepared as described in Chapter 5 (n=3).

7.2.2 Scaffold Repopulation

All scaffolds were seeded as described in Chapter 5. Briefly, scaffolds were soaked in culture medium prior to cell seeding for > 1 h. Group 1 scaffolds had 2 X 10^6 rMSCs seeded in each injection channel and were placed in static culture for 48 h to allow

complete cell adhesion and acclimation. Group 2 scaffolds had a single injection of 50-70μl of the chitosan/β-GP HGF gel in a central injection channel, which was left at 37° for > 30 mins to allow for gelation. Subsequently, 2 X 10^6 rMSCs were seeded in two injection channels, 60° each side of the central HGF channel and then placed in static culture for 48 h, as with Group 2.

7.2.3 Pulsatile Flow Bioreactor System

The pulsatile flow bioreactor was assembled as described in Chapter 6. All of the components were sterilised by either autoclaving or soaking in 100% ethanol for > 30 mins. Each scaffold was removed from static culture after 48 h and sutured onto the stainless steel specimen holders using 3-0 sutures (Tevdek® II, Teleflex Medical), within a Class II safety cabinet.

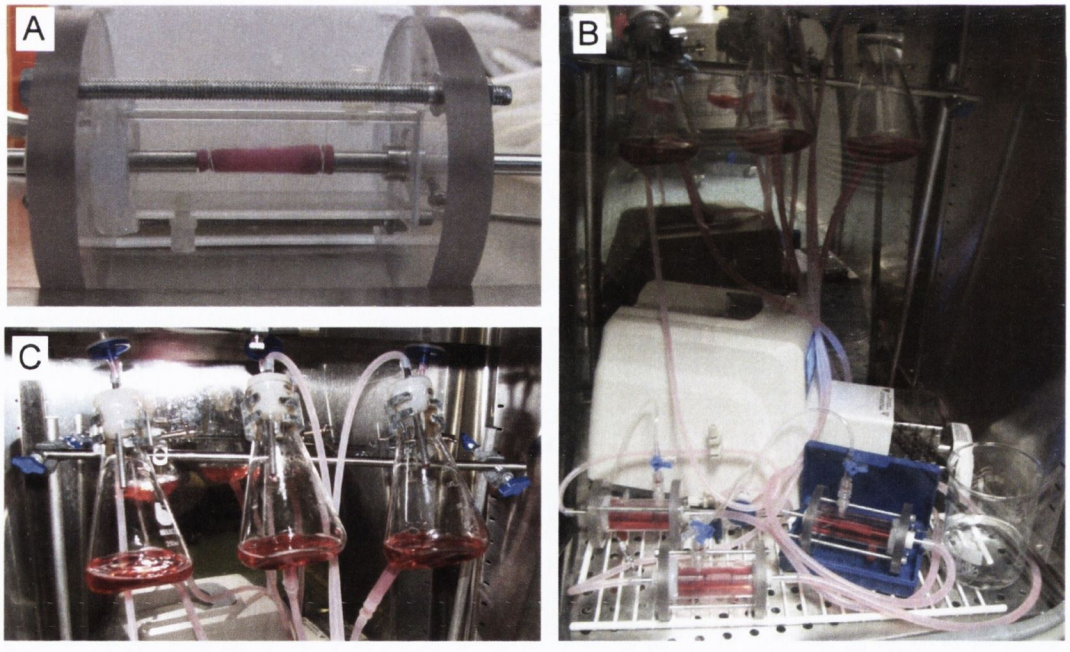

Figure 7.1 Bioreactor Assembly

(A) Specimen mounted within chamber in zero strain state. (B) Fully assembled system within incubator. (C) Culture medium reservoirs.

The mounted scaffolds were then assembled within the chamber using the step up assembly process (described in Chapter 6) and the unit was compressed to form a watertight seal. The external section of the chamber was then filled with rMSC culture medium (as described in Section 5.2.6), leaving a small air gap between the medium and outer chamber. The specimen holders were then longitudinally adjusted until the desired axial stretch of 20% was achieved. A picture was taken of the mounted specimen within the assembled chamber as reference for a 'so called' zero strain state (Figure 7.1 A). A 0.2μm syringe filter was attached via a luer connector to the outer surface of the chamber to allow for gas exchange. The assembled chamber unit was then connected to the circulation loop of the bioreactor. The reservoir was filled with 80 ml of culture medium and a 20 G needle was inserted through the silicone seal on the lid of the reservoir (Figure 7.1 B). This allowed for the attachment of a 0.2 μm filter for gas exchange. In order to maintain physiological pH, CO2, O2 and temperature, all components including the peristaltic pump were contained in a standard humidified incubator (Figure 7.1 C).This process was repeated for each of the n=3 scaffolds. Video extensometer tracking of the pulsating scaffold recorded the cyclic strain on the scaffold wall and was adjusted to achieve ~5% strain (Figure 7.2), the method of achieving desired strain level is described in Chapter 6. This tracking was carried out once a day to ensure a consistent level of cyclic strain was achieved throughout the 7 days. The scaffolds were maintained within the bioreactor system for 7 days, with a media change every second day.

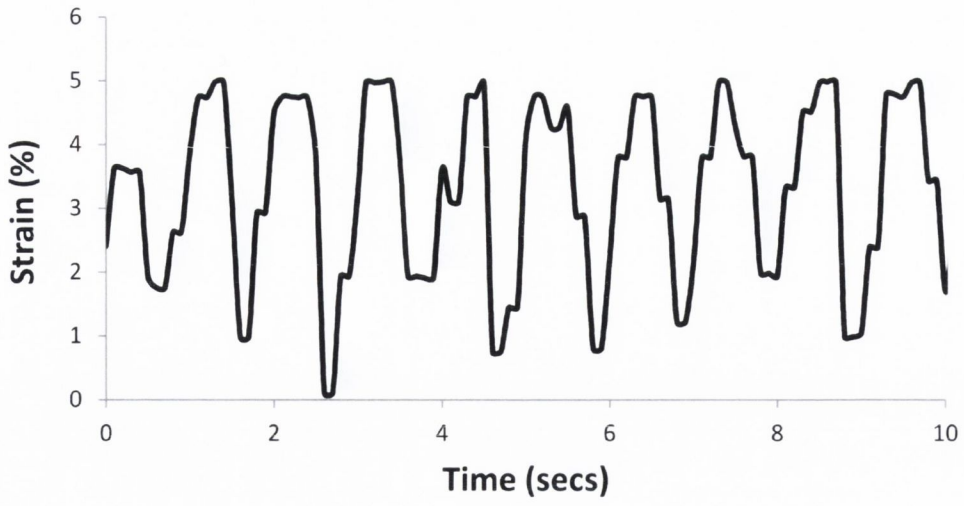

Figure 7.2 Cyclic Strain Applied to Scaffold

Consistent cyclic strain of ~5% experienced by the scaffold within the bioreactor system

7.2.4 Migration Quantification

All rMSCs were labelled with PKH26 membrane labelling prior to seeding, according to the manufacturer's protocol. Scaffolds were removed from the incubator at each time point, embedded in OCT compound (Tissue Tek) and snap frozen in liquid nitrogen for cryostat sectioning (Leica microtome, Leica, Germany). Slides were washed in PBS to remove excess OCT compound, stained for 15 mins with Alexa Flour®488 Phalloidin (Invitrogen) and mounted in Vectashield Mounting Media with DAPI. Observation under light and fluorescent microscopy and digital image acquisition was carried out with an inverted microscope (Olympus IX 71). Scaffold sections were scaled using ImageJ and the maximum cell migration in both directions away from each injection site was measured at longitudinal intervals of 300μm over the length of injected scaffold. The ratio of cell migration toward the HGF with respect to the cell migration in the direction away from the HGF was determined for Group 2. As a control, cell migration was similarly quantified for medially injected scaffolds and chitosan/β-GP HGF gel loaded scaffolds (see Chapter 5) after 7 days of static culture.

7.2.5 Endothelialisation

rMSCs

Concentration analysis was undertaken with rMSCs to determine the ideal cell number and volume to efficiently seed cells on the lumen wall of the decellularized scaffolds. A low concentration of 0.25 X 10^6 cells per cm^2 in 50µl culture medium and a high concentration of 0.5 X 10^6 cells per cm^2 in 100µl were seeded. These cell concentrations were seeded onto flat-cut sections of scaffold by directly pipetting the cell solution on the lumen surface and allowed to adhere for 20 mins prior to culture for 3 days.

In order to determine the efficiency of lumen seeding on an intact scaffold, rMSCs were seeded in the high concentration. A cell suspension of 2 X 10^6 in 100µl of culture medium was seeded on the lumen wall of the scaffold and allowed to adhere for 20 mins. Subsequently, the scaffold was rotated 120° and another cell suspension with the same concentration was seeded on the lumen wall. A final rotation and seeding allowed for complete seeding of the lumen surface. In total 6 X 10^6 cells were seeded per scaffold.

HUVEC Seeding

To demonstrate the feasibility of EC adhesion to the lumen of the decellularized scaffold HUVEC seeding was performed. HUVECs were purchased from Lonza, (Berkshire, UK) and cultured in EndoGRO™ Medium with provided supplements (Millipore, Ireland). All culture incubations were carried out at 37°C with 5% CO2 and 95% relative humidity. Media was replaced every 3 days and upon reaching 80-90% confluency cells were passaged.

The high cell concentration rotational seeding method described above was undertaken using these HUVECs and cultured for 2 days. A rMSC/HUVEC co-culture was also investigated. In the same manner as Group 1 scaffolds above, medially injected

rMSCs were statically cultured for 2 days and subsequently dynamically cultured for 7 days in the bioreactor. The next step involved seeding with HUVECs and a further 2 days dynamic culture in the bioreactor.

Individual circulation loops were taken from the incubator to the fume hood, and the chamber unit was disconnected. All rMSC media was removed and the system flushed with PBS. HUVECs were seeded as described above within the lumen of the mounted scaffolds, with 20 mins adhesion times and 120° manual rotations to ensure an even cell distribution. The circulation tubing was then reconnected, the medium reservoir filled with HUVEC medium and the bioreactor was returned to the incubator. After 12 h flow was restarted to allow the perfusion of endothelialised vessel lumens with the EndoGRO™ medium at a reduced flow rate of 15ml/min, the flow rate was gradually increased back to 60ml/min after 48 h.

7.2.6 Luminal Seeding Quantification

Quantification of the efficiency of the lumen cell seeding techniques was verified by DAPI staining. Scaffolds were cut into 2 cm^2 segments and a DAPI solution diluted to 4000:1 was applied directly to the lumen surface. These segments were placed on glass slides, held in place by cover slips and observed and imaged under fluorescent microscopy (Olympus IX 71). These DAPI stained images were thresholded in ImageJ which allowed for cell counting of the DAPI stained nuclei and quantification of seeded cell numbers.

7.2.7 Luminal Seeded Cell Viability

The rMSCs seeded scaffolds, at low and high concentration and HUVEC seeded scaffolds were assessed for viability using a Live/Dead stain (Molecular Probes, Invitrogen,

Ireland) according to the manufacturer's protocol. Digital image acquisition was carried out with an inverted fluorescent microscope (Olympus IX 71). Live cells were stained green with green-fluorescent calcein-AM and dead cells were stained red with red-fluorescent ethidium homodimer-1.

7.2.8 Statistics

Results are presented as mean ± standard deviation for the migration quantification. A Student's T-test was used to test significance between specific groups, results were considered significantly different at $p < 0.05$ and are represented with an * on each chart, if this level of significance was reached.

7.3 Results

7.3.1 rMSC Medial Injection

Group 1 - Cells Only

Adjustment of the distal pinch valve could achieve the desired 5% cyclic strain, which was confirmed by videoextensometer tracking. Histological analysis of the dynamically cultured scaffolds showed increased cell migration away from the injection site in each of the scaffolds (Figure 7.3). The rMSCs were successfully delivered to the medial layer via the injection channels. Cell migration away from the injection site in both circumferential directions was evident (Figure 7.3 A). This circumferential migration was consistent across all scaffolds, over the entire length of the injected scaffold segment, to a maximum distance of 2.7 mm from the centre of the injection cavity. The cell migration was evenly distributed in both circumferential directions (Figure 7.3 B). Radial cell migration was limited to the elastin layers which the cells were injected within. There was no evidence of enhanced radial cell migration toward the luminal or abluminal surfaces Figure 7.3 C.

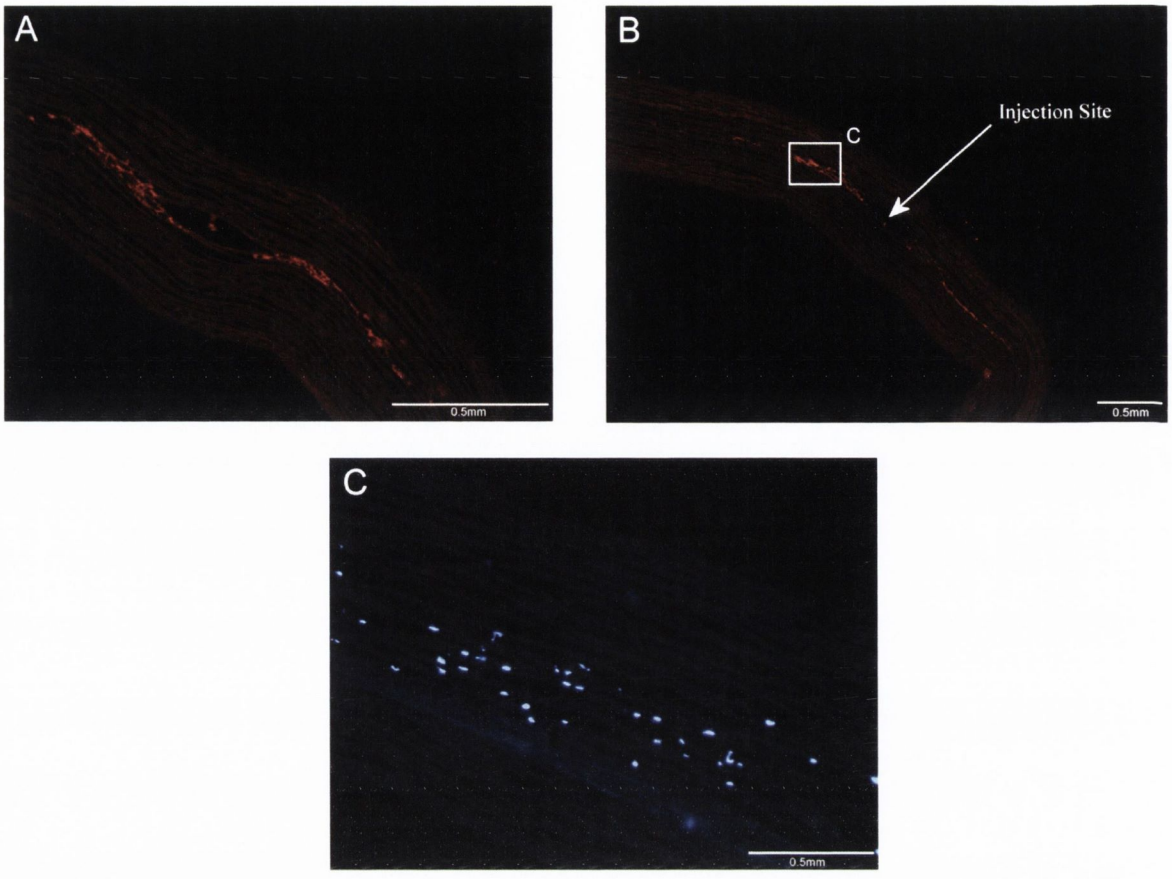

Figure 7.3 Medially Injected rMSCs after Bioreactor Culture for 7 Days

(A) Circumferential migration of rMSCs away from the injection site in both directions. (B) Increased migration was evident across all scaffolds due to the dynamic bioreactor conditioning. (C) High magnification view of migrated cells display no radial migration across elastin layers.

Figure 7.4 A displays the typical cell distribution within a bioreactor cultured scaffold in Group 1. The cells were homogenously distributed over the injected length and displayed consistent levels of migration in both directions over this length.

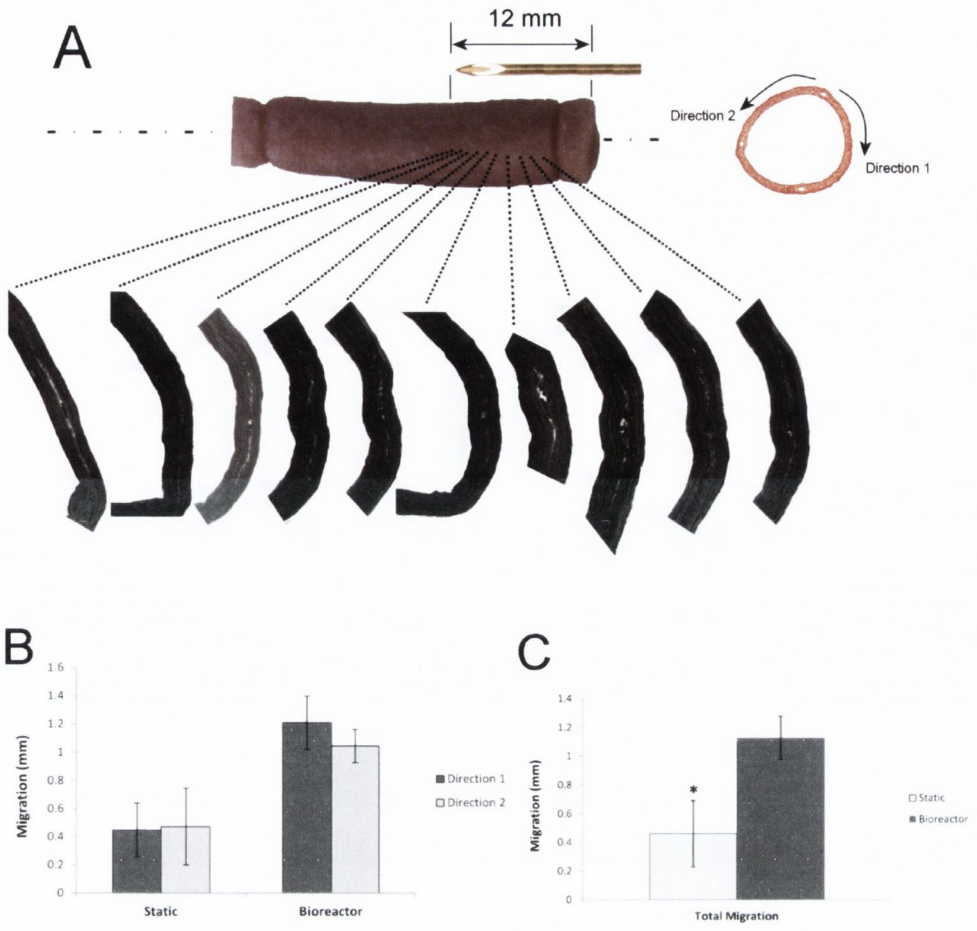

Figure 7.4 Cell Distribution and Quantification for Bioreactor Cultured Scaffold

(A) Schematic of cell distribution within a scaffold displays consistent cell migration in both directions away from the injection site. Homogenous cell distribution was evident over the entire injected length. (B) No statistically significant difference was seen in cell migration distance in either direction away from the injection site for static or bioreactor cultured scaffolds. (C) A statistically significant difference in total cell migration was seen for the bioreactor conditioned scaffolds in comparison to the statically cultured control. $p < 0.05$

Migration was evenly distributed in both directions away from the injection sites. There was no significant difference in migration in either direction for both static and bioreactor cultured scaffolds (Figure 7.4 A). The total migration for the bioreactor cultured scaffolds was determined by taking the average of the total migration distance in both directions.

There was a significant difference in the total cell migration for the bioreactor cultured scaffolds compared to the statically cultured control (Figure 7.4 B).

Group 2 – Cells and Chitosan/β-GP HGF gel

Group 2 scaffolds had consistent circumferential migration in the direction of the released HGF stimulus at each injection site (Figure 7.5). The degree of cell migration varied over the injected length and across scaffolds (Figure 7.5 A-B).

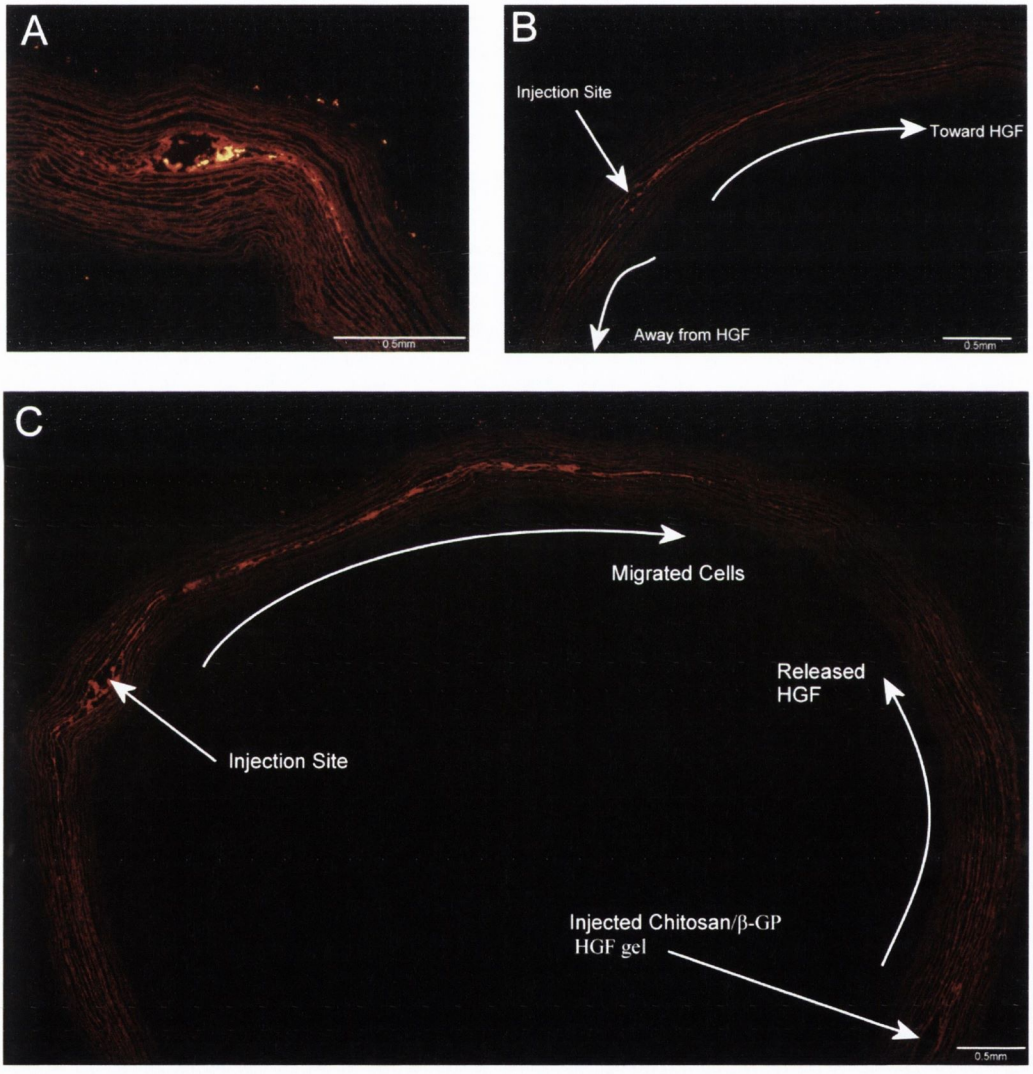

Figure 7.5 Bioreactor Cultured Chitosan/β-GP HGF Gel Loaded Scaffold

(A) Medially injected cells consistently migrated from the injection site in the direction of the released HGF stimulus. (B) The degree of cell migration varied over the injected length. (C) An increase in cell migration compared to Group 1 was evident.

There was a significant difference in migration in the direction of the released HGF for each scaffold (Figure 7.6 A). The ratio of migration toward the HGF in comparison to migration in the direction away from the HGF was calculated. The overall ratio of migration toward the HGF was not statistically significantly different compared to the chitosan/β-GP HGF gel loaded static control.

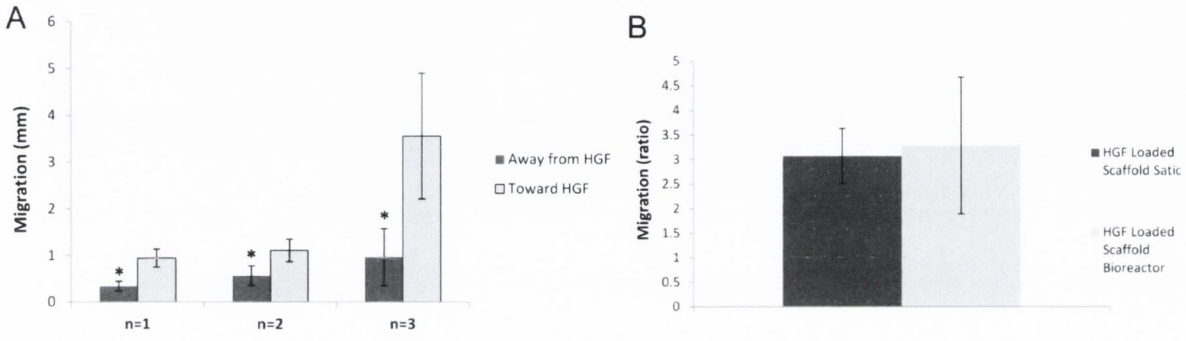

Figure 7.6 Group 2 Cell Migration

(A) Statistically significant difference in migration was seen toward the HGF stimulus for each scaffold in Group 2. (B) The ratio of migration in both directions (toward and away from HGF) was not significantly different. $p < 0.05$

The maximum cell migration achieved by bioreactor conditioning of the chitosan/β-GP HGF gel loaded scaffolds (5.2 mm) was larger than the static control (2.9 mm), (Figure 7.7). A direct comparison of both stimuli (dynamic bioreactor conditioning and HGF chemotactic) displayed a similar degree of migration. There was a significant difference in migration achieved with the bioreactor in comparison to the migration away from the released HGF in static culture (Figure 7.8 A).

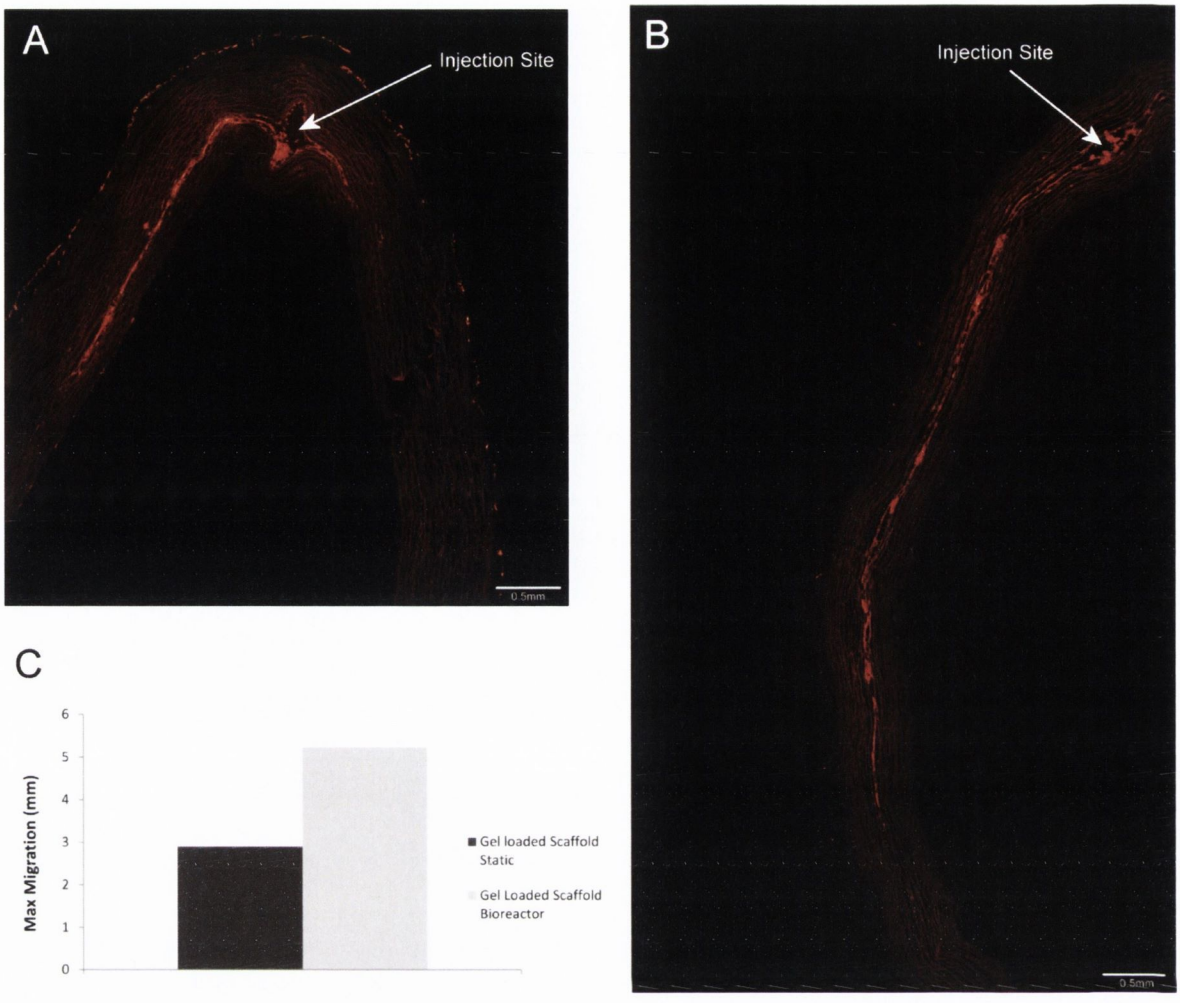

Figure 7.7 Maximum Cell Migration Utilising Chitosan/β-GP HGF Gel

(A) Maximum migration achieved in chitosan/β-GP HGF gel loaded scaffold in static culture. (B) Maximum migration achieved in chitosan/β-GP HGF gel loaded scaffold in bioreactor culture. (C) Graph displaying maximum distances.

No significant difference in cell migration was seen with the Group 1 bioreactor conditioned scaffolds compared to the Group 2 HGF loaded bioreactor cultured scaffolds. However, large deviations were noted in Group 2. Similarly, no significant difference and large deviations were present in the Group 2 HGF loaded bioreactor cultured scaffolds compared to the non-bioreactor cultured static control.

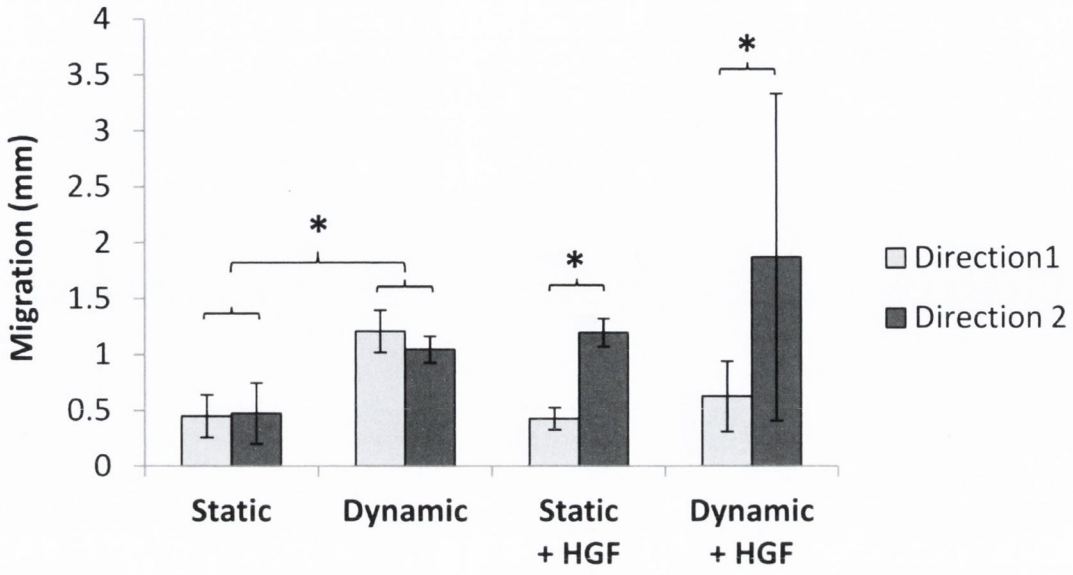

Figure 7.8 Comparison of Bioreactor Cultured Groups to Static Controls

A similar degree of migration was achieved with bioreactor conditioning as utilising the HGF stimulus in static culture. Combining these stimuli increased the migration but was not statistically significant due to the large deviations present in the bioreactor conditioned HGF loaded scaffolds. This may be attributed to HGF wash out from the scaffold. (Direction 1 is in the opposite direction to released HGF and Direction 2 is toward the released HGF).

7.3.2 Endothelialisation

rMSCs

Successful adherence of rMSCs to the luminal surface of the scaffold was achieved by both statically seeding cells and the rotational seeding method (Figure 7.9). The low cell concentration displayed widespread viable cell coverage of the luminal scaffold (viable cells stain green). However, there was evidence of non homogenous cell distribution with some areas of low cell attachment with the low concentration.

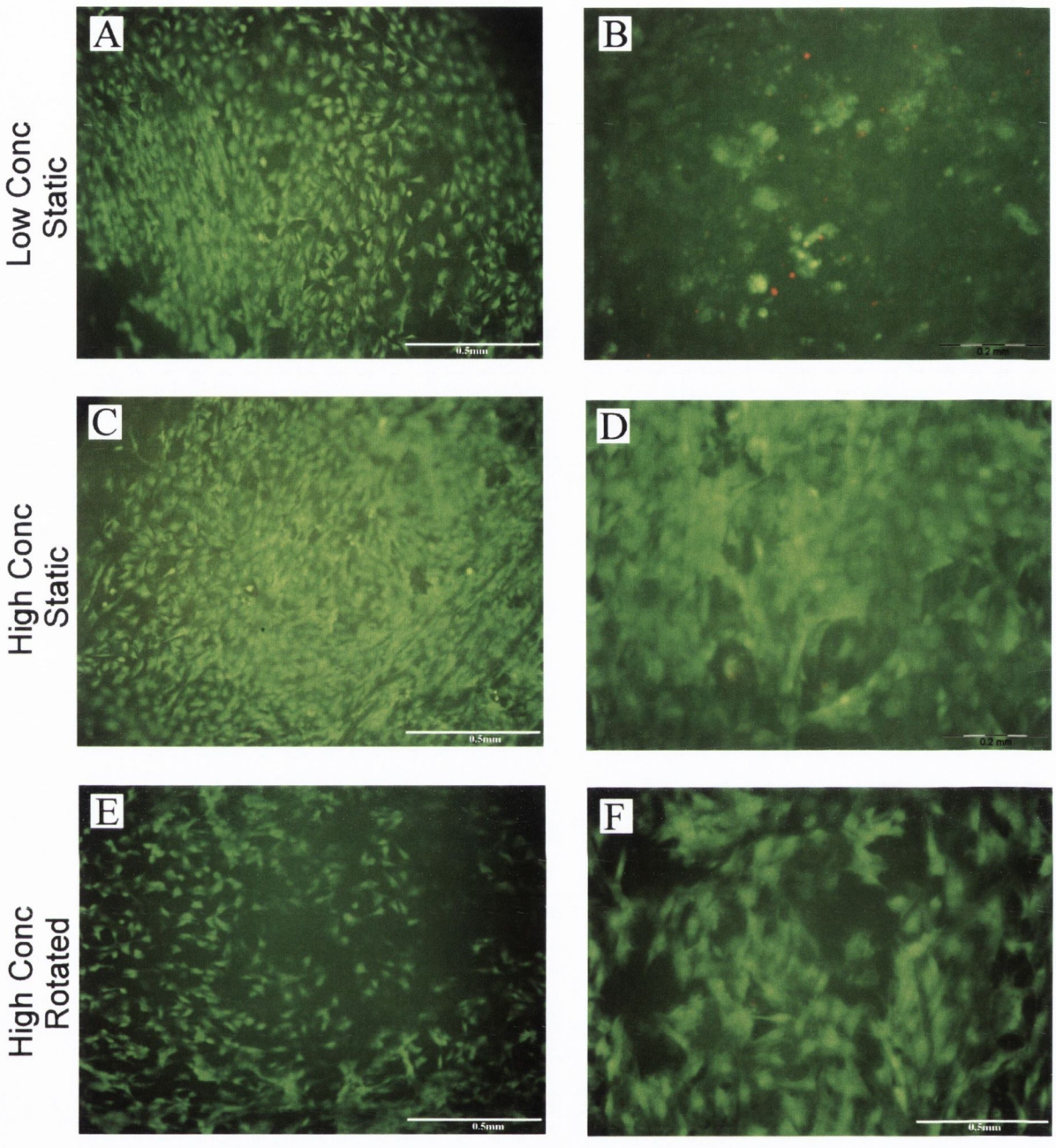

Figure 7.9 Live/Dead Stain of Luminal Seeded rMSCs

(A) Low concentration statically seeded rMSCs showed good cell coverage with some unseeded scaffold sections and large cell viability (viable cells stain green). (B) Some dead cells (red) were apparent in areas of low cell coverage. (C) The high concentration demonstrated complete cell coverage. (D) Minimal non viable cells were visible. (E) Rotational seeding demonstrated good cell coverage. (F) High cell viability was apparent.

Further investigation revealed dead cells (non viable cells stain red) present within these low cell covered scaffold sections (Figure 7.9 B). The high cell concentration achieved full cell coverage and large cell viability was maintained after 3 days of culture (Figure 7.9 C-D). The rotational seeding method displayed less confluent cell coverage; however, the cells were homogeneously distributed across the luminal surface with high cell viability present (Figure 7.9 E-F).

Quantification of seeded cell numbers was carried out to determine the efficiency of cell seeding the luminal surface. A typical DAPI stained section for a statically seeded high concentration scaffold is shown in Figure 7.10 A. 0.25cm^2 sections of DAPI stained images were thresholded and the number of cell nuclei counted. This was repeated at 10 locations across each scaffold to allow for full quantification of cell numbers (Figure 7.10 B-C). A statistically significant increase in cell number was seen between the high and low concentrations of statically seeded cells. An increase in cell number was seen with the rotational seeded scaffolds compared to the low concentration and a decrease compared to the high concentration statically seeded scaffolds. However, there was no statistically significant difference between either the low or high concentration statically seeded scaffolds and the rotationally seeded scaffolds. Figure 7.10 D displays a DAPI stained cross section of a rotationally seeded scaffold showing the complete coverage of the inner lumen with the seeded rMSCs. A homogenous cell distribution around the inner scaffold circumference was visible.

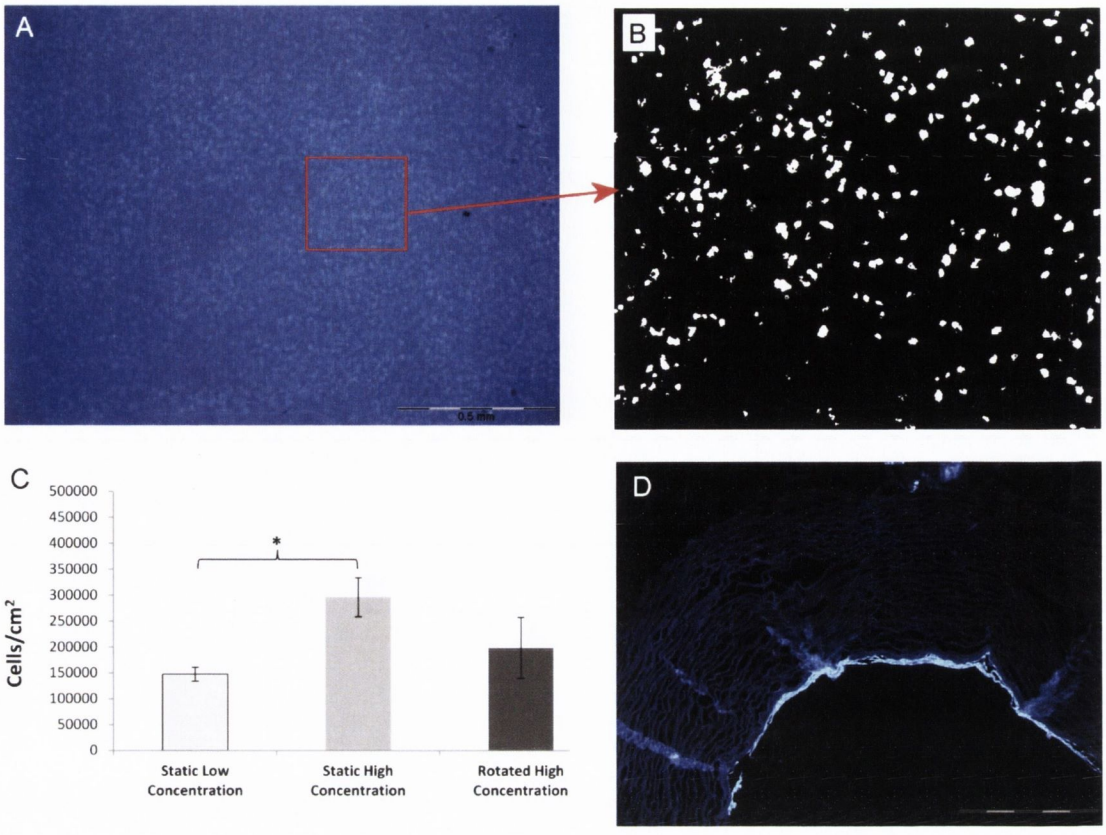

Figure 7.10 Luminal Seeded rMSC Quantification

(A) Typical DAPI stained luminal surface displaying widespread coverage of cell nuclei (blue dots). (B) 0.25cm^2 section was thresholded in ImageJ which allowed for cell counting. (C) A statistically significant difference in cell number was visible between the high and low cell seeded concentrations. The rotational seeding method with the high cell concentration fell in between the low and high statically seeded scaffolds. (D) A typical DAPI stained cross section of a scaffold showing complete cell coverage of the lumen.

HUVECs

HUVECs were successfully seeded onto the luminal scaffold surface using the high concentration (6 X 10^6 cells/scaffold) rotational method. Seeded scaffolds were cultured for 2 days in both static non bioreactor cultured and dynamic bioreactor cultured conditions. A consistent homogenous monolayer of viable HUVECs was present on the luminal surface of the non bioreactor cultured scaffolds after 2 days (Figure 7.11 A & F).

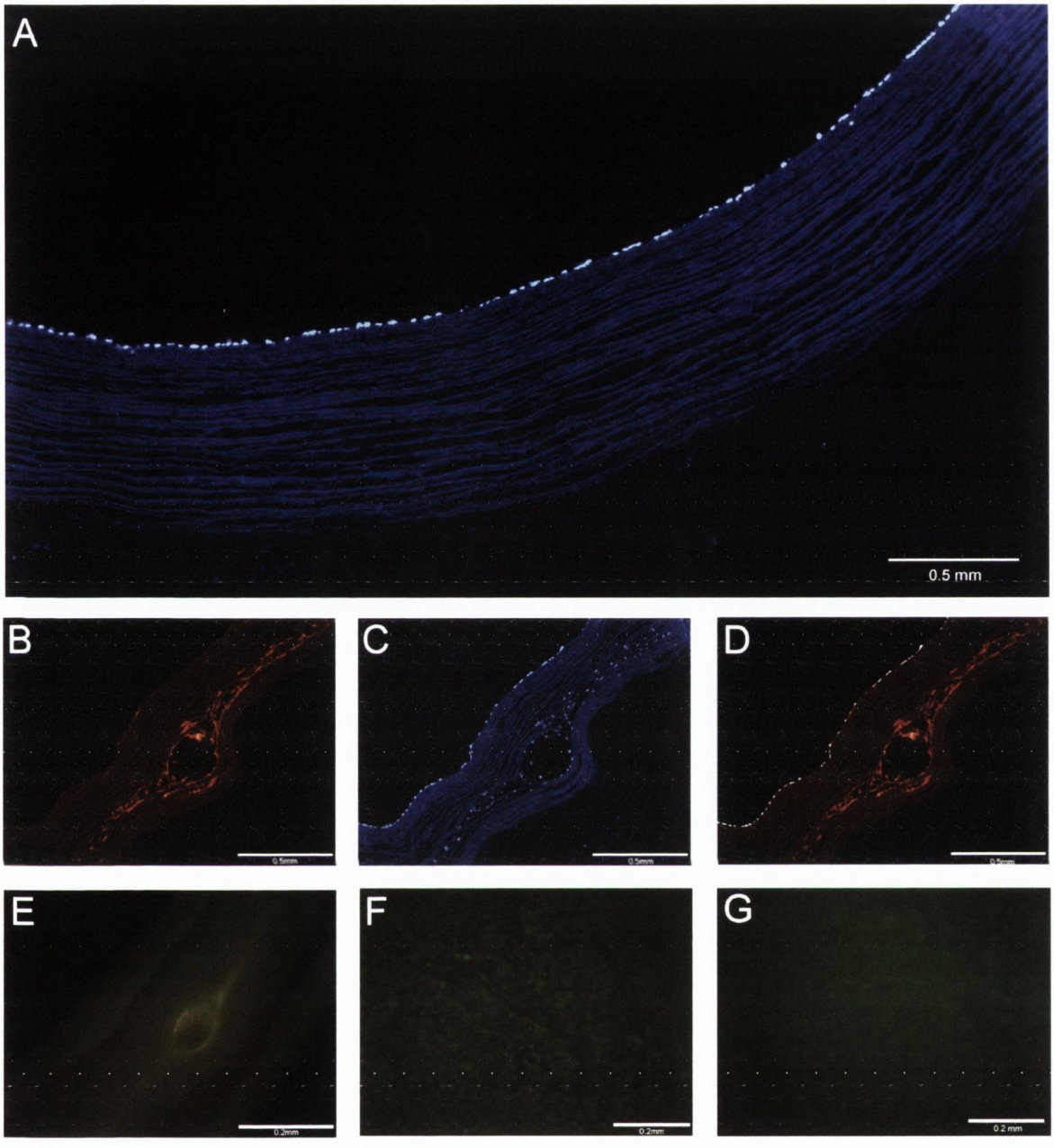

Figure 7.11 HUVEC Luminal Scaffold Seeding

(A) DAPI stained non-bioreactor cultured HUVECs displayed full cell coverage of the lumen. (B) PKH 26 labelled rMSCS medially injected. (C) Same section DAPI stained show nuclei of both rMSCs and HUVECs. (D) Merged imaged with rMSCs fluorescing red and HUVECs white. This displays endothelial coverage after 7 days bioreactor conditioning of the rMSCs and 2 days of rMSCs/HUVEC bioreactor co-culture. (E) Live/Dead of medially injected rMSCs show viability after 11 days culture. (F) Live/Dead of non-bioreactor cultured HUVECs shows high coverage and cell viability. (G) Live/Dead of bioreactor cultured HUVECs shows similar coverage and viability as the non-bioreactor static control.

Similarly, this monolayer was present in the rMSC/HUVECs co-cultured bioreactor scaffolds. The PKH26 labelled rMSCs were visible at the injection sites with similar migration to Group 1 above (Figure 7.11 B). A DAPI stain of the same section stains both rMSC and HUVEC nuclei (Figure 7.11 C). Thresholding and overlapping these images allows for the identification of each of the specific cell types. Endothelialisation of the scaffold with HUVECs in the co-cultured scaffold was evident (Figure 7.11 D). This HUVEC monolayer was consistent around the lumen and across the scaffolds. Viability of the cells within the co-cultured scaffold was verified using a Live/Dead stain with minimal non viable cells present either within the medial layer (Figure 7.11 E) or on the inner lumen surface (Figure 7.11 G). The successful endothelialisation of rMSC medially injected scaffolds with HUVECs subjected to pulsatile flow bioreactor conditioning is further shown in Figure 7.12. The PKH26 labelled cells within this full scaffold section show the migrated rMSCs in both directions away from the injection site. The DAPI stained HUVEC monolayer on the inner lumen is shown in white and is homogenous around the lumen circumference.

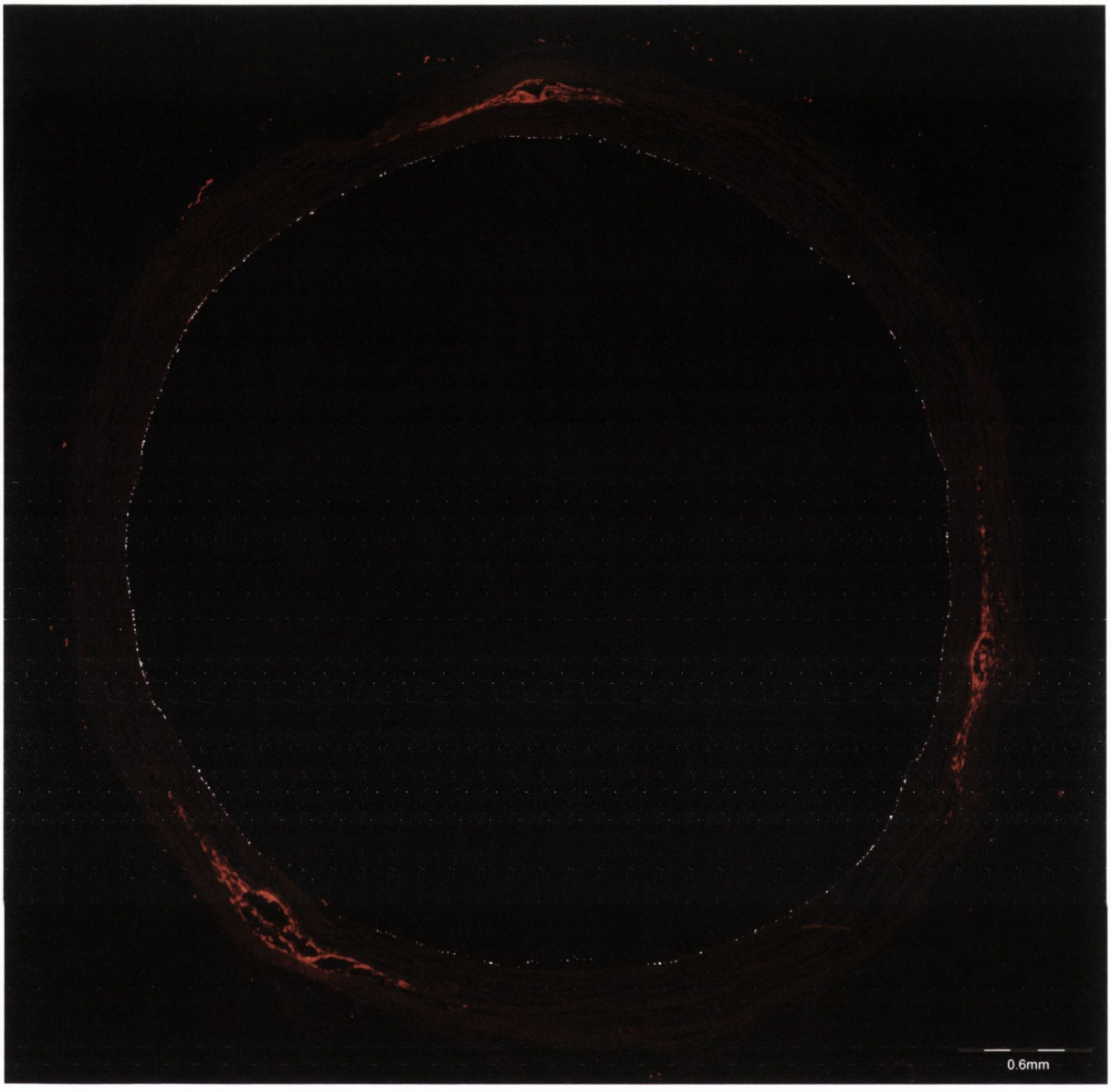

Figure 7.12 rMSC/HUVEC Bioreactor Co-cultured Scaffold

The medially injected PKH26 labelled rMSCs fluoresce red and showed increased circumferential migration due to bioreactor conditioning for 9 days. The HUVECs fluoresce white and achieved a consistent luminal monolayer around the inner scaffold circumference after 2 days of bioreactor conditioning.

7.4 Discussion

In order to investigate the possible behaviour of medially injected cells in a dynamic environment, this chapter examined the response of the cells to the pulsatile flow bioreactor described in Chapter 6. This chapter aimed to determine if complete medial layer repopulation was possible *in vitro,* and identify any limitations with the repopulation methods conceived in Chapter 3 & 5 in a dynamic environment.

Group 1 scaffolds consisted of the medial injection of rMSCs via three injection channels. Successful medial repopulation was achieved in this group with increased migration away from the injection site, evenly in both directions post mechanical conditioning (Figure 7.3). The average circumferential migration of these cells was significantly different than what was achieved by culturing medially injected cells in static conditions for the same time frame. This demonstrates that the cyclic strain experienced by these cells provided an extra stimulus for cell migration. This correlates well with the literature as enhanced migration has been consistently demonstrated in bioreactor systems (McFetridge et al., 2007, Dahan et al., 2012). However, migration within the medial layer of decellularized scaffolds in this manner, and in such a short time frame has not been previously demonstrated. Medial cell injection in static culture had shown successful medial repopulation, however, the cell retention and migration was variable and inconsistent. After 7 days of bioreactor conditioning the cell distribution was more homogenous along the length of the injected part of the scaffold. The circumferential migration was still largely confined to the elastin layers in which the cells were injected at the injection channel; no improvement in radial migration was evident. The lack of radial migration of cells is a concern; however, the *in vivo* environment may improve this, in comparison to the bio-mimetic environment. Other scaffold manipulations/customisation techniques, such as extra injection channels, may aid this. *In*

vivo, there will be more cells and signalling molecules present both luminally and abluminally which may increase migration of engrafted cells or enhance the remodelling and integration response. It has been previously shown that matrix metalloproteinases (MMPs) have been expressed by SMCs within a bioreactor system; however, an increase in radial migration was not achieved in previous studies (McFetridge et al., 2007, Dahan et al., 2012). However, these MMPs are more widely expressed *in vivo* and may allow the degradation of the dense elastin sheets to either promote engrafted cell migration or increase host cell integration (McCawley and Matrisian, 2001, Sluijter et al., 2006).

Group 2 consisted of chitosan/β-GP HGF gel loaded scaffolds, also medially injected with rMSCs, and bioreactor cultured for 7 days. A similar result to that of the statically cultured chitosan/β-GP HGF gel loaded scaffolds was seen, whereby, directional migration of the injected rMSCs toward the released HGF was evident at each injection site (Figure 7.5). The degree of migration varied across the injected length and also across scaffolds, however, the maximum migration achieved was 1.8 times more than that of the static cultured control from Chapter 5, and 10 times higher than the average migration for statically cultured scaffolds, without any HGF stimulus. There was a significant difference in the migration toward the released HGF compared to the opposite direction for each of the scaffolds. However, in the bioreactor conditioned scaffolds the ratio of migration toward the HGF was not significantly different to the statically seeded control. Also, there was no significant difference in average migration in Group 2 compared to the static controls of both the chitosan/β-GP HGF gel loaded scaffolds and cell only scaffolds (Figure 7.8 B-C). While the maximum migration was much improved it varied largely across the scaffolds, resulting in large deviations.

Washout of the released HGF from the scaffold wall, due to the cyclic expansion of the scaffold may account for the large deviations exhibited. While the scaffold wall is

highly dense, it is still porous, and the pressure within the bioreactor system will cause the culture medium to perfuse through the wall. The rate of perfusion was low (< 10ml/day), but may have been enough to gradually remove the released HGF from the medial layer. A study in the future may be required to quantify this aspect. Autofluorescence from the released HGF was visible on DAPI stained sections of static cultured HGF loaded scaffolds in Chapter 5, this allowed for identification of the path of migration of the cells toward the HGF (Figure 5.10 B-D). There was no evidence of this autofluorescence in any DAPI stained sections of the bioreactor cultured scaffolds, providing further evidence of HGF removal from the scaffold at the final time point in Group 2. Due to the natural dimensional variation between scaffolds, the amount of collagen digestion from the NaOH can vary slightly across scaffolds, and hence result in small porosity changes between scaffolds. This may account for the variation in migration. However, it should be noted that consistent directional migration was still achieved, potentially an early stimulus prior to washout could be attributed to this. This issue may be overcome by increasing the static culture time from 2 days to 5 days when the majority of the HGF is released from the chitosan/β-GP. This may allow consistent increased migration by efficiently combining the HGF stimulus with the bioreactor stimulus. Furthermore, this released HGF washout may not be an issue *in vivo* as the perfusion across the graft wall will not be as extenuated due to an endothelial layer and the compaction of the surrounding connective and adventitial tissue. In addition, HGF would be abluminally perfused from the wall and not washed out into the circulatory system, which may have positive benefits by increasing host cell infiltration across the elastin layers.

Two cell types were investigated here for luminal seeding, MSCs and HUVECs. HUVECs are widely studied for their function and pathology as ECs and were utilised

here to demonstrate the feasibility of EC adherence to our customised scaffold. rMSCs were investigated as a more clinically viable cell source as they will allow for the dual seeding of the lumen and medial layer with the same cell type, prior to implantation. Since these cells are allogenic, they will not require excessive culture times to generate large numbers, in comparison to an autologous cell source.

An initial investigation into the appropriate rMSC numbers for efficiently seeding the exposed luminal scaffold surface revealed that the low cell concentration did not provide full coverage by static seeding, with some areas of non viable cells present (Figure 7.9). In contrast, the high concentration provided full coverage and widespread viability with a significant difference in cell retention (Figure 7.10 C). Translating this to the intact scaffold surface by rotational seeding was successful but with decreased cell retention. This reduction is as a result of the rotation of the scaffold and the non adherence of cells; however, sufficient cell coverage was still achieved. This method of luminal seeding is quick and efficient and could be easily translated to a clinical setting with the combination of direct medial injection with the same cell type. Further experimentation with the rotational seeding may be required to ensure complete homogenous cell retention with sufficient cell numbers.

The high cell concentration and rotational method was used to seed HUVECs onto the luminal scaffold surface. The non-bioreactor HUVEC seeded scaffolds were statically cultured for 2 days and demonstrated excellent adherence, homogenous coverage and widespread viability (Figure 7.11 A & F). Similarly, the feasibility of using HUVECs within the bioreactor system was successfully demonstrated as the cells were viable after seeding in co-culture with medially injected rMSCs. Both rMSCs and HUVECs were viable after the combined culture period of 11 days (2 days static culture and 7 days bioreactor culture with rMSCs only, and 2 days bioreactor culture with both cell types).

This demonstrates the successful adherence of ECs to the customised scaffold in conjunction with rMSC medial layer repopulation by direct medial injection (Figure 7.12). This is an essential requirement for any TEVG and is also important for any future investigations of medially injected cells within the bioreactor system, as ECs are closely linked and important in the maintenance and control of cells within the medial layer (Reneman et al., 2006). Further optimisation of the flow rates and shear stress after luminal seeding could increase cell retention efficiency and allow for investigation into cell alignment and orientation. The gradual increase over 48 h back to the original flow rate was taken from the literature (Gong and Niklason, 2008, Yazdani et al., 2010) but may be improved with further experimentation.

Taken together, the results in this chapter show an increase in cell migration from the combined stimuli of the bioreactor and growth factor, in conjunction with successful endothelialisation. This demonstrates that medially bulk loaded cells and HGF may allow for an improved dynamic performance. These results demonstrate an initial investigation into the behaviour of rMSCs, seeded within a customised scaffold by medial injection, within a bio-mimetic environment. In this study the migration alone was investigated as the principal response of the seeded rMSCs to the bioreactor and HGF stimuli, as medial layer repopulation is the overall goal of this research. However, in order to fully characterise the effects of these stimuli on the seeded cells investigation into; proliferation, cell differentiation and the improved mechanical properties of the conditioned scaffolds would be required. Variables such as flow rate, cyclic distension and foetal pressures have been shown to affect the response of cells within bioreactor systems (Niklason et al., 1999, Yazdani et al., 2009, Couet et al., 2012). Similarly, while successful repopulation of the medial layer was achieved, complete scaffold repopulation was not. Figure 7.12 highlights that further optimisation of the cell and/or chitosan/β-GP

HGF gel delivery by the creation of multiple injection channels could lead to full scaffold repopulation. Six injection channels instead of three, with either 6 cell injections or 3 cell injections and 3 chitosan/β-GP HGF gel may achieve this.

7.5 Conclusion

The bioreactor conditioning improved the circumferential migration of cells to produce a consistent, robust construct with enhanced repopulation of the medial layer. Adding a stimulus of HGF, delivered via medial injection within a chitosan/β-GP gel, further enhanced the migration of cells within the scaffold. A luminal monolayer of cells was also demonstrated within the bioreactor system by the creation a co-culture of HUVECs on the luminal surface of this customised scaffold. The response of medially injected cells to the bio-mimetic environment demonstrated that enhanced scaffold repopulation is possible *in vitro,* which may create the capacity for improved *in vivo* performance.

Chapter 8 Overall Discussion

8.1 Introduction

Tissue engineering has advanced substantially toward addressing the clinical need of replacement vascular grafts for small diameter applications, yet full scale clinical translation still remains unfulfilled. Challenges such as viable cell sources, inefficient seeding techniques, lengthy manufacturing times, sustainable shelf life and high costs have hindered this translation. This thesis aimed to address these challenges by the manipulation of decellularized vascular scaffolds in order to advance them toward use in a clinical environment. Decellularized scaffolds have the promise to confront the shortcomings of TEVG development as they have suitable mechanical properties for direct implantation, are available in a wide variety of geometries, are non-immunogenic and have the ability to remodel and grow. The clinical translation of decellularized scaffolds has been hindered by their highly dense matrix architecture which can prevent cell repopulation. This research strived to combat this issue through precise manipulation of the scaffold to tailor its properties to increase cell repopulation but maintain mechanical integrity.

8.2 Decellularized Vascular Scaffolds

Decellularized exogenous arterial tissue offers an attractive scaffold for TEVG development, as the complex structure-function relationship between the ECM components is maintained after decellularization. The main advantages of the manipulation of decellularized scaffolds are:

- The elastin network is undisrupted, which is essential for graft compliance, and *in vitro* elastin synthesis has proven difficult.
- Chapter 3 identified a means of directly injecting cells within the scaffold via injection channels created in the medial layer. This method may overcome the

barrier of poor cell infiltration of the medial layer associated with using decellularized scaffolds.

- Excessive manufacturing times associated with TEVG development may be overcome using this bulk seeding method.
- Increased levels of cell infiltration were achieved by the controlled increase in scaffold porosity via small collagen fiber digestion. Full mechanical quantification after these scaffold manipulations verified that the mechanical integrity and tensile response of the scaffold was not sacrificed.
- The scaffold demonstrated good interaction with rSMCs and hSMCs, and the injection channels were a feasible entry point for these cell types.

8.3 Biochemical Stimulus to Enhance Repopulation

The direct injection of cells into the medial layer offers a method of introducing cells within the dense scaffold. However, cell migration throughout the scaffold was still limited to the injection sites, preventing full scaffold repopulation. Chapter 5 utilised a growth factor as a chemotactic stimulus in order to address this, the main findings from this chapter were:

- MSCs were investigated as a potentially more clinically relevant cell source due to their ease of harvesting, rapid expansion, allogenicity and therapeutic benefit.
- HGF was chosen as the biochemical stimulus as it has previously been shown to increase cell migration, and MSCs also contain HGF receptors.
- A chitosan/β-GP hydrogel was used as a delivery vehicle for both rMSCs and HGF as it was fully injectable, thermoresponsive and suitable for entry within the injection channels.

- HGF release from the chitosan/β-GP demonstrated an ideal profile, with sustained controlled release up to 20 days and a burst release up to 7 days.
- The released HGF from the chitosan/β-GP also provided the desired chemotactic stimulus to increase migration of the medially injected cells.
- Radial migration of cells across the dense elastin sheets was not successful. This highlighted the futility of the commonly used method of abluminal cell seeding decellularized scaffolds, and suggests that scaffold manipulation is necessary to obtain any degree of medial layer repopulation.
- The chitosan/β-GP delivery vehicle also offers the ability for the delivery of multiple bio-therapeutics from within the scaffold, which may further enhance the capabilities of the scaffold.

8.4 Characterisation in Dynamic Culture

To examine the response of medially injected rMSCs, the cell loaded decellularized scaffold was subjected to similar hemodynamic forces experienced *in vivo*, as detailed in Chapter 7. This was achieved by the dynamic conditioning of the scaffolds in the custom built pulsatile flow bioreactor system described in Chapter 6 which demonstrated:

- Levels of cyclic strain, comparable to those experienced by native arterial tissue, improved the circumferential migration of cells to produce a consistent, robust construct with a repopulated medial layer.
- Adding a stimulus of HGF, also delivered via medial injection within a chitosan/β-GP gel, further enhanced the migration of cells within dynamically conditioned scaffolds.
- Endothelialisation of the rMSC medially injected scaffold within the bioreactor system, by the creation of a co-culture of HUVECs on the luminal scaffold

surface demonstrating that this customised scaffold was receptive to luminal monolayer creation.

- The maximum amount of migration achieved in response to the bioreactor and HGF combined stimuli was over ten times higher than that achieved in static culture.
- The amount of migration achieved by utilising the HGF stimulus alone in static culture is significantly higher than any degree of infiltration seen in the literature by dynamically conditioning decellularized vascular scaffolds in a bioreactor system.

8.5 "Off-the-Shelf" Availability

The readily available, multi dimensional characteristics of exogenous decellularized scaffolds mean scale up for clinical use will be relatively cheap and straightforward, compared to other tissue engineering techniques. However, one major requirement of this scale up will be the creation of a feasible shelf life, i.e. the long term preservation and sterilisation of the scaffold. This challenge was addressed in Chapter 4 by the description of a new freeze drying protocol for our manipulated decellularized scaffold, which demonstrated:

- Snap freezing the scaffolds in liquid nitrogen, prior to insertion into a pre-cooled freeze-drier, below the T_f at which primary drying occurs produces a homogenously dried, robust intact scaffold with undisrupted ECM components and minimal alteration to the overall mechanical properties of the scaffold.
- This protocol does not affect the creation of the injection channels or cytocompatibility of the scaffold.

- This protocol applies to a "standard" decellularized scaffold without any manipulation, with similar success but the protocol was most optimal for the more porous customised scaffold.
- The manipulated scaffold can be delivered and stored sterile and ready for use by rapidly bulk loading with bio-therapeutics by direct injection, in theatre, prior to implantation as a vascular graft. Furthermore, the freeze-dried state of the scaffold offers increased handling properties, which may lend itself to further future manipulations of the scaffold, via laser cutting or machining.

8.6 Future work

The results described here have shown how decellularized vascular scaffolds can be advanced toward clinical use. However, there are some limitations to this work and certain aspects of this research that warrant further investigation, namely the following areas:

Incomplete medial repopulation

The customisation techniques of collagen digestion and injection channel creation were shown to successfully introduce cells and repopulate the medial layer, yet complete circumferential medial migration was not achieved. Full scaffold repopulation prior to implantation should improve host cell integration and remodelling, thus incomplete repopulation is less ideal. Only three injection channels were used in the final bioreactor study in order to determine the maximum potential migration possible in response to dynamic conditioning. Figure 8.1 highlights that the addition of an extra three injection channels could allow for complete repopulation. These extra injection channels could contain either cells only or chitosan/β-GP HGF loaded gel in order to achieve 360° cell coverage within the medial layer. The process of creating multiple injection channels

would require precise machining. The manipulation of the scaffold in its freeze-dried state may aid this, as demonstrated in Figure 8.1 B, micro-machining numerous channels within the wall of a freeze-dried scaffold is possible.

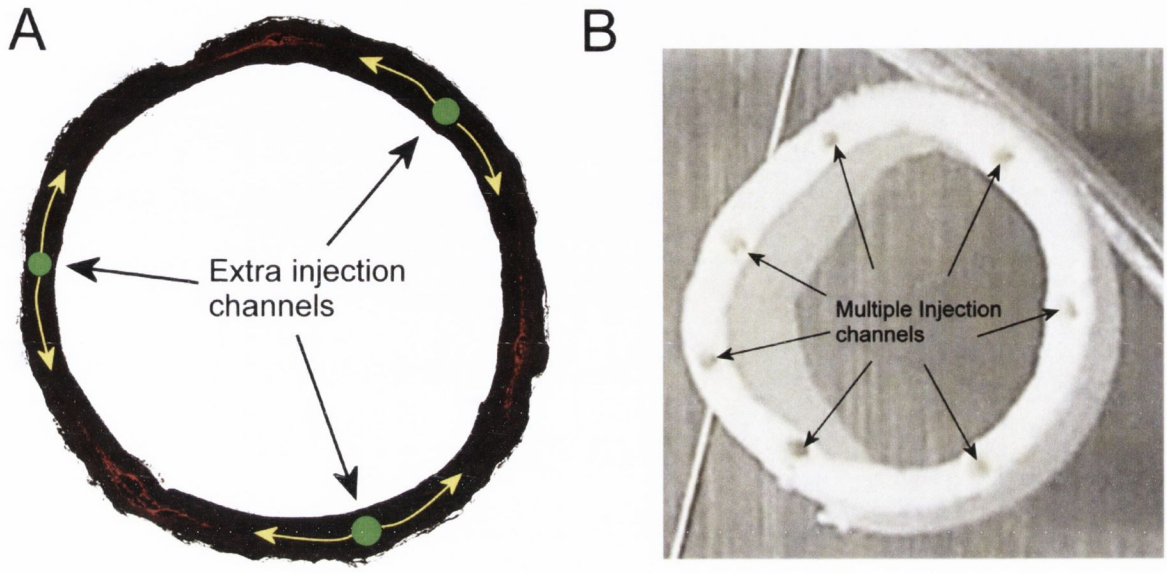

Figure 8.1 Multiple Injection Channels for Complete Repopulation

(A) *The addition of extra injection channels with either HGF or cells may allow for complete circumferential repopulation. (B) Freeze-drying allows for a robust machinable scaffold for the creation of multiple injection channels.*

Another issue is that the repopulation was limited to the circumferential direction, with minimum cell movement radially across the elastin layers. While it is hypothesised that this cell migration may not be as limited *in vivo* due to remodelling and host cell repopulation, there are still means to address this *in vitro*. Two further scaffold manipulations could achieve this: (1) increasing porosity of the dense elastin sheets, via laser cutting micro-channels radially through the scaffold wall, (2) injection channel creation across multiple elastin layers. However, any further scaffold manipulation would

require full mechanical quantification to ensure the integrity of the scaffold remains intact.

Non-mechanical manipulation of the scaffold to further increase repopulation could be achieved with the delivery of multiple bio-therapeutics. The use of the chitosan/β-GP hydrogel allowed for the controlled sustained release of HGF with a suitable release profile for this application. This is the first demonstration of protein release from this delivery vehicle and it is envisioned that other proteins will have similar release profiles. Other growth factors such as IGF, VEGF, bFGF and TGF-β have been utilised to increase proliferation, migration and differentiation in TEVG development. Further investigation into the release of these growth factors within a decellularized scaffold, and the cellular response to these bio-therapeutics is warranted.

Clinically Relevant Scaffold Length

The scaffolds described here were all 30mm in length, yet the medial repopulation was limited to only the injected length to which the needles were inserted (~12mm). The repopulation results demonstrated here served as a proof of concept for these short length scaffolds. Clinical translation of these scaffolds will require longer length scaffolds matched to patient specific cases. Overcoming this limitation by full longitudinal repopulation will therefore be required. This can be achieved with the introduction of needles into the transverse section of the proximal and distal ends of the scaffold, but also the insertion of needles from the abluminal surface, circumferentially and longitudinally to ensure full scaffold repopulation. Freeze-drying the scaffolds, as already described, offers a means of introducing these multiple needles as the dried scaffold is robust and easy to machine thus allowing consistent, repeatable needle insertion without the risk of piercing the scaffold wall (Figure 8.1).

Incomplete Bioreactor Characterisation

The study outlined here using the pulsatile flow bioreactor was an initial investigation into the migration response of medially injected rMSCs in a dynamic environment. A full characterisation study, with a completely repopulated scaffold will be required to fully determine the advantages of medial repopulation. Specifically, proliferation and differentiation of the rMSCs due to the hemodynamic forces experienced in the bioreactor should be investigated. Also mechanical testing of the bioreactor cultured scaffolds will quantify the effects of repopulation and conditioning and further determine its potential dynamic response. The efficacy of any additional growth factors explored for potential improvement in the scaffold should be investigated within a dynamic environment to observe unforeseen aspects that do not occur in the static environment.

In vivo Characterisation

The hypothesis of this thesis is that manipulation of decellularized scaffolds to increase cell repopulation by *in vitro* seeded cells and/or host cells *in vivo*, may potentially improve their performance as small diameter bypass grafts. However, this hypothesis is limited until it is verified by full *in vivo* characterisation of the scaffold. A small animal model, such as a New Zealand white rabbit common carotid interposition bypass grafting could be useful to determine the efficacy of a fully repopulated scaffold. A control for this study would be static abluminally seeded scaffolds. This bypass model is of suitable dimensions for the decellularized scaffold used here and time points of 1, 3 and 6 months would allow for full evaluation of the remodelling process. Labelling and tracking of the MSCs would determine if their role in remodelling was functional or therapeutic. Ideal study outcomes would be primary patency at each time point, with no stenosis, aneurysm formation, calcification or intimal hyperplasia. The *in vivo* response of tissue engineered constructs have been evaluated in non-load bearing settings, such as cranial defects for

bone scaffolds and even sub dermal implantation for TEVGs. However, the complexity of TEVGs requires a broad in depth *in vivo* characterisation under full hemodynamic forces, as described above, to determine the long term efficacy of the scaffold.

Clinically relevant EC source

A clinically relevant EC source that is easily harvested, expanded and integrated with a vascular scaffold is a major limitation in the translation of all TEVGs. Endothelialisation or monolayer formation of the customised decellularized scaffold was demonstrated here, though it was beyond the scope of this project to determine a clinically relevant EC source. While this is a major challenge for all vascular tissue engineering techniques, some success has been achieved to date. Endothelial progenitor cells can be harvested from circulating blood flow and offer an attractive source for endothelialisation. This could be from either direct harvesting and expansion or coating of the decellularized scaffold to attract and adhere these cells *in vivo*. The newly discovered cardiac stem cell niche would also be a cell source worth investigating as they offer high differentiation potential.

8.7 Overall Conclusion

This thesis has described a means of producing a fully acellular vascular scaffold which retains the structure-function relationship of the ECM components of the native porcine tissue from which it's derived. The poor cell infiltration associated with these decellularized scaffolds was addressed by manipulating the remaining matrix to allow a means of bulk cell seeding the medial layer. The further additions of biochemical and biomechanical stimuli increased the degree of cell infiltration of these scaffolds. This was achieved with a novel hydrogel delivery vehicle and a custom built pulsatile flow

bioreactor. Novel freeze drying techniques were also derived which allow for the long term preservation and simple sterilisation of this scaffold.

This research has addressed some of the shortcomings of decellularized arterial scaffolds for TEVG development. Bulk loading bio-therapeutics within a preserved, mechanically robust, customised decellularized vascular scaffold creates a possible platform for enhanced *in vivo* performance by increased cell repopulation, suitable mechanical properties and reduced manufacturing times. This scaffold offers the potential to produce "off-the-shelf" patient specific TEVGs and bridge the translation of TEVGs to clinical use.

References

ABBOTT, W. M., MEGERMAN, J., HASSON, J. E., L'ITALIEN, G. & WARNOCK, D. F. 1987. Effect of compliance mismatch on vascular graft patency. *Journal of Vascular Surgery,* 5, 376-382.

AMIEL, G. E., KOMURA, M., SHAPIRA, O., YOO, J. J., YAZDANI, S., BERRY, J., KAUSHAL, S., BISCHOFF, J., ATALA, A. & SOKER, S. 2006. Engineering of blood vessels from acellular collagen matrices coated with human endothelial cells. *Tissue Engineering,* 12, 2355-2365.

ASAHARA, T., MUROHARA, T., SULLIVAN, A., SILVER, M., VAN DER ZEE, R., LI, T., WITZENBICHLER, B., SCHATTEMAN, G. & ISNER, J. M. 1997. Isolation of Putative Progenitor Endothelial Cells for Angiogenesis. *Science,* 275, 964-966.

ATALA, A., BAUER, S. B., SOKER, S., YOO, J. J. & RETIK, A. B. 2006. Tissue-engineered autologous bladders for patients needing cystoplasty. *The Lancet,* 367, 1241-1246.

BABENSEE, J., MCINTIRE, L. & MIKOS, A. 2000. Growth Factor Delivery for Tissue Engineering. *Pharmaceutical Research,* 17, 497-504.

BADYLAK, S. F. 2007. The extracellular matrix as a biologic scaffold material. *Biomaterials,* 28, 3587-3593.

BADYLAK, S. F., FREYTES, D. O. & GILBERT, T. W. 2009. Extracellular matrix as a biological scaffold material: Structure and function. *Acta biomaterialia,* 5, 1-13.

BAJPAI, V. K. & ANDREADIS, S. T. 2012. Stem cell sources for vascular tissue engineering and regeneration. *Tissue Eng Part B Rev,* 18, 405-25.

BARILE, L., MESSINA, E., GIACOMELLO, A. & MARBÁN, E. 2007. Endogenous Cardiac Stem Cells. *Progress in Cardiovascular Diseases,* 50, 31-48.

BARRON, V., LYONS, E., STENSON-COX, C., MCHUGH, P. E. & PANDIT, A. 2003. Bioreactors for Cardiovascular Cell and Tissue Growth: A Review. *Annals of Biomedical Engineering,* 31, 1017-1030.

BEARZI, C., ROTA, M., HOSODA, T., TILLMANNS, J., NASCIMBENE, A., DE ANGELIS, A., YASUZAWA-AMANO, S., TROFIMOVA, I., SIGGINS, R. W., LECAPITAINE, N., CASCAPERA, S., BELTRAMI, A. P., D'ALESSANDRO, D. A., ZIAS, E., QUAINI, F., URBANEK, K., MICHLER, R. E., BOLLI, R., KAJSTURA, J., LERI, A. & ANVERSA, P. 2007. Human cardiac stem cells. *Proceedings of the National Academy of Sciences,* 104, 14068-14073.

BENDECK, M. P., KEELEY, F. W. & LANGILLE, B. L. 1994. Perinatal accumulation of arterial wall constituents: relation to hemodynamic changes at birth. *American Journal of Physiology - Heart and Circulatory Physiology,* 267, H2268-H2279.

BERGMEISTER, H., BOECK, P., KASIMIR, M.-T., FLECK, T., FITZAL, F., HUSINSKY, W., MITTLBOECK, M., STOEHR, H. G., LOSERT, U., WOLNER, E. & GRABENWOEGER, M. 2005. Effect of laser perforation on the remodeling of acellular matrix grafts. *Journal of Biomedical Materials Research Part B: Applied Biomaterials,* 74B, 495-503.

BERGMEISTER, H., PLASENZOTTI, R., WALTER, I., PLASS, C., BASTIAN, F., RIEDER, E., SIPOS, W., KAIDER, A., LOSERT, U. & WEIGEL, G. 2008. Decellularized, xenogeneic small-diameter arteries: Transition from a muscular to

an elastic phenotype *in vivo*. *Journal of Biomedical Materials Research Part B: Applied Biomaterials,* 87B, 95-104.

BERNKOP-SCHNÜRCH, A. & DÜNNHAUPT, S. 2012. Chitosan-based drug delivery systems. *European Journal of Pharmaceutics and Biopharmaceutics,* 81, 463-469.

BILODEAU, K., COUET, F., BOCCAFOSCHI, F. & MANTOVANI, D. 2005. Design of a Perfusion Bioreactor Specific to the Regeneration of Vascular Tissues Under Mechanical Stresses. *Artificial Organs,* 29, 906-912.

BOLAND, E. 2004. Electrospinning collagen and elastin: preliminary vascular tissue engineering. *Frontiers in Bioscience,* 9, 1422.

BORDEN, B. A., YOCKMAN, J. & KIM, S. W. 2010. Thermoresponsive Hydrogel as a Delivery Scaffold for Transfected Rat Mesenchymal Stem Cells. *Molecular Pharmaceutics,* 7, 963-968.

BORSCHEL, G. H., HUANG, Y.-C., CALVE, S., ARRUDA, E. M., LYNCH, J. B., DOW, D. E., KUZON, W. M., DENNIS, R. G. & BROWN, D. L. 2005. Tissue Engineering of Recellularized Small-Diameter Vascular Grafts. *Tissue Engineering,* 11, 778.

BRAR, S. & STONE, G. 2009. Advances in percutaneous coronary intervention. *Current Cardiology Reports,* 11, 245-251.

BREEN, L. T., MCHUGH, P. E., MCCORMACK, B. A., MUIR, G., QUINLAN, N. J., HERATY, K. B. & MURPHY, B. P. 2006. Development of a novel bioreactor to apply shear stress and tensile strain simultaneously to cell monolayers. *Review of Scientific Instruments,* 77.

BRENNAN, M. P., DARDIK, A., HIBINO, N., ROH, J. D., NELSON, G. N., PAPADEMITRIS, X., SHINOKA, T. & BREUER, C. K. 2008. Tissue-engineered Vascular Grafts Demonstrate Evidence of Growth and Development When Implanted in a Juvenile Animal Model. *Annals of Surgery,* 248, 370-377

BUXTON, B. F., HAYWARD, P. A. R., NEWCOMB, A. E., MOTEN, S., SEEVANAYAGAM, S. & GORDON, I. 2009. Choice of conduits for coronary artery bypass grafting: craft or science? *Eur J Cardiothorac Surg,* 35, 658-670.

CAMERON, A., DAVIS, K. B., GREEN, G. & SCHAFF, H. V. 1996. Coronary Bypass Surgery with Internal-Thoracic-Artery Grafts — Effects on Survival over a 15-Year Period. *New England Journal of Medicine,* 334, 216-220.

CARDAMONE, L., VALENTÍN, A., EBERTH, J. F. & HUMPHREY, J. D. 2009. Origin of axial prestretch and residual stress in arteries. *Biomechanics and Modeling in Mechanobiology,* 8, 431-446.

CARMELIET, P. & CONWAY, E. M. 2001. Growing better blood vessels. *Nat Biotech,* 19, 1019-1020.

CARO, C., PEDLEY, T., SCHROTER, R. & SEED, W. 1978. *The Mechanics of the Circulation*, Oxford University Press, New York.

CHAN-PARK, M. B., SHEN, J. Y., CAO, Y., XIONG, Y., LIU, Y., RAYATPISHEH, S., KANG, G. C.-W. & GREISLER, H. P. 2009. Biomimetic control of vascular smooth muscle cell morphology and phenotype for functional tissue-engineered small-diameter blood vessels. *Journal of Biomedical Materials Research Part A,* 91A, 629-634.

CHENITE, A., BUSCHMANN, M., WANG, D., CHAPUT, C. & KANDANI, N. 2001. Rheological characterisation of thermogelling chitosan/glycerol-phosphate solutions. *Carbohydrate Polymers,* 46, 39-47.

CHO, S.-W., LIM, S. H., KIM, I.-K., HONG, Y. S., KIM, S.-S., YOO, K. J., PARK, H.-Y., JANG, Y., CHANG, B. C., CHOI, C. Y., HWANG, K.-C. & KIM, B.-S. 2005.

Small-Diameter Blood Vessels Engineered With Bone Marrow-Derived Cells. *Annals of Surgery,* 241, 506-515.

CHUANG, T.-H., STABLER, C., SIMIONESCU, A. & SIMIONESCU, D. T. 2009. Polyphenol-Stabilized Tubular Elastin Scaffolds for Tissue Engineered Vascular Grafts. *Tissue Engineering Part A,* 15, 2837-2851.

CONKLIN, B. S., RICHTER, E. R., KREUTZIGER, K. L., ZHONG, D. S. & CHEN, C. 2002. Development and evaluation of a novel decellularized vascular xenograft. *Medical Engineering & Physics,* 24, 173-183.

CONKLIN, B. S., WU, H., LIN, P. H., LUMSDEN, A. B. & CHEN, C. 2004. Basic Fibroblast Growth Factor Coating and Endothelial Cell Seeding of a Decellularized Heparin-coated Vascular Graft. *Artificial Organs,* 28, 668-675.

CORNWELL, K. G., LANDSMAN, A. & JAMES, K. S. 2009. Extracellular Matrix Biomaterials for Soft Tissue Repair. *Clinics in Podiatric Medicine and Surgery,* 26, 507-523.

COUET, F., MEGHEZI, S. & MANTOVANI, D. 2012. Fetal development, mechanobiology and optimal control processes can improve vascular tissue regeneration in bioreactors: An integrative review. *Medical Engineering and Physics,* 34, 269-278.

CRAPO, P. M., GAO, J. & WANG, Y. 2008. Seamless tubular poly(glycerol sebacate) scaffolds: High-yield fabrication and potential applications. *Journal of Biomedical Materials Research Part A,* 86A, 354-363.

CRAPO, P. M., GILBERT, T. W. & BADYLAK, S. F. 2011. An overview of tissue and whole organ decellularization processes. *Biomaterials,* 32, 3233-3243.

CRAPO, P. M. & WANG, Y. 2010. Physiologic compliance in engineered small-diameter arterial constructs based on an elastomeric substrate. *Biomaterials,* 31, 1626-1635.

CRISSMAN, R. S. 1987. Comparison of Two Digestive Techniques for Preparation of Vascular Elastic Networks for SEM Observation. *Journal of Electron Microscopy Technique,* 6, 335-348.

DA SILVA MEIRELLES, L., FONTES, A. M., COVAS, D. T. & CAPLAN, A. I. 2009. Mechanisms involved in the therapeutic properties of mesenchymal stem cells. *Cytokine and Growth Factor Reviews,* 20, 419-427.

DAHAN, N., ZARBIV, G., SARIG, U., KARRAM, T., HOFFMAN, A. & MACHLUF, M. 2012. Porcine small diameter arterial extracellular matrix supports endothelium formation and media remodeling forming a promising vascular engineered biograft. *Tissue Eng Part A.,* 18, 411-22.

DAHL, S., RHIM, C., SONG, Y. & NIKLASON, L. 2007. Mechanical Properties and Compositions of Tissue Engineered and Native Arteries. *Annals of Biomedical Engineering,* 35, 348-355.

DAHL, S. L. M., BLUM, J. L. & NIKLASON, L. E. 2011. Bioengineered Vascular Grafts: Can We Make Them Off-the-Shelf? *Trends in Cardiovascular Medicine,* 21, 83-89.

DAVIES, P. F. 1995. Flow-mediated endothelial mechanotransduction. *Physiological Reviews,* 75, 519-60.

DAVIS, E. 1993. Stability of elastin in the developing mouse aorta: a quantitative radioautographic study. *Histochemistry,* 100, 17-26.

DERHAM, C., YOW, H., INGRAM, J., FISHER, J., INGHAM, E., KORROSIS, S. A. & HOMER-VANNIASINKAM, S. 2008. Tissue engineering small-diameter vascular grafts: preparation of a biocompatible porcine ureteric scaffold. *Tissue Eng Part A,* 14, 1871-82.

DESAI, M., SEIFALIAN, A. M. & HAMILTON, G. 2011. Role of prosthetic conduits in coronary artery bypass grafting. *European Journal of Cardio-Thoracic Surgery,* 40, 394-398.

DIMUZIO, P. & TULENKO, T. 2007. Tissue engineering applications to vascular bypass graft development: The use of adipose-derived stem cells. *Journal of Vascular Surgery,* 45, A99-A103.

DONG, J.-D., GU, Y.-Q., LI, C.-M., WANG, C.-R., FENG, Z.-G., QIU, R.-X., CHEN, B., LI, J.-X., ZHANG, S.-W., WANG, Z.-G. & ZHANG, J. 2009. Response of mesenchymal stem cells to shear stress in tissue-engineered vascular grafts. *Acta Pharmacol Sin,* 30, 530-536.

DUFFY, G. P., MCFADDEN, T. M., BYRNE, E. M., GILL, S. L., FARRELL, E. & O'BRIEN, F. J. 2011. Towards in vitro vascularisation of collagen-GAG scaffolds. *Eur Cell Mater,* 21, 15-30.

DURHAM, E. R., INGHAM, E. & RUSSELL, S. J. 2013. Technique for internal channelling of hydroentangled nonwoven scaffolds to enhance cell penetration. *Journal of Biomaterials Applications,* 28, 241-9.

EISENBERG, M., FILION, K. B., AZOULAY, A., BROX, A. C., S., H. & PILOTE, L. 2005. OUtcomes and cost of coronary artery bypass graft surgery in the united states and canada. *Archives of Internal Medicine,* 165, 1506-1513.

FAIKRUA, A., WITTAYA-AREEKUL, S., OONKHANOND, B. & VIYOCH, J. 2013. In vivo chondrocyte and transforming growth factor-β1 delivery using the thermosensitive chitosan/starch/β-glycerol phosphate hydrogel. *Journal of Biomaterials Applications,* 28, 175-186.

FARKOUH, M. E., DOMANSKI, M., SLEEPER, L. A., SIAMI, F. S., DANGAS, G., MACK, M., YANG, M., COHEN, D. J., ROSENBERG, Y., SOLOMON, S. D., DESAI, A. S., GERSH, B. J., MAGNUSON, E. A., LANSKY, A., BOINEAU, R., WEINBERGER, J., RAMANATHAN, K., SOUSA, J. E., RANKIN, J., BHARGAVA, B., BUSE, J., HUEB, W., SMITH, C. R., MURATOV, V., BANSILAL, S., KING, S., BERTRAND, M. & FUSTER, V. 2012. Strategies for Multivessel Revascularization in Patients with Diabetes. *New England Journal of Medicine,* 367, 2375-2384.

FONCK, E., PROD'HOM, G., ROY, S., AUGSBURGER, L., RÜFENACHT, D. A. & STERGIOPULOS, N. 2007. Effect of elastin degradation on carotid wall mechanics as assessed by a constituent-based biomechanical model. *American Journal of Physiology - Heart and Circulatory Physiology,* 292, H2754-H2763.

FORTE, G., MINIERI, M., COSSA, P., ANTENUCCI, D., SALA, M., GNOCCHI, V., FIACCAVENTO, R., CAROTENUTO, F., DE VITO, P., BALDINI, P. M., PRAT, M. & DI NARDO, P. 2006. Hepatocyte Growth Factor Effects on Mesenchymal Stem Cells: Proliferation, Migration, and Differentiation. *Stem Cells,* 24, 23-33.

FREED, A. D. & DOEHRING, T. C. 2005. Elastic Model for Crimped Collagen Fibrils. *Journal of Biomechanical Engineering,* 127, 587-593.

FUNAMOTO, S., NAM, K., KIMURA, T., MURAKOSHI, A., HASHIMOTO, Y., NIWAYA, K., KITAMURA, S., FUJISATO, T. & KISHIDA, A. 2010. The use of high-hydrostatic pressure treatment to decellularize blood vessels. *Biomaterials,* 31, 3590-3595.

FUNG, Y.-C. 1993. *Biomechanics: mechanical properties of living tissues*, New York: Springer.

FUNG, Y. C. 1991. What are the residual stresses doing in our blood vessels? *Annals of Biomedical Engineering,* 19, 237-49.

FUSTER, V., WALSH, R. & HARRINGTON, R. 2011. *Hurst's The Heart 13th Edition*, McGraw-Hill.

GAJIWALA, K. & GAJIWALA, A. L. 2004. Evaluation of lyophilised, gamma-irradiated amnion as a biological dressing. *Cell Tissue Bank,* 5, 73-80.

GAO, J., CRAPO, P., NEREM, R. & WANG, Y. 2008. Co-expression of elastin and collagen leads to highly compliant engineered blood vessels. *Journal of Biomedical Materials Research Part A,* 85A, 1120-1128.

GEORGE, J. C. 2010. Stem cell therapy in acute myocardial infarction: a review of clinical trials. *Translational Research,* 155, 10-19.

GERSH, B. J., SLIWA, K., MAYOSI, B. M. & YUSUF, S. 2010. The epidemic of cardiovascular disease in the developing world: global implications. *European Heart Journal,* 31, 642-648.

GILBERT, T. W., SELLARO, T. L. & BADYLAK, S. F. 2006. Decellularization of tissues and organs. *Biomaterials,* 27, 3675-3683.

GILBERT, T. W., WOGNUM, S., JOYCE, E. M., FREYTES, D. O., SACKS, M. S. & BADYLAK, S. F. 2008. Collagen fiber alignment and biaxial mechanical behavior of porcine urinary bladder derived extracellular matrix. *Biomaterials,* 29, 4775-4782.

GODBEY, W. T., STACEY HINDY, B. S., SHERMAN, M. E. & ATALA, A. 2004. A novel use of centrifugal force for cell seeding into porous scaffolds. *Biomaterials,* 25, 2799-2805.

GONG, Z. & NIKLASON, L. E. 2008. Small-diameter human vessel wall engineered from bone marrow-derived mesenchymal stem cells (hMSCs). *FASEB J,* 22, 1635-1648.

GOODNEY, P. P., BECK, A. W., NAGLE, J., WELCH, H. G. & ZWOLAK, R. M. 2009. National trends in lower extremity bypass surgery, endovascular interventions, and major amputations. *Journal of Vascular Surgery,* 50, 54-60.

GRAY, B. H., CONTE, M. S., DAKE, M. D., JAFF, M. R., KANDARPA, K., RAMEE, S. R., RUNDBACK, J., WAKSMAN, R. & FOR WRITING GROUP 7 2008. Atherosclerotic Peripheral Vascular Disease Symposium II: Lower-Extremity Revascularization: State of the Art. *Circulation,* 118, 2864-2872.

GREENWALD, S. E. & BERRY, C. L. 2000. Improving vascular grafts: the importance of mechanical and haemodynamic properties. *The Journal of Pathology,* 190, 292-299.

GRINES, C. L., BROWNE, K. F., MARCO, J., ROTHBAUM, D., STONE, G. W., O'KEEFE, J., OVERLIE, P., DONOHUE, B., CHELLIAH, N., TIMMIS, G. C., VLIETSTRA, R. E., STRZELECKI, M., PUCHROWICZ-OCHOCKI, S. & O'NEILL, W. W. 1993. A Comparison of Immediate Angioplasty with Thrombolytic Therapy for Acute Myocardial Infarction. *New England Journal of Medicine,* 328, 673-679.

GRÜNTZIG, A. 1978. TRANSLUMINAL DILATATION OF CORONARY-ARTERY STENOSIS. *The Lancet,* 311, 263-263.

GUI, L., MUTO, A., CHAN, S. A., BREUER, C. K. & NIKLASON, L. E. 2009. Development of Decellularized Human Umbilical Arteries as Small-Diameter Vascular Grafts. *Tissue Engineering Part A,* 15, 2665-2676.

HAHN, M., MCHALE, M., WANG, E., SCHMEDLEN, R. & WEST, J. 2007. Physiologic Pulsatile Flow Bioreactor Conditioning of Poly(ethylene glycol)-based Tissue Engineered Vascular Grafts. *Annals of Biomedical Engineering,* 35, 190-200.

HANSSON, G. K. 2009. Inflammatory mechanisms in atherosclerosis. *Journal of Thrombosis and Haemostasis,* 7, 328-331.

HARLEY, B. A., LYNN, A. K., WISSNER-GROSS, Z., BONFIELD, W., YANNAS, I. V. & GIBSON, L. J. 2010. Design of a multiphase osteochondral scaffold. II. Fabrication of a mineralized collagen–glycosaminoglycan scaffold. *Journal of Biomedical Materials Research Part A,* 92A, 1066-1077.

HASTINGS, C. L., KELLY, H. M., MURPHY, M. J., BARRY, F. P., O'BRIEN, F. J. & DUFFY, G. P. 2012. Development of a thermoresponsive chitosan gel combined with human mesenchymal stem cells and desferrioxamine as a multimodal pro-angiogenic therapeutic for the treatment of critical limb ischaemia. *Journal of Controlled Release,* 161, 73-80.

HAUGH, M. G., MURPHY, C. M. & O'BRIEN, F. J. 2010. Novel freeze-drying methods to produce a range of collagen-glycosaminoglycan scaffolds with tailored mean pore sizes. *Tissue Eng Part C Methods.,* 16, 887-94.

HAVELKA, G. E. & KIBBE, M. R. 2011. The Vascular Adventitia: Its Role in the Arterial Injury Response. *Vascular and Endovascular Surgery,* 45, 381-390.

HE, W., NIEPONICE, A., HONG, Y., WAGNER, W. & VORP, D. 2011. Rapid Engineered Small Diameter Vascular Grafts from Smooth Muscle Cells. *Cardiovascular Engineering and Technology,* 2, 149-159.

HE, W., NIEPONICE, A., SOLETTI, L., HONG, Y., GHARAIBEH, B., CRISAN, M., USAS, A., PEAULT, B., HUARD, J., WAGNER, W. R. & VORP, D. A. 2010. Pericyte-based human tissue engineered vascular grafts. *Biomaterials,* 31, 8235-8244.

HIBINO, N., MCGILLICUDDY, E., MATSUMURA, G., ICHIHARA, Y., NAITO, Y., BREUER, C. & SHINOKA, T. 2010. Late-term results of tissue-engineered vascular grafts in humans. *The Journal of Thoracic and Cardiovascular Surgery,* 139, 431-436.e2.

HIMMELFARB, J. & IKIZLER, T. A. 2010. Hemodialysis. *New England Journal of Medicine,* 363, 1833-1845.

HIRAI, J. & MATSUDA, T. 1996. Venous reconstruction using hybrid vascular tissue composed of vascular cells and collagen: Tissue regeneration process. *Cell Transplantation,* 5, 93-105.

HOERSTRUP, S. P., CUMMINGS MRCS, I., LACHAT, M., SCHOEN, F. J., JENNI, R., LESCHKA, S., NEUENSCHWANDER, S., SCHMIDT, D., MOL, A., GÜNTER, C., GÖSSI, M., GENONI, M. & ZUND, G. 2006. Functional Growth in Tissue-Engineered Living, Vascular Grafts. *Circulation,* 114, I-159-I-166.

HOERSTRUP, S. P., ZUND, G., SODIAN, R., SCHNELL, A. M., GRUNENFELDER, J. & TURINA, M. I. 2001. Tissue engineering of small caliber vascular grafts. *Eur J Cardiothorac Surg,* 20, 164-169.

HOLZAPFEL, G., GASSER, T. & OGDEN, R. 2000. A New Constitutive Framework for Arterial Wall Mechanics and a Comparative Study of Material Models. *Journal of Elasticity,* 61, 1-48.

HOLZAPFEL, G. A. 2008. Collagen in Arterial Walls: Biomechanical Aspects. *In:* FRATZL, P. (ed.) *Collagen Structure and Mechanics.* Springer-Verlag, Heidelberg.

HSU, S.-H., TSAI, I. J., LIN, D.-J. & CHEN, D. C. 2005. The effect of dynamic culture conditions on endothelial cell seeding and retention on small diameter polyurethane vascular grafts. *Medical engineering & physics,* 27, 267-272.

HUA, Z.-Z., LI, B.-G., LIU, Z.-J. & SUN, D.-W. 2003. Freeze-Drying of Liposomes with Cryoprotectants and Its Effect on Retention Rate of Encapsulated Ftorafur and Vitamin A. *Drying Technology,* 21, 1491-1505.

HUANG, N. F. & LI, S. 2008. Mesenchymal stem cells for vascular regeneration. *Regenerative Medicine,* 3, 877-892.

HUMPHREY, J. 2002. Cardiovascular Solid Mechanics: Cells, Tissues, and Organs. *Applied Mechanics Reviews,* 55, B103-B104.

ISENBERG, B. C., WILLIAMS, C. & TRANQUILLO, R. T. 2006. Endothelialization and flow conditioning of fibrin-based media-equivalents. *Annals of Biomedical Engineering,* 34, 971-85.

ISO, Y., SPEES, J. L., SERRANO, C., BAKONDI, B., POCHAMPALLY, R., SONG, Y.-H., SOBEL, B. E., DELAFONTAINE, P. & PROCKOP, D. J. 2007. Multipotent human stromal cells improve cardiac function after myocardial infarction in mice without long-term engraftment. *Biochemical and Biophysical Research Communications,* 354, 700-706.

JOHNSON, B. D., MATHER, K. J. & WALLACE, J. P. 2011. Mechanotransduction of shear in the endothelium: basic studies and clinical implications. *Vascular Medicine,* 16, 365-77.

KAKISIS, J. D., LIAPIS, C. D., BREUER, C. & SUMPIO, B. E. 2005. Artificial blood vessel: The Holy Grail of peripheral vascular surgery. *Journal of Vascular Surgery,* 41, 349-354.

KANDA, K., MATSUDA, T. & OKA T 1993. Mechanical stress induced cellular orientation and phenotypic modulation of 3-D cultured smooth muscle cells. *ASAIO J,* 39, M686-90.

KANNAN, R. Y., SALACINSKI, H. J., BUTLER, P. E., HAMILTON, G. & SEIFALIAN, A. M. 2005. Current status of prosthetic bypass grafts: A review. *Journal of Biomedical Materials Research Part B: Applied Biomaterials,* 74B, 570-581.

KASYANOV, V., HODDE, J., HILES, M., EISENBERG, C., EISENBERG, L., DE CASTRO, L., OZOLANTA, I., MUROVSKA, M., DRAUGHN, R., PRESTWICH, G., MARKWALD, R. & MIRONOV, V. 2009. Rapid biofabrication of tubular tissue constructs by centrifugal casting in a decellularized natural scaffold with laser-machined micropores. *Journal of Materials Science: Materials in Medicine,* 20, 329-337.

KAUSHAL, S., AMIEL, G. E., GULESERIAN, K. J., SHAPIRA, O. M., PERRY, T., SUTHERLAND, F. W., RABKIN, E., MORAN, A. M., SCHOEN, F. J., ATALA, A., SOKER, S., BISCHOFF, J. & MAYER, J. E. 2001. Functional small-diameter neovessels created using endothelial progenitor cells expanded ex vivo. *Nat Med,* 7, 1035-1040.

KAWAMOTO, A. & ASAHARA, T. 2007. Role of progenitor endothelial cells in cardiovascular disease and upcoming therapies. *Catheterization and Cardiovascular Interventions,* 70, 477-84.

KIM, B.-S., NIKOLOVSKI, J., BONADIO, J. & MOONEY, D. J. 1999. Cyclic mechanical strain regulates the development of engineered smooth muscle tissue. *Nat Biotech,* 17, 979-983.

KLINKERT, P., SCHEPERS, A., BURGER, D. H. C., BOCKEL, J. H. V. & BRESLAU, P. J. 2003. Vein versus polytetrafluoroethylene in above-knee femoropopliteal bypass grafting: Five-year results of a randomized controlled trial. *Journal of Vascular Surgery,* 37, 149-155.

KONIG, G., MCALLISTER, T. N., DUSSERRE, N., GARRIDO, S. A., IYICAN, C., MARINI, A., FIORILLO, A., AVILA, H., WYSTRYCHOWSKI, W., ZAGALSKI, K., MARUSZEWSKI, M., JONES, A. L., CIERPKA, L., DE LA FUENTE, L. M. & L'HEUREUX, N. 2009. Mechanical properties of completely autologous human tissue engineered blood vessels compared to human saphenous vein and mammary artery. *Biomaterials,* 30, 1542-1550.

KRAWIEC, J. T. & VORP, D. A. 2012. Adult stem cell-based tissue engineered blood vessels: A review. *Biomaterials,* 33, 3388-3400.

KRENNING, G., MOONEN, J.-R. A. J., VAN LUYN, M. J. A. & HARMSEN, M. C. 2008. Generating New Blood Flow: Integrating Developmental Biology and Tissue Engineering. *Trends in Cardiovascular Medicine,* 18, 312-323.

KU, D. N. 1997. BLOOD FLOW IN ARTERIES. *Annual Review of Fluid Mechanics,* 29, 399-434.

KURANE, A., SIMIONESCU, D. T. & VYAVAHARE, N. R. 2007. In vivo cellular repopulation of tubular elastin scaffolds mediated by basic fibroblast growth factor. *Biomaterials,* 28, 2830-2838.

KURPINSKI, K., PARK, J., THAKAR, R. & LI, S. 2006. Regulation of Vascular Smooth Muscle Cells and Mesenchymal Stem Cells by Mechanical Strain. *Molecular and Cell Biology,* 3, 21-34.

L'HEUREUX, N., DUSSERRE, N., KONIG, G., VICTOR, B., KEIRE, P., WIGHT, T. N., CHRONOS, N. A. F., KYLES, A. E., GREGORY, C. R., HOYT, G., ROBBINS, R. C. & MCALLISTER, T. N. 2006. Human tissue-engineered blood vessels for adult arterial revascularization. *Nature Medicine,* 12, 361-365.

L'HEUREUX, N., GERMAIN, L., LABBÉ, R. & AUGER, F. A. 1993. In vitro construction of a human blood vessel from cultured vascular cells: A morphologic study. *Journal of Vascular Surgery,* 17, 499-509.

L'HEUREUX, N., MCALLISTER, T. N. & DE LA FUENTE, L. M. 2007. Tissue-Engineered Blood Vessel for Adult Arterial Revascularization. *New England Journal of Medicine,* 357, 1451-1453.

L'HEUREUX, N., PAQUET, S., LABBE, R., GERMAIN, L. & AUGER, F. A. 1998. A completely biological tissue-engineered human blood vessel. *FASEB J.,* 12, 47-56.

LAUGHLIN, M. H., NEWCOMER, S. C. & BENDER, S. B. 2008. Importance of hemodynamic forces as signals for exercise-induced changes in endothelial cell phenotype. *Journal of Applied Physiology,* 104, 588-600.

LEE, K. W., STOLZ, D. B. & WANG, Y. 2011. Substantial expression of mature elastin in arterial constructs. *Proceedings of the National Academy of Sciences of the United States of America,* 108, 2705-2710.

LEUNG, D., GLAGOV, S. & MATHEWS, M. 1976. Cyclic stretching stimulates synthesis of matrix components by arterial smooth muscle cells in vitro. *Science,* 191, 475-477.

LIBBY, P. 2002. Inflammation in atherosclerosis. *Nature,* 420, 868-874.

LIBBY, P., RIDKER, P. M. & HANSSON, G. K. 2011. Progress and challenges in translating the biology of atherosclerosis. *Nature,* 473, 317-325.

LIU, G.-F., HE, Z.-J., YANG, D.-P., HAN, X.-F., GUO, T.-F., HAO, C.-G., MA, H. & NIE, C.-L. 2008. Decellularized aorta of fetal pigs as a potential scaffold for small diameter tissue engineered vascular graft. *Chinese Medical Journal,* 121, 9.

LIU, J. Y., SWARTZ, D. D., PENG, H. F., GUGINO, S. F., RUSSELL, J. A. & ANDREADIS, S. T. 2007. Functional tissue-engineered blood vessels from bone marrow progenitor cells. *Cardiovascular Research,* 75, 618-628.

LU, Q., GANESAN, K., SIMIONESCU, D. T. & VYAVAHARE, N. R. 2004. Novel porous aortic elastin and collagen scaffolds for tissue engineering. *Biomaterials,* 25, 5227-5237.

MACCHIARINI, P., JUNGEBLUTH, P., GO, T., ASNAGHI, M. A., REES, L. E., COGAN, T. A., DODSON, A., MARTORELL, J., BELLINI, S., PARNIGOTTO, P. P., DICKINSON, S. C., HOLLANDER, A. P., MANTERO, S., CONCONI, M. T. & BIRCHALL, M. A. 2008. Clinical transplantation of a tissue-engineered airway. *The Lancet,* 372, 2023-2030.

MAILLARD, L., HAMON, M., KHALIFE, K., STEG, P. G., BEYGUI, F., GUERMONPREZ, J.-L., SPAULDING, C. M., BOULENC, J.-M., LIPIECKI, J., LAFONT, A., BRUNEL, P., GROLLIER, G., KONING, R., COSTE, P., FAVEREAU, X., LANCELIN, B., VAN BELLE, E., SERRUYS, P., MONASSIER, J.-P. & RAYNAUD, P. 2000. A comparison of systematic stenting and conventional balloon angioplasty during primary percutaneous transluminal coronary angioplasty for acute myocardial infarction. *Journal of the American College of Cardiology,* 35, 1729-1736.

MANCHIO, J. V., GU, J., ROMAR, L., BROWN, J., GAMMIE, J., PIERSON III, R. N., GRIFFITH, B. & POSTON, R. S. 2005. Disruption of Graft Endothelium Correlates With Early Failure After Off-Pump Coronary Artery Bypass Surgery. *The Annals of Thoracic Surgery,* 79, 1991-1998.

MARTIN, N. D., SCHANER, P. J., TULENKO, T. N., SHAPIRO, I. M., DIMATTEO, C. A., WILLIAMS, T. K., HAGER, E. S. & DIMUZIO, P. J. 2005. In Vivo Behavior of Decellularized Vein Allograft. *The Journal of surgical research,* 129, 17-23.

MATSUMURA, G., HIBINO, N., IKADA, Y., KUROSAWA, H. & SHIN'OKA, T. 2003a. Successful application of tissue engineered vascular autografts: clinical experience. *Biomaterials,* 24, 2303-2308.

MATSUMURA, G., MIYAGAWA-TOMITA, S., SHIN'OKA, T., IKADA, Y. & KUROSAWA, H. 2003b. First Evidence That Bone Marrow Cells Contribute to the Construction of Tissue-Engineered Vascular Autografts In Vivo. *Circulation,* 108, 1729-1734.

MCALLISTER, T. N., DUSSERRE, N., MARUSZEWSKI, M. & L'HEUREUX, N. 2008. Cell-based therapeutics from an economic perspective: primed for a commercial success or a research sinkhole? *Regenerative Medicine,* 3, 925-937.

MCALLISTER, T. N., MARUSZEWSKI, M., GARRIDO, S. A., WYSTRYCHOWSKI, W., DUSSERRE, N., MARINI, A., ZAGALSKI, K., FIORILLO, A., AVILA, H., MANGLANO, X., ANTONELLI, J., KOCHER, A., ZEMBALA, M., CIERPKA, L., DE LA FUENTE, L. M. & L'HEUREUX, N. 2009. Effectiveness of haemodialysis access with an autologous tissue-engineered vascular graft: a multicentre cohort study. *The Lancet,* 373, 1440-1446.

MCCAWLEY, L. J. & MATRISIAN, L. M. 2001. Matrix metalloproteinases: they're not just for matrix anymore! *Current Opinion in Cell Biology,* 13, 534-540.

MCFETRIDGE, P. S., ABE, K., HORROCKS, M. & CHAUDHURI, J. B. 2007. Vascular Tissue Engineering: Bioreactor Design Considerations for Extended Culture of Primary Human Vascular Smooth Muscle Cells. *ASAIO Journal,* 53, 623-630

MCFETRIDGE, P. S., BODAMYALI, T., HORROCKS, M. & CHAUDHURI, J. B. 2004a. Endothelial and Smooth Muscle Cell Seeding onto Processed Ex Vivo Arterial Scaffolds Using 3D Vascular Bioreactors. *ASAIO Journal,* 50, 591-600.

MCFETRIDGE, P. S., DANIEL, J. W., BODAMYALI, T., HORROCKS, M. & CHAUDHURI, J. B. 2004b. Preparation of porcine carotid arteries for vascular tissue engineering applications. *Journal of Biomedical Materials Research Part A,* 70A, 224-234.

MEYERROSE, T., OLSON, S., PONTOW, S., KALOMOIRIS, S., JUNG, Y., ANNETT, G., BAUER, G. & NOLTA, J. A. 2010. Mesenchymal stem cells for the sustained in vivo delivery of bioactive factors. *Advanced Drug Delivery Reviews,* 62, 1167-1174.

MIRZA, A., HYVELIN, J.-M., ROCHEFORT, G. Y., LERMUSIAUX, P., ANTIER, D., AWEDE, B., BONNET, P., DOMENECH, J. & EDER, V. 2008. Undifferentiated mesenchymal stem cells seeded on a vascular prosthesis contribute to the restoration of a physiologic vascular wall. *Journal of Vascular Surgery,* 47, 1313-1321.

MOGUES, T., LI, J., COBURN, J. & KUTER, D. J. 2005. IgG antibodies against bovine serum albumin in humans—their prevalence and response to exposure to bovine serum albumin. *Journal of Immunological Methods,* 300, 1-11.

MOHR, F. W., MORICE, M.-C., KAPPETEIN, A. P., FELDMAN, T. E., STÅHLE, E., COLOMBO, A., MACK, M. J., HOLMES JR, D. R., MOREL, M.-A., DYCK, N. V., HOULE, V. M., DAWKINS, K. D. & SERRUYS, P. W. 2013. Coronary artery bypass graft surgery versus percutaneous coronary intervention in patients with three-vessel disease and left main coronary disease: 5-year follow-up of the randomised, clinical SYNTAX trial. *The Lancet,* 381, 629-638.

MOLINA, J. E., EDWARDS, J. E., BIANCO, R. W., CLACK, R. W., LANG, G. & MOLINA, J. R. 1995. Composite and plain tubular synthetic graft conduits in right ventricle-pulmonary artery position: fate in growing lambs. *J Thorac Cardiovasc Surg,* 110, 427-435.

MORICE, M.-C., SERRUYS, P. W., SOUSA, J. E., FAJADET, J., BAN HAYASHI, E., PERIN, M., COLOMBO, A., SCHULER, G., BARRAGAN, P., GUAGLIUMI, G., MOLNÀR, F. & FALOTICO, R. 2002. A Randomized Comparison of a Sirolimus-Eluting Stent with a Standard Stent for Coronary Revascularization. *New England Journal of Medicine,* 346, 1773-1780.

MOSES, J. W., LEON, M. B., POPMA, J. J., FITZGERALD, P. J., HOLMES, D. R., O'SHAUGHNESSY, C., CAPUTO, R. P., KEREIAKES, D. J., WILLIAMS, D. O., TEIRSTEIN, P. S., JAEGER, J. L. & KUNTZ, R. E. 2003. Sirolimus-Eluting Stents versus Standard Stents in Patients with Stenosis in a Native Coronary Artery. *New England Journal of Medicine,* 349, 1315-1323.

NAGHAVI, M., LIBBY, P., FALK, E., CASSCELLS, S. W., LITOVSKY, S., RUMBERGER, J., BADIMON, J. J., STEFANADIS, C., MORENO, P., PASTERKAMP, G., FAYAD, Z., STONE, P. H., WAXMAN, S., RAGGI, P., MADJID, M., ZARRABI, A., BURKE, A., YUAN, C., FITZGERALD, P. J., SISCOVICK, D. S., DE KORTE, C. L., AIKAWA, M., JUHANI AIRAKSINEN, K. E., ASSMANN, G., BECKER, C. R., CHESEBRO, J. H., FARB, A., GALIS, Z. S., JACKSON, C., JANG, I.-K., KOENIG, W., LODDER, R. A., MARCH, K., DEMIROVIC, J., NAVAB, M., PRIORI, S. G., REKHTER, M. D., BAHR, R., GRUNDY, S. M., MEHRAN, R., COLOMBO, A., BOERWINKLE, E., BALLANTYNE, C., INSULL, W., SCHWARTZ, R. S., VOGEL, R., SERRUYS, P. W., HANSSON, G. K., FAXON, D. P., KAUL, S., DREXLER, H., GREENLAND, P., MULLER, J. E., VIRMANI, R., RIDKER, P. M., ZIPES, D. P., SHAH, P. K. & WILLERSON, J. T. 2003. From Vulnerable Plaque to

Vulnerable Patient: A Call for New Definitions and Risk Assessment Strategies: Part I. *Circulation,* 108, 1664-1672.

NAIL, S. L., JIANG, S., CHONGPRASERT, S. & KNOPP, S. A. 2002. Fundamentals of freeze-drying. *Pharm Biotechnol,* 14, 281-360.

NAKAMURA, T., YOSHITANI, M., RIGBY, H., FULLWOOD, N. J., ITO, W., INATOMI, T., SOTOZONO, C., NAKAMURA, T., SHIMIZU, Y. & KINOSHITA, S. 2004. Sterilized, Freeze-Dried Amniotic Membrane: A Useful Substrate for Ocular Surface Reconstruction. *Investigative Ophthalmology & Visual Science,* 45, 93-99.

NARITA, Y., KAGAMI, H., MATSUNUMA, H., MURASE, Y., UEDA, M. & UEDA, Y. 2008. Decellularized ureter for tissue-engineered small-caliber vascular graft. *Journal of Artificial Organs,* 11, 91-99.

NEFF, L. P., TILLMAN, B. W., YAZDANI, S. K., MACHINGAL, M. A., YOO, J. J., SOKER, S., BERNISH, B. W., GEARY, R. L. & CHRIST, G. J. 2011. Vascular smooth muscle enhances functionality of tissue-engineered blood vessels in vivo. *Journal of Vascular Surgery,* 53, 426-434.

NEREM, R. M. & SELIKTAR, D. 2001. VASCULAR TISSUE ENGINEERING. *Annual Review of Biomedical Engineering,* 3, 225-243.

NETTLES, D. L., ELDER, S. H. & GILBERT, J. A. 2002. Potential Use of Chitosan as a Cell Scaffold Material for Cartilage Tissue Engineering. *Tissue Engineering,* 8, 1009-1016.

NEUSS, S., BECHER, E., WÖLTJE, M., TIETZE, L. & JAHNEN-DECHENT, W. 2004. Functional Expression of HGF and HGF Receptor/c-met in Adult Human Mesenchymal Stem Cells Suggests a Role in Cell Mobilization, Tissue Repair, and Wound Healing. *Stem Cells,* 22, 405-414.

NIEPONICE, A., SOLETTI, L., GUAN, J., DEASY, B. M., HUARD, J., WAGNER, W. R. & VORP, D. A. 2008. Development of a tissue-engineered vascular graft combining a biodegradable scaffold, muscle-derived stem cells and a rotational vacuum seeding technique. *Biomaterials,* 29, 825-833.

NIKLASON, L. E., GAO, J., ABBOTT, W. M., HIRSCHI, K. K., HOUSER, S., MARINI, R. & LANGER, R. 1999. Functional Arteries Grown in Vitro. *Science,* 284, 489-493.

O'CEARBHAILL, E. D., MURPHY, M., BARRY, F., MCHUGH, P. E. & BARRON, V. 2010. Behavior of human mesenchymal stem cells in fibrin-based vascular tissue engineering constructs. *Annals of Biomedical Engineering,* 38, 649-57.

O'CONNELL, M. K., MURTHY, S., PHAN, S., XU, C., BUCHANAN, J., SPILKER, R., DALMAN, R. L., ZARINS, C. K., DENK, W. & TAYLOR, C. A. 2008. The three-dimensional micro- and nanostructure of the aortic medial lamellar unit measured using 3D confocal and electron microscopy imaging. *Matrix Biology,* 27, 171-181.

O'FLAHERTY, M., BUCHAN, I. & CAPEWELL, S. 2013. Contributions of treatment and lifestyle to declining CVD mortality: why have CVD mortality rates declined so much since the 1960s? *Heart,* 99, 159-162.

O'BRIEN, F. J., HARLEY, B. A., YANNAS, I. V. & GIBSON, L. J. 2005. The effect of pore size on cell adhesion in collagen-GAG scaffolds. *Biomaterials,* 26, 433-441.

OLAUSSON, M., PATIL, P. B., KUNA, V. K., CHOUGULE, P., HERNANDEZ, N., METHE, K., KULLBERG-LINDH, C., BORG, H., EJNELL, H. & SUMITRAN-HOLGERSSON, S. 2012. Transplantation of an allogeneic vein bioengineered with autologous stem cells: a proof-of-concept study. *The Lancet,* 380, 230-237.

OPITZ, F., SCHENKE-LAYLAND, K., COHNERT, T. U., STARCHER, B., HALBHUBER, K. J., MARTIN, D. P. & STOCK, U. A. 2004a. Tissue engineering of aortic tissue: dire consequence of suboptimal elastic fiber synthesis in vivo. *Cardiovascular Research,* 63, 719-730.

OPITZ, F., SCHENKE-LAYLAND, K., RICHTER, W., MARTIN, D. P., DEGENKOLBE, I., WAHLERS, T. & STOCK, U. A. 2004b. Tissue Engineering of Ovine Aortic Blood Vessel Substitutes Using Applied Shear Stress and Enzymatically Derived Vascular Smooth Muscle Cells. *Annals of Biomedical Engineering,* 32, 212-222.

OSOL, G. 1995. Mechanotransduction by vascular smooth muscle. *Journal of Vascular Research,* 32, 275-92.

OTT, H. C., MATTHIESEN, T. S., GOH, S.-K., BLACK, L. D., KREN, S. M., NETOFF, T. I. & TAYLOR, D. A. 2008. Perfusion-decellularized matrix: using nature's platform to engineer a bioartificial heart. *Nat Med,* 14, 213-221.

OWENS, G. K., KUMAR, M. S. & WAMHOFF, B. R. 2004. Molecular Regulation of Vascular Smooth Muscle Cell Differentiation in Development and Disease. *Physiological Reviews,* 84, 767-801.

PATEL, A., FINE, B., SANDIG, M. & MEQUANINT, K. 2006. Elastin biosynthesis: The missing link in tissue-engineered blood vessels. *Cardiovascular Research,* 71, 40-49.

PAWLOWSKI, K. J., RITTGERS, S. E., SCHMIDT, S. P. & BOWLIN, G. L. 2004. Endothelial cell seeding of polymeric vascular grafts. *Frontiers in Bioscience,* 9, 1412-21.

PECK, M., GEBHART, D., DUSSERRE, N., MCALLISTER, T. N. & L'HEUREUX, N. 2012. The evolution of vascular tissue engineering and current state of the art. *Cells Tissues Organs,* 195, 144-58.

PEREA, H., AIGNER, J., HOPFNER, U. & WINTERMANTEL, E. 2006. Direct magnetic tubular cell seeding: a novel approach for vascular tissue engineering. *Cells Tissues Organs,* 183, 156-65.

PETERSEN, T. H., CALLE, E. A., ZHAO, L., LEE, E. J., GUI, L., RAREDON, M. B., GAVRILOV, K., YI, T., ZHUANG, Z. W., BREUER, C., HERZOG, E. & NIKLASON, L. E. 2010. Tissue-Engineered Lungs for in Vivo Implantation. *Science,* 329, 538-541.

POLAK, R. & PITOMBO, R. N. M. 2011. Care during freeze-drying of bovine pericardium tissue to be used as a biomaterial: A comparative study. *Cryobiology,* 63, 61-66.

QUINT, C., KONDO, Y., MANSON, R. J., LAWSON, J. H., DARDIK, A. & NIKLASON, L. E. 2011. Decellularized tissue-engineered blood vessel as an arterial conduit. *Proceedings of the National Academy of Sciences,* 108, 9214-9219.

RADISIC, M., PARK, H., CHEN, F., SALAZAR-LAZZARO, J. E., WANG, Y., DENNIS, R., LANGER, R., FREED, L. E. & VUNJAK-NOVAKOVIC, G. 2006. Biomimetic approach to cardiac tissue engineering: oxygen carriers and channeled scaffolds. *Tissue Engineering,* 12, 2077-91.

RENEMAN, R. S., ARTS, T. & HOEKS, A. P. 2006. Wall shear stress--an important determinant of endothelial cell function and structure--in the arterial system in vivo. Discrepancies with theory. *Journal of Vascular Research,* 43, 251-69.

RENSEN, S. S., DOEVENDANS, P. A. & VAN EYS, G. J. 2007. Regulation and characteristics of vascular smooth muscle cell phenotypic diversity. *Neth Heart J.,* 15, 100-8.

RIEDER, E., KASIMIR, M.-T., SILBERHUMER, G., SEEBACHER, G., WOLNER, E., SIMON, P. & WEIGEL, G. 2004. Decellularization protocols of porcine heart valves differ importantly in efficiency of cell removal and susceptibility of the matrix to recellularization with human vascular cells. *J Thorac Cardiovasc Surg,* 127, 399-405.

ROACH, M. R. & BURTON, A. C. 1957. The reason for the shape of the distensibility curves of arteries. *Canadian journal of biochemistry and physiology,* 35, 681-90.

RODGERS, U. R. & WEISS, A. S. 2005. Cellular interactions with elastin. *Pathologie Biologie,* 53, 390-398.

ROGER, V. L., GO, A. S. & LLOYD-JONES, D. M. 2011. Heart Disease and Stroke Statistics--2011 Update: A Report From the American Heart Association. *Circulation,* 123, e18-209.

ROGER, V. L., GO, A. S., LLOYD-JONES, D. M., BENJAMIN, E. J., BERRY, J. D., BORDEN, W. B., BRAVATA, D. M., DAI, S., FORD, E. S., FOX, C. S., FULLERTON, H. J., GILLESPIE, C., HAILPERN, S. M., HEIT, J. A., HOWARD, V. J., KISSELA, B. M., KITTNER, S. J., LACKLAND, D. T., LICHTMAN, J. H., LISABETH, L. D., MAKUC, D. M., MARCUS, G. M., MARELLI, A., MATCHAR, D. B., MOY, C. S., MOZAFFARIAN, D., MUSSOLINO, M. E., NICHOL, G., PAYNTER, N. P., SOLIMAN, E. Z., SORLIE, P. D., SOTOODEHNIA, N., TURAN, T. N., VIRANI, S. S., WONG, N. D., WOO, D. & TURNER, M. B. 2012. Heart Disease and Stroke Statistics—2012 Update: A Report From the American Heart Association. *Circulation,* 125, e2-e220.

ROH, J. D., BRENNAN, M. P., LOPEZ-SOLER, R. I., FONG, P. M., GOYAL, A., DARDIK, A. & BREUER, C. K. 2007a. Construction of an autologous tissue-engineered venous conduit from bone marrow-derived vascular cells: optimization of cell harvest and seeding techniques. *Journal of Pediatric Surgery,* 42, 198-202.

ROH, J. D., NELSON, G. N., UDELSMAN, B. V., BRENNAN, M. P., LOCKHART, B., FONG, P. M., LOPEZ-SOLER, R. I., SALTZMAN, W. M. & BREUER, C. K. 2007b. Centrifugal seeding increases seeding efficiency and cellular distribution of bone marrow stromal cells in porous biodegradable scaffolds. *Tissue Engineering,* 13, 2743-9.

ROSE, F. R., CYSTER, L. A., GRANT, D. M., SCOTCHFORD, C. A., HOWDLE, S. M. & SHAKESHEFF, K. M. 2004. In vitro assessment of cell penetration into porous hydroxyapatite scaffolds with a central aligned channel. *Biomaterials,* 25, 5507-5514.

ROSS, R. 1999. Atherosclerosis — An Inflammatory Disease. *New England Journal of Medicine,* 340, 115-126.

ROY, S., SILACCI, P. & STERGIOPULOS, N. 2005. Biomechanical proprieties of decellularized porcine common carotid arteries. *Am J Physiol Heart Circ Physiol,* 289, H1567-1576.

RUEL-GARIÉPY, E., CHENITE, A., CHAPUT, C., GUIRGUIS, S. & LEROUX, J. C. 2000. Characterization of thermosensitive chitosan gels for the sustained delivery of drugs. *International Journal of Pharmaceutics,* 203, 89-98.

RZUCIDLO, E. M., MARTIN, K. A. & POWELL, R. J. 2007. Regulation of vascular smooth muscle cell differentiation. *Journal of vascular surgery : official publication, the Society for Vascular Surgery [and] International Society for Cardiovascular Surgery, North American Chapter,* 45, A25-A32.

SALACINSKI, H. J., GOLDNER, S., GIUDICEANDREA, A., HAMILTON, G., SEIFALIAN, A. M., EDWARDS, A. & CARSON, R. J. 2001. The Mechanical

Behavior of Vascular Grafts: A Review. *Journal of Biomaterials Applications,* 15, 241-278.

SCHANER, P. J., MARTIN, N. D., TULENKO, T. N., SHAPIRO, I. M., TAROLA, N. A., LEICHTER, R. F., CARABASI, R. A. & DIMUZIO, P. J. 2004. Decellularized vein as a potential scaffold for vascular tissue engineering. *Journal of Vascular Surgery,* 40, 146-153.

SCHWAB, S. J. 2007. Hemodialysis vascular access: The Achilles' heel remains. *Kidney Int,* 72, 665-666.

SCHWARTZ, C. F. & GALLOWAY, A. C. 2004. Coronary Artery Disease. *In:* ROBERT, C. M., JR, MD, GREGORY, V. S. & BEN, E. (eds.) *Surgical Decision Making (Fifth Edition).* Philadelphia: W.B. Saunders.

SEARLES, J. A., CARPENTER, J. F. & RANDOLPH, T. W. 2001. Annealing to optimize the primary drying rate, reduce freezing-induced drying rate heterogeneity, and determine Tg′ in pharmaceutical lyophilization. *Journal of Pharmaceutical Sciences,* 90, 872-887.

SEDDON, A. M., CURNOW, P. & BOOTH, P. J. 2004. Membrane proteins, lipids and detergents: not just a soap opera. *Biochimica et Biophysica Acta (BBA) - Biomembranes,* 1666, 105-117.

SEGERS, V. M. & LEE, R. 2010. Protein Therapeutics for Cardiac Regeneration after Myocardial Infarction. *Journal of Cardiovascular Translational Research,* 3, 469-477.

SELIKTAR, D., BLACK, R., VITO, R. & NEREM, R. 2000. Dynamic Mechanical Conditioning of Collagen-Gel Blood Vessel Constructs Induces Remodeling In Vitro. *Annals of Biomedical Engineering,* 28, 351-362.

SERRUYS, P. W., DE JAEGERE, P., KIEMENEIJ, F., MACAYA, C., RUTSCH, W., HEYNDRICKX, G., EMANUELSSON, H., MARCO, J., LEGRAND, V., MATERNE, P., BELARDI, J., SIGWART, U., COLOMBO, A., GOY, J. J., VAN DEN HEUVEL, P., DELCAN, J. & MOREL, M.-A. 1994. A Comparison of Balloon-Expandable-Stent Implantation with Balloon Angioplasty in Patients with Coronary Artery Disease. *New England Journal of Medicine,* 331, 489-495.

SHIMIZU, K., ITO, A., ARINOBE, M., MURASE, Y., IWATA, Y., NARITA, Y., KAGAMI, H., UEDA, M. & HONDA, H. 2007. Effective cell-seeding technique using magnetite nanoparticles and magnetic force onto decellularized blood vessels for vascular tissue engineering. *Journal of Bioscience and Bioengineering,* 103, 472-478.

SHIN'OKA, T., IMAI, Y. & IKADA, Y. 2001. Transplantation of a Tissue-Engineered Pulmonary Artery. *New England Journal of Medicine,* 344, 532-533.

SHIN'OKA, T., MATSUMURA, G., HIBINO, N., NAITO, Y., WATANABE, M., KONUMA, T., SAKAMOTO, T., NAGATSU, M. & KUROSAWA, H. 2005. Midterm clinical result of tissue-engineered vascular autografts seeded with autologous bone marrow cells. *The Journal of Thoracic and Cardiovascular Surgery,* 129, 1330-1338.

SILVA, G. V., LITOVSKY, S., ASSAD, J. A. R., SOUSA, A. L. S., MARTIN, B. J., VELA, D., COULTER, S. C., LIN, J., OBER, J., VAUGHN, W. K., BRANCO, R. V. C., OLIVEIRA, E. M., HE, R., GENG, Y.-J., WILLERSON, J. T. & PERIN, E. C. 2005. Mesenchymal Stem Cells Differentiate into an Endothelial Phenotype, Enhance Vascular Density, and Improve Heart Function in a Canine Chronic Ischemia Model. *Circulation,* 111, 150-156.

SIMIONESCU, D. T., LU, Q., SONG, Y., LEE, J., ROSENBALM, T. N., KELLEY, C. & VYAVAHARE, N. R. 2006. Biocompatibility and remodeling potential of pure arterial elastin and collagen scaffolds. *Biomaterials,* 27, 702-713.

SLUIJTER, J. P. G., DE KLEIJN, D. P. V. & PASTERKAMP, G. 2006. Vascular remodeling and protease inhibition–bench to bedside. *Cardiovascular Research,* 69, 595-603.

SMITH, R. R., BARILE, L., CHO, H. C., LEPPO, M. K., HARE, J. M., MESSINA, E., GIACOMELLO, A., ABRAHAM, M. R. & MARBAN, E. 2007. Regenerative potential of cardiosphere-derived cells expanded from percutaneous endomyocardial biopsy specimens. *Circulation,* 115, 896-908.

SOLETTI, L., HONG, Y., GUAN, J., STANKUS, J. J., EL-KURDI, M. S., WAGNER, W. R. & VORP, D. A. 2010. A bilayered elastomeric scaffold for tissue engineering of small diameter vascular grafts. *Acta biomaterialia,* 6, 110-122.

SOLETTI, L., NIEPONICE, A., GUAN, J., STANKUS, J. J., WAGNER, W. R. & VORP, D. A. 2006. A seeding device for tissue engineered tubular structures. *Biomaterials,* 27, 4863-4870.

STANKUS, J. J., SOLETTI, L., FUJIMOTO, K., HONG, Y., VORP, D. A. & WAGNER, W. R. 2007. Fabrication of cell microintegrated blood vessel constructs through electrohydrodynamic atomization. *Biomaterials,* 28, 2738-2746.

STEGEMANN, J. P., HONG, H. & NEREM, R. M. 2005. Mechanical, biochemical, and extracellular matrix effects on vascular smooth muscle cell phenotype. *J Appl Physiol,* 98, 2321-2327.

STEGEMANN, J. P., KASZUBA, S. N. & ROWE, S. L. 2007. Review: Advances in Vascular Tissue Engineering Using Protein-Based Biomaterials. *Tissue Engineering,* 13, 2601-2613.

STEGEMANN, J. P. & NEREM, R. M. 2003. Phenotype Modulation in Vascular Tissue Engineering Using Biochemical and Mechanical Stimulation. *Annals of Biomedical Engineering,* 31, 391-402.

STEKELENBURG, M., RUTTEN, M. C., SNOECKX, L. H. & BAAIJENS, F. P. 2009. Dynamic straining combined with fibrin gel cell seeding improves strength of tissue-engineered small-diameter vascular grafts. *Tissue Eng Part A,* 15, 1081-9.

STEMPER, B. D., YOGANANDAN, N., STINEMAN, M. R., GENNARELLI, T. A., BAISDEN, J. L. & PINTAR, F. A. 2007. Mechanics of Fresh, Refrigerated, and Frozen Arterial Tissue. *Journal of Surgical Research,* 139, 236-242.

SYEDAIN, Z. H., MEIER, L. A., BJORK, J. W., LEE, A. & TRANQUILLO, R. T. 2011. Implantable arterial grafts from human fibroblasts and fibrin using a multi-graft pulsed flow-stretch bioreactor with noninvasive strength monitoring. *Biomaterials,* 32, 714-722.

TAYALIA, P. & MOONEY, D. J. 2009. Controlled Growth Factor Delivery for Tissue Engineering. *Advanced Materials,* 21, 3269-3285.

TEEBKEN, O. E., BADER, A., STEINHOFF, G. & HAVERICH, A. 2000. Tissue Engineering of Vascular Grafts: Human Cell Seeding of Decellularised Porcine Matrix. *European Journal of Vascular and Endovascular Surgery,* 19, 381-386.

TILLMAN, B. W., YAZDANI, S. K., NEFF, L. P., CORRIERE, M. A., CHRIST, G. J., SOKER, S., ATALA, A., GEARY, R. L. & YOO, J. J. 2012. Bioengineered vascular access maintains structural integrity in response to arteriovenous flow and repeated needle puncture. *Journal of Vascular Surgery,* 56, 783-793.

TRANQUILLO, R. T. 2002. The Tissue-Engineered Small-Diameter Artery. *Annals of the New York Academy of Sciences,* 961, 251-254.

TSCHOEKE, B., FLANAGAN, T. C., CORNELISSEN, A., KOCH, S., ROEHL, A., SRIHARWOKO, M., SACHWEH, J. S., GRIES, T., SCHMITZ-RODE, T. & JOCKENHOEVEL, S. 2008. Development of a Composite Degradable/Nondegradable Tissue-engineered Vascular Graft. *Artificial Organs,* 32, 800-809.

TSCHOEKE, B., FLANAGAN, T. C., KOCH, S., HARWOKO, M. S., DEICHMANN, T., ELLÅ, V., SACHWEH, J. S., KELLOMÅKI, M., GRIES, T., SCHMITZ-RODE, T. & JOCKENHOEVEL, S. 2009. Tissue-Engineered Small-Caliber Vascular Graft Based on a Novel Biodegradable Composite Fibrin-Polylactide Scaffold. *Tissue Engineering Part A,* 15, 1909-1918.

VAN VLIERBERGHE, S., DUBRUEL, P. & SCHACHT, E. 2011. Biopolymer-Based Hydrogels As Scaffolds for Tissue Engineering Applications: A Review. *Biomacromolecules,* 12, 1387-1408.

VANDEVORD, P. J., MATTHEW, H. W. T., DESILVA, S. P., MAYTON, L., WU, B. & WOOLEY, P. H. 2002. Evaluation of the biocompatibility of a chitosan scaffold in mice. *Journal of Biomedical Materials Research,* 59, 585-590.

VEITH, F. J., MOSS, C. M., SPRAYREGEN, S. & MONTEFUSCO, C. 1979. Preoperative saphenous venography in arterial reconstructive surgery of the lower extremity. *Surgery,* 85, 253-6.

VENKATASUBRAMANIAN, R., GRASSL, E., BAROCAS, V., LAFONTAINE, D. & BISCHOF, J. 2006. Effects of Freezing and Cryopreservation on the Mechanical Properties of Arteries. *Annals of Biomedical Engineering,* 34, 823-832.

VENNEMANN, P., LINDKEN, R. & WESTERWEEL, J. 2007. In vivo whole-field blood velocity measurement techniques. *Experiments in Fluids,* 42, 495-511.

VILLALONA, G. A., UDELSMAN, B., DUNCAN, D. R., MCGILLICUDDY, E., SAWH-MARTINEZ, R. F., HIBINO, N., PAINTER, C., MIRENSKY, T., ERICKSON, B., SHINOKA, T. & BREUER, C. K. 2010. Cell-Seeding Techniques in Vascular Tissue Engineering. *Tissue Engineering Part B: Reviews,* 16, 341-350.

WAGENSEIL, J. E. & MECHAM, R. P. 2009. Vascular Extracellular Matrix and Arterial Mechanics. *Physiological Reviews,* 89, 957-989.

WALLES, T., GÖRLER, H., PUSCHMANN, C. & MERTSCHING, H. 2004. Functional neointima characterization of vascular prostheses in human. *The Annals of Thoracic Surgery,* 77, 864-868.

WALTER, J. & MAGOMETSCHNIGG, H. 2007. The role of vein grafts in peripheral vascular disease and carotid artery disease. *European Surgery,* 39, 76-82.

WANG, F., LI, Z., KHAN, M., TAMAMA, K., KUPPUSAMY, P., WAGNER, W. R., SEN, C. K. & GUAN, J. 2010. Injectable, rapid gelling and highly flexible hydrogel composites as growth factor and cell carriers. *Acta Biomaterialia,* 6, 1978-1991.

WANG, S., GOECKE, T., MEIXNER, C., HAVERICH, A., HILFIKER, A. & WOLKERS, W. F. 2012a. Freeze-dried heart valve scaffolds. *Tissue Eng Part C Methods,* 18, 517-25.

WANG, S., QU, X. & ZHAO, R. 2012b. Clinical applications of mesenchymal stem cells. *Journal of Hematology & Oncology,* 5, 19.

WEINBERG, C. & BELL, E. 1986. A blood vessel model constructed from collagen and cultured vascular cells. *Science,* 231, 397-400.

WHITE, J. J., BANDER, S. J. & SCHWAB, S. J. 2005. Opinion: Is Percutaneous Transluminal Angioplasty an Effective Intervention for Arteriovenous Graft Stenosis? *Seminars in Dialysis,* 18, 190-192.

WILLIAMS, C., LIAO, J., JOYCE, E. M., WANG, B., LEACH, J. B., SACKS, M. S. & WONG, J. Y. 2009. Altered structural and mechanical properties in decellularized rabbit carotid arteries. *Acta biomaterialia,* 5, 993-1005.

WILLIAMS, C. & WICK, T. M. 2004. Perfusion Bioreactor for Small Diameter Tissue-Engineered Arteries. *Tissue Engineering,* 10, 930-941.

WILLIAMS, C. & WICK, T. M. 2005. Endothelial Cell–Smooth Muscle Cell Co-Culture in a Perfusion Bioreactor System. *Annals of Biomedical Engineering,* 33, 920-928.

WILSHAW, S. P., ROONEY, P., BERRY, H., KEARNEY, J. N., HOMER-VANNIASINKAM, S., FISHER, J. & INGHAM, E. 2012. Development and characterization of acellular allogeneic arterial matrices. *Tissue Eng Part A,* 18, 471-83.

WISH, J. B. 2010. Vascular Access for Dialysis in the United States: Progress, Hurdles, Controversies, and the Future. *Seminars in Dialysis,* 23, 614-618.

WOLINSKY, H. & GLAGOV, S. 1967. A Lamellar Unit of Aortic Medial Structure and Function in Mammals. *Circulation Research,* 20, 99-111.

WORTH, N. F., ROLFE, B. E., SONG, J. & CAMPBELL, G. R. 2001. Vascular smooth muscle cell phenotypic modulation in culture is associated with reorganisation of contractile and cytoskeletal proteins. *Cell Motility and the Cytoskeleton,* 49, 130-145.

WU, Y. F., ZHANG, J., GU, Y. Q., LI, J. X., WANG, L. C. & WANG, Z. G. 2008. Reendothelialization of tubular scaffolds by sedimentary and rotative forces: a first step toward tissue-engineered venous graft. *Cardiovascular Revascularization Medicine,* 9, 238-247.

WYSTRYCHOWSKI, W., CIERPKA, L., ZAGALSKI, K., GARRIDO, S., DUSSERRE, N., RADOCHONSKI, S., MCALLISTER, T. N. & L'HEUREUX, N. 2011. Case study: first implantation of a frozen, devitalized tissue-engineered vascular graft for urgent hemodialysis access. *J Vasc Access,* 12, 67-70.

YANG, E. Y., DOKAINISH, H., VIRANI, S. S., MISRA, A., PRITCHETT, A. M., LAKKIS, N., BRUNNER, G., BOBEK, J., MCCULLOCH, M. L., HARTLEY, C. J., BALLANTYNE, C. M., NAGUEH, S. F. & NAMBI, V. 2011. Segmental Analysis of Carotid Arterial Strain Using Speckle-Tracking. *Journal of the American Society of Echocardiography,* 24, 1276-1284.e5.

YAZDANI, S. K., TILLMAN, B. W., BERRY, J. L., SOKER, S. & GEARY, R. L. 2010. The fate of an endothelium layer after preconditioning. *Journal of Vascular Surgery,* 51, 174-183.

YAZDANI, S. K., WATTS, B., MACHINGAL, M., JARAJAPU, Y. P. R., VAN DYKE, M. E. & CHRIST, G. J. 2009. Smooth Muscle Cell Seeding of Decellularized Scaffolds: The Importance of Bioreactor Preconditioning to Development of a More Native Architecture for Tissue-Engineered Blood Vessels. *Tissue Engineering Part A,* 15, 827-840.

YOW, K.-H., INGRAM, J., KOROSSIS, S. A., INGHAM, E. & HOMER-VANNIASINKAM, S. 2006. Tissue engineering of vascular conduits. *British Journal of Surgery,* 93, 652-661.

YUSUF, S., HAWKEN, S., ÔUNPUU, S., DANS, T., AVEZUM, A., LANAS, F., MCQUEEN, M., BUDAJ, A., PAIS, P., VARIGOS, J. & LISHENG, L. 2004. Effect of potentially modifiable risk factors associated with myocardial infarction in 52 countries (the INTERHEART study): case-control study. *The Lancet,* 364, 937-952.

ZELLER, P. J. & SKALAK, T. C. 1998. Contribution of individual structural components in determining the zero-stress state in small arteries. *J Vasc Res,* 35, 8-17.

ZHANG, L., ZHOU, J., LU, Q., WEI, Y. & HU, S. 2008. A novel small-diameter vascular graft: in vivo behavior of biodegradable three-layered tubular scaffolds. *Biotechnology and Bioengineering,* 99, 1007-15.

ZHAO, F. & MA, T. 2005. Perfusion bioreactor system for human mesenchymal stem cell tissue engineering: dynamic cell seeding and construct development. *Biotechnology and Bioengineering,* 91, 482-93.

ZHAO, Y., ZHANG, S., ZHOU, J., WANG, J., ZHEN, M., LIU, Y., CHEN, J. & QI, Z. 2010. The development of a tissue-engineered artery using decellularized scaffold and autologous ovine mesenchymal stem cells. *Biomaterials,* 31, 296-307.

ZHOU, J., FRITZE, O., SCHLEICHER, M., WENDEL, H.-P., SCHENKE-LAYLAND, K., HARASZTOSI, C., HU, S. & STOCK, U. A. 2010. Impact of heart valve decellularization on 3-D ultrastructure, immunogenicity and thrombogenicity. *Biomaterials,* 31, 2549-2554.

ZHOU, M., LIU, Z., WEI, Z., LIU, C., QIAO, T., RAN, F., BAI, Y., JIANG, X. & DING, Y. 2009. Development and Validation of Small-diameter Vascular Tissue From a Decellularized Scaffold Coated With Heparin and Vascular Endothelial Growth Factor. *Artificial Organs,* 33, 230-239.

ZHU, C., YING, D., MI, J., LI, L., ZENG, W., HOU, C., SUN, J., YUAN, W., WEN, C. & ZHANG, W. 2008. Development of anti-atherosclerotic tissue-engineered blood vessel by A20-regulated endothelial progenitor cells seeding decellularized vascular matrix. *Biomaterials,* 29, 2628-2636.